Investigating the distributions of zinc and cadmium in the subarctic northeast Pacific Ocean

by

David Janssen
B.Sc., Humboldt State University, 2011

A Dissertation Submitted in Partial Fulfillment
of the Requirements for the Degree of

DOCTOR OF PHILOSOPHY

in the School of Earth and Ocean Sciences

Supervisory Committee

Investigating the distributions of zinc and cadmium in the subarctic northeast Pacific Ocean

by

David Janssen
B.Sc., Humboldt State University, 2011

Supervisory Committee

Dr. Jay T. Cullen, School of Earth and Ocean Sciences
Supervisor

Dr. Roberta C. Hamme, School of Earth and Ocean Sciences
Departmental Member

Dr. J. Scott McIndoe, Department of Chemistry
Outside Member

Dr. Maeve C. Lohan, Earth and Ocean Science, University of Southampton
Additional Member

Abstract

Supervisory Committee
Dr. Jay T. Cullen, School of Earth and Ocean Sciences
Supervisor

Dr. Roberta C. Hamme, School of Earth and Ocean Sciences
Departmental Member

Dr. J. Scott McIndoe, Department of Chemistry
Outside Member

Dr. Maeve C. Lohan, Earth and Ocean Science, University of Southampton
Additional Member

Zinc (Zn) and cadmium (Cd) have nutrient-type vertical distributions reflecting control driven by biological uptake in surface waters and remineralization of sinking biogenic particles at depth. Both metals show strong correlations with major algal nutrients (Cd with phosphate (PO_4^{3-}) and Zn with silicic acid (Si)) in the world ocean. Through their roles as micronutrients and toxins to marine phytoplankton, Zn and Cd can influence surface biological community composition. Preserved Zn and Cd records have been employed as proxies to gain insight into nutrient distributions, circulation, and organic carbon export in the paleocean. A thorough and mechanistic understanding of the biogeochemical cycling of Zn and Cd is necessary for accurate paleoceanographic reconstructions as well as predicting alterations in metal supply to the modern surface ocean and its impacts on primary productivity due to oceanic changes. My dissertation aims to further this understanding through an investigation of Zn and Cd distributions in the subarctic northeast Pacific through samples collected along the Line P transect.

A major focus of this dissertation was identifying and characterizing depletions of metals in O_2-depleted waters relative to global and basin scale metal:macronutrient correlations. Dissolved Cd profiles from the subarctic northeast Pacific and the eastern North Atlantic show a deficit of Cd relative to regional Cd:PO_4^{3-} relationships. Particulate Cd and Cd stable isotopes ($\varepsilon^{112/110}$Cd) from low-O_2 North Atlantic waters and published sedimentary data from the subarctic northeast Pacific point to a previously undocumented water-column metal removal process acting in O_2-depleted waters. Metal sulphide formation, likely in association with particulate microenvironments, can explain the

observed deficits. Other metals with similar sulphide coordination chemistry should also form metal sulphides if this process is occurring. Dissolved Zn from Line P showed distributions and Zn:Si relationships that are consistent with the removal of metal in O_2-depleted waters through sulphide formation. A first order approximation of the Cd deficit suggests that sulphide formation may be an important sink term in the global Cd cycle.

Surface and upper nutricline Zn:Si and Cd:PO_4^{3-} relationships in the chronically iron (Fe)-limited subarctic northeast Pacific showed distinct trends, which differ from those seen in Fe-replete regions. Distributions suggest the formation of surface biogenic particles with high Cd:PO_4^{3-} and Zn:Si, leaving surface waters depleted in metals relative to macronutrients and resulting in high metal:macronutrient ratios in the nutricline as these particles sink and are remineralized. This is consistent with understandings of phytoplankton physiology and uptake of divalent metals under Fe-limitation, and corresponds well with global data for dissolved Cd:PO_4^{3-} patterns in Fe-limited regions. Subsurface high Cd:PO_4^{3-} and Zn:Si may also be influenced by the advection of water enriched in trace metals. The distinct shallow remineralization horizon observed for Zn compared to Si in the subarctic northeast Pacific by this and previous work presents a fundamentally different distribution than observed in global Zn:Si compilations. Directed sampling in the subarctic northeast Pacific should help elucidate the mechanism behind the oceanographically distinct distributions in this basin.

Dissolved $\varepsilon^{112/110}$Cd from Line P demonstrates a remarkably uniform subarctic northeast Pacific deepwater reflecting an advected source signal. Particulate $\varepsilon^{112/110}$Cd samples show an active Cd cycle, which is not imprinted upon the dissolved phase. Particulate $\varepsilon^{112/110}$Cd from 200-600 m depth is among the lightest $\varepsilon^{112/110}$Cd ever reported for natural telluric samples. This may be an important sink for light Cd in the global ocean, which at present is heavy with respect to known sources. Line P surface waters with very low Cd concentrations are not accurately represented by a closed-system Rayleigh model, which can describe $\varepsilon^{112/110}$Cd in the Southern Ocean. This suggests spatially and/or temporally variable surface $\varepsilon^{112/110}$Cd fractionation. A large difference is observed in reported dissolved $\varepsilon^{112/110}$Cd at very low Cd concentrations between different instrumentations. An intercalibration is necessary to determine if this is an analytical artefact or reflects real oceanic variability.

Table of Contents

List of Tables

List of Figures

Acknowledgments

I would like to begin by thanking Jay Cullen first and foremost. Thank you for giving me a spot in your lab and for the thorough mentorship over the years. Thank you for supporting my research endeavors, whether they were oceanographic or not. Thanks for the encouragement during long lab stretches, the countless pieces of advice on a range of challenges, from promoting science through public outreach to fixing winches to life in general, and for lessons learned in organizing successful field campaigns. Finally thank you for inviting me into your family. I value the beer and cheese nights, story time with Luke, and overall the examples on the importance of balancing work and family/personal life, more than anyting I learned in the lab, office, or field.

I likely would not have found trace metal work or oceanography at all if it wasn't for Matt Hurst. Thanks Matt for the many years of mentorship and the introduction to research work, and for guiding me toward UVic for my PhD. Thank you for all your work, recognized and not, to teach me the tools for a successful career in academic research. Thanks for forgiving me for contaminating that whole set of samples with Zn and for providing a great spilled sample story. I'm glad we can laugh about that.

Thank you to my supervisory committee: Roberta Hamme, Scott McIndoe, Maeve Lohan and, in an earlier iteration, Ken Bruland. Thanks to Roberta for regular and thorough comments on my work and for taking an interest in my preparation for a successful academic future beyond my PhD. Special thanks to Maeve for filling in late in the game and still providing excellent advice. Thanks additionally to Ken for giving me a chance on my first research cruise and for his intervention to get me my first email response from Jay, a notoriously challenging feat.

A fundamental part of this PhD labwork took place in Germany. Thank you to Wafa Abouchami and Steve Galer who made this great opportunity possible. Thanks Wafa & Steve for all the energy you put into introducing me to isotope geochemistry (and maybe winning me over to the field) and for inviting me into your home.

Thanks to the members of the Cullen lab, especially Christina and Sarah. Of all the support I've had, Christina deserves special mention. Thank you for welcoming me to the

lab from my first visit and for making sure I was always well fed, including that first visit. Thanks also for providing the necessary impetus to turn a somewhat serious joke into reality and knit myself short shorts. I'm sure many others share this gratitude to you for the shorts. May you always live with the joy of knowing that you made that dream a reality. Thanks to Sarah for NZ fun facts, cheesy positivity cards, cross-cubicle plant invasions and conversations, pretending to be serious and for general commiseration.

Thanks to all my friends at UVic, especially Stinky Stanley, Jess & Neil and many more than can be listed here. I greatly appreciate your support, assistance and friendship. Thanks also to the many non-academic friends in Victoria and elsewhere, especially to the supper club. Thank you to Markus and Dana for being my European family and giving me a place that felt like home. Thanks to Andrea who kept me fed and sane in Germany (and Italy). The following people also contributed to my success and/or sanity in Germany: Heinz for extensive TIMS assistance, Ruifang, Ran, Brad, Sonja and the country & people of Belgium (especially Niels, Kevin, and the Van Roy family).

Thanks to the many people who provided me with the resources and assistance that made this degree possible, especially Allison, Kimberly and Terry in the SEOS office. Everything you do to make the department function is greatly appreciated. Thanks to Marie Robert for always working in my sampling requests and for organizing such a smoothly running program. Thanks also to the captains and crews of the *CCGS J.P. Tully*, the Canadian Coast Guard, and the Line P cruise participants. Thank you to UVic Science Stores, especially Glenda and Bev (who are probably concerned about what I will ask them to ship every time they see me). I'm very grateful to Phoebe Lam for the significant amount of energy and equipment she sent my way to make this work possible.

Lastly, none of this would have been possible without my family. Thanks to my parents for fostering my enthusiasm in science from a young age. And for yielding to my dramatic negotiation tactics by providing swimming lessons at age 5 (how could I study the ocean if I couldn't swim?!). Thanks to my sister Rebecca, who has the amazing talent to, at times, make it appear that I am the normal one in the family. Finally thanks to my grandparents Dorothy, Joan and Harvey for all their energy directed toward my education and interests, whether it was instilling in me the value of being self-sufficient, conducuting spelling tests in the sand, or answering questions about nuclear spin.

Dedication

This dissertation is dedicated to my parents, who exposed me to science and academic research from an early age and have always supported me, and to a series of excellent mentors (listed chronologically: Amy Schwentor, Matt Hurst and Jay Cullen) who instilled in me a deep interest in chemistry and chemical oceanography and who gave me the tools to follow that interest.

Chapter 1

Introduction

1.1 Trace metals in the ocean

Trace metals include transition row and P block metals, rare earth elements, and certain S block metals, which are present in the ocean in vanishingly small concentrations (nmol kg^{-1} to fmol kg^{-1}) (Bruland and Lohan, 2006; see also the MBARI periodic table of elements in the ocean[†] and references therein). While the concentrations of these trace metals are orders of magnitude below concentrations of the main cations in seawater and below macronutrient concentrations (phosphate (PO_4^{3-}), inorganic nitrogen species such as nitrate (NO_3^-) and ammonium (NH_4^+), and silicic acid (Si)), trace metals serve a critical function for marine biota through their roles in the active sites of essential enzymes. In addition to the beneficial and necessary roles that trace metals serve, some metals can also be toxic to certain organisms at oceanographically relevant concentrations. Because of these micronutrient and toxin roles, trace metals can exert control on biological production in the ocean. By either limiting phytoplankton growth (e.g. iron (Fe): Martin et al., 1989) or influencing phytoplankton community composition (e.g. zinc (Zn): Coale, 1991; Crawford et al., 2003; cobalt (Co): Ahlgren et al., 2014; copper (Cu): Mann et al., 2002), trace metals can alter the efficiency of the ocean's biological carbon pump - the process in which phytoplankton transform dissolved inorganic carbon in the ocean surface into particulate organic carbon that is subsequently transferred out of the surface ocean to depth. In this way trace metals impact the degree to which the ocean can store carbon and therefore they impact global carbon cycling.

In addition to the control trace metals can exert on phytoplankton in the ocean, plankton may also exert control on metal distributions and bioavailability. Trace metals such as Fe (Rue and Bruland, 1995), Zn (Bruland, 1989), Cu (Moffett et al., 1990), Co (Saito et al., 2005) and cadmium (Cd) (Bruland, 1992) are primarily bound to organic chelating ligands in the surface ocean (see also Bruland and Lohan, 2006; Vraspir and Butler, 2009 and references therein). The exact origin and function of these ligands are poorly known at present, but it is clear that ligands alter the availability of metals to phytoplankton (e.g. Hutchins et al., 1999; Semeniuk et

[†]http://www.mbari.org/science/upper-ocean-systems/chemical-sensor-group/periodic-table-of-elements-in-the-ocean/

al., 2009) and that they can be produced by marine microbes, for example in response to Fe additions (e.g. Rue and Bruland, 1997) or to elevated concentrations of toxic metals (e.g. Cu: Leal et al., 1999; Croot et al., 2000).

Trace metals and their isotopes also have utility to the oceanographic community through their roles as tracers of ocean processes and the record they provide of paleoceanographic conditions. Studies of trace metal distributions in seawater, marine sediments and corals have provided fundamental information regarding physical, chemical and biological processes in the ocean. In the modern ocean, trace metals have helped to identify and quantify the input of lithogenic material (e.g. aluminum: Measures and Vink, 2000; scandium: Parker et al., 2016), anthropogenic inputs to the ocean (e.g. lead: Shen and Boyle, 1987; Wu and Boyle, 1997; Bridgestock et al., 2016), track deepwater circulation (e.g. neodymium isotopes: Lambelet et al., 2016) and determine biological export production (e.g. thorium and uranium isotopes: Buesseler et al., 1992). Trace metals in paleo records have been used to infer past ocean condition including dust flux on glacial-interglacial scales (Fe: Martinez-Garcia et al., 2011), ocean circulation and macronutrient conditions (e.g. Cd: Boyle, 1988) and the extent of low-oxygen waters through multiple redox-sensitive elements (e.g. Nameroff et al., 2004).

In order to better interpret paleoceanographic records and constrain the impacts of trace metals on biological communities, it is important to have a thorough and mechanistic understanding of the processes influencing the biogeochemical cycling of individual metals. To make further progress toward this goal, this dissertation will examine the distributions of Zn and Cd in the subarctic northeast Pacific and the mechanisms driving their distributions.

1.2 Cadmium in the global ocean

Physical and chemical properties of Cd, including average oceanic and crustal concentrations, are shown in Table 1.1. The dissolved speciation of Cd in seawater is shown in Table 1.2. Dissolved Cd has a nutrient-type distribution in the global ocean driven by biological uptake in surface waters and enrichments at depth due to the sinking and subsequent decomposition of biogenic material (Boyle et al., 1976; Bruland et al., 1978). Cadmium may act as a nutrient for certain phytoplankton via substitution into the carbonic anhydrase enzyme (Price and Morel, 1990) or in a Cd-specific form of the enzyme (Lane and Morel, 2000; Lane et

al., 2005). Cadmium is also known to be a toxin for marine phytoplankton, with a taxa-dependent susceptibility that is strongest for prokaryotic plankton (Brand et al., 1986; Tortell and Price, 1996; Sunda and Huntsman, 1996; Saito et al., 2003). Dissolved profiles and distributions of Cd in the global ocean show a strong relationship with dissolved PO_4^{3-}, and estimates of Cd residence times in the global ocean, roughly 10^4 years (Boyle et al., 1976; Bruland, 1980; de Baar et al., 1994), are of the same order of magnitude as the residence time of PO_4^{3-} (Froelich, 1982; Ruttenberg and Berner 1993; Ruttenberg, 1993). The accuracy of Cd residence time estimates is limited by incomplete understanding of sources and sinks of Cd at present.

Property	
Atomic Number	48
Atomic weight	112.411
Atomic Radius (10^{-10} m)	1.55[a]
Electron Configuration	[Kr] $4d^{10}5s^2$
Melting Point	321.07 °C
Boiling Point	767 °C
Density (g cm^{-3})	8.69
Oxidation States	+2
Ionic Radius (coordination # of 4, 6) (10^{-10} m)	0.78, 0.95
Reduction Potential (E^o) for $Cd^{2+} + 2e^- \leftrightarrow Cd$ (V)	-0.403
First Ionization Energy (KJ mol^{-1})	868
Second Ionization Energy (KJ mol^{-1})	1631
Deepwater concentration range (nmol kg^{-1})	0.3[b] (North Atlantic) to 1.0[c] (North Pacific)
Average crustal composition (ng g^{-1})	100[a]

Table 1.1 Physical and chemical properties of cadmium
Adapted from Rehkämper et al., 2012. Except where noted, values from Lide, 2006.
[a]Slater, 1964.
[b]Bruland and Franks, 1983.
[c]Boyle et al., 1976; Bruland, 1980.

Special attention has been paid to the dissolved Cd:PO_4^{3-} relationship in the global ocean due to the preservation of Cd in marine carbonates resulting in a paleo record of seawater [Cd] and its potential utility for Cd as a paleoceanographic proxy for nutrient distributions and water mass circulation (e.g. Boyle, 1988). The utility of Cd as a paleoproxy is especially clear in the South Atlantic, where strong gradients in [Cd] are seen between North Atlantic Deep

Water (NADW) water and southern component sources (Antarctic Intermediate Water and Antarctic Deepwater) (e.g. Boyle and Keigwin, 1987; Boyle, 1988). In order to infer past nutrient conditions from Cd preserved in sediments, it is of fundamental importance to constrain the variability in dissolved $Cd:PO_4^{3-}$ and the driving mechanisms of any deviations in the relationship.

Organic complexation	**%**	**Source**
Surface water	67%	Bruland, 1992
Subsurface water	Not detected	Sakamoto-Arnold et al., 1987; Bruland, 1992
Inorganic Species	**% of inorganic**	
$CdCl^+$	36%	Byrne, 2002
$CdCl_2$	45%	Byrne, 2002
$CdCl_3^-$	16%	Byrne, 2002
Cd^{2+}	2.8%	Byrne et al., 1988

Table 1.2 Dissolved speciation of cadmium in seawater

A primary driver of variability in regional dissolved $Cd:PO_4^{3-}$ is the biological uptake of $Cd:PO_4^{3-}$ in surface waters, and therefore the Cd:phosphorus (P) exported to depth associated with biogenic particles. Cadmium:P in biological particles is known to vary due to community compositions (e.g. Ho et al., 2003) and physiochemical environmental controls. Perhaps foremost among these environmental factors is Fe bioavailability. Incubation experiments in natural communities and in laboratory isolates show elevated $Cd:PO_4^{3-}$ uptake at low Fe (Sunda and Huntsman, 1998; Sunda and Huntsman, 2000; Cullen et al., 2003; Cullen and Sherrell, 2005; Lane et al., 2008; Lane et al., 2009) and coherent global gradients in $Cd:PO_4^{3-}$ uptake and dissolved $Cd:PO_4^{3-}$ systematics exist across Fe-replete and Fe-limited regions (Cullen, 2006; Lane et al., 2009; Quay et al., 2015). Other metals such as manganese (Mn), cobalt (Co) and Zn show similar antagonistic interactions (Sunda and Huntsman, 1995; Sunda and Huntsman, 1998; Cullen et al., 1999; Sunda and Huntsman, 2000; Cullen and Sherrell, 2005; Baars et al., 2014). These antagonistic interactions between Cd and metals such as Mn, Fe, Co and Zn are driven by competitive metal binding and cellular regulation of non-specific metal transport proteins (e.g. Sunda and Huntsman, 1998; Sunda and Huntsman, 2000; Lane et al., 2009) and

interreplacement of metals in cells (Sunda and Huntsman, 1995; Price and Morel, 1990; Lane et al., 2000).

1.3 Stable cadmium isotopes

Table 1.3 shows the natural stable isotopes of Cd. The alteration of oceanic Cd stable isotope composition through biological and chemical interactions can provide insight into the mechanisms driving the marine Cd cycle. Cadmium stable isotopes are presented in one of three ways by the oceanographic community: $\delta^{114/110}$Cd, $\varepsilon^{114/110}$Cd and $\varepsilon^{112/110}$Cd, all relative to the reference standard NIST SRM-3108 (Abouchami et al., 2012). Exact conversions between the three different units are shown in Table 1.4. In the initial $\varepsilon^{112/110}$Cd studies, individual labs did not all use the same reference standard. Conversions between different reference standards can be found in Abouchami et al. (2012). I will present Cd isotope data in both $\varepsilon^{112/110}$Cd and $\delta^{114/110}$Cd and will discuss the data in units of $\varepsilon^{112/110}$Cd, which is the derivation of the $^{112/110}$Cd ratio in parts per ten thousand relative to NIST SRM-3108 as calculated by Equation 1.1.

$$\varepsilon^{112/110}Cd = \left(\frac{^{110}Cd/^{112}Cd_{NIST\ SRM\ 3108}}{^{110}Cd/^{112}Cd_{Sample}} - 1 \right) \times 10{,}000 \qquad \text{(Equation 1.1)}$$

Lower and negative $\varepsilon^{112/110}$Cd values reflect enrichment of light isotopes while higher positive values reflect enrichment of heavy isotopes. Biological uptake of Cd in surface waters is believed to sequester light isotopes into the particulate phase leaving surface waters enriched in heavy isotopes relative to both deepwater and phytoplankton (Lacan et al., 2006; John and Conway, 2014; S.C. Yang et al., 2015). A deepwater dissolved $\varepsilon^{112/110}$Cd gradient is observed with NADW elevated in $\varepsilon^{112/110}$Cd relative to Southern Component Water (SCW). The oceanic $\varepsilon^{112/110}$Cd inventory of around +1 to +2 (Ripperger et al., 2007; Abouchami et al., 2014; Conway and John, 2015a; Conway and John, 2015b; Chapter 4 / Janssen et al., in revision) is heavy relative to bulk silicate earth (Schmitt et al., 2009a), suggesting a light sink for Cd in the global ocean. The identity, isotope composition, and magnitude of this sink is currently unknown. The incorporation Cd into ferromanganese crusts and the abiotic incorporation into calcite reflects the water column signal without fractionation (Schmitt et al., 2009a; Horner et

al., 2010) while preliminary data on the non-quantitative formation of Cd sulphides suggests that the solid sulphide phase is enriched in light isotopes, leaving surrounding water enriched in heavy isotopes (Schmitt et al. 2009a). This suggests that sulphide formation may be a relevant potential sink to explain the isotopic imbalance of oceans and source material. Uptake of Cd by phytoplankton has been shown to sequester light Cd in the particulate phase (Lacan et al., 2006; John and Conway, 2014; see also e.g. Ripperger et al., 2007; Abouchami et al., 2011), and therefore this may also be an important sink of isotopically light Cd.

Mass number	Atomic Mass	Natural Abundance (%)	Half-life (years)	Decay Mode	Nuclear Spin
106	105.906	1.25	$>5.8*10^{17}$	Electron Capture	0
108	107.904	0.89	$>4.1*10^{17}$	Electron Capture	0
110	109.903	12.49	Stable	NA	0
111	110.904	12.8	Stable	NA	1/2
112	111.903	24.13	Stable	NA	0
113	112.904	12.22	$8.2*10^{15}$	Beta Emission	1/2
114	113.903	28.73	$>6.0*10^{17}$	Double Beta Emission	0
116	115.905	7.49	$3.8*10^{19}$	Double Beta Emission	0

Table 1.3 Natural isotopes of cadmium
Values from Lide, 2006.

	$\varepsilon^{112/110}Cd$	$\varepsilon^{114/110}Cd$	$\delta^{114/110}Cd$
$\varepsilon^{112/110}Cd$	*1	*2.000425	*0.2000425
$\varepsilon^{114/110}Cd$	*0.499894	*1	*0.1
$\delta^{114/110}Cd$	*4.99894	*10	*1

Table 1.4 Interconversion factors for notations used in the Cd stable isotope literature
Table presented as row notation value*conversion factor = column notation value. Values from Abouchami et al., 2012.

1.4 Zinc in the global ocean

Physical and chemical properties of Zn are shown in Table 1.5 and the dissolved speciation of Zn in seawater is shown in Table 1.6. Dissolved Zn also has a nutrient-type

distribution in the global ocean (Bruland et al., 1978). While Zn in phytoplankton is primarily associated with organic tissue and not mineral phases (e.g. Twining et al., 2004; Twining et al., 2014), and Zn is released from cells along with other organic-phase elements such as P (Twining et al., 2014), depth profiles of dissolved Zn suggest a deeper remineralization than the macronutrients PO_4^{3-} and NO_3^- and other nutrient-type trace metals like Cd. Instead, depth profiles and global distributions of Zn correlate strongly with the "hard-part" associated macronutrient Si (e.g. Bruland et al., 1978). Considerable uncertainty exists regarding the residence time of Zn in the ocean, with estimates ranging from 10^3-10^4 years (e.g. Shiller and Boyle, 1985; Roshan et al., 2016).

Property	
Atomic Number	30
Atomic weight	65.409
Atomic Radius	1.35[a]
Electron configuration	$[Ar]3d^{10}4s^2$
Melting Point °C	416
Boiling Point °C	907
Density g cm^{-3}	7.13
Oxidation States	+2
Ionic Radius (coordination # of 4, 6) (10^{-10} m)	0.60, 0.74
Reduction Potential (E^o) for $Zn^{2+} + 2e^- \leftrightarrow Zn$ (V)	-0.762
First Ionization Energy (KJ mol^{-1})	906
Second Ionization Energy (KJ mol^{-1})	1733
Deepwater concentration range (nmol kg^{-1})	1.5[b] (North Atlantic) to 10[c] (North Pacific)
Average crustal composition (μg g^{-1})	55-65[d]

Table 1.5 Physical and chemical properties of zinc
Except where noted, values from Lide, 2006.
[a]Slater, 1964.
[b]Bruland and Franks, 1983.
[c]Martin et al., 1989.
[d]Wedepohl, 1995; McDonough and Sun, 1995.

The biochemical roles for Zn in marine prokaryotes and eukaryotes are more clear and widespread phylogenetically when compared to Cd. Zinc is active in carbonic anhydrase, which catalyzes the interconversion of dissolved inorganic carbon species to help supply CO_2 needed for photosynthesis. Additionally Zn is believed to play a role in alkaline phosphatase, which is

involved in the acquisition of organic phosphorus, and in DNA repair and RNA transcription (e.g. Morel et al., 2003; Saito et al., 2008; Dupont et al., 2010 and references therein). As with Cd, Zn requirements vary across phytoplankton taxa. Eukaryotic organisms have a higher Zn demand relative to their proteome size than prokaryotic organisms (Dupont et al., 2006), suggesting that eukaryotic phytoplankton may be more susceptible to Zn limitation than prokaryotic phytoplankton. Experiments with laboratory isolates (*cf.* Morel et al., 1994; Saito et al., 2003; Saito and Goepfert, 2008) and natural assemblages of phytoplankton in the field (Franck et al., 2003; Chappell et al., 2016) show general support for this idea.

Organic Complexation	**% Complexed**
Surface water	>98%[a], >96%[b], ~96%[c]
Subsurface water	~70%[a], 75-90%[b],
Inorganic Species	**% of inorganic**
Zn^{2+}	64%[d]
$ZnCl^{+}$	16%[d]
$ZnCO_3$	10%[e]
$ZnOH^{+}$	6%[e]
$ZnSO_4$	5%[e]

Table 1.6 Dissolved speciation of zinc in seawater
[a]North Pacific, Bruland, 1989.
[b]Atlantic, Ellwood and Van den Berg, 2000.
[c]Subarctic North Pacific, Jakuba et al., 2012.
[d]Byrne, 2002.
[e]Byrne et al., 1988.

Although phytoplankton isolates grown in chemically defined media have illustrated the potential for Zn to act as a limiting or co-limiting nutrient (e.g. Anderson et al., 1978; Brand et al., 1983; Morel et al., 1994; Saito and Goepfert, 2008), field data showing Zn limitation are scarce. Incubation studies with Zn amendments have generally not shown a strong influence on total primary productivity (e.g. Coale, 1991; Crawford et al., 2003; Leblanc et al., 2005; Jakuba et al., 2012; Goes et al., 2016; see also the discussion of challenges in observing Zn-carbon co-limitation in the field, Saito et al., 2008 section: Thoughts on the potential for colimitation in the marine environment). Evidence where Zn has been shown to limit or co-limit natural phytoplankton communities is restricted to select environments in the North Pacific (Franck et al., 2003; Jakuba et al., 2012; Chappell et al., 2016). More generally, while Zn availability has

not been shown to be the proximate limiting nutrient for primary producers in the global ocean, Zn can exert control on community composition (Coale, 1991; Crawford et al., 2003; Leblanc et al., 2005; Jakuba et al., 2012; Goes et al., 2016). Incubation experiments from natural systems with amendments of Zn, either alone or along with Fe, have generally been shown to favor small eukaryotic phytoplankton such as diatoms and flagellates, in contrast to the large diatoms favored by additions of Fe alone (Crawford et al., 2003; Franck et al., 2003 Costa Rica dome site; Leblanc et al., 2005; Goes et al., 2016; note that some Zn addition studies have also shown larger diatoms to be favored; Franck et al., 2003 California sites). This is in agreement with trends seen for phytoplankton isolates grown in defined media, which showed an absolute Zn requirement in diatoms but not in the prymnesiophyte *Emiliania huxleyi* or the prokaryotic genus *Synechococcus* (Sunda and Huntsman, 1992; Sunda and Huntsman, 1995). Community composition can influence the trophic transfer of carbon as well as the degree to which carbon and other major nutrients may be exported to depth.

In addition to the biological relevance of Zn in primary productivity and community composition, Zn also has shown some potential as a paleoceanographic proxy. While the paleoceanographic potentials of Zn have received less attention than Cd-based proxies, Zn may be useful for tracing deepwater circulation (Marchitto et al., 2000; Marchitto et al., 2002) and organic carbon export (Ellwood et al., 2004). It is therefore important to understand the loss terms of Zn and the sensitivity of these terms to changing ocean conditions as it pertains to the ocean carbon pump and paleoceanographic reconstructions.

1.5 Oxygen and sulphide in the open ocean

Substantial expanses of low-oxygen (O_2) water can be found throughout the global ocean. Such regions exist as intermediate depth waters, which are isolated from the atmosphere due to natural ocean overturning circulation. The depletion of O_2 is driven by respiration which, in the absence of a replenishment of O_2 from the atmosphere, results in diminishing O_2 concentrations. The degree of O_2 depletion is regulated by the water's initial [O_2] and the amount of aerobic respiration in the water, which is influenced by respiration rates and the water age ("older" waters, waters that have been removed from the surface for longer, have more time to develop significant depletions). Respiration rates are higher in regions with higher

organic carbon flux, such as regions underlying productive upwelling environments, and in the upper ocean because the flux of organic matter from the surface ocean decreases exponentially with depth (Wytrtki, 1962; Martin et al., 1987; Gilly et al., 2013). For these reasons, O_2-depleted waters are found at intermediate depths at a broad scale in ocean basins with "older" water such as in the North Pacific, the Indian Ocean, and the Eastern Tropical South Pacific as well as more localized O_2-depleted regions around upwelling environments (e.g. near Mauritania and Angola/Namibia in the eastern Atlantic Ocean). Time series data show that dissolved O_2 concentrations are decreasing in the global ocean (Whitney et al., 2007; Stramma et al., 2010; Keeling et al., 2010), leading to intensification and spatial expansion of these regions. Model projections predict that trends of increased oxygen depletion will continue (Shaffer et al., 2009; Keeling et al., 2010; Bopp et al., 2013).

The terminology used to describe O_2-depleted regions in the literature can be confusing and inconsistent. Terms such as dysoxic, hypoxic, suboxic, Oxygen Limited Zone (OLZ). Oxygen Minimum Zone (OMZ), Oxygen Deficient Zone (ODZ), Anoxic Marine Zone (AMZ) and functionally anoxic have all been used to describe different low-O_2 regions of the world ocean, at times with variable definitions depending on the publication, geographic region and biological species being discussed (*cf*. Diaz and Rosenberg, 2008; Shaffer et al., 2009; Ulloa and Pantoja, 2009; Ulloa et al., 2012; Thamdrup et al., 2012; Wright et al., 2012; Gilly et al., 2013). While O_2-depletion limits the capacity for aerobic respiration in these waters, it allows for a variety of different biologically catalyzed redox transformations affecting the more major (e.g. sulphate (SO_4^{2-}) and NO_3^-) and minor (e.g. Mn, Fe) chemical species in seawater (Wright et al., 2012). Following this metabolic diversity, Canfield and Thamdrup (2009) have argued for the phasing out of some terminology in favour of describing regions of O_2-depletion and non-oxic respiration by the chemical signatures of the region.

In sections of this dissertation which were previously published I have used the term ODZ. For similar motivations to those used by Canfield and Thamdrup (2009), I have not bounded this term with specific O_2 concentrations ($[O_2]$) and instead have applied it to signify anomalies in chemical fields (trace metal concentrations in my case) which may indicate respiration using electron acceptors other than O_2. The $[O_2]$ that corresponds to these metal anomalies in the subarctic northeast Pacific are roughly 50 μmol kg^{-1} for the subarctic northeast

Pacific and 75 μmol kg^{-1} in the Mauritanian upwelling in the eastern North Atlantic. As my use of the term ODZ is in disagreement with the O_2 ranges presented in the literature, I have selected not to use these terms in chapters which have not yet been published and instead have used phrases such as low-O_2 and O_2-depleted to describe waters with significant oxygen depletion in which I see anomalous metal behavior.

While spatial expansions and intensifications of O_2-depleted regions result in a loss of habitat for many pelagic metazoans, shifting ecosystem dynamics and selecting for a few more hypoxia-tolerant species (e.g. Stramma et al., 2010; Gilly et al., 2013 and references therein), microbial communities of high metabolic diversity exist in these ecosystems which make use of multiple electron acceptors even under thermodynamically unfavourable conditions (cf. Wright et al., 2012; Froelich et al., 1979). Sulphate reduction in the presence of dissolved O_2 is well documented (e.g. Hastings and Emerson, 1988; Marschall et al., 1993). However, in the open ocean, sulphide is not generally measured in O_2-depleted regions (notable exceptions are transient and spatially expansive sulphide plumes which have been detected in the ODZ off of Peru (Dugdale et al., 1977; Schunck et al., 2013)). Until recently proof of dissimilatory SO_4^{2-} reduction in a water column with measurable O_2 and without detectable dissolved free sulphide was lacking. Recent microbial work has helped to solve this puzzle. Genomic, transcriptomic and incubation data show that organisms metabolizing sulphur through dissimilatory pathways are both present and active in ODZ waters (Canfield et al., 2010; Stewart, 2011; Podlaska et al., 2012; Stewart et al., 2012; Ulloa et al., 2012; Wright et al., 2012; Carolan et al., 2015). In what is termed the “cryptic sulphur cycle”, sulphur compounds are cycled through redox states by both SO_4^{2-} reducing and sulphide oxidizing bacteria in ODZs, possibly in association with anoxic microenvironments in sinking particles (Stewart et al., 2011; Wright et al., 2012), which have been identified as potentially important in nitrogen (N) cycling in low-O_2 waters (Glud et al., 2015; Ploug and Bergkvist, 2015). There is some disagreement as to the exact rates at which these processes occur as measured by incubations (Canfield et al., 2010) and as constrained by theoretical stable isotope calculations (Johnston et al., 2014); however, it is clear that S redox reactions are occurring in these environments.

1.6 Zn and Cd solubility in the presence of sulphide

Group 12 elements Zn and Cd (as well as Group 11 metals Cu and silver (Ag)) form very strong metal sulphides (Pearson, 1963) that are insoluble in water. So, while these metals are soluble in oxic waters, their concentrations are much diminished in sulphidic waters found in certain fjords, inlets, marginal basins and inland seas with restricted circulation (e.g. Jacobs and Emerson, 1982; Jacobs and Emerson, 1985; Dyrssen and Kremling, 1990). Once formed, these metal sulphides are highly stable and their existence is not restricted to anoxic and sulphidic waters. Metal sulphides have been detected in oxic environments and sulphides of Zn and Cd have half-lives in oxic water of more than one month (Rozan et al., 2000; Mullaugh and Luther, 2011). Due to the kinetic inertness of metal-sulphide complexes and particles, these metal sulphides play an important role in stabilizing reduced sulphur in oxic environments (e.g. Luther and Tsamakis, 1989; Zhang and Millero, 1994; Theberge et al., 1997; Rozan et al., 2000; Mullaugh and Luther, 2011).

The formation of metal sulphides has been invoked to explain the accumulation of Cd in oxygen-depleted sediments and sedimentary Cd enrichments therefore show potential as a paleoceanographic proxy for the redox conditions under which sediments were deposited (e.g. Van Geen et al., 1995; Rosenthal et al., 1995a; Morford and Emerson, 1999). In certain environments, there appears to be a mass balance between sedimentary Cd enrichments and water column Cd deficits (Van Geen et al., 1995). The potential for metal sulphides to form in low oxygen water columns has been documented for silver in the northeast Pacific (McKay and Pedersen, 2008; Kramer et al., 2011). Due to the proclivity of Cd and Zn to form insoluble sulphides, the presence of reduced sulphur in O_2-depleted but not anoxic water columns, and the stability of Zn and Cd sulphides in oxic environments, a similar water column sulphide formation mechanism may be acting to remove dissolved Zn and Cd in O_2-depleted waters. Sulphides of Zn and Cd are expected to be isotopically light relative to the dissolved phase from which they formed (John et al., 2008; Schmitt et al., 2009a; J. Yang et al., 2015). Therefore a sulphide removal mechanism may be important in resolving imbalances between the isotopic composition of source material and the oceanic inventories of Zn (Little et al., 2014; Little et al., 2016; Vance et al., 2016) and possibly other metals forming highly insoluble sulphides such as Cd.

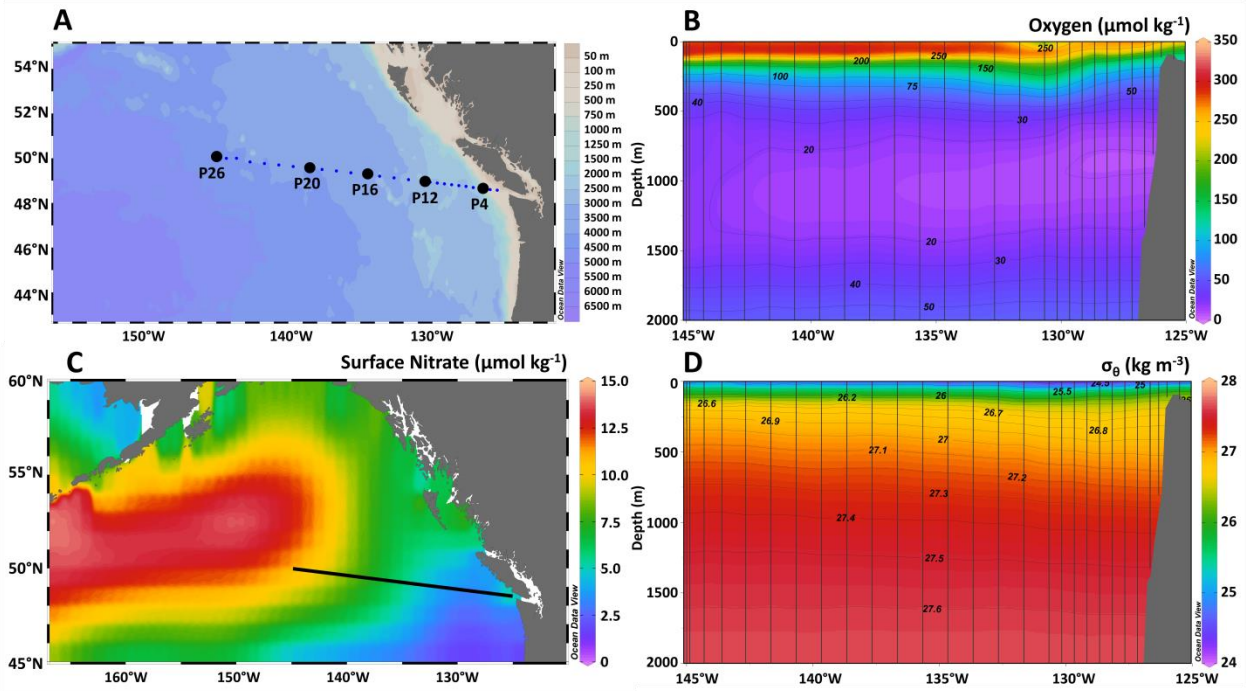

Figure 1.1 The Line P transect
Stations along the Line P transect are shown as blue dots in panel A, with stations where trace metals samples were collected in black and labeled. Panel B shows [O_2] in the upper 2000 m from CTD casts (black lines) (cruise 2012-13, data courtesy of the Line P program). Panel C shows surface NO_3^- in the subarctic northeast Pacific (data from the World Ocean Atlas, Garcia et al., 2010) with the Line P transect shown as a black line. Panel D shows density in the upper 2000 m along the transect from CTD casts (black lines) (cruise 2012-13, data courtesy of the Line P program). Line P CTD data is available at: https://www.waterproperties.ca/linep/cruises.php. Adapted from Chapter 4 / Janssen et al., in revision.

1.7 Dissertation motivation and focus

This dissertation is focused on understanding the distributions and biogeochemical cycling of Zn and Cd in the subarctic northeast Pacific, with field work conducted along the Line P time series transect (Figure 1.1). The Line P transect extends westward off of the British Columbia shelf to the open subarctic northeast Pacific and the Alaskan Gyre. The eastern more coastally-influenced end of the transect shows high nutrient drawdown consistent with Fe-replete conditions while the open ocean side is chronically Fe-limited (Martin et al., 1989, Coale, 1991; Peña and Varela, 2007) (Figure 1.1 panel C). A spatially expansive O_2-depleted water mass is found along the entire transect with [O_2] falling below 50 µmol kg^{-1} near 400 m

depth, reaching a minimum of ~10-20 μmol kg^{-1} near 1000 m and not exceeding 50 μmol kg^{-1} again until below roughly 2000 m (Figure 1.1 panel B). These strong gradients in nutrient limitation and [O_2] along the transect make this an ideal environment to study the influence of such forcings on trace metal and metal isotope cycling.

Historically, processes controlling the distribution of trace metals and their utility as tracers of physical and chemical processes in the ocean have been inferred from regional and global dissolved trace metal-macronutrient correlations. Here I will investigate the degree of correlation between metals and macronutrients in the Pacific and take advantage of the dramatic chemical and biological gradients that characterize the onshore-offshore section and depth profiles along Line P to probe for factors that markedly impact the basin scale distribution of Cd and Zn. Likewise, insight gained from the subarctic northeast Pacific is relevant to the global ocean for determining the potential of similar mechanisms to act elsewhere, their potential implications to Zn and Cd distributions and the resulting potential impact on surface phytoplankton communities. Additionally, accurate interpretation of paleoceanographic Cd and Zn records requires a thorough and mechanistic understanding of the cycling of Zn and Cd in the modern ocean and how the biogeochemical cycles of these elements may be altered under different oceanographic conditions, which have been known to vary on glacial-interglacial time scales, such as oxygenation (Van Geen et al., 1995; Jaccard et al., 2014) and micronutrient supply (Martin, 1990; Martinez-Garcia et al., 2011).

A central theme to this work is the impact of O_2-depleted, but not anoxic, environments on the distributions of Zn and Cd. **Chapter 2** focuses on depletions of Cd in low-O_2 waters in literature and new data. This chapter combines data from the Pacific (dissolved Cd) and from the Atlantic (dissolved and particulate Cd and $\varepsilon^{112/110}$Cd) to introduce the formation of water column sulphides as a potential mechanism to explain the observed depletions. This chapter was published in the Proceedings of the National Academy of Sciences of the United States of America (Janssen et al., 2014). **Chapter 3** investigates Zn distributions in the subarctic northeast Pacific, highlighting Zn:Si relationships that are fundamentally distinct from the global average, including similar Zn behavior to that observed for Cd in low-O_2 water. This chapter was published in Marine Chemistry (Janssen and Cullen, 2015).

Chapters 4 and 5 present $\varepsilon^{112/110}$Cd measurements in the dissolved and particulate phases along Line P to better understand vertical and horizontal controls on Cd cycling. **Chapter 4** focuses on dissolved Cd and $\varepsilon^{112/110}$Cd from 2012-2014. Surface and nutricline data show Cd:PO_4^{3-} trends indicative of HNLC control on Cd:PO_4^{3-} uptake as well as interannual variability in Cd and $\varepsilon^{112/110}$Cd cycling, highlighting remaining questions in isotope fractionation during Cd uptake. Subsurface data highlight distinct isotope distributions in the Pacific compared to the Atlantic and strengthen a global data set supporting the potential of $\varepsilon^{112/110}$Cd as a tracer of global deepwater circulation. This chapter is in review at Earth and Planetary Science Letters. **Chapter 5** presents sinking and suspended particulate samples from Line P in 2014. These data demonstrate alteration of the Cd isotope composition of particles without leaving an imprint on the dissolved phase, pointing to unknown processes driving marine Cd cycling, and identify an isotopically light Cd sink to help balance the marine $\varepsilon^{112/110}$Cd inventory with known sources and sinks.

Chapter 2

Undocumented water column sink for cadmium in open ocean oxygen-deficient zones

Janssen, D.J., Conway, T.M., John, S.G., Christian, J.R., Kramer, D.I., Pedersen, T.F., Cullen, J.T. (2014). Undocumented water column sink for cadmium in open ocean oxygen-deficient zones. *Proceedings of the National Academy of Sciences of the United States of America*. 111:6888-6893. doi: 10.1073/pnas.1402388111.

2.1 Abstract

Cadmium (Cd) is a micronutrient and a tracer of biological productivity and circulation in the ocean. The correlation between dissolved Cd and the major algal nutrients in seawater has led to the use of Cd preserved in microfossils to constrain past ocean nutrient distributions. However, linking Cd to marine biological processes requires constraints on marine sources and sinks of Cd. Here, we show a decoupling between Cd and major nutrients within oxygen deficient zones (ODZs) in both the Northeast Pacific and North Atlantic Oceans, which we attribute to Cd sulphide (CdS) precipitation in euxinic microenvironments around sinking biological particles. We find that dissolved Cd correlates well with dissolved phosphate in oxygenated waters, but is depleted compared with phosphate in ODZs. Additionally, suspended particles from the North Atlantic show high Cd content and light Cd stable isotope ratios within the ODZ, indicative of CdS precipitation. Globally, we calculate that CdS precipitation in ODZs is an important, and to our knowledge a previously undocumented marine sink of Cd. Our results suggest that water column oxygen depletion has a substantial impact on Cd biogeochemical cycling, impacting the global relationship between Cd and major nutrients and suggesting that Cd may be a previously unidentified tracer for water column oxygen deficiency on geological timescales. Similar depletions of copper and zinc in the Northeast Pacific indicate that sulphide precipitation in ODZs may also have an influence on the global distribution of other trace metals.

2.2 Introduction

Cadmium has a nutrient-type depth profile in the open ocean, with low concentrations in surface water due to phytoplankton uptake and higher concentrations in deep water where sinking biological material remineralizes, releasing Cd (Boyle et al., 1976; Bruland et al., 1978; de Baar et al., 1994). Cadmium can act either as a nutrient or a toxin, and therefore influences both phytoplankton growth and community composition (Lane and Morel, 2000; Lee et al., 1995; Price and Morel, 1990; Xu et al., 2008). In addition to the direct impact of Cd on marine microbial communities, dissolved Cd is strongly correlated with the major algal nutrient phosphate (PO_4^{3-}) (Boyle et al., 1976; Bruland et al., 1978), in seawater. A paleoceanographic proxy for dissolved PO_4^{3-} therefore takes advantage of Cd incorporation into foraminiferal calcite tests, preserved in the sedimentary record (Boyle, 1988; Elderfield and Rickaby, 2000). Foraminiferal records of Cd have been used by a number of studies to reconstruct water mass distribution and nutrient utilization in past oceans (Boyle, 1988; Elderfield and Rickaby, 2000; Rosenthal et al., 1997).

Reliable tracers of paleoceanographic nutrient distributions in the ocean are vital to understanding past climate variability, and thus to predicting the potential impacts of anthropogenic climate change. Successful use of the foraminiferal Cd proxy to reconstruct past macronutrients requires a detailed understanding of Cd cycling and of factors which may influence the Cd:PO_4^{3-} of the ocean. For example, it is well established that correlations between dissolved Cd and PO_4^{3-} may vary due to regional differences in the rates at which phytoplankton take up Cd and PO_4^{3-} (de Baar et al., 1994; Cullen, 2006). Recent studies (Conway et al., 2013) of dissolved Cd isotope ratios in the ocean ($\varepsilon^{112/110}$Cd) indicate a restricted isotopic range of the deep ocean (~+1 to +2) which is heavier than crustal $\varepsilon^{112/110}$Cd of near 0 (Schmitt et al., 2009a), indicative of an as-yet unattributed sink for isotopically light Cd. The extent to which this sink induces local changes in Cd:PO_4^{3-} must be understood to correctly interpret paleoceanographic records.

2.3 Methods

Northeast Pacific Cd samples were collected along an onshore–offshore transect from the coast of Vancouver Island, BC, Canada to Ocean Station P (50°N, 145°W, depth 4,220 m) February 12–18, 2005, on board the *CCGS J.P. Tully* (Kramer et al., 2011). Filtered (0.2 μm, Millipore Opticap) samples from 0 to 50 m were collected using a Teflon bellows pump. Samples from 50 to 600 m depth were collected using X-Niskin or GO-FLO (General Oceanics) bottles on a Kevlar line and were filtered immediately after collection through a 0.2-μm filter (Millipore Opticap). Samples below 600 m were collected on a standard metal frame rosette equipped with Niskin bottles and were not filtered. Duplicate samples were collected from the non-trace metal clean rosette and clean bottles on the Kevlar line to confirm that the standard rosette was of sufficient cleanliness for analysis (Kramer et al., 2011). Samples were acidified with 12 mol L^{-1} ultrapure HCl (SEASTAR Chemicals Inc.) within 48 h of collection. Cadmium was analyzed using the 1-pyrrolidine dithiocarbamate–diethylammoniumdiethyldithiocarbamate organic extraction method followed by isotope dilution inductively coupled plasma mass spectrometry, and nutrients were determined with standard colorimetric techniques (Kramer et al., 2011).

North Atlantic samples were collected as part of the US GEOTRACES A03 North Atlantic transect at stations USGT10-9 (17.4°N, 18.3°W) and USGT11-14 (27.6°N, 49.6°W). Dissolved samples (0.2-μm filtered) were collected using the US GEOTRACES trace-metal clean sampling system, and particulate samples were collected onto 0.8-μm Supor filters using in situ large-volume pumps. Seawater samples were acidified onshore with 1 mL 12 mol L^{-1} ultrapure HCl (VWR) and allowed to sit for several months before processing. Dissolved Cd was extracted from seawater onto Nobias PA-1 chelating resin, purified by an anion exchange chromatographic technique, and analyzed by Thermo Neptune multicollector inductively coupled plasma mass spectrometer at the Center for Elemental Mass Spectrometry at the University of South Carolina according to previously published methods (Conway et al., 2013). Particulate $\varepsilon^{112/110}$Cd was determined following a pH 8 oxalate-EDTA (0.1–0.05 mol L^{-1}) leach of particles; purification and analysis was performed according to the same procedures used for seawater. The stable isotope values for Cd are reported as $\varepsilon^{112/110}$Cd relative to the National

Institute of Standards and Technology Standard Reference Material 3108 standard and have been converted from their original notation ($\delta^{114/110}$Cd) by the conversion factors found in Table 1.4. Original $\delta^{114/110}$Cd values were calculated by:

$$\delta^{114/110}Cd = \left(\frac{^{114}Cd/^{110}Cd_{sample}}{^{114}Cd/^{110}Cd_{NIST\ SRM\ 3108}} - 1 \right) \times 1{,}000$$

Cd*, which tracks enrichments and depletions of Cd relative to PO_4^{3-} and an average deepwater Cd:PO_4^{3-} ratio, was calculated by:

$$Cd^* = Cd_{measured} - PO_4^{3-}{}_{measured} \times \frac{Cd}{PO_4^{3-}}_{deep}$$

where $\frac{Cd}{PO_4^{3-}}_{deep}$ represents the average deepwater ratio in either the Pacific or Atlantic samples. A value of 0.25 is used for the deepwater ratio for Atlantic samples and 0.35 is used for Pacific and Southern Ocean–subantarctic samples (see appendix A for further discussion of Pacific Cd* based on the further data generated during this dissertation). These values represent a best average composition for our North Atlantic and northeast Pacific samples and show agreement with published values. Because the absolute value of Cd* will vary depending on the value chosen for deepwater Cd:PO_4^{3-}, we focus mainly on trends in Cd* within profiles and basins, which illustrate relative enrichments or depletions of Cd compared with PO_4^{3-} independent of the Cd:PO_4^{3-} used. Figures in the manuscript were produced using Ocean Data View (Schlitzer, 2014).

2.4 Results and Discussion

Cadmium and other trace metals such as copper (Cu) and zinc (Zn) are known to form solid sulphide precipitates in the ocean under conditions of anoxia where sulphide is present. For example, precipitation of Cd sulphide (CdS) (Al-Farawati and van den Berg, 1999) leading to dissolved Cd depletion is observed at oxic–anoxic interfaces in stratified basins with permanently or seasonally anoxic waters (Jacobs and Emerson, 1984; Jacobs et al., 1985). Here, for the first time to our knowledge, we provide evidence that CdS precipitation may occur in

oxic open-ocean waters, operationally defined as containing measureable O_2 (detection limit of typically <3 μmol kg^{-1}using common methods) (Berner, 1981). At the surface of the ocean, oxygen saturation in seawater is usually 200–300 μmol kg^{-1}. In regions where we observe evidence of CdS precipitation, oxygen concentrations are significantly depleted by heterotrophic respiration, but significantly above detection limits. The northeast subarctic Pacific hosts the world's most extensive oxygen-deficient zones (ODZ) (Figure 2.1), with oxygen depletion (<50 μmol kg^{-1}) extending from 400 to 1,800 m depth and minimum oxygen concentrations of 10–20 μmol kg^{-1} at ~1,000 m (Figure 2.2) (Whitney et al., 2007). The ODZ in the eastern subtropical North Atlantic underlies the Mauritanian upwelling region and, like the Pacific ODZ, is most intense along the eastern margin (Figure 2.1), where oxygen deficiency (<75 μmol kg^{-1}) extends from 100 to 750 m depth, with a minimum of 45 μmol kg^{-1} near 400 m (Figure 2.2).

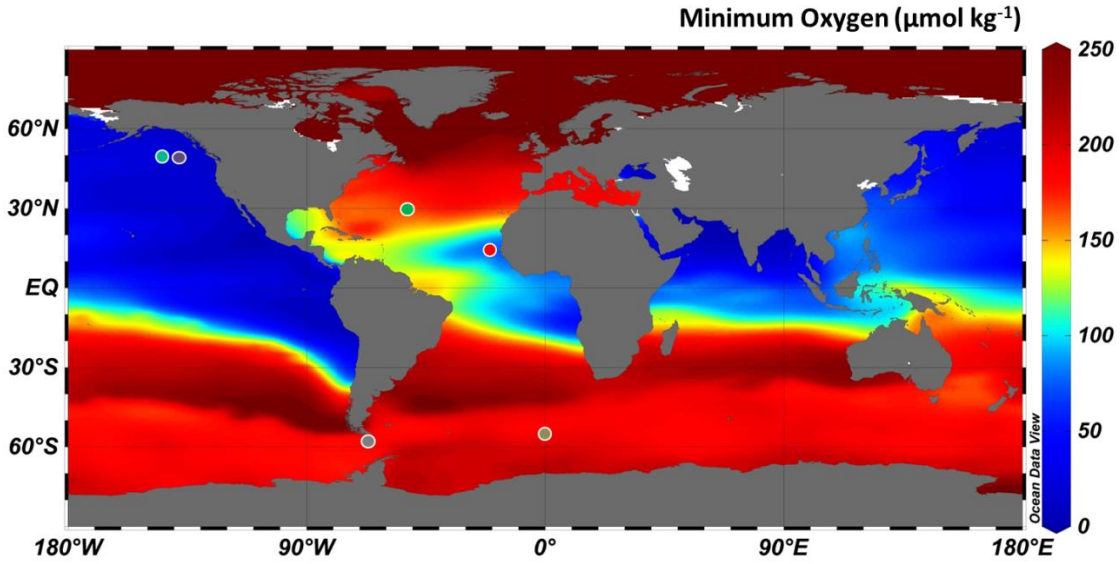

Figure 2.1 Sampling locations for this study overlain on water column minimum dissolved oxygen concentrations
New data are presented here from the eastern North Pacific at station P20 (49.6°N, 139.7°W, purple) and North Atlantic at stations USGT11-14 (27.6°N, 49.6°W, green) and USGT10-9 (17.4°N, 18.25°W,red). Previously published data are presented from station T7/P26 in the eastern North Pacific (50.0°N, 145.0°W, light blue) (Martin et al., 1989), and Southern Ocean/subantarctic stations 249 (56.1°S, 63.8°W, gray) (Xue et al., 2013), and PS71-113 (53.0°S, 0.3°W, tan) (Abouchami et al., 2014).

In the Pacific and Atlantic ODZs we observe a decoupling between concentrations of dissolved Cd and PO_4^{3-}, compared with more oxygenated sites in the Southern Ocean and

subantarctic South Atlantic, and the central North Atlantic (Figures 2.1 and 2.2), where Cd and PO_4^{3-} are well correlated throughout deep waters with average Cd:PO_4^{3-} ratios of 0.33 ± 0.03 nmol μmol^{-1} and 0.23 ± 0.04 nmol μmol^{-1}, respectively (1σ SD) (de Baar et al., 1994). However, within the northeast Pacific and Mauritanian ODZs, dissolved Cd decreases relative to PO_4^{3-} beginning near the point where dissolved O_2 falls below about 75 μmol kg^{-1}. In the northeast Pacific this is observed beginning at a depth of 400 m; whereas PO_4^{3-} continues to increase in a nutrient-like fashion to a maximum at 1,000 m, Cd concentrations do not (Figure 2.2). In the eastern North Atlantic, the decoupling between PO_4^{3-} and Cd is observed as a much slower rate of increase in Cd concentrations below 80 m, compared with the rate at which PO_4^{3-} increases. The departure of Cd from expected concentrations within the ODZs, based on average deepwater Cd:PO_4^{3-}, can be visualized by plotting the variable Cd*, which is the excess or depletion of Cd compared with PO_4^{3-}. Depletions in Cd* of up to 100 pmol kg^{-1} and 250 pmol kg^{-1} are observed within the ODZs at the northeast Pacific sites and eastern North Atlantic sites, respectively. At depths where the water column is more oxygenated, Cd* depletions are generally <50 pmol kg^{-1} (Figure 2.2).

Suspended particles provide additional evidence of Cd precipitation within the North Atlantic ODZ (Figure 2.3). The concentrations of both particulate Cd and P, like surface primary productivity, are higher in the eastern basin compared with the central basin. In the central North Atlantic where oxygen concentrations are higher, suspended particulate Cd and P are both high in surface waters where phytoplankton grow, and decrease monotonically with depth. Whereas suspended particulate P in the eastern basin also follows this trend, suspended particulate Cd concentrations and the Cd:P ratio reach a maximum within the ODZ. Elevated particulate Cd concentration and Cd:P ratios in the ODZ, compared with overlying waters including the chlorophyll maximum, suggests a source of particulate Cd within the ODZ in addition to sinking biogenic material. Particulate $\varepsilon^{112/110}$Cd within the ODZ is consistent with CdS precipitation (Figure 2.3). Because Cd is nearly quantitatively removed by phytoplankton growing within the euphotic zone, we expect the biogenic particulate $\varepsilon^{112/110}$Cd flux out of the surface ocean to match the upward mixing flux of dissolved $\varepsilon^{112/110}$Cd into the euphotic zone. Thus, assuming that the suspended biogenic particulate $\varepsilon^{112/110}$Cd accurately reflects the biogenic flux, it should be 3.85, which is equivalent to dissolved $\varepsilon^{112/110}$Cd at the base of the

euphotic zone (89 m). Instead we observe particulate $\varepsilon^{112/110}$Cd from -0.05 to +1.75, significantly lighter than the expected biogenic signature. Isotopically lighter particulate $\varepsilon^{112/110}$Cd compared with seawater is consistent with CdS precipitation, assuming non-quantitative precipitation of seawater Cd with a preferential precipitation of lighter Cd isotopes into sulphides, as observed in low-temperature hydrothermal systems (Schmitt et al., 2009a). The highest $\varepsilon^{112/110}$Cd (1.75) is observed just below the chlorophyll a maximum, perhaps reflecting a greater contribution of biogenic particulate Cd at this depth. The lowest $\varepsilon^{112/110}$Cd values (-0.05 and -0.10 at 185 and 235 m respectively) are found within the ODZ at the same depths where we observe a maximum in particulate Cd:P. Together, the lighter $\varepsilon^{112/110}$Cd of particles compared with seawater, and the increasing particulate [Cd] with depth within the ODZ, support a local dissolved source of Cd to particles rather than gradual remineralization of sinking biogenic Cd.

Several hypotheses have been advanced to explain the decoupling of Cd and P concentrations in the global ocean, although none seems appropriate to describe the decoupling observed in ODZs. Differences in the remineralization with depth of Cd and P are inconsistent with the relatively similar remineralization rates of Cd and P observed in a majority of existing vertical profiles (de Baar et al., 1994). Biological uptake rates of Cd compared with PO_4^{3-} have been observed to vary with species composition, irradiance, trace metal concentration, and carbon dioxide availability (Xu and Morel, 2013). One consequence of this is that preformed dissolved Cd:PO_4^{3-} is lower in waters which ventilate in the Southern Ocean (Frew, 1995). Recent measurements of dissolved Cd:PO_4^{3-} and $\varepsilon^{112/110}$Cd suggest that Cd and PO_4^{3-} mix conservatively along isopycnals in the well-oxygenated ocean interior (Abouchami et al., 2014), meaning that some portion of the lowered Cd:PO_4^{3-} we observe in the northeastern subarctic Pacific may reflect mixing with low Cd:PO_4^{3-} subantarctic and Antarctic waters. However, Cd:PO_4^{3-} values at similar densities in the Southern Ocean are not low enough to account for the observed minimum Northeast Pacific Cd:PO_4^{3-} values. The low Cd:PO_4^{3-} North Atlantic ODZ waters do not outcrop in the Southern Ocean and therefore cannot be explained by mixing of low Cd:PO_4^{3-} Southern Ocean water. Particulate Cd and $\varepsilon^{112/110}$Cd in the North Atlantic ODZ also cannot be accounted for by mixing of water masses.

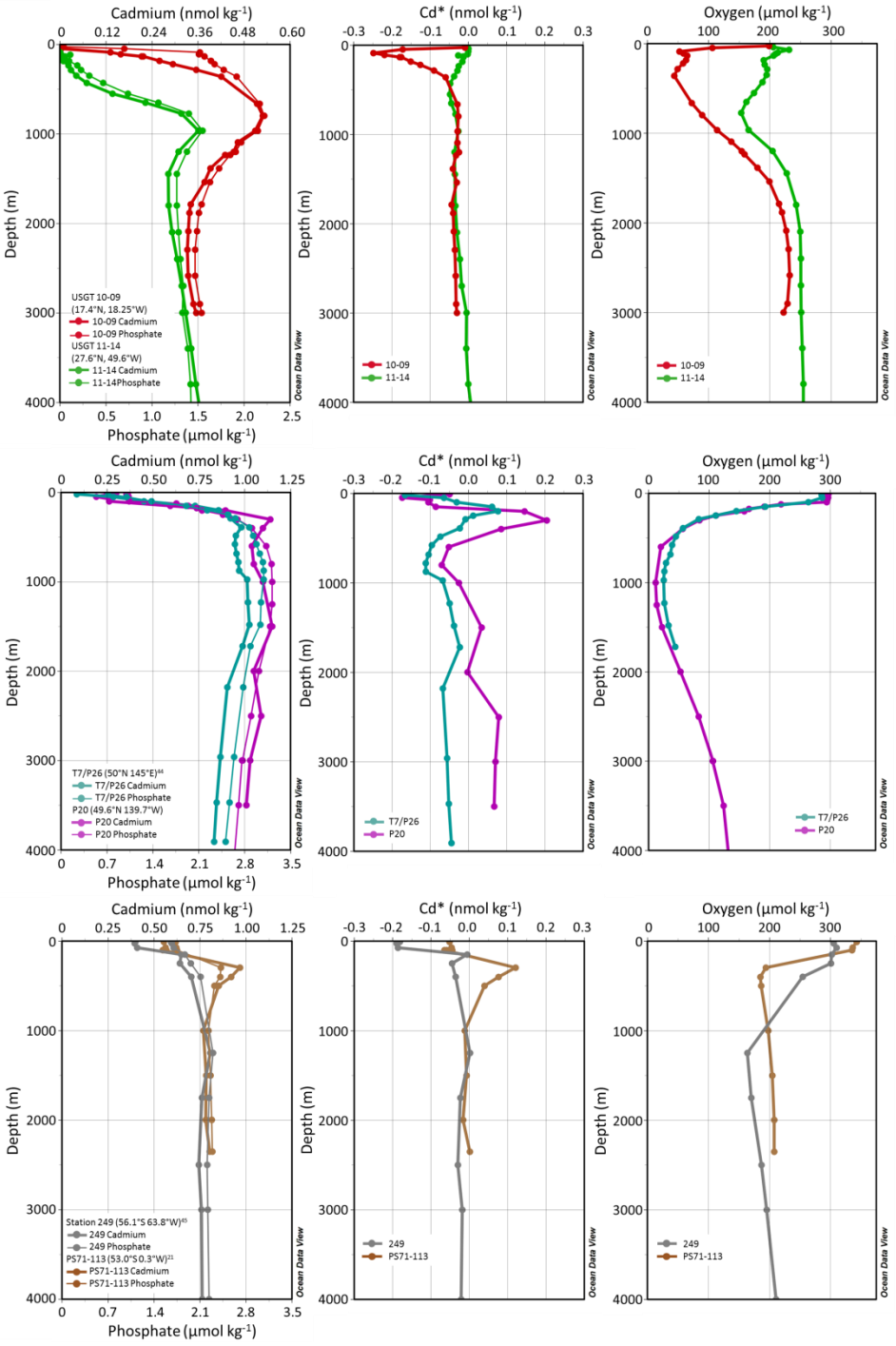

Figure 2.2 Profiles of dissolved oxygen, cadmium, and phosphate in the North Atlantic, Pacific, and Southern Oceans with calculated Cd*

(Top) Atlantic data; (Middle) Pacific data, and (Bottom) Southern Ocean–subantarctic data. Trace metal concentrations are shown in thick lines and macronutrients in thin lines, and colors correspond to station locations and studies in Figure 2.1.

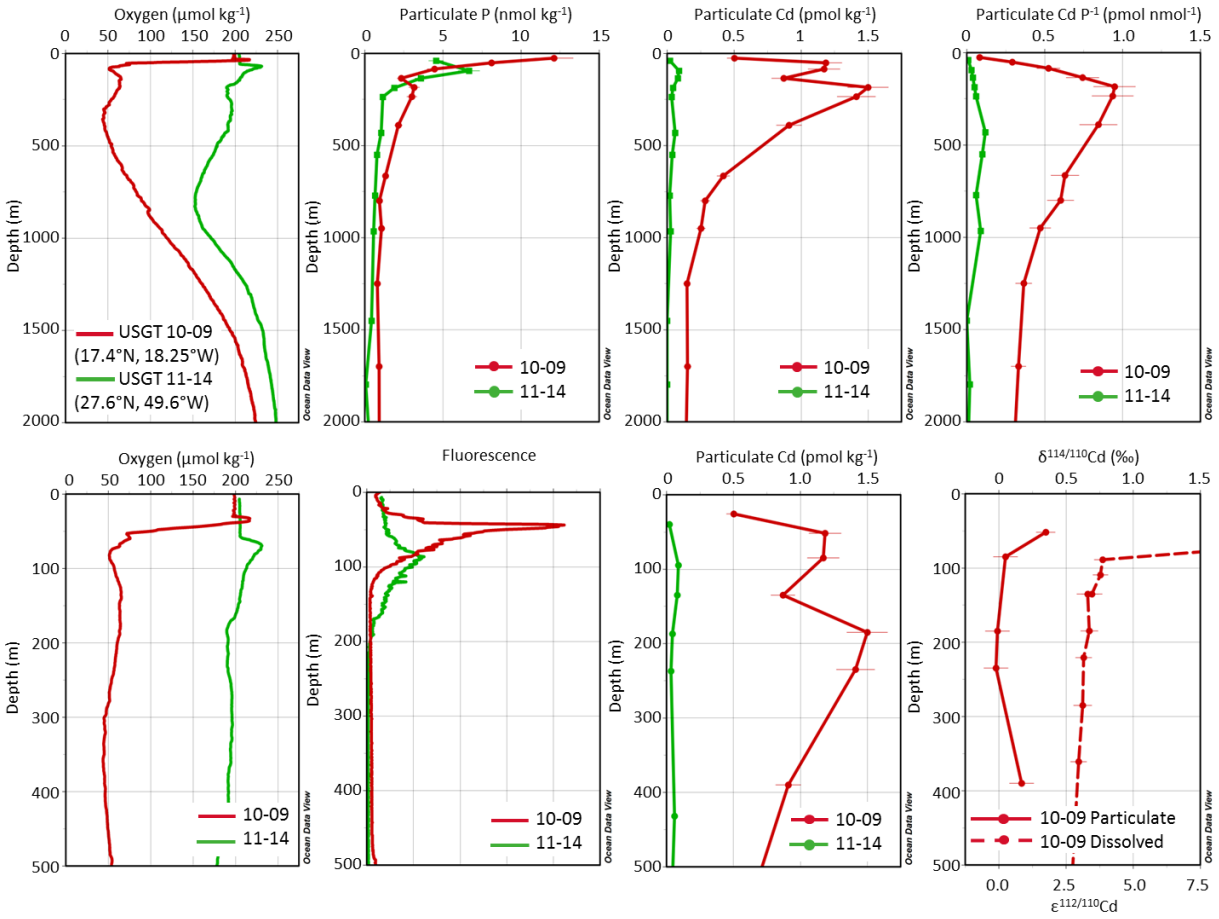

Figure 2.3 Particulate Cd, P and $\varepsilon^{112/110}$Cd from the US GEOTRACES North Atlantic Transect, shown with oxygen concentrations and fluorescence
Station USGT11-14 (27.6°N, 49.6°W) is shown in green and station USGT10-09 (17.4°N, 18.25°W) is shown in red. (Upper) Depth range of 0–2,000 m; (Lower) ODZ range from 0 to 500 m.

We have considered the possibility that low Cd:PO_4^{3-} anomalies observed in the ocean interior could reflect lateral advection of waters modified by contact with reducing shelf sediments, which tend to concentrate Cd (Rosenthal et al., 1995a, van Geen et al., 1995), and to release P (van Cappellen and Ingall, 1996). However, we believe that these signals represent a water column process, rather than a sedimentary process, based on comparison with dissolved Fe stable isotope data (δ^{56}Fe). Low δ^{56}Fe at station USGT10-9 is a sensitive tracer of reduced Fe input, demonstrating that sedimentary inputs are strongest at the base of the water column near the sediments, rather than at shallower depths where the water column minimum in O_2 coincides with low Cd*, high particulate Cd/P, and low particulate $\varepsilon^{112/110}$Cd (Conway and

John, 2013). Additionally, using maximum Cd accumulation rates into reducing sediments of 10 ng Cd cm^{-2} y^{-1} (van Geen et al., 1995) the time necessary to form observed volume-specific Cd anomalies along an isopycnal would be ~10^4 y, an order of magnitude greater than ocean circulation time (see Appendix A for an updated calculation and discussion). Ocean mixing would therefore be expected to obscure low Cd:PO_4^{3-} signals formed along ocean margins well before they could reach the ocean interior.

We propose that CdS precipitation occurs in response to sulphide generated within low-oxygen microenvironments associated with sinking organic matter (Wright et al., 2012), in analogy to the precipitation of barite (Bishop, 1988). Differences in the oxygen threshold below which CdS precipitates in the Atlantic and Pacific may therefore be related to both the quantity and the composition of sinking organic particles. Microbial sulphide production in oxic waters of the Pacific ODZ is supported by genomic evidence for the presence of both heterotrophic sulphate reducing bacteria and sulphur oxidizing autotrophs (Wright et al., 2012, Canfield et al., 2010) and isotopically labeled incubation experiments showing sulphate reduction rates of up to 0.5–1 nmol L^{-1} S h^{-1} in the core of the nearly anoxic eastern tropical South Pacific ODZ (Canfield et al., 2010). CdS may also precipitate in waters with more extreme oxygen depletion such as the eastern tropical South Pacific ODZ, where sulphide concentrations of 1–5 μmol L^{-1} have been found throughout an extensive region (Schunck et al., 2013). CdS is supersaturated at these sulphide concentrations, allowing Cd to be rapidly scavenged from the water column (Al-Farawati and van den Berg, 1999).

The enrichment of Cd in oxygen-depleted sediments has previously led to the suggestion that CdS precipitation from sediment porewaters is the primary sink for Cd from the oceans (Rosenthal et al., 1995a, van Geen et al., 1995). Based on the areal extent of low oxygen sediments in the modern ocean and calculated Cd flux into the sediments, Rosenthal et al. (1995a) calculated a removal rate of 0.6–2.3 × 10^7 mol y^{-1}, which is similar to calculated Cd input from the atmosphere and world rivers (0.6–2.5 × 10^7 mol y^{-1}). Because the Pacific ODZ is the largest worldwide, we use the observed Cd depletion from the northeast Pacific ODZ (~100 pmol L−1) and the volume of the global ocean with dissolved O_2 < 50 μmol L^{-1} (1.3–6.0 × 10^{19} L) (Bianchi et al., 2012), to estimate a global depletion of 0.1–0.5 ×10^{10} mol dissolved Cd from sulphide precipitation. Assuming that this depletion occurs on a timescale as short as

the residence time of water in an ODZ (~100 y) or as long as that of ocean mixing (~10^3 y) yields a Cd removal rate range from 0.1×10^7 mol Cd y^{-1} to 0.5×10^8 mol Cd y^{-1} (see Appendix A for an updated version of this calculation and discussion). This calculation suggests that CdS precipitation in ODZs is an important vector for Cd delivery to suboxic sediments, possibly the primary sink for Cd from the oceans. As Cd associated with sinking particles is known to be the primary route to burial in suboxic sediments (Klinkhammer and Palmer, 1991), the formation of particulate CdS species which are stable in oxic water (Luther and Rickard, 2005) allows for distributed Cd burial in sediments and may represent a significant contribution to the sedimentary Cd enrichments seen in oxygen-depleted sediments.

A globally significant water column sink for Cd via Cd sulphide precipitation suggests that the distributions of other biologically used metals disposed to forming highly insoluble sulphides, such as Cu and Zn, may be similarly affected. Although particle and isotope data are not available for Cu and Zn, we note that Cu and Zn are depleted relative to Si for the same depths at which Cd is depleted relative to phosphate within the northeast Pacific ODZ (Figure 2.4), suggesting they may also be precipitated as sulphides. Cu and Zn are known to influence biological production and community composition (Sunda and Huntsman, 1992; Morel et al., 1994; Tortell and Price, 1996; Saito and Goepfert, 2008; Mann et al., 2002; Peers and Price, 2006) through taxon-specific requirements and toxic sensitivity. Indeed, removal of these metals relative to other bioessential trace metals like iron (Fe) and cobalt (Co) in the ocean interior could influence biogeochemical cycling through metal–metal antagonisms and co-limitation when deep waters are brought to the surface in ocean upwelling zones. For example, within oxygen-deficient upwelling regions observations have been made of Zn limitation in eukaryotic phytoplankton (Franck et al., 2003), and of an increased biogeochemical significance of prokaryotes (Stukel et al., 2013), perhaps reflecting Zn deficiency in upwelling waters combined with the higher Zn requirements of eukaryotic plankton compared with prokaryotic plankton (Twining and Baines, 2013, Dupont et al., 2006).

2.4 Conclusions

The implications for decoupling of Cd concentrations from macronutrient concentrations in ODZs span a wide range of timescales. On geological timescales, it suggests

that in situ water column precipitation is at least a significant sink, if not the predominant sink of Cd from the oceans. Consequently, global variability in marine dissolved Cd concentrations and $\varepsilon^{112/110}$Cd will be crucially dependent on the extent of ODZs in the world's oceans over geological timescales. For studies investigating macronutrient distributions on glacial–interglacial timescales, our results suggest that the commonly used foraminiferal Cd proxy must be interpreted with caution in oxygen-depleted regions. In the future, the predicted expansion of oxygen depletion in the global oceans (Stramma et al., 2010) means that water column sulphide precipitation may be an increasingly important sink for Cd as well as Cu and Zn from the ocean, with significant consequences for marine biogeochemical cycles due to the dual roles of these metals as both toxins and essential micronutrients.

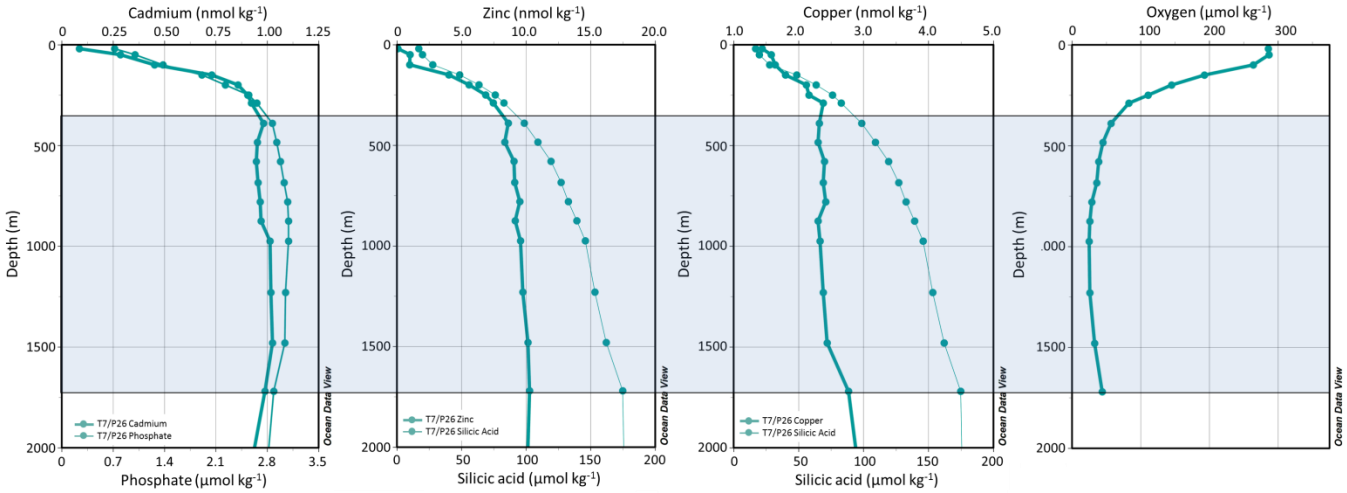

Figure 2.4 Concurrent decoupling of Cadmium, Zinc and Copper from corresponding macronutrients in the northeast subarctic Pacific

The trace metal-macronutrient pairs of Cd-PO_4^{3-} , Zn-Si and Cu-Si all show decoupling in the northeast subarctic Pacific ODZ (station P26, 50.0°N 145.0°W). While macronutrients continue to increase monotonically throughout the ODZ, the trace metals reach stable values or decrease slightly. The onset of decoupling, which begins near the depth where oxygen concentrations drop below ~50 µmol kg^{-1} (shaded region), shows strong agreement between the three trace metal-macronutrient pairs. Data from Martin et al., 1989.

Chapter 3

Decoupling of zinc and silicic acid in the subarctic northeast Pacific interior

Janssen, D.J., Cullen, J.T. (2015). Decoupling of zinc and silicic acid in the subarctic northeast Pacific interior. *Marine Chemistry*. 177:124-133. doi: 10.1016/j.marchem.2015.03.014.

3.1 Abstract

Zinc (Zn) is an essential micronutrient for marine phytoplankton that plays a role in regulating community composition and may limit primary productivity in localized regions. Depth profiles of dissolved Zn throughout the world ocean are tightly correlated with dissolved silicic acid (Si). New and previously published data from the subarctic northeast Pacific show a decoupling of dissolved Zn and Si. Waters above 400-500 m depth are characterized by elevated Zn compared to Si and the global average. The oxygen deficient zone of the subarctic northeast Pacific is characterized by a dissolved Zn:Si trend with slopes below the global average. The deficit of Zn relative to Si in the oxygen-depleted water column is consistent with a specific removal process for dissolved Zn in the subarctic northeast Pacific oxygen deficient zone. We propose that this data adds to a growing body of evidence implicating the formation of solid Zn sulphides in low oxygen, particle-associated microenvironments as an important loss term in the oceanic Zn budget. Time series data indicate dissolved oxygen concentrations are diminishing in the ocean interior, expanding and intensifying oxygen deficient zones, and model results predict this trend will continue in the future. An oxygen-sensitive removal process affecting dissolved Zn may impact global ocean productivity and carbon cycling due to the role of Zn in regulating community composition and even total primary productivity in select regions.

3.2. Introduction

Zinc (Zn) is a biologically important trace metal with a nutrient type distribution and a strong correlation to dissolved silicic acid (Si) concentration in seawater (Bruland et al., 1978; Bruland and Lohan 2006). As with other nutrient type trace metals, dissolved Zn is depleted and strongly complexed in surface waters by a dynamic pool of organic ligands (~98%) (Bruland 1989) that can exhibit production and consumption cycles on time scales less than one day (Lohan et al., 2005). The sources, sinks and lability of these ligands are poorly understood (Bruland and Lohan 2006). While laboratory-based experiments with phytoplankton isolates maintained in culture have shown that Zn may act as a limiting nutrient (Anderson et al., 1978; Brand et al., 1983; Tortell and Price, 1996; De La Rocha et al., 2000; Shaked et al., 2006), field evidence of Zn limitation in marine microalgae is scarce, with only a few clear examples of community composition regulation (Crawford et al., 2003) and total primary productivity limitation (Franck et al. 2003; Jakuba et al., 2012) in the literature.

Zinc correlates strongly with Si, generally showing a deeper remineralization signal than the other macronutrients nitrate (NO_3^-) and phosphate (PO_4^{3-}) as well as other biologically utilized trace metals like cadmium (Cd) (Bruland et al., 1978; GEOTRACES, 2014). The reasons for this Zn-Si correlation are not entirely clear and while some Zn may be found associated with diatom frustules (i.e. ‘hard parts’), the vast majority of Zn in biological particles is found associated with nitrogen (N) and phosphorus (P) in organic tissues (i.e. ‘soft parts’) in marine algae (Ellwood and Hunter, 2000; Twining et al., 2003; Twining and Baines, 2004). As Zn is associated with N and P intracellularly, it would follow that remineralization of organic matter would release Zn in concordance with macronutrients NO_3^- and PO_4^{3-} and trace metals such as Cd rather than the observed deeper remineralization signal of Zn matching ‘hard part’ associated elements like Si. John and Conway (2014) have recently shown that while Zn is remineralized from the particulate phase to the dissolved pool concurrently with Cd in cultured plankton, Zn is reversibly re-adsorbed onto particles, temporarily re-entering the particulate phase. While temporarily trapped back onto the particulate phase, this Zn can be released as the particles degrade further, therefore maintaining a nutrient-type profile for Zn rather than an adsorbed/scavenged profile. This may explain the incongruity between the intracellular co-location of Zn and other organic phase macro- and micro-nutrients and their disparate

respective oceanic depth profiles. Deeper apparent remineralization of Zn may also reflect an association with more refractory organic matter that degrades more slowly than average cellular organic matter (Lohan et al., 2002), or the coupling may be driven by some other currently unidentified mechanism.

Zinc is one of several 'class B' metals (following the distinction of Jacobs and Emerson, 1982) which form highly insoluble sulphides (approximate K_{sp} for ZnS (sphalerite) = $10^{-18.47}$, $ZnS + H_2S \leftrightarrow Zn^{2+} + 2HS^-$ (Daskalakis and Helz, 1993)). These metals (including Cd, copper (Cu), and silver (Ag) in addition to Zn) are known to be depleted below oxic-anoxic boundaries of fjords, inlets, and seas with restricted circulation and ventilation due to the formation of solid metal sulphides (Jacobs and Emerson, 1985). While sulphidic regions are not generally observed in the open ocean - though measurable hydrogen sulphide has been found in the oxygen-depleted waters of the eastern tropical South Pacific (ETSP) (Schunck et al., 2013) - large volumes of oxygen depleted water, called oxygen deficient zones (ODZs), exist in the ocean interior. Although there is generally still measurable oxygen (O_2) and no measurable free sulphide in these ODZs, a complex and active community of sulphate reducing and sulphide oxidizing bacteria exists in water column ODZ environments presenting a sulphide source (Canfield et al., 2010; Stewart, 2011; Wright et al., 2012; Podlaska et al., 2012; Johnston et al., 2014). Regions with less than 50 µmol kg^{-1} dissolved O_2 account for approximately 1.0-4.6% of the ocean's volume (Bianchi et al., 2012). These ODZs are found at nearly basin-wide scales in the eastern tropical Pacific, the subarctic northeast Pacific, and the Indian Ocean and in localized upwelling regions off of the coast of Mauritania as well as Namibia and Angola in the eastern Atlantic. Time series data show that oxygen depleted regions are expanding spatially while the degree of O_2 depletion itself is intensifying (Whitney et al., 2007; Stramma et al., 2010; Keeling et al., 2010) and model projections predict that this will to continue in the future (Shaffer et al., 2009; Keeling et al., 2010).

We report data from Line P, a time series transect beginning at 48.5° N 125.5° W and extending westward off of the continental shelf of Vancouver Island, BC to Ocean Station PAPA/P26 (50° N 145° W) in the subarctic northeast Pacific (Figure 3.1). Surface waters in this region are influenced by the North Pacific Current, having both subtropical and subarctic components (Whitney et al., 2007). Isopycnal surfaces along Line P shoal slightly heading

westward (offshore) along the transect and a permanent halocline is observed at around 100-150 m depth (Crawford et al., 2007). Density surfaces found at depths ~200 m along the Line P transect may outcrop periodically in the subarctic northwest Pacific in the East Kamchatka and Oyashio Currents but depths below do not ventilate in the open North Pacific (Ono et al., 2001; Shcherbina et al., 2003; Mecking et al., 2006; Whitney et al., 2007). The density range corresponding with North Pacific Intermediate Water (NPIW, σ_θ = 26.5-27.0, Talley et al., 1993) is found at ~150 – 500 m depth; however the Line P transect lies near the eastern extent of NPIW (Talley et al., 1993) and a prominent salinity minimum is not observed along the transect (Line P hydrographic data has been made available by the Institute of Ocean Sciences (Sidney, BC) at https://www.waterproperties.ca/linep/index.php). Below this depth range, the subarctic North Pacific has a pronounced ODZ which is strongest along the eastern margin and weakens heading westward (Whitney et al., 2007). At a depth of approximately 400 m [O_2] falls below 50 µmol kg^{-1}, reaching minimum values of < 10-20 µmol kg^{-1} near 900-1000 m depth before increasing, reaching 50 µmol kg^{-1} again near 1900 m depth. At more coastal stations, the transect receives the northern reach of the California Undercurrent (Thomson and Krassovski, 2010). Surface and near-surface waters (≤ 200 m depth) of the Line P transect have previously been sampled for Zn, providing information about seasonal and onshore-offshore trends in Zn in the upper water column (Lohan et al., 2002). Additionally, the VERTEX T transect, intersecting the Line P transect at station T7/Ocean Station Papa/P26, has been sampled for Zn to a depth of ~1500 m for stations T5, T6, T8 and T9, and to a depth of 3910 m for station T7/P26 (Martin et al., 1989).

3.3. Methods

3.3.1 Sample collection and sampling site

The Line P transect (Figure 3.1) was sampled between August 14th and 30th 2012 (cruise 2012-13) on board the *CCGS J.P. Tully*. Sample and reagent bottles were cleaned according to GEOTRACES protocols. Samples for Zn determination were collected using a 12 bottle powder coated trace metal clean rosette system modified according to Measures et al. (2008) equipped with 12 L Teflon-coated GO-FLO (General Oceanics, FL USA) bottles. The GO-FLO bottles were gravity filtered through 0.2 µm Acropak filters (Pall Corporation). Samples were

acidified to pH = 1.7 with 12 mol L^{-1} HCl (SeaStar Chemical) after collection and stored for at least 6 hours before analysis. Unfiltered samples for Si, NO_3^- and PO_4^{3-} were analyzed according to Barwell-Clarke and Whitney (1996). Dissolved O_2 data was obtained with a Seabird SBE43 dissolved oxygen sensor calibrated against Winkler titrations. Nutrient and O_2 data are courtesy of the Line P Program (Chief Scientist Marie Robert, Institute of Ocean Sciences, Canada)

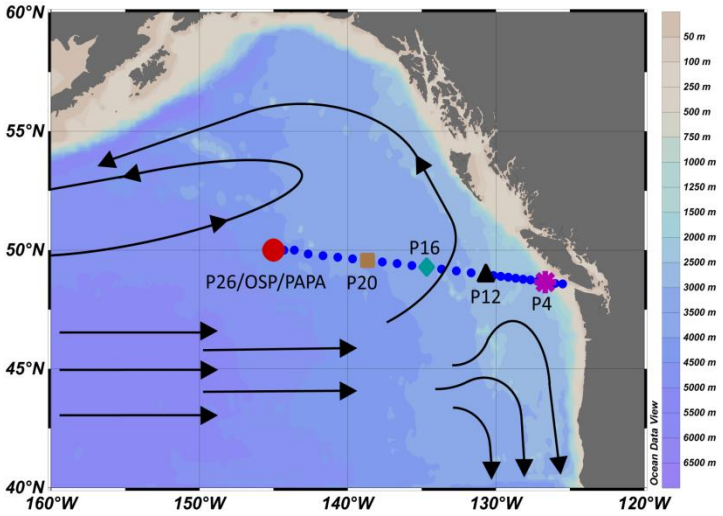

Figure 3.1 The Line P transect
The Line P transect, extending westward off of Vancouver Island, British Columbia Canada is shown with all stations in blue and with major stations for which trace metal data was collected labeled and in larger coloured symbols (P4 as a purple star, P12 as a black triangle, P16 as a light blue diamond, P20 as a brown square and P26/OSP as a red dot). Surface currents are adapted from Whitney et al. (2007) and Freeland (2007). The small scale structure of the currents near to the margins and the degree to which subtropical origin North Pacific Gyre water reaches the Line P transect is variable year to year (e.g. Cummins and Freeland, 2007; Freeland, 2006).

3.3.2 Zinc Analysis

Zinc samples were analyzed at sea with a flow injection method, shown in Figure 3.2, based on Nowicki et al. (1994) utilizing the fluorescent binding ligand p-tosyl-8-aminoquinoline (p-taq) (Chemica Inc, Los Angeles Ca, USA). The methodology of Nowicki et al. (1994) was followed with the following modifications: pre-acidification and on-line buffering of samples, changing the chelating resin to a commercially available resin which eliminates Cd interference, and minor changes in the p-taq buffer solution and elution acid strength.

Reagents and samples were pumped using an eight channel peristaltic pump (Rainin Dynamax) at a pump speed of 9.50 RPM and flow was directed using 6 and 12 port injection valves (Valco Instruments Co. Inc., Cheminert). FlowZF software (Global FIA) was used to control the injection sequence and record fluorescence. Fluorescence was measured using a Shimadzu RF-535 fluorometer connected to a data acquisition module (Omega). PVC 2 stop pump tubing (Fisher) was used as follows: sample line, rinse line and p-taq buffer lines coded yellow-blue (1.52 mm id), elution line coded orange-orange (0.89 mm id), on-line buffer line coded black-black (0.76 mm id).

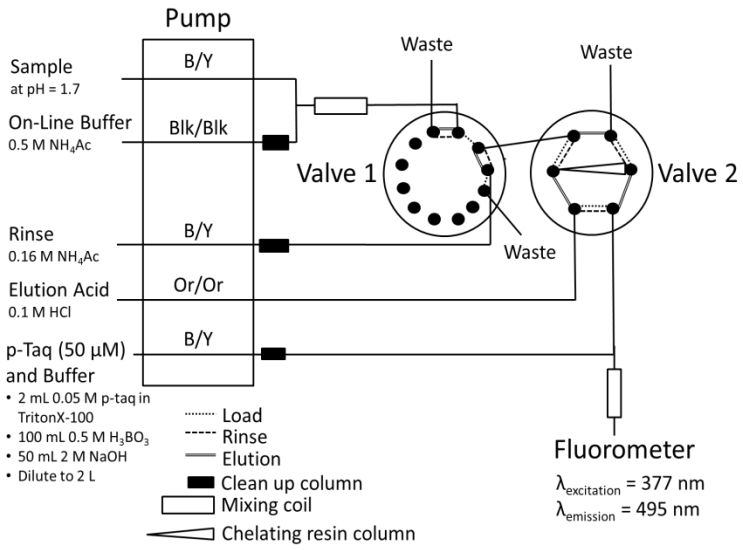

Figure 3.2 Flow injection analysis schematic
Solid lines show tubing not influenced by valve position. Dotted lines show flow direction under loading valve orientation, dashed lines show rinse orientation, and doubled lines show elution orientation.

Acidified samples (pH = 1.7) were buffered online to pH = 4.3 using an 0.50 mol L^{-1} ammonium acetate (NH_4Ac) buffer and an 80 cm mixing coil (type KOT2 from Selavka et al., 1987) and loaded onto a 2 cm mini column (Global FIA) of NTA Superflow resin (Qiagen). Samples below 150 m depth were loaded for two minutes and samples above 150 m were loaded for four minutes. Previous applications of this method were susceptible to a Cd interference via a fluorescent p-taq complex with excitation and emission wavelengths that overlap with those of the Zn complex (Nowicki et al., 1994; Wyatt et al., 2014). Choosing a loading pH of 4.3 allows Zn to be retained on the NTA column while allowing much of the Cd

to pass through the column (Lohan et al., 2005), minimizing the interference of Cd. One and two cm clean-up columns of Nobias chelate PA1 resin (Hitachi High-Technologies) were used on on-line buffer, p-taq and rinse solution lines. Clean up columns were flipped every couple of days to minimize compaction of the resin in the columns and back pressure issues.

Samples were rinsed for one minute with 0.16 mol L^{-1} NH_4Ac and eluted for two minutes using 0.1 mol L^{-1} HCl (SeaStar Chemicals, Sidney BC). Ammonium acetate solutions were prepared from a saturated solution of NH_4Ac made by bubbling pure ammonia gas (Praxair) into glacial acetic acid (SeaStar Chemicals) until saturation. Excess acetic acid was poured off and the NH_4Ac precipitate was dissolved in MQ water. Samples were eluted for two minutes and mixed with a p-taq buffer solution using an 80 cm mixing coil (type KOT2 from Selavka et al., 1987). The p-taq buffer solution was prepared by mixing 100 mL of 0.5 mol L^{-1} boric acid (ACP chemicals) with 50 mL of 2 mol L^{-1} NaOH (ACP Chemicals) and diluting to 2 L. Finally, 2 mL of 0.5 mol L^{-1} p-taq stock solution in TritonX-100 was added. The solution was mixed for at least 24 hours on a shaker table before using. This mixture contains half as much boric acid as called for by Nowicki et al. (1994) and was suggested to improve sensitivity (M. Lohan, Southampton, personal communication). No problems due to instability of the p-taq – borate buffer solution were encountered, though prepared p-taq buffer solutions were not stored long term (greater than 1-2 months). Due to batch to batch variability in the sensitivity of the fluorescent reagent buffer solution, each set of analyses were restricted to one batch of the p-taq buffer solution.

Zinc working standards in pH = 4 MQ water prepared from a 1000 ppm Zn ICP-MS standard (SPEX CertiPrep) were used to prepare Zn running standards in 0.22 µm filtered (Opticap, Millipore) low Zn surface seawater collected using a Teflon bellows pump during previous Line P cruises. Reagent blanks were determined by loading acidified (pH = 1.7) 18.2 MΩ MQ water treated as a sample. The SAFe D2 standard (consensus value of 7.43 ± 0.25 nmol kg^{-1} Zn) was measured each day of analysis to ensure accuracy. The average value based on 11 analyses over the course of the cruise was 7.38 ± 0.09 nmol kg^{-1} Zn. Seawater samples were analyzed in triplicate and typically yielded relative standard deviations (1σ) at or below 2%. The detection limit, as determined by three times the standard deviation of the blank, was typically 200 pmol kg^{-1} for 2 minute load times and 65 pmol kg^{-1} for four minute load times.

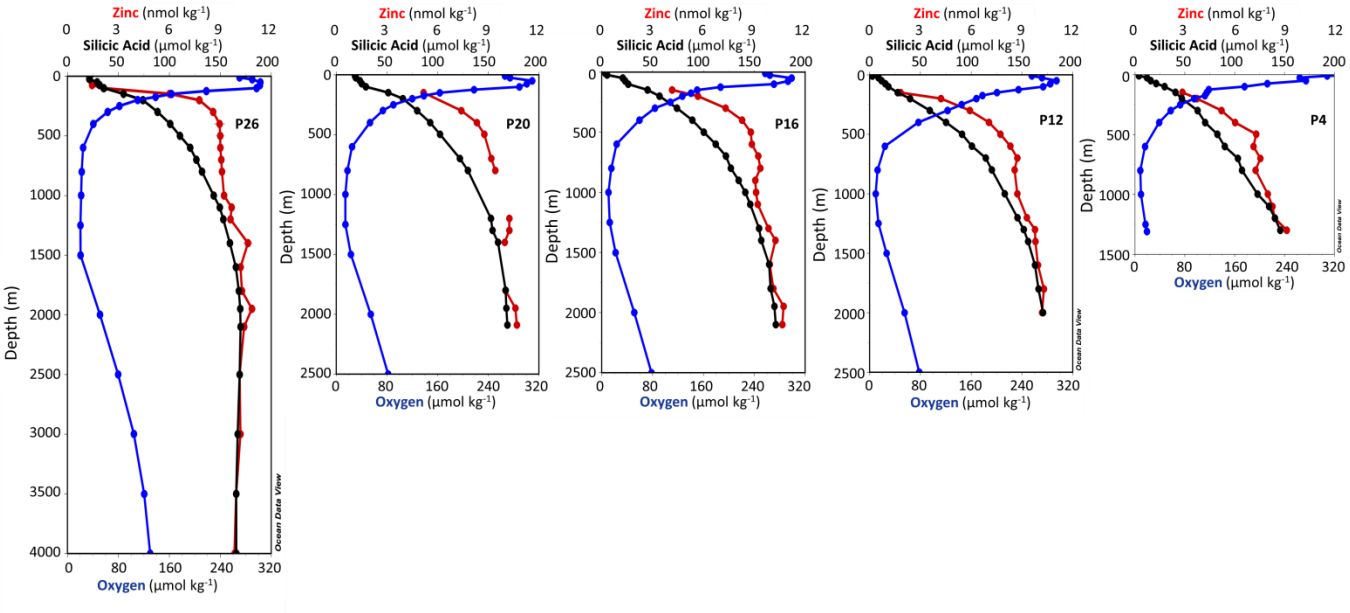

Figure 3.3 August 2012 Line P data
Dissolved Zn (red), Si (black) and O_2 (blue) depth profiles from samples collected in August 2012 along Line P with P4, the most coastal station, at right and P26/Ocean Station PAPA at left. The Zn profile at station P20 is broken due to missing samples. Sections are not connected spanning the range of missing samples to avoid suggesting that the profile is linear between section endpoints as depth profiles from other stations with data covering these depth ranges suggest that the profile at P20 may not be linear between sections. Dissolved O_2 data is courtesy of the Line P program, which is run by the Institute of Ocean Sciences (Sidney, BC).

3.4 Results

3.4.1 Dissolved Zn data

The dissolved Zn data from August 2012 (Figure 3.3) are oceanographically consistent (Boyle and Edmund, 1975) and similar to previously published data from the subarctic northeast Pacific (surface to 1500-3900 m, Martin et al., 1989; see Appendix B, Figure B.1) and previous work by the Line P Time Series (upper 200 m, Lohan et al., 2002). Dissolved Zn displays a nutrient-type depth profile with low values (1.9-6.3 nmol kg^{-1} Zn at 150 m depth) in the upper water column and concentrations increasing with depth (average of 36 samples below 1000 m = 9.90 ± 0.63 nmol kg^{-1} Zn). In the upper 150-500 m (σ_θ < 27.1), Zn concentrations increase moving westward along the transect (Figure C.1 panel A in depth space, panel B in density space), the reverse of the trend seen in the upper 200 m by Lohan et al. (2002). While

Zn concentrations below 500 m also increase from the more coastal stations P4 and P12, concentrations do not show this distinct longitudinal trend below 500 m for the more offshore stations P16-P26. Isopycnal surfaces shoal ~100-200 m in upper and intermediate waters (upper ~500-1000 m) with distance from shore while deepwater isopycnal depths tend to be more stable along the transect. Dissolved Zn trends along isopycnal surfaces are similar to the [Zn] depth trends, with [Zn] increasing moving westward in upper isopycnal surfaces and [Zn] remaining more stable longitudinally on deeper isopycnal surfaces.

The result of these longitudinal Zn trends progressing westward along the transect is that profiles shift away from a single more smoothly increasing curve throughout the water column seen in coastal stations toward profiles with two distinct sections: a surface to approximately 400-500 m section of enhanced shallow Zn remineralization within the nutricline and a section below 500 m of relatively stable deepwater values. This depth trend contrasts sharply with more continuous dissolved Zn profiles from the eastern Pacific at lower latitude (e.g. Bruland et al., 1978 at 37° N), from the South Atlantic (e.g. Wyatt et al 2014), and from the North Atlantic (e.g. Conway and John, 2014) which closely mimic silicic acid in terms remineralization horizons.

3.4.2 Zinc and Si in the ODZ

A compilation of dissolved Zn versus Si measurements from the subarctic northeast Pacific (this study; Lohan et al., 2002; and Martin et al., 1989) result in a generally similar slope, but not intercept, to previously reported values in the Pacific (Bruland et al., 1978) and to a global average trend (Figure 3.4; Table 3.1; Figure C.2) (global data from GEOTRACES, 2014; only paired Zn and Si measurements in the GEOTRACES data set are used). While the subarctic northeast Pacific data result in a similar slope to the global compilation when considering the full depth range of the subarctic northeast Pacific data, the relationship between Zn and Si in the northeast Pacific does not follow the global trend line. The slope of the relationship is characterized by a kink in the subarctic northeast Pacific Zn:Si relationship with two distinct trends, primarily related to variability in dissolved Zn depth profiles mentioned above. The piecewise nature of the northeast Pacific data, which results in a deepwater Zn:Si near the single global correlation line, is evident against global average data (Figure 3.4 panel

A), and the transition from a greater Zn:Si slope to a lower slope occurs where O_2 concentrations drop below 50 µmol kg^{-1} (Figure 3.4 panel C).

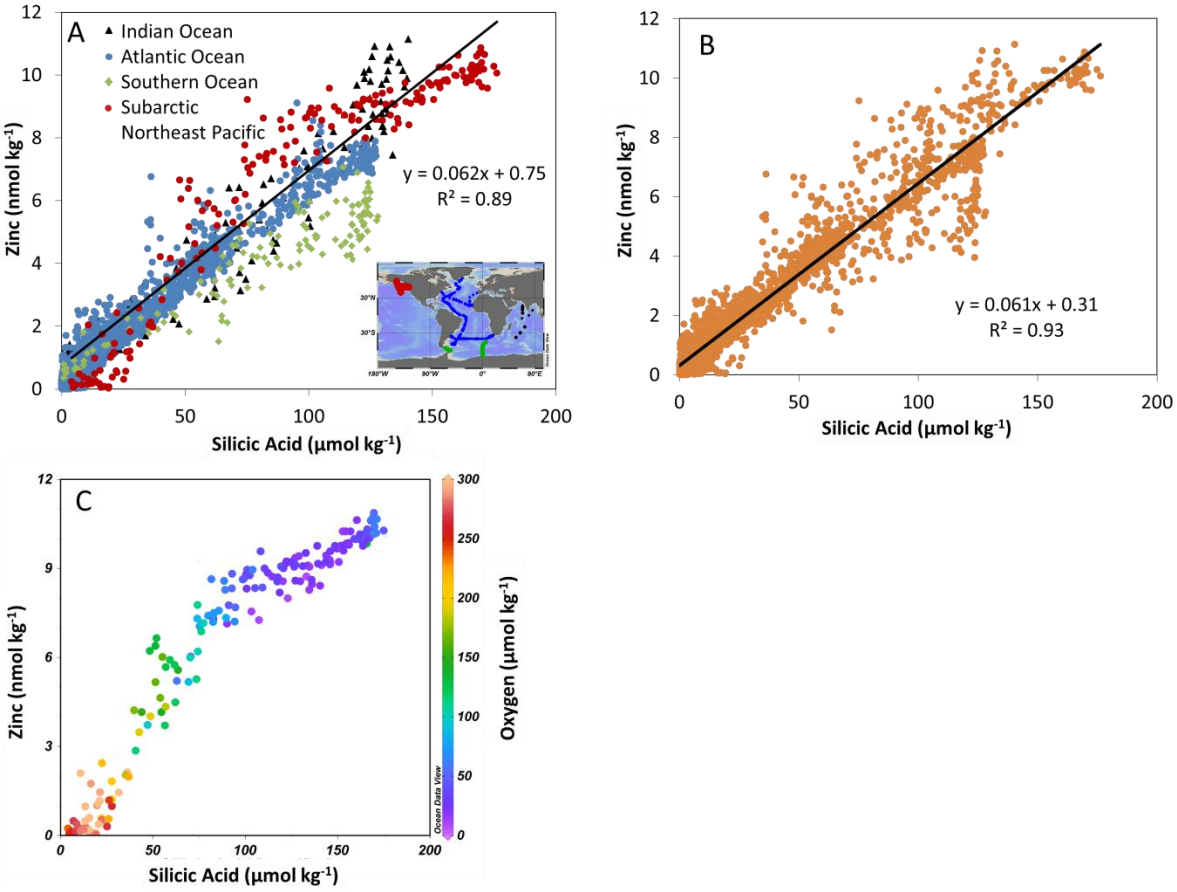

Figure 3.4 Dissolved Zn:Si trends for the subarctic northeast Pacific and the global ocean
Panel A shows the subarctic northeast Pacific composite Zn:Si relationship (red dots; data from this study; Lohan et al., 2002 (station P4 is omitted); and Martin et al., 1989) on top of the global data set from the GEOTRACES intermediate data product (station locations in panel A inset) which includes data from the Indian Ocean (black triangles), Atlantic Ocean (blue dots), and Southern Ocean (green diamonds). The trend line shown in panel A is for only the subarctic northeast Pacific data. The subarctic northeast Pacific data is added to the GEOTRACES data set to provide a global average relationship (panel B). Panel C shows the subarctic northeast Pacific data with [O_2].

From the surface to approximately 400-500 m in the subarctic northeast Pacific, where O_2 concentrations remain above 50 µmol kg^{-1}, greater Zn increase occurs relative to Si when compared to global trend (Table 3.1). Northeast Pacific data with [O_2] > 50 µmol kg^{-1} and within the upper 400-500 m of the water column have a Zn:Si slope nearly double that of global

data over this same depth range (0.102 Zn:Si nmol µmol Si^{-1} for the northeast Pacific compared to 0.052 Zn:Si nmol µmol^{-1} for the GEOTRACES data set).

The second Zn:Si trend, with a much lower slope, begins where dissolved O_2 concentrations fall below 50 µmol kg^{-1} (approximately 400-500 m depth, Figure 3.4 panel C). Dissolved Zn:Si ratios for the subarctic northeast Pacific ODZ are approximately 0.030 Zn:Si nmol µmol^{-1} while the global average full water column slope is 0.059 Zn:Si nmol µmol^{-1}. This low Zn:Si slope highlights the lack of Zn regeneration relative to Si and relative to the GEOTRACES global data set within these oxygen-depleted waters.

	O_2 > 50 µmol kg^{-1} depth < 510 m (Above ODZ)				**O_2 < 50 µmol kg^{-1} (ODZ)**				**Full Water Column**			
	Slope Zn:Si nmol µmol^{-1}	Intercept nmol kg^{-1} Zn	r^2	N	Slope Zn:Si nmol µmol^{-1}	Intercept nmol kg^{-1} Zn	r^2	N	Slope Zn:Si nmol µmol^{-1}	Intercept nmol kg^{-1} Zn	r^2	N
This Study	0.109	-1.01	0.93	19	0.033	4.66	0.77	49	0.048	2.68	0.86	78
Subarctic Northeast Pacific	0.102	-0.88	0.92	93	0.030	5.09	0.73	80	0.062	0.89	0.89	184
GEOTRACES Global Data	0.052	0.18	0.85	1173	0.045	0.65	0.84	36	0.059	0.34	0.92	2760

Table 3.1 Dissolved Zn:Si in the subarctic northeast Pacific and the global ocean
Dissolved Zn:Si trends for the subarctic northeast Pacific and the global ocean. Slopes, intercepts, and coefficients of determination (r^2) for Zn:Si trendlines as well as the number of samples included (N) are given for three data sets at three depth and dissolved oxygen groupings. Subarctic northeast Pacific data is composed of Martin et al. (1989), Lohan et al. (2002) (excepting station P4), and this study. GEOTRACES global data is from the intermediate data product (2014) and does not include the subarctic northeast Pacific data. The first column grouping shows data where both the dissolved oxygen concentration is above 50 µmol kg^{-1} and the depth is less than 510 m (510 m was chosen to include samples targeting a depth of 500 m but where the actual collection depth was slightly deeper). In the subarctic northeast Pacific, this column grouping contains all samples above the ODZ. The second column grouping includes ODZ samples from all depths where dissolved oxygen concentrations are below 50 µmol kg^{-1}. The third column grouping, the full water column, is a composite of samples from all depths and oxygen concentrations.

3.5 Discussion

3.5.1 Zn:Si dynamics in the upper 400 m

A global compilation of dissolved Zn:Si data in the subarctic northeast Pacific along with data from the GEOTRACES intermediate data product (2014) in the North and South

Atlantic (GA02: H. de Baar, unpublished data; GA03: Conway and John, 2014; GA10: Wyatt et al., 2014), the Atlantic sector of the Southern Ocean (GIPY5: Croot et al., 2011), and the Indian Ocean (GI04: Vu and Sohrin, 2013) is shown in Figure 3.4, Table 3.1, and Figure C.2. The two trends observed in subarctic northeast Pacific Zn:Si combine to form a composite relationship broadly similar to data from the Atlantic, Southern, and Indian Oceans; however, in comparison to these data, the detailed structure of subarctic northeast Pacific data show fundamentally different distributions with an apparent decoupling of Zn and Si.

Previously published data from the upper water column of the northeast Pacific show nutrient depleted surface waters (0-25 μmol kg^{-1} Si) are deficient in Zn relative to Si compared to the global mean. This may be due to enhanced divalent metal uptake in Fe limited high-nutrient, low-chlorophyll (HNLC) regions (Sunda and Huntsman, 2000; Cullen et al., 2003; Lane et al., 2008). Although work from HNLC regions has also shown that Fe limited cells may become more heavily silicified, either with more silica per cell (*e.g.* Hutchins and Bruland, 1998) or more silica per organic matter due to cell morphology changes (*e.g.* Marchetti and Harrison, 2007), HNLC enhanced Zn uptake appears to have a stronger impact on the dissolved Zn-Si dynamics, resulting in low nutrient surface water with Zn depleted relative to Si (Figure 3.4 panel A, Figure C.2 panel B, data from Lohan et al., 2002 and Martin et al., 1989).

From this point until approximately 400 m depth (25 to roughly 90 μmol kg^{-1} Si) Zn concentrations show a greater gradient in the upper water column than Si as shown by a greater slope for the northeast Pacific trend in Zn:Si space (Figure 3.4 panel A, Table 3.1). The same can be seen in open ocean depth profiles for the two nutrients. By a depth of 400 m at P26, Zn concentrations reach a value within 15% of the stable deepwater concentration while [Si] is only at 60% of its deepwater value. The resulting profile of shallow remineralization in the upper 400 m resembles other 'soft part' species such as NO_3^- (Figure 3.3), which reaches a value within 10% of its maximum value by a depth of 400 m.

The reasons for this apparent shallow Zn remineralization in the subarctic northeast Pacific nutricline as shown by the slope of the Zn:Si trend are unclear. The Zn:Si trend over the upper 400 m may be influenced by remineralization of Zn-enriched organic matter sinking from the HNLC surface waters. If the deeper remineralization seen in other basins is the result of reversible scavenging (John and Conway, 2014), this suggests less active scavenging of Zn in

the upper 400 m of the subarctic northeast Pacific. The apparent shallow remineralization signal may be advected and may not be derived from in-situ remineralization. Recent data from the subarctic northwest Pacific also found elevated Zn:Si at intermediate depths and higher Zn in surface waters than in subtropical North Pacific waters (Kim et al., 2015). This was attributed to aeolian or riverine sources transported to depth by increased vertical mixing or settling biogenic material; however surface water is not enriched in Zn relative to Si when compared to the subtropical North Pacific trend (i.e. the Zn:Si intercepts are comparable, Kim et al., 2015), suggesting that an additional perturbation such as enhanced surface Zn uptake may drive the high Zn:Si trends observed in the nutricline rather than, or in addition to, the penetration of an aeolian Zn source into the ocean interior.

3.5.2 Zn:Si dynamics below 400 m and Zn removal in the ODZ

At depth greater than approximately 400 m ([Si] > 90 μmol kg^{-1}) dissolved O_2 concentrations fall below 50 μmol kg^{-1}. In the subarctic northeast Pacific ODZ, Zn and Si remain decoupled relative to the global relationship. This decoupling, however, is characterized by a shift to lower slopes in the Zn:Si relationship relative to global average. Silicic acid concentrations continue increasing while Zn concentrations decrease slightly, remain stable, or increase to a lesser degree with increasing depth. This ODZ decoupling driven by a deficit Zn relative to Si can be seen along the entire transect. Coastal stations show depleted Zn concentrations and a 'bite' can be seen in dissolved [Zn] over this depth range (Figure 3.3). Zinc concentrations do not increase over the range of 400-1000 m at open ocean station P26, while Si does and respiration of organic matter continues, albeit to a lesser degree than in overlying waters, as demonstrated by O_2 and macronutrient (NO_3^- and PO_4^{3-}) profiles.

The continued respiration of organic matter and increasing dissolved macronutrient concentrations over the ODZ depth range in the absence of measureable [Zn] increase is consistent with a Zn-specific removal term in this low O_2 environment. Sulphide precipitation has been proposed as a significant removal mechanism for Cd in low O_2 water, and the same mechanism has been suggested for Zn and Cu (Janssen et al., 2014 / Chapter 2). Recent data from low-O_2 Mauritania Upwelling in the eastern Atlantic supports the proposal of dissolved Cd and Zn removal by sulphide precipitation (Conway and John, 2014; Conway and John,

2015; Figure C.4). We propose that this water column removal mechanism is also acting for Zn in the subarctic northeast Pacific. Once formed these solid sulphide species would be stable and resistant to oxidation even in the presence of a more oxic water column (Luther et al., 1999), allowing solid sulphides to sink out of the water column without being quantitatively remineralized.

3.5.3 A proposed mechanism for water column metal sulphide formation

Oxygen deficient zone sulphide precipitation of dissolved Zn may occur in anoxic microenvironments associated with sinking particles, and the degree to which the interior of the particle may become anoxic is likely controlled by the ambient seawater [O_2] and particle structure and composition. (Janssen et al., 2014 / Chapter 2; John et al., 2014). Particle-associated water column sulphide formation, if occurring, would be more intense closer to the coast due to the higher particulate load (Charette et al. 1999) and lower [O_2] found there. If particulate sulphides form in the water column, this may occur via a combination of processes in the ODZ (Figure 3.5). As has been well documented, heterotrophic sulphate (SO_4^{2-}) reduction (Step 1) and chemoautotrophic sulphide oxidation (Step 2) occur on and/or around this heterogeneous particulate environment (e.g. Wright et al., 2012). We propose that a small amount of reduced sulphur (denoted as HS^-) leaks out of this sulphur cycle loop (Step 3) and is available to react with dissolved metals such as Zn. Zinc may be supplied by diffusion toward the particle from the ambient seawater ($Zn_{(aq)}$, Step 4) to form solid sulphides (Step 5) or may originate from the particle ($Zn_{(part)}$, this designation is meant only to describe the origin of the Zn and not its phase when reacting to form solid sulphides). This particle-origin Zn may form solid sulphides (Step 6) as Zn is released from the respiration of particulate organic matter, effectively re-trapping Zn back onto the particle in an inert phase. Such an effect would lead to lower apparent remineralization rates of dissolved Zn and other metals relative to macronutrients in ODZ waters and may not necessarily lead to a subsurface particulate metal maximum

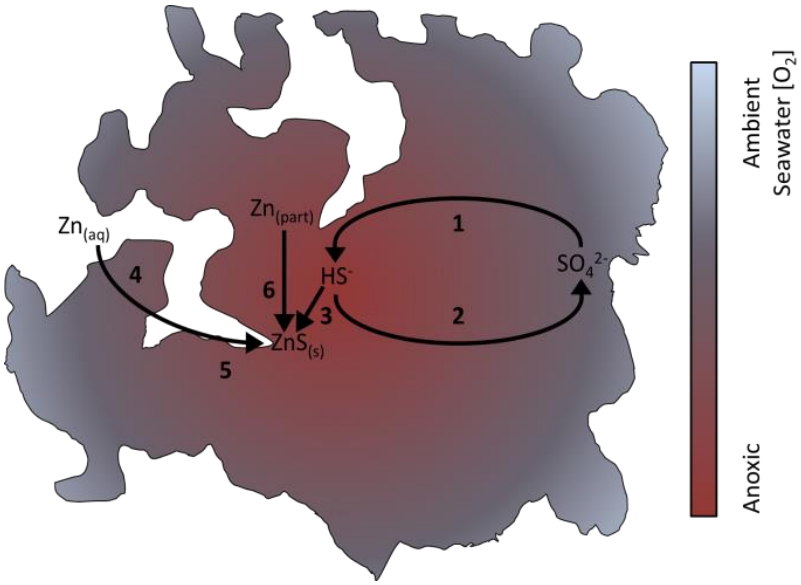

Figure 3.5 Proposed mechanism of water-column zinc sulphide formation
A 2D section of a sinking marine particle is shown with dissolved O_2 gradients from the particle exterior (ambient seawater O_2, gray) to anoxic interior and inner microenvironments (red).

These proposed mechanisms could simultaneously occur in ODZ particle environments and both mechanisms would yield a similar result – that of dissolved Zn and other 'class B' metals depleted in ODZ environments relative to dissolved macronutrients. In addition, both would yield Zn and other 'class B' metals enriched in ODZ particles relative to particulate macronutrients. A necessary test of this mechanism for Zn removal is the identification of ZnS in sinking particles, which may also help to distinguish the provenance of Zn associated with reduced sulphur. Particulate Cd data from the eastern Atlantic showing a secondary particulate maximum in ODZ waters (Janssen et al., 2014 / Chapter 2; Conway and John, 2015) suggests that the former mechanism (metal originating from the water column) may be dominant in that region, which predicts a similar pattern for Zn.

3.*5.4 Alternate explanations of Zn:Si decoupling in the ODZ*

A decoupling of Zn from Si in the northeast Pacific ODZ assumes that the two nutrients are otherwise coupled in the world ocean. While no clear mechanistic reasoning for such a coupling is known, a large body of dissolved data from the Atlantic, Southern, Indian and Pacific Oceans shows a strong correlation between the two. Whether the relationship exists

because of coincident remineralization depths from biogenic particles (Lohan et al., 2002; John and Conway, 2014), export from a distal source such as the Southern Ocean (analogous to the control of the Southern Ocean on Si:N ratios (Sarmiento et al., 2004)) or from another causal mechanism is uncertain at present. In any case, the distinctly different behavior in the subarctic northeast Pacific ODZ relative to the global data set provides information which can aid understanding of the global Zn:Si relationship and the mechanisms acting to control their respective distributions on global ocean scale. A set of suspended particulate samples spanning the ODZ and targeted to observe the presence or absence of water column sulphides would be necessary in order to differentiate between water column sulphide formation and the possible mechanisms mentioned below.

3.5.4.1 Zn removal in local sediments

Sediments in contact with oxygen deficient, but not anoxic or sulphidic, water can show enrichments of sulphide-insoluble metals such as Cd, Cu, and Zn, and these enrichments may be sensitive to changes in O_2 availability at the sediment surface over geological time (Calvert and Pedersen, 1993; Rosenthal et al., 1995a; Rosenthal et al., 1995b; van Geen et al., 1995; Morford and Emerson, 1999; Nameroff et al., 2002; Nameroff et al., 2004). It is possible that the observed deficit of Zn within the subarctic northeast Pacific ODZ is not formed in the water column and rather is an advected signal formed through contact with oxygen deficient and anoxic sediments in the western and eastern North Pacific. Dissolved Zn concentrations increase along isopycnals from the more coastally influenced station P4 to the more oceanic P16, lending support to a shelf removal along the western margin of North America. However, this increase of dissolved Zn is seen above the ODZ as well as within it, requiring either two different mechanisms to explain the longitudinal trend or significant Zn removal in sediments not in contact with the ODZ as well as those within it. Additionally, organic carbon flux is higher closer to the continental margin (Charette et al., 1999) and O_2 is lower, proving a greater potential for particulate microenvironments to remove metal in the water column.

In our data set the sample closest to shelf sediments (Station P4 1300 m, bottom depth = 1324 m) shows the highest [Zn] at this station. In addition, [Zn] at 1300 m at P4 shows a greater relative difference from concentrations at the nearest 2 depths (1200 m and 1100 m) than either

PO_4^{3-}, NO_3^- and Si. Unfortunately this is our only data point in close proximity to shelf sediments. While this is only a single data point, it is inconsistent with the idea that ODZ shelf sediments in this area are a significant sink for Zn and that these sediments would lead to a depletion of Zn relative to macronutrients. More dissolved metal data along the margin, including at the core of the ODZ, would help to determine whether margin removal of Zn is a significant process affecting water column inventories.

We can examine the water column and sediment behavior of the elements Cd and Ag, which have similar coordination chemistry and sulphide affinity, to help determine how likely a strong margin sediment sink might exist for Zn. In the case of Cd, the possibility of shelf sediments removing sufficient metal to explain the observed basin-scale trend was investigated and was determined to be unlikely due to the small spatial extent of sediments in contact with the ODZ relative to the volume of ODZ water in the basin (Janssen et al., 2014 / Chapter 2). The availability of sedimentary Zn data is poor relative to other sulphide-insoluble metals in the subarctic northeast Pacific, which precludes a similar analysis here. McKay et al. (2007) found that Cd and other redox sensitive elements were not enriched in western Canadian margin surface sediments in contact with the ODZ near our sampling transect. Down-core enrichments were observed in these samples, suggesting little sulphide formation occurs at the sediment-water interface. McKay and Pedersen (2008) showed that in marine sediments lying in and below the core of the subarctic northeast Pacific ODZ, Ag was more enriched in sediments below the ODZ core. In contrast with these observations, if Ag sulphides were formed in the sediments or at the sediment-seawater interface a maximum would be expected at or above the ODZ core, where O_2 availability is lower and the particulate organic load is higher. The authors suggested that Ag sulphides were formed in the water column and were delivered to the sediments, resulting in the observed sedimentary Ag maximum below the O_2 minimum (McKay and Pedersen, 2008). Due to the similar sulphide chemistry of Zn to Ag and Cd, we expect Zn to behave analogously.

3.5.4.2 An advected signal from the northwest Pacific

Recent work in the western subarctic Pacific by Kim et al (2015) may offer some insight into the possibility of an advected water column signal. These data show a similar Zn:Si linear

trend (0.065 nmol μmol^{-1}) to the composite trend (0.062 nmol μmol^{-1}) from both oxic ($[O_2]$ > 50 $\mu mol\ kg^{-1}$) and ODZ ($[O_2]$ < 50 $\mu mol\ kg^{-1}$) waters of the subarctic northeast Pacific (Martin et al., 1989; Lohan et al., 2002; this study). The authors observe that intermediate depth samples are enriched with Zn relative to the global average Zn:Si relationship and suggest that this is driven by elevated inputs (dust and fluvial discharge) combined with enhanced vertical mixing and remineralization of biogenic material. The elevated Zn:Si water in the western subarctic Pacific (Kim et al., 2015) and eastern subarctic Pacific (this study, Martin et al., 1989; Lohan et al., 2002) may be influenced by the mechanisms described by Kim et al. (2015); however these mechanisms are not able to address the trend observed in ODZ water, which is depleted in Zn relative to Si compared to the global Zn:Si relationship.

Below these high Zn:Si intermediate waters reported by Kim et al. (2015), a similar decoupling of Zn from Si, driven by steadily increasing [Si] without a corresponding [Zn] increase, is observed in the subarctic northwest Pacific ODZ (e.g. see station CR-27)). The persistence of a Zn depletion in the ODZ relative to Si across the entire subarctic North Pacific basin highlights is consistent with a process resulting in decoupling of Zn from Si acting in low $[O_2]$ regions of the world ocean. The apparent spatial extent of this anomaly in the Pacific, and the presence of the same type of anomaly for Zn and Cd in the Atlantic basin (Conway and John, 2014; Conway and John, 2015; Figure C.4) suggests that this removal process may act globally wherever water column $[O_2]$ is sufficiently low.

The possibility of a sediment removal signal advected from the western Pacific is subject to the same limitations discussed above in section 3.5.4.1 – namely that the large extent of missing metal is difficult to explain by scavenging into low $[O_2]$ surface sediments when the coverage of the sediments is very small relative to the basin volume and that data so far for sediments in such conditions in the North Pacific either do not show an enrichment or show an enrichment inconsistent with sufficient removal occurring at the sediment-water interface. Further data covering ODZ margin sediments in the western and eastern subarctic North Pacific would help to constrain the role of shelf sediment removal in explaining the observed depletions.

The low Zn:Si slope and high Zn intercept (Table 3.1) and the strong imprint of aerobic respiration in the subarctic northeast Pacific ODZ are inconsistent with the ODZ observations

being the result of a preformed anomalous Zn:Si relationship and point to a modification resulting in decoupling of Zn and Si. Cd depletions in the subarctic northeast Pacific (Janssen et al., 2014 / Chapter 2) and Zn and Cd depletions in an Atlantic ODZ (Conway and John 2014, Conway and John 2015; Figure C.4) are also inconsistent with a preformed explanation and lend further support to post-outcrop modifications acting to perturb the Zn:Si relationship in ODZs.

3.5.4.3 HNLC perturbation of the Si cycle

Increased diatom silicification - either by increased Si per diatom (e.g. Hutchins and Bruland 1998) or by changes in morphology driving increased Si per organic matter (e.g. Marchetti and Harrison 2007) - has been documented in chronically Fe-limited regions. Furthermore, coastal environments with elevated Si input may result in more heavily silicified cells and increased cellular sinking rates, although grazing rates may also decrease, altering the export of organic matter from the surface (Durkin et al., 2013). This elevated silicification could lower cellular Zn:Si and may alter Zn:Si export by the influences of particle sinking and grazing rates. Either of these processes may perturb the Zn or Si cycle, resulting in decoupling of Zn and Si and increased export of Si to intermediate and deep waters rather than a deficit of Zn.

As briefly mentioned in section 3.5.1, Fe limitation has also been shown to increase Zn uptake in marine diatoms. Phytoplankton from chronically Fe-limited regions show enhanced uptake of other divalent metals including Zn (Sunda and Huntsman, 2000; Cullen et al., 2003; Lane et al., 2008). Whether Fe limitation has a greater relative influence on uptake of Zn or Si in the surface waters of the subarctic northeast Pacific, and therefore if the net effect is an increased export of Si to depth, Zn to depth, or no change in Zn:Si, is unclear. The lack of a comprehensive global data set for suspended and sinking particles in HNLC and non-HNLC regions limits the ability to conclusively determine the influence of chronic Fe stress on exported Zn:Si ratios; however dissolved metal ratios in this region compared to the global average may offer some insight.

Dissolved metal data from the subarctic northeast Pacific show substantial drawdown of both Zn and Si, however dissolved Zn:Si data for [Si] < 40 μmol kg^{-1} sit predominantly below

the global average (Figure 3.4). Samples from the subarctic northeast Pacific show lower Zn:Si than the entire GEOTRACES compilation for the range of 10-25 μmol kg^{-1} Si (generally the upper 100 m in the subarctic northeast Pacific). These global dissolved ratios suggest that if surface phytoplankton incorporation of Zn and Si is altered by Fe limitation, the result is either no Zn:Si change or greater uptake of Zn relative to Si, leaving the water Si-rich relative to the global Zn:Si average, and not increased uptake of Si relative to Zn. If cells are Zn enriched relative to Si, any trends with depth driven by these sinking cells should then reflect this, with greater Zn export to intermediate and deep waters compared to Si. Therefore, with the available data, any perturbation of nutrient uptake in the HNLC region seems unable to explain the observed ODZ Zn deficit.

3.5.4.4 The Cascadia Plume

We considered that sedimentary Si inputs might explain Zn:Si decoupling, as a plume of water enriched in Si exists at depth in the subarctic northeast Pacific. This plume originates at the shelf in the Cascadia Basin at a depth of approximately 2500 – 3000 m and extends westward, but is constrained to depths greater than 2000 m (Johnson et al., 2006; Esther et al., 2010). Thus, this plume does not influence the observed anomalous Zn:Si relationship in and above the subarctic northeast Pacific ODZ.

3.5.5 Implications for ODZ Zn removal

A sink term for dissolved Zn in oxygen-depleted waters, whether in the water column or advected from ocean margins, will alter trace metal micronutrient ratios in the ocean interior. Many O_2-deficient regions of the global ocean are found underlying upwelling environments (Diaz and Rosenberg 2008; Keeling et al., 2010) like the eastern North Pacific, the ETSP, and the Mauritania and Benguela upwelling environments. If Zn is removed from the dissolved phase due to [O_2] depletion in subsurface waters that are subsequently upwelled, there exists the potential for Zn limitation in surface waters. The altered trace metal ratios of affected water masses will be additionally perturbed if other similar trace metal micronutrients and toxins are affected by the same process, as has been proposed for Cd and suggested for Cu (Janssen et al., 2014 / Chapter 2). While metals forming insoluble sulphides such as Cu, Zn, and Cd may be

depleted in these subsurface waters, other trace metal micronutrients such as Fe, Mn and Co which form more soluble reduced species tend to be enriched in these waters either in open ocean ODZs or as the oxygen depleted waters upwell, passing over shelf sediments (Martin and Knauer, 1984; Martin et al., 1985; Blain et al., 2008; Lohan and Bruland, 2008; Homoky et al., 2012; Ahlgren et al., 2014). When these waters are upwelled to the surface, the altered trace metal micronutrient and toxin ratios may have an effect on surface phytoplankton community structure and productivity (Ahlgren et al., 2014).

Phytoplankton show taxa-dependent nutrient demands and toxicity resistance for trace metals, with eukaryotic phytoplankton such as diatoms generally showing higher biological demand for Zn and greater resistance to Cu and Cd toxicity while prokaryotic plankton such as cyanobacteria, which show much lower toxicity resistance to Cd and Cu, have low Zn requirements (Brand et al., 1986; Saito et al., 2003; Dupont et al., 2006, Dupont et al., 2010). Upwelling of oxygen-depleted water with altered trace metal ratios to the surface ocean may lead to a shift in phytoplankton community composition away from eukaryotic phytoplankton taxa with a higher Zn demand and a greater Cu and Cd tolerance toward plankton with lower demands such as cyanobacteria, with implications for oceanic carbon transport and storage as well as food web structure.

The Costa Rica upwelling dome, which sits above the ETSP ODZ and is dominated by blooms of cyanobacteria (Li et al., 1983; Saito et al., 2005), may be an environment where the removal of dissolved Zn in oxygen-depleted water is already influencing the surface phytoplankton community. Franck et al. (2003) found that while individual additions of Fe promoted slight growth, combined additions of both Zn and Fe promoted higher diatom and flagellate cell counts by orders of magnitude, showing that growth of these eukaryotic phytoplankton are likely co-limited by both Zn and Fe in the Costa Rica dome. While Zn was not measured at the Costa Rica dome station, other stations in the ETSP showed surface dissolved Zn concentrations of 0.06 - 0.10 nmol L^{-1}, which were lower than concentrations of dissolved Fe at those stations. Furthermore, incubation experiments in the northeast Pacific at Pt. Arena and Pt. Conception along the California coast showed enhanced growth with additions of both Zn and Fe when compared to Fe additions alone, and for the Pt. Arena incubation, greater phytoplankton stimulation from Zn additions than from Fe additions (Franck

et al., 2003). These northeast Pacific sites also lie in upwelling environments on top of oxygen-depleted waters (Garcia et al., 2010). Phytoplankton-trace metal synergisms in these oxygen-depleted upwelling environments support the hypothesis that removal of Zn as well as Cu and Cd coupled with potential enrichment of Fe and Co (Ahlgren et al., 2014) in oxygen-depleted water may induce or exacerbate growth limitation by Zn while relieving or alleviating the much more frequently observed Fe limitation.

3.6 Conclusion

Regionality in the Zn:Si relationship, specifically the depth dependent variability in the slope of the correlation in the subarctic northeast Pacific, point to a removal process in low O_2 waters that acts to control the relative distributions of these essential nutrients in the ocean. Decoupling of Zn from Si is observed to occur in the form of departures from the global average slope across two depth ranges in the subarctic northeast Pacific. The upper 400-500 m is characterized by shallower remineralization of Zn than of Si. The slope of the Zn:Si relationship in this region is 0.102 Zn:Si nmol μmol^{-1}, nearly double the global averages of 0.052 Zn:Si nmol μmol^{-1} and 0.059 Zn:Si nmol μmol^{-1} for the upper 500 m and the whole water column respectively (GEOTRACES intermediate data product, 2014, omitting subarctic northeast Pacific data from the global average). Reversible scavenging has recently been proposed as a mechanism responsible for the deeper remineralization of Zn and its correlation with Si (John and Conway, 2014). Remineralization of Zn closer to the surface, resulting in Zn depth profiles similar to other 'soft part' elements, might indicate decreased Zn scavenging in the upper 400 m of the subarctic northeast Pacific if this mechanism is the driving factor for the deeper remineralization typically observed for Zn.

Low Zn:Si slopes compared to the global average are observed where $[O_2]$ is less than 50 $\mu mol\ kg^{-1}$ in the subarctic northeast Pacific (0.030 Zn:Si nmol μmol^{-1}). This is nearly half of the full water column global average (0.059 Zn:Si nmol μmol^{-1}) and is also lower than the 0.045 Zn:Si nmol μmol^{-1} slope observed in Mauritanian upwelling and Indian Ocean ODZs (GEOTRACES intermediate data product, 2014). Depth profiles for dissolved Zn along Line P show depletions in ODZ waters in the more coastal stations and show stable concentrations with depth at the open ocean station P26. The observed low Zn:Si slopes in the northeast

Pacific ODZ relative to the global data, and the features observed in dissolved Zn depth profiles within the subarctic northeast Pacific ODZ, are consistent with a Zn removal mechanism acting in the ODZ. This supports the recently suggested Zn removal mechanism of solid sulphide formation within particle-associated microenvironments in the ODZ (Janssen et al., 2014 / Chapter 2) and is supported by recent data showing similar Zn and Cd depletions in the Mauritanian ODZ (Conway and John, 2014; Conway and John, 2015; Figure 3.4). Collection and analysis of a high-quality set of particulate samples in oceanic ODZs for Zn and other class B trace metals should be prioritized to disambiguate possible mechanisms for the observed depletions.

An oxygen-sensitive Zn removal mechanism in ODZ water, whether formed in situ or advected from oxygen deficient margin sediments, would result in perturbed trace metal micronutrient ratios in ODZs. Due to the role of Zn as a micronutrient with taxa-dependent requirements (Saito et al., 2003; Dupont et al., 2006; Dupont et al., 2010; Crawford et al., 2003), imprints left from oxygen-depleted water could influence surface phytoplankton community composition where ODZ water upwells. Incubation experiments in ODZ upwelling environments have already shown some signs of Zn limitation (Franck et al., 2003). Time series data show O_2 loss within ODZs and model results predict further expansion and intensification of ODZs (Whitney et al., 2007; Stramma et al., 2010; Keeling et al., 2010; Shaffer et al., 2009), which may lead to further perturbed trace metal ratios in ODZ waters and may induce or exacerbate Zn limitation in ODZ upwelling environments, altering surface phytoplankton community composition and subsequently ocean carbon transport and food web dynamics.

Chapter 4

Dissolved cadmium concentration and isotopes in the subarctic northeast Pacific

This chapter is in revision at Earth and Planetary Science Letters as the following manuscript: Janssen, D.J., Abouchami, W., Galer, S.J.G., Cullen, J.T. Dissolved cadmium concentration and isotopes in the subarctic northeast Pacific.

4.1 Abstract

We present dissolved cadmium (Cd) concentrations, [Cd], and stable isotope compositions, $\varepsilon^{112/110}$Cd, in high-resolution depth profiles from five stations along the Line P transect in the subarctic northeast Pacific Ocean. In addition to the profiles collected in 2012, subsurface isopycnal samples and surface samples were collected in 2013 and 2014 respectively, providing both temporal and spatial coverage. Surface waters are characterized by Cd depletion relative to phosphate (PO_4^{3-}) compared to deepwater Cd:PO_4^{3-}, and high inferred remineralization ratios in the nutricline (0.45 nmol μmol^{-1}) are observed, consistent with Cd enrichment relative to phosphorus (P) in surface-derived biogenic particles. The correlation between Cd and PO_4^{3-} weakens at depths where oxygen is highly depleted as shown by local minima in dissolved [Cd] and the tracer Cd*. The decoupling, which is driven by a deficit of Cd relative to PO_4^{3-}, appears consistent with the recent hypothesis of dissolved Cd removal in oxygen-depleted regions by insoluble metal sulphide formation.

Dissolved $\varepsilon^{112/110}$Cd indicates a biologically driven fractionation in surface waters with more positive (heavy) values in the upper water column and lower (light) values in deeper waters. The highest $\varepsilon^{112/110}$Cd observed in our sample set (5.19 ± 0.23) is comparable to observations from the Southern Ocean but is significantly lighter than maximum reported surface values from the subtropical North Pacific of $\varepsilon^{112/110}Cd \geq 15$. Samples in the upper 100 m from the 2012 sampling campaign fit a closed-system Rayleigh fractionation model;

however, surface waters sampled in 2014 had much lower [Cd] with relatively constant $\varepsilon^{112/110}$Cd that cannot be explained by a closed-system Rayleigh model. These results, which occurred with a warm water surface anomaly found along Line P in 2014, demonstrate that there is inter-annual variability in the biogeochemical cycling of Cd and Cd isotopes in the subarctic North Pacific. A high degree of $\varepsilon^{112/110}$Cd variability is observed in literature data for surface waters at very low [Cd], with significant differences in maximum $\varepsilon^{112/110}$Cd. The observed $\varepsilon^{112/110}$Cd range may be due to analytical artefacts or could reflect true physical or biological variability. An intercalibration using low [Cd] surface water should be prioritized to help determine the cause of the observed $\varepsilon^{112/110}$Cd variability. In contrast to other ocean basins where vertical variability in $\varepsilon^{112/110}$Cd is observed at depth, deep and intermediate waters in the North Pacific have a near-uniform $\varepsilon^{112/11}$0Cd value (mean of 1.14 ± 0.37, n = 43, 2SD) representative of nearly all samples at or below 1000 m depth. The nearly constant Cd isotopic composition of subsurface North Pacific water is consistent with the inflow of Southern Component Water at depth in the Pacific basin, along with deep remineralization, and supports the potential of $\varepsilon^{112/110}$Cd as a tracer of global deepwater circulation.

4.2 Introduction

Cadmium (Cd) behaves as a trace metal micronutrient in the global ocean with dissolved depth profiles reflecting biological uptake in surface waters and remineralization of particulate matter at depth. The distribution of Cd (unless otherwise stated, Cd will refer to dissolved Cd rather than particulate) in the global ocean shows a strong correlation with phosphate (PO_4^{3-}) (Boyle et al., 1976; Bruland et al., 1978). There exist distinct Cd:PO_4^{3-} relationships in the major ocean basins and water masses (de Baar et al., 1994; Quay et al., 2015). These regional differences must ultimately be the result of processes that alter the relative concentrations of Cd ([Cd]) versus PO_4^{3-} ([PO_4^{3-}]) compared to the deepwater average Cd:PO_4^{3-}, such as (1) the formation of biogenic particles in the surface ocean (e.g. Sunda and Huntsman, 2000; Cullen et al., 2003; Cullen and Sherrell, 2005; Lane et al., 2009), (2) depth-dependent remineralization or scavenging with sinking particles in the ocean interior (Janssen et al., 2014 / Chapter 2; Conway and John 2015a; Waeles et al., 2016) and (3) scavenging and remobilization at ocean margins (e.g. Van Geen et al., 1995; Rosenthal et al., 1995a).

Cadmium:PO_4^{3-} anomalies generated regionally from the above mechanisms can be subducted or advected, resulting in transport of "pre-formed" Cd:PO_4^{3-} by water mass circulation and mixing in the global ocean (e.g. Abouchami et al. 2014; Baars et al., 2014; Quay et al. 2015, Xie et al., 2015).

Both species composition and the physical-chemical environment can contribute to variability in particulate Cd:phosphorus (P) that is set primarily by phytoplankton Cd:P composition. Laboratory cultures of 15 eukaryotic phytoplankton representing major marine phyla maintained under identical growth conditions were found to have cellular Cd:P that varied by two orders of magnitude (0.007 – 0.73 mmol mol^{-1}) (Ho et al., 2003). Within phyla, Cd uptake and cellular Cd:P are known to be modulated by the availability of other trace metals such as iron (Fe) and zinc (Zn) through antagonistic interactions at phytoplankton cell surface transport proteins which can be non-specific with respect to cation binding and permeability (e.g. Sunda and Huntsman 2000; Cullen et al., 2003; Cullen and Sherrell, 2005; Lane et al., 2009; Baars et al., 2014). Uptake of Cd can be linked to carbonic anhydrase, an enzyme with a Zn cofactor involved in algal inorganic carbon acquisition, through the substitution of Cd for Zn (e.g. Price and Morel, 1990) or the incorporation of Cd into a Cd-specific form of the enzyme (e.g. Lane and Morel, 2000). Thus the species composition and physical-chemical conditions in ocean surface waters during phytoplankton growth can result in the formation and export of particles with a wide range of Cd:P. The relative importance of biological versus physical processes for shaping the global Cd:PO_4^{3-} correlation, and consequently the sensitivity of the relationship to changing environmental conditions in space and time, is at present unresolved.

The distribution of Cd stable isotopes ($\varepsilon^{112/110}$Cd, the deviation of the $^{112}Cd/^{110}Cd$ ratio in parts per ten thousand relative to that of the reference material NIST SRM-3108) in the oceans has shed light on important processes controlling Cd cycling and, by extension, the variability of Cd:PO_4^{3-} in the global ocean. To a first order, dissolved [Cd] and $\varepsilon^{112/110}$Cd are inversely correlated with each other in the ocean. Surface waters with lower [Cd] - due to biological uptake of dissolved Cd - have elevated $\varepsilon^{112/110}$Cd due to isotopic fractionation during uptake (e.g. Lacan et al., 2006; Ripperger et al., 2007; Abouchami et al., 2011). As particulate Cd is remineralized back into the dissolved pool, [Cd] is expected to increase while dissolved

$\varepsilon^{112/110}$Cd decreases. Note that not all studies have seen a biological $\varepsilon^{112/110}$Cd fractionation signature in surface waters, potentially due to extremely low [Cd] resulting in diffusion-limited Cd supply to phytoplankton (Gault-Ringold et al., 2012) or local aeolian Cd inputs to the surface layer (Yang et al., 2012).

In addition to the insight supplied by $\varepsilon^{112/110}$Cd into biological uptake and remineralization processes, Cd stable isotopes show potential utility as a water mass tracer and a paleoceanographic proxy. For example, in the subsurface Atlantic and the Atlantic sector of the Southern Ocean $\varepsilon^{112/110}$Cd is elevated in North Atlantic Deep Water (NADW) ($\varepsilon^{112/110}$Cd = 2.42 ± 0.45, 2SD, Boyle et al. 2012; see also Conway and John, 2015a; Xue et al., 2012), where [Cd] is lower, compared to Cd-rich Southern Component Water ($\varepsilon^{112/110}$Cd = 1.21 ± 0.36, 2SD, Xue et al., 2013; Abouchami et al., 2014; see also Conway and John, 2015a; Xie et al., in revision).

To date, depth profiles of dissolved $\varepsilon^{112/110}$Cd are available for transects in the North Atlantic (Conway and John, 2015a) and the Southern Ocean (Xue et al., 2013; Abouchami et al., 2014); however, data from the Pacific are limited to only a few isolated stations in the open North Pacific and marginal seas (Lacan et al., 2006; Ripperger et al., 2007; Yang et al., 2012; Yang et al., 2014) Conway and John, 2015b) and a seasonally sampled surface transect in the South Pacific (Gault-Ringold et al., 2012). Here we present the first $\varepsilon^{112/110}$Cd transect data in the North Pacific, with five high-resolution dissolved $\varepsilon^{112/110}$Cd and [Cd] depth profiles from the Line P time series transect, extending from the margin to the open ocean and spanning oxygen (O_2)-depleted waters.

Spatially extensive oceanic O_2-depleted regions, sometimes called oxygen deficient zones or oxygen minimum zones, are found in the North Pacific, the eastern tropical Pacific, and the Arabian and Bengal Seas, as well as regionally in the eastern Atlantic in upwelling environments near Mauritania and in the Benguela current, near Angola and Namibia. Data from oceanographic time series show that the degree of O_2 depletion in these regions is intensifying (e.g. Whitney et al., 2007; Gilly et al., 2013 and references therein) and models predict continued O_2 loss (Gilly et al., 2013 and references therein). These low-O_2 regions generally contain measureable dissolved [O_2] and, although free sulphide is generally not detected, active communities of sulphur metabolizing bacteria - both sulphate-reducing and

sulphide-oxidizing - are found in O_2-depleted water columns (e.g. Canfield et al., 2010; Wright et al., 2012 and references therein). These bacteria, which either produce reduced sulphur species or require them for metabolism, provide evidence for the presence of free sulphide and an active sulphur cycle in non-anoxic low-O_2 waters, with possibly elevated concentrations in particle-associated microenvironments.

Cadmium concentrations are depleted in waters with oxic-anoxic boundaries such as fjords, inlets, and seas with restricted circulation. This is due to the formation of highly insoluble metal sulphides (Jacobs and Emerson, 1985; Dyrssen and Kremling, 1990). Other metals such as Zn and copper (Cu) also form highly insoluble sulphides in these anoxic environments (Jacobs and Emerson, 1985; Dyrssen and Kremling, 1990). Recent data suggest that insoluble Cd sulphides may form in the water column in O_2-depleted, but not anoxic, regions and that this process may be a significant removal term in the oceanic dissolved Cd budget (Janssen et al., 2014 / Chapter 2; Conway and John, 2015a; Conway and John, 2015b). Water column sulphide formation can act to deliver metal sulphides to sediments in addition to sulphides being formed in reducing sedimentary environments (McKay and Pedersen, 2008). Preliminary data on the formation of solid Cd sulphides and similar metal sulphides from hydrothermal systems suggest that this process may be accompanied by an isotope fractionation with lighter isotopes enriched in the solid phase, leaving the remaining dissolved pool enriched in heavier isotopes (Schmitt et al., 2009a; John et al., 2008; Abouchami et al., 2015). This hydrothermal Cd sulphide isotope effect is supported by theoretical investigations of Cd sulphides (Yang et al., 2015) and similar isotopic signatures are also found in particulates from Cd-depleted low-O_2 water (Janssen et al., 2014 / Chapter 2; Conway and John, 2015a). However, no experimental studies of fractionation during sulphide formation have been carried out and not all studies suggesting removal of dissolved Cd by sulphide formation in O_2-depleted regions have seen evidence in the dissolved pool of an associated fractionation (Conway and John, 2015b).

4.3 Sampling Site: The subarctic northeast Pacific

The Line P time series transect (Figure 4.1) is a zonal onshore-offshore transect in the subarctic northeast Pacific which begins at 48.5° N, 125.5° W in coastally-influenced waters

near Vancouver Island, BC and extends westward to Ocean Station PAPA/P26 (50° N, 145° W) in the Alaskan Gyre. Cadmium concentrations have been reported previously in the region along the north-south VERTEX T transect, which intersects Line P at station T7/P26, to a depth of around 1500 m (3910 m at T7/P26) (Martin et al., 1989). The Line P transect covers environments with elevated Fe near the continental shelf as well as the chronically Fe-limited High-Nutrient Low-Chlorophyll (HNLC) open subarctic northeast Pacific Ocean and Alaskan Gyre (e.g. Martin et al., 1989). Line P lies within O_2-depleted waters in the North Pacific, with O_2-depletion strongest in the east along the margin and weakening heading westward (Whitney et al., 2007). Minimum dissolved [O_2] within this region are 10-20 μmol kg^{-1}, with [O_2] generally below 50 μmol kg^{-1} in the depth range of 400 - 1900 m (Figure 4.1).

Line P receives influence from both subarctic and subtropical waters from the western Pacific via the North Pacific Current, which splits near Line P sending a component heading north to the Alaskan Gyre and a component heading south along the western shelf of North America (Whitney et al., 2007). The subarctic Alaskan Gyre system is dynamic and can vary on seasonal, annual, interannual and decadal timescales, e.g. the bifurcation of the North Pacific Current influencing both the strength of the Alaska Current and the extent of the Alaskan Gyre (e.g. Cummins and Freeland, 2007), El Niño-Southern Oscillation (ENSO) and Pacific Decadal Oscillation (PDO) (e.g. Chandler et al., 2015).

Moving offshore (westward) along the Line P transect, isopycnal surfaces shoal slightly (by ~100 m in the upper 500 m) (Figure 4.1). The winter mixed layer can extend to roughly 100-125 m depth, overlying a permanent halocline (Crawford et al., 2007). Waters at or above the σ_θ = 26.6 isopycnal surface (~200 m along the Line P transect) may outcrop in the open western North Pacific (Talley et al., 1993; Whitney et al., 2007). The more coastal stations along the Line P transect lie within the northern reaches of the California Undercurrent, centered around the σ_θ = 26.5 isopycnal surface (~200 m depth at coastal stations) (Thomson and Krassovski, 2010). The northeastern extent of North Pacific Intermediate Water (NPIW) approaches but does not reach the Line P transect; and no broad salinity minimum, characteristic of NPIW, is seen on the isopycnal range of σ_θ = 26.6-27.0 (Figure 4.1) (Talley, 1993). North Pacific Deep Water, derived ultimately from southern water sources, is found below intermediate depths (Macdonald et al., 2009).

A strong warm temperature anomaly in northeast Pacific surface waters (colloquially called the "Blob") developed in the winter of 2013-2014 due to a high atmospheric pressure anomaly that reduced wintertime surface heat loss and altered ocean advection (Bond et al., 2015). The Blob hosted biological anomalies as well such as altered phytoplankton and zooplankton community composition, abundances, and reproductive dynamics (Chandler et al., 2015; Peterson et al., 2016). The warm water anomaly was not related to an ENSO event (Bond et al., 2015). This anomaly was sustained into 2015 and extends to roughly 100 m depth (Bond et al., 2015); therefore our 2014 samples were taken from within the feature while our 2012 samples were taken under 'normal' conditions, allowing us to determine the effect of changing conditions on the distribution of Cd in the region. Hydrographic data from the Line P transect time series are available at: https://www.waterproperties.ca/linep/cruises.php.

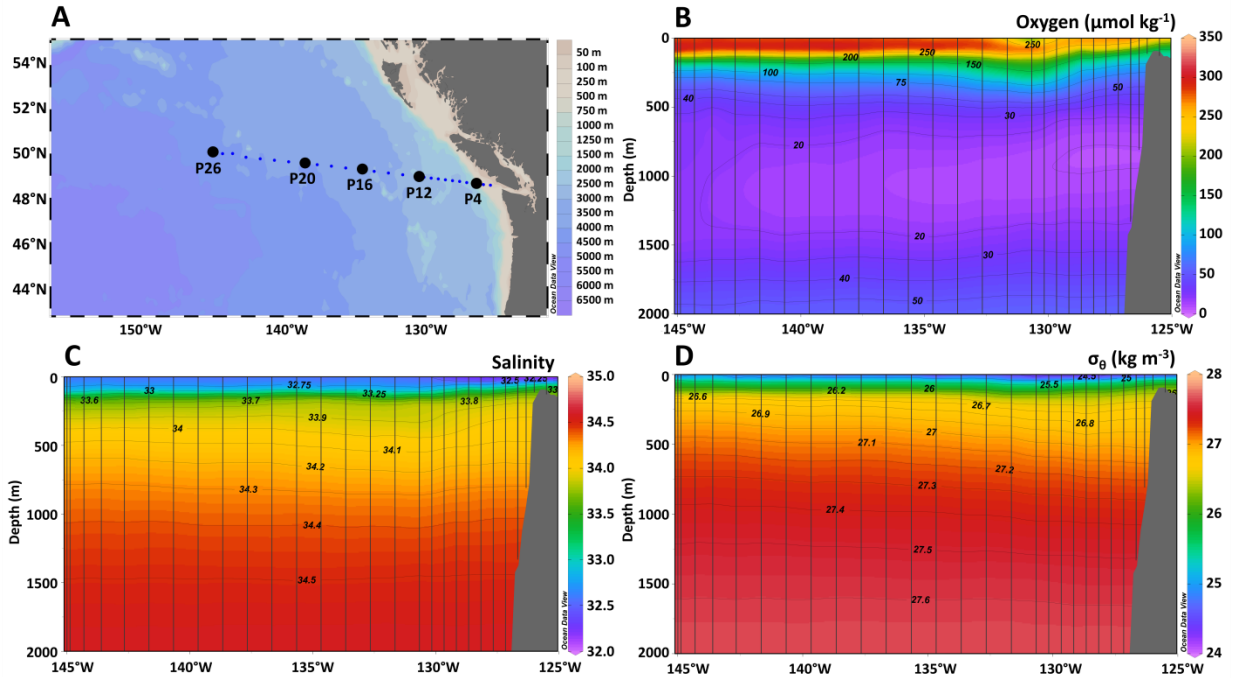

Figure 4.1 Line P transect map (A), dissolved oxygen (B), salinity (C) and density (σ_θ, D) to 2000 m depth

In panel A, major stations sampled for Cd analyses are shown in black and minor stations are shown in blue. Oxygen, salinity, and density are from the August 2012 cruise CTD data (cruise 2012-13) and are courtesy of the Line P program, Institute of Ocean Sciences, Fisheries and Oceans Canada (www.waterproperties.ca/linep). Vertical lines in panels B-D show station locations where there are CTD data.

4.4 Methods

The Line P transect was sampled during three cruises from 14-30 August 2012 (n = 104 samples, cruise 2012-13), 20 August - 6 September 2013 (n = 23 samples, cruise 2013-18), and 19 August - 4 September 2014 (n = 12 samples, cruise 2014-19) on board the *CCGS John P. Tully*. Sample depth ranges for [Cd] and $\varepsilon^{112/110}$Cd are shown in Table 4.1. Samples were collected in one of three ways: one surface sample (2012 cruise, P26 25 m depth) was collected using an air-driven Teflon bellows pump and filtered through a 0.4 µm filter (Millipore Opticap). Samples throughout most of the water column were collected using 12 L Teflon-coated GO-FLO bottles (General Oceanics, Fl USA) mounted on a 12 bottle powder-coated trace metal clean rosette system (Measures et al., 2008) with a CTD. Samples below 2100 m were collected using 12 L Teflon-coated GO-FLO bottles attached to a Kevlar line and tripped using Teflon messengers. The GO-FLO bottles were gravity-filtered through 0.2 µm Acropak filters (Pall Corporation) into acid cleaned 250 mL and 1 L LDPE bottles (Nalgene). Samples were acidified to pH = 2 using 12 mol L^{-1} hydrochloric acid (HCl) (SeaStar Chemicals) and stored until analysis (approximately 4-18 months). Unfiltered macronutrient samples (PO_4^{3-}, NO_3^-, silicic acid (Si)) were collected from the GO-FLO bottles as well as from a conventional rosette and analyzed according to Barwell-Clarke and Whitney (1996). Dissolved O_2 data was obtained with a Seabird SBE43 dissolved O_2 sensor calibrated by Winkler titration. Macronutrient and O_2 data are courtesy of the Line P program run by the Institute of Ocean Sciences (DFO, Canada).

Cruise ID (Year)	**$\varepsilon^{112/110}$Cd**	**[Cd]**
2012-13 (2012)	P26: surface to 4000 m P12-P20: 100 m to 2100 m P4: 100 m to 1300 m	P26: Surface to 4000 m P12-P20: Surface to 2100 m P4: Full water column (surface to 1300 m)
2013-18 (2013)	P4-P16, P26: Subsurface isopycnals, (200-1100 m)	P4-P16, P26: Subsurface isopycnals, (200-1100 m)
2014-19 (2014)	P4-P20: Surface (upper 50 m)	P4-P20: Surface (upper 50 m)

Table 4.1 Samples collected for $\varepsilon^{112/110}$Cd and [Cd] in 2012, 2013 and 2014

The procedures for chemical separation of Cd and analysis of $\varepsilon^{112/110}$Cd follow Abouchami et al. (2011, 2014). Briefly, samples were weighed and spiked with a ^{106}Cd-^{108}Cd double spike (Schmitt et al., 2009b) and left to equilibrate for at least 24 hours. Equilibrated samples (pH = 2) were acidified to pH = 1 with 12 mol L^{-1} HCl (sub-boiling distilled) and the Cd was separated in a two-step process by anion exchange chromatography utilizing Bio-Rad AG1-X8 resin (100-200 mesh). The initial separation of Cd for nearly all samples was accomplished using the resin in chloride form. For eight surface samples from 2014 (P12 all depths, P16 all depths, P20: 10 and 25 m), the initial separation was accomplished with the resin in bromide form and with samples (pH = 2, HCl) further acidified with 6 mL L^{-1} of 8.5 mol L^{-1} hydrobromic acid (sub-boiling distilled) rather than HCl, following Xie et al. (in revision). In both cases the initial separation of Cd was followed by final Cd purification using the resin in bromide form in a 100 μL 4:1 shrink-fit PFA column. Dried samples were loaded onto degassed single rhenium filaments and analyzed by thermal ionization mass spectrometry (TIMS) with a Thermo-Fisher Triton instrument. The consensus reference material NIST SRM-3108 (Abouchami et al., 2013) was analyzed along with every set of samples. The procedural blank (3 pg Cd or 0.06 pmol kg^{-1} Cd) was determined by processing a 500 mL acidified aliquot of 18.2 MΩ water (MilliQ, Millipore) through the chemical separation and analytical procedure, and is a maximum value since this includes the water blank itself. Raw data were corrected for instrumental mass bias offline with the double-spike reduction algorithm using the exponential fractionation law. All cadmium isotope data are reported as $\varepsilon^{112/110}$Cd (Equation 4.1) relative to NIST SRM-3108.

$$\varepsilon^{112/110}Cd = \left(\frac{^{110}Cd/^{112}Cd_{NIST\ SRM\ 3108}}{^{110}Cd/^{112}Cd_{Sample}} - 1 \right) \times 10{,}000 \qquad \text{(Equation 4.1)}$$

Analyses of the NIST-3108 reference standard were carried out with different amounts of Cd loaded onto the filament and a small offset was observed at low Cd (≤ 10 ng Cd) (Table D.1). When applicable, sample data were referenced to the weighted mean NIST ^{110}Cd/^{112}Cd value of comparably low Cd loads rather than the ^{110}Cd/^{112}Cd ratio of 0.520121 from normal loads (Abouchami et al., 2011; this study, Table D.1).

While data in this study are discussed in terms of $\varepsilon^{112/110}$Cd, figures and tables are presented in both $\varepsilon^{112/110}$Cd and $\delta^{114/110}$Cd. Notations and standard reference materials have been converted as needed to $\varepsilon^{112/110}$Cd and $\delta^{114/110}$Cd relative to NIST SRM-3108 using the conversion factors reported in Abouchami et al. (2013). Cadmium concentrations were determined by isotope dilution from the fractionation-corrected ^{106}Cd/^{112}Cd ratio measured simultaneously with the isotopic composition run. The uncertainty of [Cd] is below 1% (Abouchami et al., 2014), and is governed largely by weighing error for the spike rather than the measurement error.

Analysis of the SAFe D1 and D2 reference materials resulted in $\varepsilon^{112/110}$Cd = 1.58 ± 0.12 (n = 3, 2σ), [Cd] = 1.008 ± 0.008 nmol kg^{-1} (n = 3), which compares well with previously published data (Table 4.2, consensus [Cd] = 0.991 ± 0.031 nmol kg^{-1} as of May 2013). The long-term external reproducibility is shown in Figure D.1 for double-spiked NIST SRM-3108 standards with ≥ 50 ng Cd. The average $^{110/112}$Cd ratio of 0.520121 ± 0.00009 (2SD, n = 54 standards analyzed between October 2013 and April 2016) agrees with the value reported by Abouchami et al. (2011).

Source	$\varepsilon^{112/110}$Cd	$\delta^{114/110}$Cd	N
This study	1.58 ± 0.12	0.316 ± 0.024	3
Conway and John, 2013	1.30 ± 0.10	0.260 ± 0.020	5
Conway and John 2015b	1.55 ± 0.20	0.320 ± 0.040	8

Table 4.2 SAFe standard intercomparison
$\varepsilon^{112/110}$Cd values (with 2σ) are from SAFe D1 and D2 standards (this study, Conway et al., 2013) and deep samples (500-4500 m) from the SAFe site (Conway and John, 2015b). SAFe D1 and D2 standards are from 1000 m depth. Note that the individual measurement from a sample collected at 1000 m depth during a 2009 reoccupation of the SAFe station gave $\varepsilon^{112/110}$Cd = 1.55 ± 0.20 ($\delta^{114/110}$Cd = 0.31 ± 0.04) (Conway and John, 2015b), agreeing well with the reported SAFe site deepwater mean.

4.5 Results and Discussion

4.5.1 *Concentration depth profiles and Cd:PO_4^{3-} remineralization*

Dissolved [Cd], [PO_4^{3-}] and [O_2] are presented in Figure 4.2 (2012 and 2014) and Table D.2 (all data). Our data agree well with previous [Cd] from the region (Martin et al., 1989) and show nutrient-type behavior of Cd and a strong correlation with PO_4^{3-}. With the exception of station P4, where surface [Cd] is high, surface [Cd] in both 2012 and 2014 follow a pattern of elevated values on the oceanic end of the transect and lower values toward the coastal end, similar to those reported previously for macronutrients along Line P (Peña and Varela, 2007). Surface dissolved [Cd] and macronutrient concentrations were significantly lower in 2014 than in 2012 at stations P12-P20 while remaining similar at P4 for these two samplings (Figure 4.2, Table D.2). These inter-annual variations are consistent with the diminished vertical mixing and advection, responsible for the warm temperature anomaly and resulting stratification (Bond et al., 2015), which would limit nutrient resupply to the mixed layer.

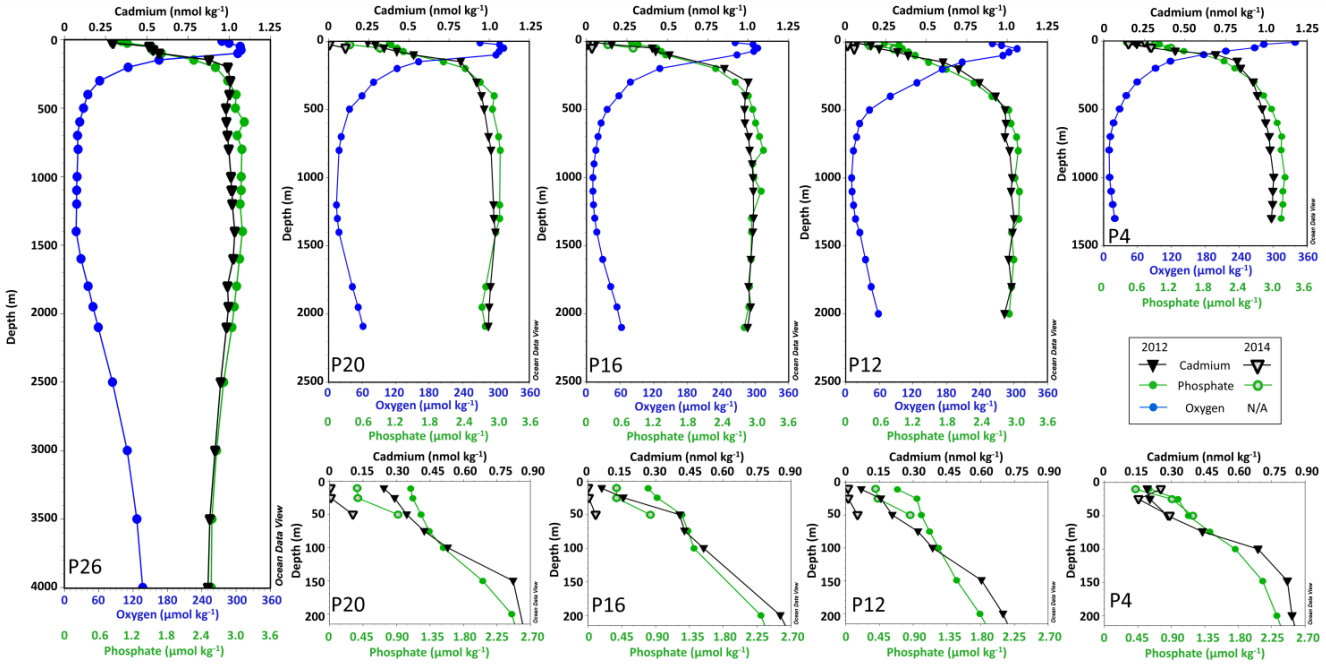

Figure 4.2 Dissolved [Cd], [PO_4^{3-}] and [O_2] from August 2012 and 2014
Cadmium concentrations are presented as black inverted triangles, [PO_4^{3-}] as green dots and [O_2] as blue dots. Cadmium and PO_4^{3-} concentration data from the upper 200 m are shown again in the lower plots for stations P4-P20, with 2012 data as solid symbols and 2014 data as open symbols. Note that the x axis scales are different for the surface plots and full water column plots; however, the relative scaling of Cd and PO_4^{3-} is kept approximately constant. 2013 data are not shown here but are included in Table D.2. Phosphate (bottle data) and O_2 (CTD data) are courtesy of the Line P program.

Remineralization ratios of particulate Cd:P were estimated by linear regression of dissolved [Cd] and [PO_4^{3-}] in the nutricline (Table 4.3). Calculated Cd:P remineralization values of 0.42-0.52 nmol Cd (μmol P)$^{-1}$ (composite value = 0.45 nmol Cd (μmol P)$^{-1}$) compare well with those previously calculated for the HNLC North Pacific and other HNLC regions and are much higher than non-HNLC regions (Lane et al., 2009; Quay et al., 2015). The same can be seen in Cd* (Figure A.4; Table D.2), a tracer analogous to N* that tracks enrichments and depletions of Cd relative to PO_4^{3-} and regional Cd:PO_4^{3-} relationships. Cd* is calculated from observed [Cd] and [PO_4^{3-}] by the following:

$$Cd^* = [Cd_{obs}] - [PO_4^{3-}{}_{obs}] \times 0.345 \text{ nmol } \mu\text{mol}^{-1} \qquad \text{(Equation 4.2)}$$

with a 0.345 nmol μmol^{-1} slope of the Cd:PO_4^{3-} relationship selected to result in Cd* ≈ 0 in subarctic northeast Pacific deepwater (>2000 m) (see also Baars et al., 2014; Janssen et al., 2014 / Chapter 2; Conway and John, 2015a, 2015b). Surface samples show negative Cd* and values increase in the nutricline at all stations, which is consistent with elevated biological Cd uptake in HNLC surface waters and remineralization of sinking Cd-rich particles (e.g. Sunda and Huntsman, 2000; Cullen 2006; Lane et al., 2009; Baars et al., 2014; Quay et al., 2015). Elevated nutricline Cd* may also reflect advection of high Cd:PO_4^{3-} waters from the western North Pacific, where a comparable but smaller subsurface Cd* maximum (Cd:PO_4^{3-} maximum) is seen (Abe, 2002; see also Conway and John, 2015b). Note that Cd* is less positive in western North Pacific waters and therefore, advection alone is insufficient to fully account for the trends seen along Line P.

As depth increases and dissolved [O_2] diminishes, Cd* begins to decrease. This sharp reversal in Cd* occurs at around 200-300 m and is seen at all stations. Cd* continues decreasing and reaches a minimum between 500 and 1000 m. The mid-depth deficit of Cd relative to PO_4^{3-} at low [O_2] (see Figures 4.1B, 4.2, A.4) along with mid-depth local [Cd] minima at some stations, suggests a removal process is acting in this depth range as suggested previously for Cd (Janssen et al., 2014 / Chapter 2) and Zn (Janssen and Cullen, 2015 / Chapter 3).

Dissolved [Cd] appear to decouple from [PO_4^{3-}] in the upper nutricline at station P26, with more complete apparent remineralization of Cd than P at shallower depths. Rather than the

Cd depth profile showing a gradual increase toward a maximum value near 1000 m depth, mirroring the PO_4^{3-} profile and apparent oxygen utilization, [Cd] reaches a near-maximum value at 200 m followed by relatively constant [Cd] with depth while [PO_4^{3-}] continues to increase and [O_2] continues to decrease (see the nutricline gradients at station P26, Figure 4.2, and percent of maximum Cd, Table D.2). The same trend is apparent, though less pronounced, at other stations along the transect as well as for Zn:Si at P26 (Janssen and Cullen, 2015 / Chapter 3). This apparent remineralization of Cd before P may be caused by a decoupling of Cd from P during particle remineralization resulting in more rapid loss of Cd from particles or it may be driven by physical processes acting on water with perturbed Cd:PO_4^{3-} such as a distal supply of metal-rich water along isopycnal surfaces.

Station	**Cd:PO_4^{3-} Slope (nmol µmol^{-1})**	**N (Samples)**	**r^2**
P26	0.43	8	0.98
P20	0.43	7	0.95
P16	0.49	7	0.97
P12	0.52	8	0.95
P4	0.42	8	0.95
Composite	0.45	38	0.96
Literature data (Quay et al., 2015)			
Region	**Cd:PO_4^{3-} Slope (nmol µmol^{-1})**	**N (Stations)**	
HNLC	0.49 ± 0.23	102	
Non-HNLC	0.21 ± 0.09	58	

Table 4.3 Remineralization ratios of Cd and PO_4^{3-}
Remineralization ratios, following Quay et al. (2015) and Lane et al. (2009), are calculated from the slope of the linear regression of dissolved [Cd] and [PO_4^{3-}] in the upper 300 m using 2012 data. For each station, the slopes, number of data points for the regression (N) and r^2 values for each regression are given. The composite is a single regression from all the data points. For comparison, the mean HNLC and non-HNLC Cd:PO_4^{3-} slopes calculated by Quay et al. (2015) are shown, with N referring to the number of stations rather than the number samples.

4.5.2 *Cd isotope fractionation in the subarctic North Pacific water column*

4.5.2.1 $\varepsilon^{112/110}$Cd data from 2012 and 2013

Dissolved $\varepsilon^{112/110}$Cd data are shown in Figure 4.3 (2012 and 2014) and Table D.2 (all data). Surface waters (≤ 100 m), where [Cd] is lower, have higher $\varepsilon^{112/110}$Cd values and show stable isotope fractionation patterns seen in many of the previous $\varepsilon^{112/110}$Cd studies (e.g. Lacan et al., 2006; Ripperger et al., 2007; Abouchami et al., 2011; Xue et al., 2013). As depth and [Cd] increases, $\varepsilon^{112/110}$Cd decreases to a deepwater mean of 1.14 ± 0.34 (n = 43 samples with depth ≥ 1000 m, 2SD), which is indistinguishable from the $\varepsilon^{112/110}$Cd of Upper Circumpolar Deep Water and Antarctic Bottom Water $\varepsilon^{112/110}$Cd of 1.21 ± 0.36 (n = 40 samples with depth ≥ 1000 m, 2SD, Xue et al., 2013; Abouchami et al., 2014). The near-constant deepwater $\varepsilon^{112/110}$Cd (this study; Conway and John 2015b) illustrates greater uniformity along the Line P transect and in the northeast Pacific compared to other basins such as the North and South Atlantic (Xue et al., 2013; Abouchami et al, 2014; Conway and John, 2015a; Xie et al., in revision). Note that any vertical mixing of Pacific deepwater and Southern Component Water would go undetected since both water bodies have similar $\varepsilon^{112/110}$Cd and elevated [Cd]. Near-uniform deep Pacific $\varepsilon^{112/110}$Cd begins within the nutricline, while [Cd] is still increasing, at depths as shallow as 150 m (P26), though generally closer to the range of 300-400 m. The increasing [Cd] in the nutricline is likely due to respiration of organic matter, and we expect Cd in organic matter from surface biological activity to be light relative to the dissolved pool, as found in previous studies (e.g. Lacan et al., 2006; Ripperger et al., 2007; Abouchami et al., 2011). It is likely that this apparent lack of a $\varepsilon^{112/110}$Cd signal with [Cd] remineralization is driven by the relatively small change to the large dissolved Cd pool. In addition to the depth profiles collected at all stations in 2012, which show near-uniform deepwater $\varepsilon^{112/110}$Cd, subsurface isopycnals were sampled from the August 2013 cruise (stations P4-P16, P26 along targeted isopycnals of 26.7 to 27.25, approximately 200-1100 m depth, n = 23 samples). Nearly all overlapping samples from these two years agree within error for [Cd] and $\varepsilon^{112/110}$Cd (Table D.2; see also Figure 4.6), suggesting that subsurface [Cd] and $\varepsilon^{112/110}$Cd in the subarctic northeast Pacific are relatively invariant on inter-annual timescales.

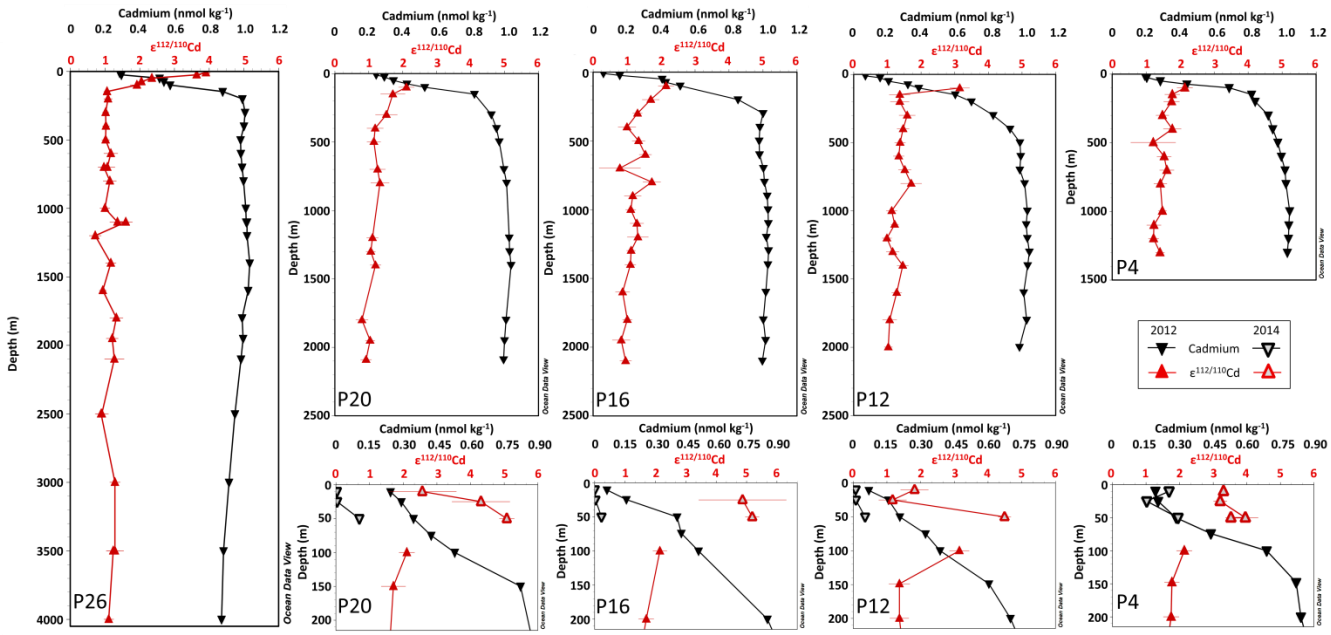

Figure 4.3 Dissolved [Cd] and $\varepsilon^{112/110}$Cd from August 2012 and August 2014
Cadmium concentrations are presented as black inverted triangles and $\varepsilon^{112/110}$Cd as red triangles. Duplicate analyses (station P26 700 m, 1100 m, 2500 m and 3500 m) are shown for $\varepsilon^{112/110}$Cd. The upper plots show only 2012 data. $\varepsilon^{112/110}$Cd and [Cd] data from the upper 200 m are shown again in the lower plots for stations P4-P20,with 2012 data as solid symbols and 2014 data as open symbols. Note that the [Cd] scaling is different for the surface plots and full water column plots and that the surface plot for station P16 has different [Cd] and $\varepsilon^{112/110}$Cd scaling than the other surface plots. 2013 are not shown here but are included in Table D.2. Figure D.2 presents a version of this figure in $\delta^{114/110}$Cd notation.

From 500-1000 m, where a 'bite' is observed in dissolved [Cd] and [O_2] is depleted, there is no accompanying $\varepsilon^{112/110}$Cd shift that is resolvable outside analytical uncertainty. A similar lack of a dissolved $\varepsilon^{112/110}$Cd signal in Cd- and O_2-depleted North Pacific water was observed by Conway and John (2015b). This is in contrast to dissolved $\varepsilon^{112/110}$Cd observations in the eastern Atlantic (Conway and John, 2015a) where $\varepsilon^{112/110}$Cd signals in low-[O_2] water were attributed to a fractionation during sulphide formation (see also Janssen et al., 2014 / Chapter 2). The difference between the Pacific data and those from the North Atlantic might be related to the greater [Cd] and the smaller Cd deficit (less negative Cd*) in the North Pacific than the North Atlantic. The peak Cd depletion from Cd* is roughly 10% of the dissolved Pacific inventory (Table A.2), while it is up to 50% in the North Atlantic (Janssen et al., 2014 / Chapter 2; Conway and John, 2015a). The smaller relative Cd depletion in the Pacific along

with the large Cd inventory may lead to a "dilution" effect of the $\varepsilon^{112/110}$Cd signal imparted during Cd removal by sulphides.

Alternatively, the process(es) driving the Cd depletion may have only minor or no Cd isotope fractionation effect(s). In order for a Cd deficit of up to 0.1 nmol kg^{-1} to exist in the subarctic northeast Pacific while maintaining a remaining dissolved $\varepsilon^{112/110}$Cd similar to the deepwater mean (weighted mean $\varepsilon^{112/110}$Cd = +1.13), given an analytical uncertainty on individual measurements of ca. 0.15, the 'missing' Cd must have an $\varepsilon^{112/110}$Cd ≥ -0.37 (supplemental section D.3; Table D.3). In terms of fractionation factors for removal of dissolved Cd ($\alpha_{sw\text{-}removed}$), this constrains the removal process to an $\alpha_{sw\text{-}removed} \leq 1.00016$ (Supplemental Section D.3). This 'missing'$\varepsilon^{112/110}$Cd estimates falls within observations for Cd sulphides from hydrothermal systems (Schmitt et al., 2009a), suggesting that sulphide formation is capable of causing the observed Cd deficit without an associated resolvable $\varepsilon^{112/110}$Cd signal in the water column. Analysis of suspended particulate $\varepsilon^{112/110}$Cd from the northeast Pacific combined with dissolved $\varepsilon^{112/110}$Cd data should help constrain the isotopic effect of a dissolved to particulate Cd transfer, such as sulphide formation.

Samples from the upper 100 m from the 2012 and 2013 cruises fit well to a closed-system Rayleigh fractionation model with a fractionation factor ($\alpha^{112/110}$Cd) of 1.0002 (Figure 4.4). This is similar to fractionation factors reported in previous studies in the HNLC Southern Ocean (Abouchami et al., 2011; Xue et al., 2013). The highest surface $\varepsilon^{112/110}$Cd observed along the transect in 2012 was 3.91 ± 0.12 and is comparable to observations in the Southern Ocean of 4.96 ± 0.32 (Abouchami et al., 2011) and 3.79 ± 0.34 (Xue et al., 2013). However, this surface value is significantly lower than those previously reported in the North Pacific at lower latitudes (up to +18.5) (Ripperger et al., 2007; Conway and John, 2015b) and in the North Atlantic (up to +25.2) (Ripperger et al., 2007; Xue et al., 2012; Boyle et al., 2012; Conway and John, 2015a).

4.5.2.2 Surface $\varepsilon^{112/110}$Cd and fractionation trends: comparison of 2012 and 2014 Line P data

Surface [Cd] were generally much lower in 2014 than in 2012 (Table D.2; Figure 4.3) while the highest $\varepsilon^{112/110}$Cd value observed in 2014 ($\varepsilon^{112/110}$Cd = 5.19 ± 0.23) is only roughly 1 epsilon unit higher than our 2012 maximum value (Table D.2, Figure 4.3). Our 2014 data do

not fit a simple closed-system Rayleigh fractionation model (Figure 4.4) but instead follow more of an open system trend with $\varepsilon^{112/110}$Cd remaining relatively invariant or decreasing slightly with decreasing [Cd]. Lower $\varepsilon^{112/110}$Cd values are observed at extremely low [Cd] (near and below 0.01 nmol kg^{-1}) compared to the elevated values where [Cd] is between 0.03-0.10 nmol kg^{-1}. The absence of a Rayleigh fractionation signal in surface $\varepsilon^{112/110}$Cd has been documented in the South Pacific and has been attributed to very low [Cd], limiting the supply of Cd to cells (Gault-Ringold et al., 2012).

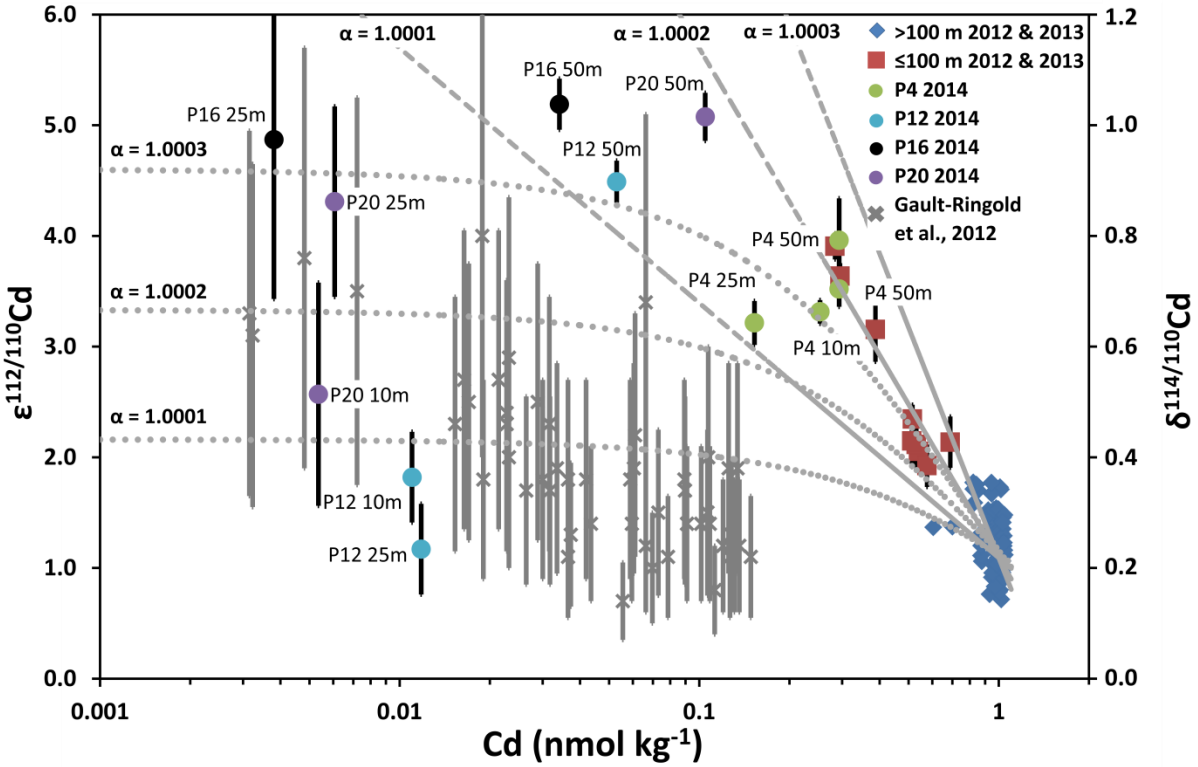

Figure 4.4 Closed-system Rayleigh and open-system fractionation models for 2012, 2013 and 2014 data

For 2012 and 2013 data, samples from the upper 100 m are shown in red and all others in blue. 2014 data are shown as circles with P20 in purple, P16 in black, P12 in light blue, and P4 in green. Literature data from the South Pacific (Gault-Ringold et al., 2012) are denoted by grey crosses. Trendlines corresponding to fractionation factors (α) of 1.0001, 1.0002, and 1.0003 for $\varepsilon^{112/110}$Cd are shown for a closed-system Rayleigh model (dashed lines, α labels at top of plot) and an open-system model (dotted lines, labels at left of plot). Model trendlines were calculated based on the initial conditions of Cd = 1 nmol kg^{-1} and $\varepsilon^{112/110}$Cd = +1.1 following Ripperger et al. (2007) and Abouchami et al. (2014).

Surface waters along the Line P transect in 2014 are characterized by the anomalous 'Blob' conditions observed from 2013 until at least 2015 - warmer temperature anomalies, higher stratification (Bond et al., 2015) - and are not representative of typical conditions along the transect. Consequently, it is possible that the observed differences in $\varepsilon^{112/110}$Cd between 2012 and 2014 are related to an advected signal in 2014. However, it should be noted that the 'Blob' water likely originated offshore to the south of the transect (Peterson et al., 2016), toward the locations of previous subtropical North Pacific stations where $\varepsilon^{112/110}$Cd values roughly two to eight times higher than our data have been reported at comparable [Cd] (Ripperger et al., 2007; Conway and John 2015b).

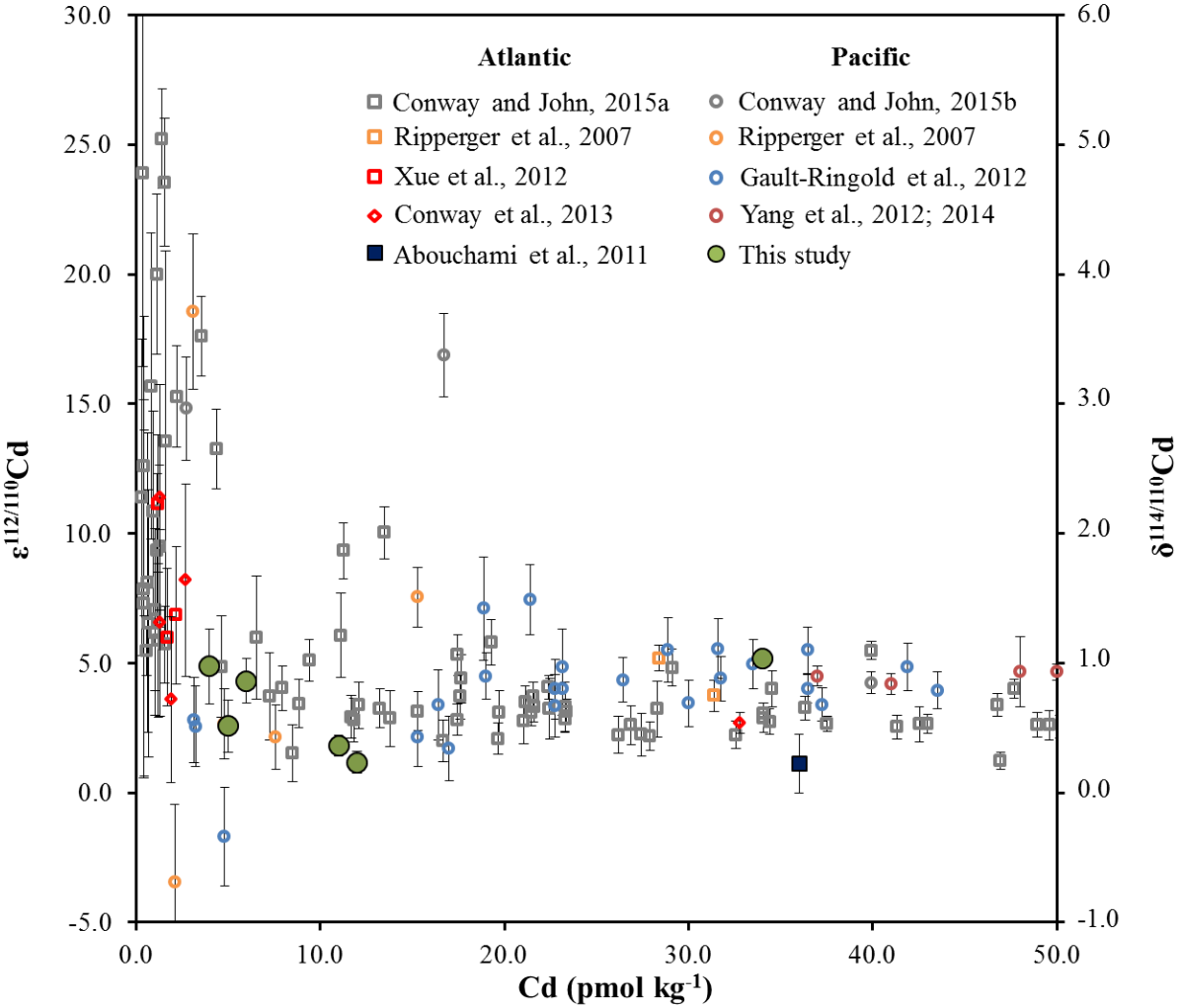

Figure 4.5 Compilation of literature $\varepsilon^{112/110}$Cd at [Cd] < 50 pmol kg^{-1}
Open symbols are samples measured with MC-ICP-MS and closed symbols are samples measured with TIMS. The data are also presented in Table D.4.

The 2014 chemical and physical 'Blob' conditions were also associated with changes in the phytoplankton community structure (Chandler et al., 2015). It is possible that this may influence some of the observed differences in 2014 surface $\varepsilon^{112/110}$Cd, given the variability in Cd uptake among phytoplankton taxa (Ho et al., 2003) and nutrient limitation conditions (e.g. Sunda and Huntsman 2000; Cullen et al., 2003; Cullen and Sherrell, 2005; Lane et al., 2009). Different Cd isotope fractionation factors have been associated with high and low Cd:Zn (α = 1.0002 and α < 1.0001 respectively) in surface waters of the Southern Ocean and the South Pacific (Abouchami et al., 2014). Our data support differentiating between fractionation effects at low to high [Cd] compared to very low [Cd], where a strong biologically-driven $\varepsilon^{112/110}$Cd signal is not observed; however, surface [Zn] is not available for our sample set to test the hypothesis of Cd-Zn interactions influencing Cd fractionation during uptake. The potential of a Zn influence on Cd uptake is discussed further in section 4.5.3.1. More culture studies of Cd isotopic fractionation during uptake across phytoplankton taxa and across varying nutrient conditions would help to elucidate the potential for nutrient- and taxa-dependent fractionation signals. Nevertheless, our data suggest that the closed-system Rayleigh model is not appropriate at extremely low [Cd], at least in the subarctic northeast Pacific.

4.5.3 Evaluation of surface water $\varepsilon^{112/110}$Cd variability at low [Cd]

The 2014 surface layer $\varepsilon^{112/110}$Cd maximum is comparable the values observed in 2012 along Line P, as well as those in the Atlantic sector of the Southern Ocean (Abouchami et al., 2011). However, it is much lower ($\varepsilon^{112/110}$Cd = 5.19 ± 0.23) than some previous observations from lower latitudes in the North Pacific of up to $\varepsilon^{112/110}$Cd = 18.5 ± 3.0 (Ripperger et al., 2007) and $\varepsilon^{112/110}$Cd = 16.9 ± 1.6 (Conway and John, 2015b), even though our data cover a comparably low [Cd] range (Figure 4.5, Table D.4). Our data show relatively constant $\varepsilon^{112/110}$Cd across a wide range of [Cd], and therefore, variability in [Cd] cannot be the sole cause for the surface $\varepsilon^{112/110}$Cd differences between our dataset and published data from the subtropical North Pacific. Similarly, Xie et al. (in revision) found lighter (less positive) surface $\varepsilon^{112/110}$Cd in the Atlantic than previously reported at comparable low [Cd] (Ripperger et al., 2007; Xue et al., 2012; Boyle et al., 2012; Conway and John, 2015a). The reason for these large

differences in both the Atlantic and Pacific surface $\varepsilon^{112/110}$ Cd is puzzling, considering the good agreement seen in subsurface $\varepsilon^{112/110}$Cd where [Cd] are higher, including at intercalibration stations such as the SAFe station (this work; Conway et al., 2013; Conway and John 2015b) and the BATS station (Boyle et al., 2012).

4.5.3.1 Factors governing surface water Cd isotope variability at low [Cd]

The differences between reported surface $\varepsilon^{112/110}$Cd could reflect either real $\varepsilon^{112/110}$Cd variability or an analytical artefact. Both physical and biological processes and external sources of Cd can locally impact surface layer $\varepsilon^{112/110}$Cd. One such possibility is via input of low levels of Cd with $\varepsilon^{112/110}$Cd ≈ 0, which would significantly lower the high $\varepsilon^{112/110}$Cd signal predicted by the Rayleigh fractionation model at very low [Cd]. Atmospheric input of terrestrially sourced Cd, which has $\varepsilon^{112/110}$Cd ≈ 0, is unlikely given that elevated $\varepsilon^{112/110}$Cd values (up to +20; Ripperger et al., 2007; Conway and John, 2015a) are observed in the North Atlantic but not in the subarctic North Pacific despite significantly higher dust input in the North Atlantic (Han et al., 2008). Additionally, a first order estimation of the dust deposition necessary to explain our subarctic northeast Pacific data suggests that dust cannot explain our low $\varepsilon^{112/110}$Cd observations at low [Cd] (see supplemental section D.5 for calculation details). Taking our observations from station P16, 10 m ([Cd] = 4 pmol kg^{-1}, $\varepsilon^{112/110}$Cd = 4.87 ± 1.44) and assuming that this represents an equal mixture of seawater and dust-derived Cd, a dust addition of ~20 g m^{-2} is required to explain our observations. This deposition must occur in a sufficiently short timeframe such that added Cd is not mixed out of the 10 m surface layer (i.e. much less than one year). However, this deposition is an order of magnitude larger than the yearly deposition for the subarctic northeast Pacific of ~1 g m^{-2} y^{-1} or less (e.g. Han et al., 2008). Consequently, the potential of dust addition to significantly lower surface $\varepsilon^{112/110}$Cd in the subarctic North Pacific appears negligible

Upwelling or mixing of subsurface water may also lower surface $\varepsilon^{112/110}$Cd; however, among all of our low [Cd] 2014 data, $\varepsilon^{112/110}$Cd below the mixed layer are higher than or equivalent to $\varepsilon^{112/110}$Cd within the mixed layer. Therefore, our low surface $\varepsilon^{112/110}$Cd cannot purely be the result of mixing between surface waters with very low [Cd] and high $\varepsilon^{112/110}$Cd and near-surface waters with higher [Cd] and lower $\varepsilon^{112/110}$Cd. On a global scale, observations

from upwelling and downwelling environments show no clear trend between upwelling and $\varepsilon^{112/110}$Cd values at comparable [Cd]. Both high (e.g. Conway and John, 2015a stations 9 and 10 from cruise KN199-4) and low (e.g. this study) $\varepsilon^{112/110}$Cd values have been reported for upwelling regions. Similarly, both high (e.g. Ripperger et al., 2007 station 7; Conway and John 2015b) and low (e.g. Ripperger et al., 2007 station 9; Xue et al., 2012; Conway and John, 2015a) $\varepsilon^{112/110}$Cd values have been reported for surface samples in regions without upwelling at similarly low [Cd]. These observations suggest that the influence of subsurface water is not the primary driver of surface $\varepsilon^{112/110}$Cd variability at very low [Cd].

Biological Cd uptake under different macro- and micronutrient conditions may result in different fractionation patterns explaining the observed differences in surface $\varepsilon^{112/110}$Cd at low [Cd] in the Pacific. At least two transport mechanisms exist for Cd uptake by marine phytoplankton – a nonspecific divalent metal transporter which is active for Mn, Cd and Zn, as well as a high-affinity Zn uptake system which becomes active at low [Zn] (Sunda and Huntsman, 2000; Xu and Morel, 2013 and references therein). A difference in Zn isotope fractionation during uptake is seen when comparing these high and low-affinity uptake systems, with lower Zn isotope fractionation under high-affinity Zn uptake. This is attributed to dissolved Zn speciation and diffusion, rather than binding and transport of Zn at the cell surface, as the main controlling factors for isotope fractionation during uptake at very low [Zn] (John et al., 2007). Distinct $\varepsilon^{112/110}$Cd fractionation trends under different ambient [Zn] have also been observed; however these consisted of higher Cd fractionation at lower [Zn] (Abouchami et al., 2014). This may be due to the intermediate Zn and Cd concentrations observed in the Southern Ocean of [Zn] > 0.3 nmol kg^{-1} (Zhao et al., 2014) and [Cd] generally > 0.1 nmol kg^{-1} (Abouchami et al., 2011; 2014) and it is possible that lower [Cd] and [Zn] might result in lower $\varepsilon^{112/110}$Cd fractionation (i.e. lower α) during biological uptake (see also, Abouchami et al., 2014 Figure 10c).

A lower $\varepsilon^{112/110}$Cd fractionation has been reported by Gault-Ringold et al. (2012) at [Zn] < 0.1 nmol kg^{-1} and [Cd] generally < 0.1 nmol kg^{-1}. This was attributed to diffusion-limited supply of Cd to cell surfaces and agrees with the reported controls on biological Zn isotope fractionation. Therefore a control on fractionation during biological Cd uptake at very low [Cd] and [Zn] such as Cd speciation and diffusion, has the potential to explain the lack of a strong

fractionation effect observed in our data set. The potential for organic ligand bound Cd has been suggested to explain the $\varepsilon^{112/110}$Cd signature of Cd-deficient waters of the SW Atlantic (Xie et al., in revision). Further investigation of the control of speciation and diffusion on $\varepsilon^{112/110}$Cd fractionation is warranted.

4.5.3.2 Inter-laboratory differences in surface $\varepsilon^{112/110}$Cd at low [Cd]

While physical or biological controls may cause real oceanographic $\varepsilon^{112/110}$Cd variability, the observed variability at low [Cd] might also be due to analytical artefacts. At present, two types of analytical instrumentation are used for stable Cd isotope measurements: multi-collector inductively coupled plasma mass spectrometry (MC-ICP-MS) and TIMS. To date no values above $\varepsilon^{112/110}$Cd = 5, considering 2σ errors, have been reported using TIMS (this study, Abouchami et al., 2011; 2014; Xie et al., in revision). Conversely, multiple measurements of $\varepsilon^{112/110}$Cd > 10 have been reported using MC-ICP-MS in both the North Atlantic and the North Pacific (Ripperger et al., 2007; Conway and John, 2015a; Conway and John, 2015b) (Figure 4.5; Table D.4). Organic residues have previously been shown to be potential sources of interference in MC-ICP-MS analyses (Shiel et al., 2009; Gault-Ringold and Stirling, 2012; Murphy et al., 2016). It should be noted that many studies using MC-ICP-MS have also reported low $\varepsilon^{112/110}$Cd at low [Cd] similar to our own $\varepsilon^{112/110}$Cd observations (see Figure 4.5, Table D.4 and references therein), including the same studies that report very high $\varepsilon^{112/110}$Cd. Therefore any analytical artefact that may exist does not universally affect MC-ICP-MS measurements. A stable Cd isotope intercalibration has been carried out for deepwater, where [Cd] is higher (Boyle et al., 2012) and two MC-ICP-MS labs have reported good agreement in low [Cd], high $\varepsilon^{112/110}$Cd surface waters (c.f. Xue et al., 2012; Conway et al., 2013). The oceanic Cd stable isotope community should prioritize a more complete intercalibration at low [Cd], including different instrumentation, to help determine if the observed ranges identify real oceanic variability or reflects artefacts due to differences in instrumentation and/or Cd pre-concentration procedures. Such an intercalibration would need to target low [Cd] water which previously yielded high $\varepsilon^{112/110}$Cd measurements to increase the likelihood that intercalibration samples capture a genuine high $\varepsilon^{112/110}$Cd signal.

4.5.4 *Subsurface $\varepsilon^{112/110}$Cd trends along Line P and in the North Pacific*

While depth profiles at individual stations show a lack of variability in deepwater $\varepsilon^{112/110}$Cd, and these deepwater $\varepsilon^{112/110}$Cd values are nearly uniform along the transect, it is possible that real spatial $\varepsilon^{112/110}$Cd variability exists in the North Pacific and is not properly resolved by our dataset. Average deepwater from the SAFe site in the subtropical North Pacific has an $\varepsilon^{112/110}$Cd = +1.60 ± 0.28 (n = 6 samples at depth ≥ 1000 m, 2SD, Conway and John, 2015b), a value in agreement with our deep SAFe standard measurements. While we observe a deepwater arithmetic mean of $\varepsilon^{112/110}$Cd = 1.14 ± 0.37 in the subarctic northeast Pacific (n = 43 samples at depth ≥ 1000 m, 2SD) that is equivalent to the SAFe site deepwater mean within error, the weighted mean of subarctic northeast Pacific deepwater ($\varepsilon^{112/110}$Cd = 1.13 ± 0.02) is distinct from the subtropical North Pacific average. The reasons for this difference are unclear, especially considering the observed similarities between Southern Component Water and subarctic northeast Pacific water. The potential existence of North Pacific deepwater $\varepsilon^{112/110}$Cd variability may reflect differences in the surface ocean, water masses or water age between the subtropical and subarctic North Pacific.

Additional fine-scale differences may be apparent along the Line P transect, with heavier deepwater $\varepsilon^{112/110}$Cd toward the margin than in the open subarctic northeast Pacific. Some of the deep $\varepsilon^{112/110}$Cd values from P26 are distinguishable from those at P4 at equivalent depths and densities (Figure D.4); however, there is no consistent difference between the two and not all depths or densities show a difference outside of error at 95% confidence. The Line P transect (roughly 1600 km) may not be long enough to resolve fully spatial differences in deepwater $\varepsilon^{112/110}$Cd between stations. High-precision $\varepsilon^{112/110}$Cd measurements along basin-scale zonal and meridional transects will help to determine if such fine scale trends exist.

In addition to potential deepwater $\varepsilon^{112/110}$Cd variability along the Line P transect, a distinct trend of increasing $\varepsilon^{112/110}$Cd moving toward the shelf (station P26 toward station P4; Figure 4.6) is seen along isopycnal surfaces in intermediate waters (the upper 500-700 m). While a similar [Cd] decrease is seen for some isopycnals, [Cd] trends are more variable and a

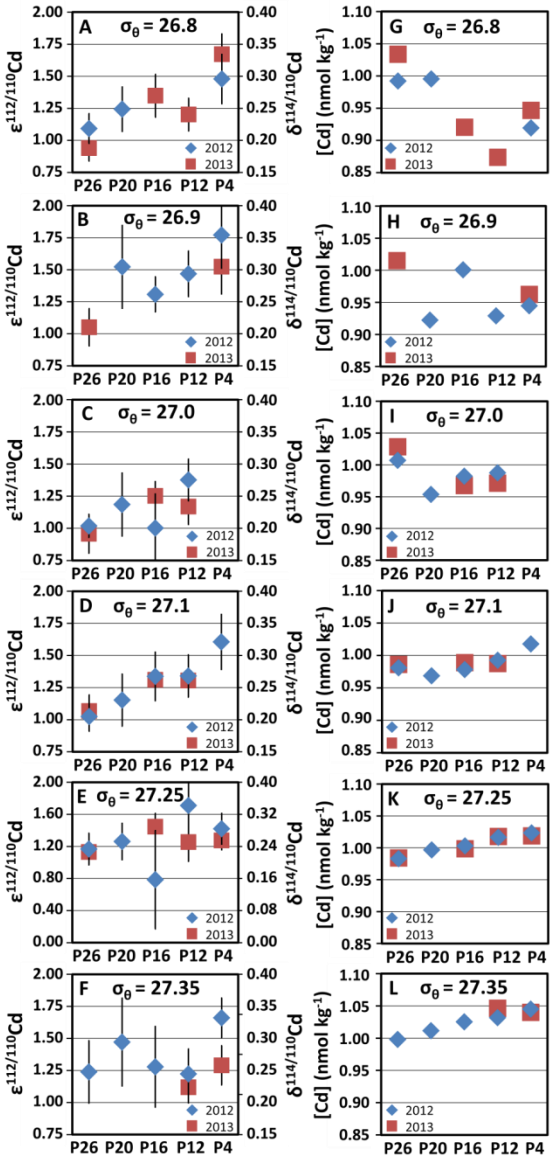

Figure 4.6 $\varepsilon^{112/110}$Cd and [Cd] along isopycnal surfaces in 2012 and 2013

2012 data are shown as blue diamonds and 2013 data as red squares. Panels A-F show $\varepsilon^{112/110}$Cd and panels G-L show [Cd]. For clarity a weighted mean is given in place of duplicates analyses from the same sample. Not all stations have all isopycnals represented for a given year; however, interannual agreement is strong along these isopycnal surfaces between 2012 and 2013 in all our overlapping samples. The tolerated density ranges are as follows: panels A and G (σ_θ = 26.8): 26.79-26.84; panels B and H (σ_θ = 26.9): 26.88-26.92; panels C and I (σ_θ = 27.0): 26.95-27.01; panels D and J (σ_θ = 27.1): 27.08-27.15; panels E and K (σ_θ = 27.25): 27.22-27.27; panels F and L (σ_θ = 27.35): 27.32-27.37. Approximate depths for these ranges vary by station due to isopycnal shoaling along the transect and are 200-350 m (A and G), 250-425 m (B and H), 300-500 m (C and I), 500-700 m (D and J), 700-800 m (E and K) and 800-1000 m (F and L). Note the different y-axis range on panels E and K. σ_θ is from CTD data and is courtesy of the Line P program.

decrease is not seen for all isopycnals (Figure 4.6). Therefore decreasing [Cd] alone cannot explain for the observed $\varepsilon^{112/110}$Cd trends. The California Undercurrent, which reaches latitudes of the Line P transect (Thomson and Krassovski, 2010), may influence this isopycnal $\varepsilon^{112/110}$Cd structure in upper intermediate waters on the coastal side of the transect, though $\varepsilon^{112/110}$Cd data are presently unavailable for the California Undercurrent for comparison purposes.

4.5.5 North Pacific deepwater in a global context

A global compilation of deepwater [Cd] and $\varepsilon^{112/110}$Cd data is presented in Figure 4.7. Pacific deepwater $\varepsilon^{112/110}$Cd (mean $\varepsilon^{112/110}$Cd = 1.14 ± 0.37, 2SD, n = 43 samples at or below 1000 m, this study) are similar to those of Southern Ocean deepwaters (mean $\varepsilon^{112/110}$Cd = 1.21 ± 0.36, 2SD, n = 40 samples at or below 1000 m, Abouchami et al., 2014; Xue et al., 2013). This similarity supports the idea that the ocean interior $\varepsilon^{112/110}$Cd on a global scale reflects conditions at deepwater formation sites such as the Southern Ocean and subsequent deepwater circulation and mixing (Abouchami et al., 2014; Conway and John, 2015b). In contrast to $\varepsilon^{112/110}$Cd, dissolved [Cd] is approximately 33% higher in North Pacific deepwater (1.01± 0.04 nmol kg^{-1}, this study, n = 43 samples at or below 1000 m) compared to that of the Southern Ocean (0.76 ± 0.08 nmol kg^{-1}, n = 40 samples at or below 1000 m, Abouchami et al., 2014; Xue et al., 2013). A 33% increase in [Cd] in Pacific deepwater from Southern Component Water, without a corresponding change in $\varepsilon^{112/110}$Cd, puts constraints on the isotopic range of the net accumulated Cd over the course of deepwater transport from the Southern Ocean into the Pacific.

Considering the mean deepwater $\varepsilon^{112/110}$Cd in the Southern Ocean (1.21 ± 0.36) and North Pacific (1.14 ± 0.37) deepwater $\varepsilon^{112/110}$Cd, the accumulated Cd in the subarctic North Pacific must have an $\varepsilon^{112/110}$Cd lying between -1.75 and +3.61. This range on the estimated accumulated Cd is inflated due to the arithmetic mean 2SD, which is much larger than both the 2σ error for single measurements (approximately ± 0.2 for the Southern Ocean and ± 0.15 for the subarctic North Pacific) and the 2σ error around weighted deepwater mean values. Weighted means for the Southern Ocean ($\varepsilon^{112/110}$Cd = 1.219 ± 0.033) and subarctic northeast Pacific ($\varepsilon^{112/110}$Cd = 1.130 ± 0.0230) constrain the accumulated $\varepsilon^{112/110}$Cd to be between 0.65 and 1.05 (see supplemental section D.7, Table D.5). As accumulated dissolved Cd in the

subarctic North Pacific is likely derived from remineralization of sinking biogenic particles, which are expected to be light relative to surface water, this relatively narrow $\varepsilon^{112/110}$Cd range suggests that remineralized Cd in these particles must have an $\varepsilon^{112/110}$Cd slightly lighter than Pacific deepwater $\varepsilon^{112/110}$Cd.

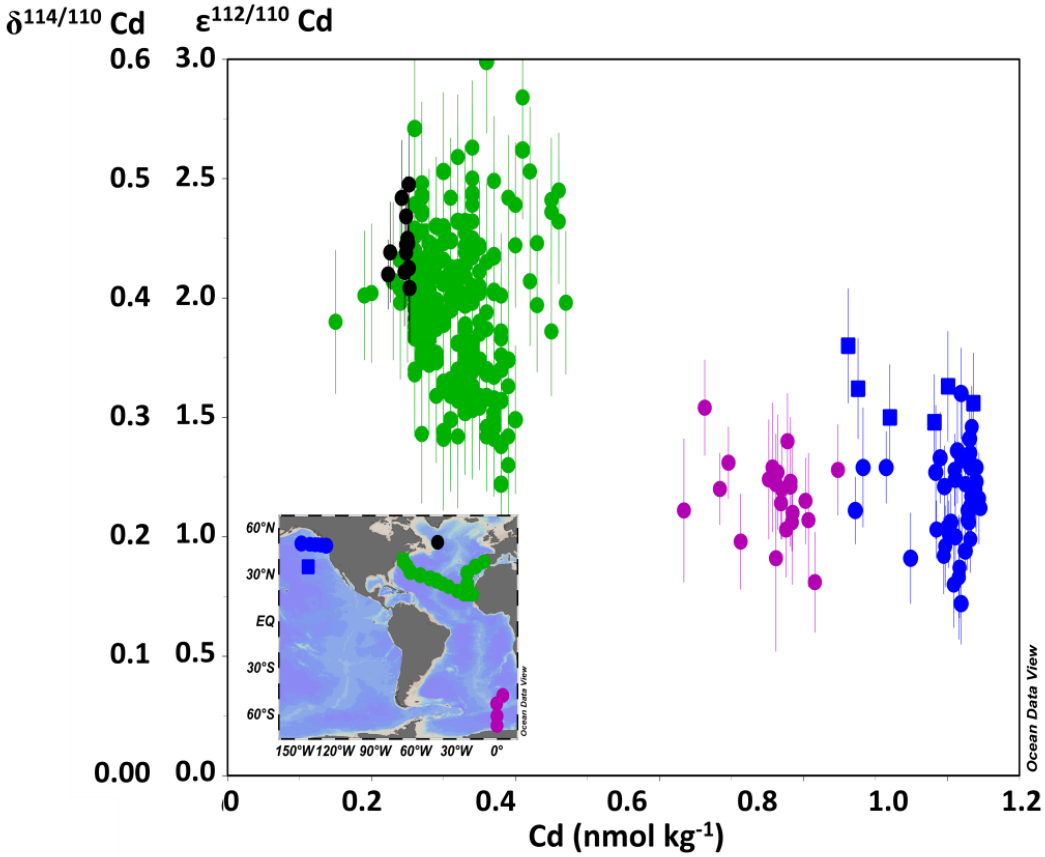

Figure 4.7 Global deepwater $\varepsilon^{112/110}$Cd and [Cd] distributions
Data shown are from below 1000 m depth. Southern Ocean data are shown in purple circles (Abouchami et al., 2014). Atlantic data are shown in green squares (Conway and John 2015a). Pacific data are shown in blue circles (this study) and blue squares (Conway and John, 2015b). Station locations are shown in the inset map.

4.6 Conclusions

Dissolved Cd is depleted relative to PO_4^{3-} at low [O_2] along the Line P transect as shown by concentration depth profiles and the derived tracer Cd*. Similar observations in the Pacific (Janssen et al., 2014 / Chapter 2; Conway and John 2015b) and in other O_2-depleted regions

(Waeles et al., 2013; Janssen et al., 2014 / Chapter 2; Conway and John, 2015a; Xie et al., 2015) have been attributed to removal of dissolved Cd by the formation of insoluble sulphides in association with sinking particles in low-O_2 water. The Cd depletion we observe is consistent with such a hypothesis. The lack of a resolvable $\varepsilon^{112/110}$Cd shift in the O_2-depleted North Pacific (this study; Conway and John, 2015b) indicates that the process causing Cd depletion either does not generate any $\varepsilon^{112/110}$Cd fractionation or that the isotope effect is too small to be resolved due to the large inventory of dissolved [Cd] in the Pacific. This 'missing' Cd is constrained to $\varepsilon^{112/110}$Cd > -0.37, or a seawater-removal term fractionation factor $\alpha_{sw\text{-}removed} \leq 1.00016$. The calculated isotopic composition of the putative sulfide removal term is within the range previously reported for marine Cd sulfides (Schmitt et al., 2009a). An analysis of suspended or sinking particulate material in the O_2-depleted northeast Pacific would help to confirm if a water column removal process is taking place and, if so, if this is associated with a resolvable $\varepsilon^{112/110}$Cd fractionation. Laboratory studies involving the formation metal sulfides could help to constrain the isotopic fractionation of seawater Cd sulfide formation.

The dissolved depth profiles of [Cd] and $\varepsilon^{112/110}$Cd show biologically-driven cycling with low [Cd] and elevated $\varepsilon^{112/110}$Cd in surface waters. Samples with [Cd] > 0.1 nmol kg^{-1} fit a closed-system Rayleigh fractionation model with a fractionation factor (α) of 1.0002, in agreement with previous studies from the HNLC Southern Ocean (Abouchami et al., 2011; Xue et al., 2013). However, $\varepsilon^{112/110}$Cd values do not increase further with decreasing [Cd] below 0.1 nmol kg^{-1}, as would be predicted from a simple closed-system Rayleigh fractionation model. Instead our 2014 surface data feature relatively low $\varepsilon^{112/110}$Cd, deviating from the Rayleigh fractionation line, demonstrating that the closed-system model is inadequate for explaining $\varepsilon^{112/110}$Cd in low [Cd] waters, at least in the subarctic northeast Pacific. Here, surface biological uptake of Cd may induce a different isotopic fractionation at very low [Cd].

Subarctic northeast Pacific deepwater $\varepsilon^{112/110}$Cd is remarkably consistent along the transect, suggesting its $\varepsilon^{112/110}$Cd signature is nearly uniform. The arithmetic mean deepwater $\varepsilon^{112/110}$Cd of the northeast Pacific is indistinguishable, within error, from that of Southern Ocean deepwater and the weighted means, while distinguishable, are nearly identical. This supports the hypothesis that deepwater $\varepsilon^{112/110}$Cd largely reflects the signature of its source, and therefore can be used as a tracer of ocean circulation and mixing (Abouchami et al., 2014). Some fine-

scale $\varepsilon^{112/110}$Cd variability may exist in deep North Pacific waters, for example between the subtropical North Pacific (the SAFe site, Conway and John, 2015b) and the subarctic northeast Pacific (this study), and warrants further attention. There is good agreement among laboratories regarding global deepwater $\varepsilon^{112/110}$Cd values; however, significant differences are observed in surface samples at very low [Cd] in both the North Pacific (this work compared to Conway and John, 2015b and Ripperger et al., 2007) and the Atlantic (Xie et al., in revision compared to Conway and John 2015a; Ripperger et al., 2007; Xue et al., 2012). There is an urgent need for a laboratory intercalibration of low [Cd] samples to determine if the observed differences in $\varepsilon^{112/110}$Cd at very low [Cd] (< 0.01 nmol kg^{-1}) reflect true natural variability in surface waters.

Chapter 5

Particulate cadmium concentrations and stable isotopes in the subarctic northeast Pacific

5.1 Abstract

The distribution of dissolved cadmium (dCd) strongly correlates with that of algal nutrients like phosphate (PO_4^{3-}) in the global ocean. This empirical observation implies a distribution controlled by association with biogenic particles through uptake of dCd in surface waters and regeneration of particulate Cd (pCd) at depth. Depth profiles of dCd stable isotope composition ($d\varepsilon^{112/110}Cd$), while sparse in coverage, exist for most of the major ocean basins, with spatial coverage improving through the efforts of the GEOTRACES program (e.g. GEOTRACES Atlantic transects GA02 and GA03, Southern Ocean transect ANT XXIV/3 and Pacific cruise IC2). However, particulate $\varepsilon^{112/110}Cd$ ($p\varepsilon^{112/110}Cd$) depth profiles with a resolution approaching that for the dissolved phase are lacking, placing restrictions on our application of stable isotope information to better understand Cd cycling in the global ocean. Here we present two $p\varepsilon^{112/110}Cd$ depth profiles from the subarctic northeast Pacific which demonstrate more complicated $\varepsilon^{112/110}Cd$ cycling than dissolved profiles would suggest. Surface $p\varepsilon^{112/110}Cd$, while lighter than surface dissolved $\varepsilon^{112/110}Cd$ ($d\varepsilon^{112/110}Cd$), is heavy relative to Pacific deepwater and crustal $p\varepsilon^{112/110}Cd$ components. Particulate $\varepsilon^{112/110}Cd$ becomes lighter as pCd is remineralized in the nutricline, reaching a minimum $p\varepsilon^{112/110}Cd$ of around -2.5, among the lightest values reported in natural telluric samples. In our sample set, it is not the formation of especially light $p\varepsilon^{112/110}Cd$ in surface biogenic particles but the modification of $p\varepsilon^{112/110}Cd$ with depth in the nutricline which results in the retention of heavy $d\varepsilon^{112/110}Cd$ in surface waters, explaining the surface-deep $d\varepsilon^{112/110}Cd$ gradient. Isotopically light $p\varepsilon^{112/110}Cd$ in intermediate depths may act as an important oceanic sink, helping to balance the known sources ($\varepsilon^{112/110}Cd$ ~0 in bulk continental crust, +0.5 to +1.5 in Siberian river flux) and sinks with the global deepwater

inventory, which has an isotopic composition of roughly +1.1 in the Pacific and +2.4 in the North Atlantic. At intermediate depths, $d\varepsilon^{112/110}Cd$ profiles show uniform isotope composition while calculated remineralized $p\varepsilon^{112/110}Cd$ is isotopically variable and distinct from the bulk dissolved pool. Our data are inconsistent with both closed system Rayleigh and open system models of Cd cycling in surface waters but are consistent with advected Southern Component Water controlling $d\varepsilon^{112/110}Cd$ in intermediate and deep North Pacific waters.

5.2 Introduction

The oceanic distribution of cadmium (Cd) reflects a biological control with uptake in surface waters and elevated concentrations at depth due to remineralization of sinking particulate matter. Dissolved Cd shows a strong correlation with phosphate (PO_4^{3-}) in the global ocean (Boyle et al., 1976; Bruland et al., 1978), although there is regional variability in dissolved Cd:PO_4^{3-} trends among ocean basins (de Baar et al., 1994). Biological uptake of Cd:PO_4^{3-} is known to vary across phytoplankton taxa (Ho et al., 2003) as well as within species due to environmental factors, which likely contribute to regional and basin-scale variability in dissolved Cd:PO_4^{3-} (e.g. Cullen et al., 2006; Lane 2009; Quay et al., 2015). Within species, Cd:P content of phytoplankton can be modulated by carbon dioxide concentrations and antagonistic relationships between Cd and metals such as iron (Fe), zinc (Zn), cobalt (Co) and manganese (Mn) through non-specific uptake of divalent metals (e.g. Sunda and Huntsman, 2000; Cullen and Sherrell, 2005) and the activity of Cd in carbonic anhydrase enzymes (Price and Morel, 1990; Lane and Morel, 2000). Regional variability in subsurface particulate Cd:P may reflect variability in exported Cd:P as well as decoupling in Cd:P remineralization in sinking particulates, potentially due to Cd retention or capture via sulphide formation in anoxic microenvironments in oxygen (O_2) depleted waters (e.g. Chapter 2 / Janssen et al., 2014; Conway and John, 2015a; Waeles et al., 2016).

Cadmium stable isotope composition ($\varepsilon^{112/110}Cd$), presented as the deviation of $^{110}Cd/^{112}Cd$ in parts per ten thousand relative to the NIST SRM-3108 reference material (Abouchami et al., 2012; see Equation 5.1 in section 5.2.3), can be used to track biological, chemical and physical cycling of Cd in the marine environment. Depth profiles for dissolved $\varepsilon^{112/110}Cd$ ($d\varepsilon^{112/110}Cd$) show elevated values in surface water, suggesting biological uptake of

light Cd isotopes, and lower values at depth (e.g. Lacan et al., 2006; Ripperger et al., 2007). Culture studies (Lacan et al., 2006, a freshwater alga; John and Conway, 2014, a marine chlorophtye) and field samples (S.C. Yang et al., 2015) have confirmed that biological Cd uptake can result in an enrichment of light Cd in the particulate phase. This fractionation during uptake has led to a potential role for $\varepsilon^{112/110}$Cd in marine sediments as a tracer of paleoceanographic productivity (Georgiev et al., 2015; Hohl et al., 2017), though some uncertainty remains regarding the fractionation from biological Cd uptake (Table D.4 and Figures 4.4 and 4.5; *cf.* Ripperger et al., 2007; Abouchami et al., 2011; Gault-Ringold et al., 2012; Xue et al., 2012; Yang et al., 2012; Conway and John, 2015a; Conway and John, 2015b; S.C. Yang et al., 2015; Chapter 4 / Janssen et al., in revision; Xie et al., in revision). Cadmium release from degrading biological particles has been shown to proceed either without isotopic fractionation (John and Conway, 2014, culture study) or with an inferred a release of light Cd based on the enrichment of heavy isotopes in sinking particulates (S.C. Yang et al., 2015, South China Sea sediment trap samples).

A distinct geographic trend in global deepwater $d\varepsilon^{112/110}$Cd is observed with elevated $d\varepsilon^{112/110}$Cd in North Atlantic deep waters and lower $d\varepsilon^{112/110}$Cd in Southern Component Water (SCW) (e.g. Ripperger et al., 2007; Xue et al., 2013; Abouchami et al., 2014; Conway and John, 2015a; Conway and John, 2015b; Chapter 4 / Janssen et al., in revision; Xie et al., in review), showing utility of $d\varepsilon^{112/110}$Cd as a tracer of deepwater circulation. The sequestration of dissolved Cd into particulate phases during the formation of ferromanganese crusts (Schmidt et al., 2009a; Horner et al., 2010) results in no discernable isotopic fractionation and therefore particulate Cd reflects the isotopic composition of ambient seawater in which the minerals were formed. This presents potential paleoceanographic utility for $\varepsilon^{112/110}$Cd as a tracer of water masses. While Cd may be incorporated into certain mineral phases without fractionation, enrichment of light isotopes in the particulate phase of sulphides is found in natural samples (Schmitt et al., 2009a; Abouchami et al., 2015) and theoretical calculations (J. Yang et al., 2015) for Cd sulphide formation in hydrothermal vent systems. Zinc behaves similarly in vent systems, with light isotopes enriched in the particulate phase relative to ambient water (John et al., 2008).

As Cd is a biologically-controlled element in the global ocean, understanding the isotopic composition and magnitude of Cd fluxes from the surface ocean are key to understanding the oceanic Cd cycle. The bulk of marine solid-phase $\varepsilon^{112/110}$Cd data have been collected on marine sediments, terrestrial deposits of marine origin, or in laboratory-based studies. Comparatively few data exist for suspended and sinking marine particles (5 depths from the North Atlantic, Chapter 2 / Janssen et al., 2014 and Conway and John, 2015a; 5 distinct size classes of surface particle samples and 3 depths of sinking particulates at 4 time points, S.C. Yang et al 2015) (a global compilation of all suspended and sinking marine $p\varepsilon^{112/110}$Cd) data is presented in Table E.1). Measurements of the isotopic composition of suspended and sinking particles show promise in helping to answer outstanding questions in the current understanding of the marine Cd cycle, including: 1) the nature of biological fractionation in surface waters (as presented in Chapter 4, sections 4.5.2.2 and 4.5.3, Figure 4.5); 2) determining the mechanism driving the recently discovered dCd sink terms in low O_2 water columns (*cf*. Chapter 2 / Janssen et al., 2014; Ohnemus et al., 2016); and 3) resolving an imbalance in global ocean $d\varepsilon^{112/110}$Cd between sources (bulk silicate earth $\varepsilon^{112/110}$Cd of approximately -0.3 ± 0.5 and bulk continental crust $\varepsilon^{112/110}$Cd = -0.05 ± 0.2, Schmitt et al., 2009a as presented in Rehkämper et al, 2012; Arctic river flux $d\varepsilon^{112/110}$Cd = +0.5 to +1.5, Lambelet et al., 2013) and global deepwater ($d\varepsilon^{112/110}$Cd = +1.1 to +2.4; Ripperger et al., 2007; Boyle et al., 2012; Abouchami et al., 2014; Conway and John, 2015a; Conway and John, 2015b; Chapter 4 / Janssen et al., in revision; Xie et al., in revision) by determining the isotopic composition and magnitude of sink terms. Recent advancements have been made by analysis and compilation of source terms (riverine flux, rainwater) and sink terms (marine sediments and particulates) to address similar isotopic imbalances in the global Cu (e.g. Little et al., 2014; Takano et al., 2014) and Zn (e.g. Little et al., 2014; Little et al., 2016; Vance et al., 2016) cycles. Here we present high resolution particulate Cd (pCd) and $p\varepsilon^{112/110}$Cd depth profiles from two stations along Line P in the subarctic northeast Pacific to further the understanding of Cd biogeochemical cycling in these areas.

5.3 Methods

Data in this manuscript are discussed as $\varepsilon^{112/110}$Cd relative to NIST SRM-3108, though figures include units of both $\varepsilon^{112/110}$Cd and $\delta^{114/110}$Cd relative to NIST SRM-3108. These two units are interconverted by the factors presented in Table 1.4 (interconversion values Abouchami et al. (2012)). Any literature data discussed in this manuscript which were originally referenced to another isotopic standard or presented in another unit have been converted to $\varepsilon^{112/110}$Cd and/or $\delta^{114/110}$Cd relative to the reference standard NIST SRM-3108 by the conversion factors reported in Abouchami et al. (2012).

5.3.1 Sample Sites

The Line P transect (Figure 5.1) begins in the waters of the British Columbia continental shelf in a coastal environment and extends ~1600 km westward into the open subarctic Northeast Pacific to Ocean Station PAPA/P26. A permanent halocline is found along the transect at 100-150 m, constraining the depth of winter mixing (Crawford et al., 2007). Lower nutrient concentrations and high productivity are found in coastally influenced waters at the eastern end of the transect (Peña and Varela, 2007) while offshore stations are found in a High-Nutrient Low Chlorophyll (HNLC) region characterized by chronic iron (Fe) limitation (e.g. Martin et al., 1989). Line P covers a region with a substantial expanse of low-O_2 subsurface waters with O_2 concentrations which decrease toward the continental shelf. Oxygen concentrations drop below 50 μmol kg^{-1} at around 300-400 m depth, reaching a minimum of 10-20 μmol kg^{-1} near 1000 m and not exceeding 50 μmol kg^{-1} until near 2000 m depth (CTD data from Line P cruises are available at www.waterproperties.ca/linep/; see also Figure 4.1 / Figure 1, Janssen et al., in revision). Cadmium data are available along Line P or regionally in the subarctic northeast Pacific for dissolved Cd (dCd) depth profiles (Martin et al., 1989; Chapter 4 / Janssen et al., in revision), $d\varepsilon^{112/110}$Cd depth profiles (Chapter 4 / Janssen et al., in revision) and pCd to a depth of 200 meters (Martin et al., 1989). See Figure 5.1 for locations of these previous data.

The Line P transect was sampled during cruise 2014-19 (August 2014) for suspended particulates at two stations representing the coastally-influenced (P4 at 48.65°N, 126.67°W; bottom depth roughly 1320 m) and open ocean (P26 at 50.0°N 145.0°W, bottom depth roughly

4300 m) ends of the transect. Note that while $d\varepsilon^{112/110}Cd$ are available for the transect, the only 2014 $d\varepsilon^{112/110}Cd$ data which overlap with our particulate samples are surface samples from P4. All other $d\varepsilon^{112/110}Cd$ data from P4 and P26 were collected in either 2012 or 2013. Beginning in winter 2013, a high pressure system caused decreased winter heat loss and weakened cold water advection, resulting in a warm-water anomaly colloquially termed 'The Blob'. This feature was present from surface waters to a depth of around 100 m in the subarctic northeast Pacific (Bond et al., 2015). These conditions decreased winter mixing, persisted from winter 2013 through at least 2015 (Peterson et al., 2016), and were coincident with anomalies in physical, chemical, and biological conditions. These surface water anomalies included decreased macronutrient (Chandler et al., 2015) and dCd (Chapter 4 / Janssen et al., in revision) concentrations as well as altered phytoplankton community composition and reproductive dynamics (Chandler et al., 2015). Our samples were collected in August 2014 and therefore surface samples were taken from the 'Blob' waters.

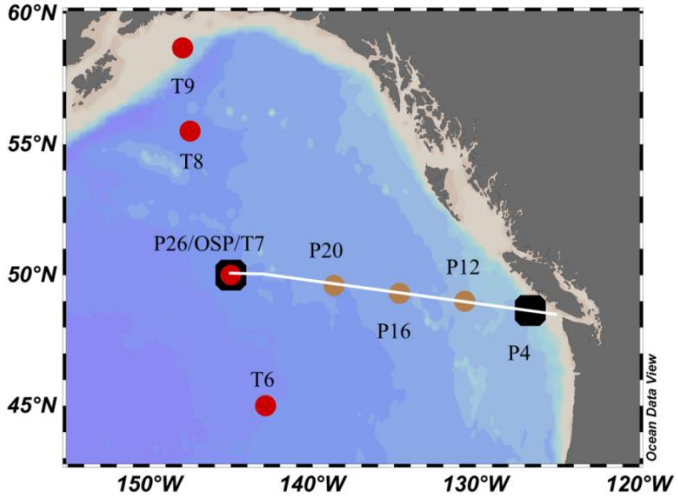

Figure 5.1 Map of subarctic northeast Pacific
The Line P transect is shown in white with major stations labeled. Stations for which particulate samples were collected (P26 and P4) are shown as black squares. Stations of relevant literature data are also shown. The VERTEX T transect is shown as red dots. Data for pCd (upper 200 m only) and dCd are available for these stations (Martin et al., 1989). For Line P, shown as tan dots or black squares, $d\varepsilon^{112/110}Cd$ and dCd are available and are presented in Chapter 4 (Janssen et al., in revision).

5.3.2 Sample Collection

Particulate samples (0.8-51 μm) were collected with in-situ large volume pumps (WST-LV, McLane) modified for dual flow (see Cutter et al., 2010; Lam and Morris, 2013). Sampling

heads were equipped with doubled 142 mm 0.8 μm polysulfone Supor^{TM} filters below 51 μm polyester prefilters, giving a 0.8-51 μm size fraction on the filters. Note that this sampling method and size restriction on our samples will influence the characteristics of our particles class. McLane pumps are known to under-sample large particles (Bishop et al., 2012), so the size restriction may result in a more representative collection of the available size class. However, our smaller sample size class and collection methodology will combine suspended, or more neutrally buoyant particles, along with smaller sinking particles, both of which may include living microbes. Therefore our size class and methodology will influence the degree to which our samples can be compared to other particulate samples collected by the same methods (Chapter 2/Janssen et al., 2014; Conway and John, 2015a) or with sediment traps (Yang et al., 2012; S.C. Yang et al., 2015).

Filters were acid cleaned prior to use following Cutter et al. (2010). The pumps were deployed on a stainless line wrapped with duct tape in the region of the pump to minimize potential influence from the line (P. Lam, UC Santa Cruz, personal communication). Pumping times varied from 2-4 hours, depending on anticipated particle loading, at an initial rate of 8 L min^{-1}. Flow through the filter head was monitored with a flow meter and was generally 500 L or more, except in surface waters. Filters for blank analyses (termed "dipped blanks") were placed in a perforated acid cleaned plastic container which was attached to the frame of a pump and deployed with the pump. Sample filters were stored frozen until subsampling and analysis (roughly 18 months).

One dCd sample (P26 50 m cruise 2014-19) is presented here for the first time. The dissolved sample was collected using GO-FLO bottles mounted on a trace metal clean rosette as described in section 4.3.

5.3.3 Sample Processing and Analysis

Filter subsamples were cut from the top filter only and were digested in sealed acid-cleaned Teflon vials for 4 hours at 80° C with a mixture of 90% 16 mol L^{-1} nitric acid (HNO_3) and 10% 29 mol L^{-1} hydrofluoric acid (HF) (e.g. 1.35 mL 16 mol L^{-1} HNO_3 + 0.15 mL 29 mol L^{-1} HF) (modified from Sherrell and Boyle, 1992; Cullen and Sherrell, 1999; referred to hereafter as HNO_3 digest). The exact size of the subsample, and therefore digest volume, was

varied to obtain roughly 10 ng Cd in the subsample based on preliminary ICP-MS data. The digest solution was transferred to a new beaker and the remaining filter was rinsed with 2×3 ml aliquots of 18.2 MΩ water, which were collected with the digest. Combined digest and rinse solutions were spiked with a ^{106}Cd-^{108}Cd double spike (Schmitt et al., 2009b) and dried overnight. Dried digests were acidified and re-dried two times with a 200 µL aliquot of 16 mol L^{-1} HNO_3, followed by a conversion first to chloride form by spiking with 150 µL 12 mol L^{-1} hydrochloric acid (HCl) (sub-boiling distilled) and drying, and then converted to bromide form by spiking with 150 µL 8.5 mol L^{-1} hydrobromic acid (HBr, sub-boiling distilled) and drying.

Dried digests in HBr form were processed through two identical steps of column purification in 100 µL 4:1 shrink fit PFA columns with AG1-X8 resin (100-200 mesh, Bio-Rad) as described in Schmidt et al. (2009b). Samples were loaded onto single degassed rhenium filaments and masses ^{106}Cd, ^{108}Cd, ^{110}Cd, ^{111}Cd, ^{112}Cd, ^{113}Cd and ^{114}Cd were analyzed by thermal ionization mass spectrometry (TIMS) with a Thermo-Fisher Triton. A double-spiked aliquot of the consensus reference standard NIST-3108 (Abouchami et al., 2012) was analyzed with every set of samples. The double-spike reduction algorithm was used offline with the exponential law to correct data for mass bias. Measured $^{110/112}$Cd ratios were converted to $\varepsilon^{112/110}$Cd notation by the following equation:

$$\varepsilon^{112/110}Cd = \left(\frac{^{110}Cd/^{112}Cd_{NIST\ SRM\ 3108}}{^{110}Cd/^{112}Cd_{Sample}} - 1\right) \times 10{,}000 \qquad \text{(Equation 5.1)}$$

Filter blank subsamples were carried through the same analytical procedure and yielded a blank value of 0.026 pmol Cd cm^{-2} and a detection limit, defined as 3 times the standard deviation of the blank, of 0.1 pmol Cd cm^{-2}. The blank was generally below 1% of our signal, though it was as high as 6% for one sample (P26 1500 m). A small $\varepsilon^{112/110}$C offset was observed with loads of low levels of standard and, when applicable, the measured $p\varepsilon^{112/110}$Cd was corrected with this offset (see Table D.1 / Janssen et al., in revision Table A.1). A pCd error of 10% has been applied following Conway and John (2015a), to encompass errors in subsampling and analysis.

The dCd sample was pre-concentrated offline using an SC4-DX sea*FAST* pico System (Elemental Scientific) following Lagerström et al. (2013) and analyzed on an 8800 ICP-MS Triple Quad (Agilent Technologies). The dissolved datum is courtesy of Sarah Jackson.

Date	Station	Digest	Depth	$p\varepsilon^{112/110}Cd$	Error	$p\delta^{114/110}Cd$	Error	pCd
			m		2σ		2σ	nmol kg^{-1}
14-Mar-16	P4	HCl	25	1.10	0.42	0.22	0.084	35.2
14-Mar-16	P4	HNO_3	25	1.68	0.30	0.36	0.060	35.7
14-Mar-16	P4	H_2O_2+HCl	25	2.27	0.39	0.45	0.078	22.7
07-Mar-16	P4	HNO_3	75	0.22	0.77	-0.04	0.154	7.1
07-Mar-16	P4	HCl	75	-0.64	0.23	-0.13	0.046	4.8
10-Mar-16	P4	HCl	75	-0.47	0.23	-0.094	0.046	7.7
10-Mar-16	P4	HNO_3	75	-0.19	0.84	-0.038	0.168	7.3
10-Mar-16	P4	H_2O_2+HCl	75	-0.44	0.39	-0.088	0.078	10.1
10-Mar-16	P4	HNO_3 from HCl	75	NA	NA	NA	NA	0.0
14-Mar-16	P4	H_2O_2 from HNO_3	25	NA	NA	NA	NA	-0.2
14-Mar-16	P4	H_2O_2 from HCl	25	NA	NA	NA	NA	-0.1

Table 5.1 Filter digestion method comparison
Particulate $\varepsilon^{112/110}Cd$ and pCd from subsamples of the same filter samples (P4 25 m and P4 75 m). Date refers to date of analysis. Digest procedures are outlined in section 5.3.1. Note that all initial digests (HNO_3, HCl, H_2O_2+HCl) contained HF. HNO_3 from HCl is a secondary HNO_3 digest of a filter processed through an HCl digestion. H_2O_2 from HNO_3 and H_2O_2 from HCl are secondary H_2O_2+HCl digests of filters already processed through HNO_3 or HCl digestions.

5.4. Results and Discussion

5.4.1 Digest procedure and reproducibility

Multiple digestion procedures were investigated before deciding on the HNO_3 digest (Table 5.1). Overnight digests with a mixture composed of 90% 12 mol L^{-1} HCl and 10% 29 mol L^{-1} HF (termed HCl digest) yielded equivalent $p\varepsilon^{112/110}Cd$ to HNO_3 digests within a 2σ error. Overnight digests with a mixture of 87.5% 12 mol L^{-1} HCl, 7.5% 29 mol L^{-1} HF and 5% hydrogen peroxide (termed HCl + H_2O_2 digest) attacked the filter in such a way that samples were difficult to process, but also gave $p\varepsilon^{112/110}Cd$ equivalent to HNO_3 digests within a 2σ error. Both HCl and HCl+ H_2O_2 digestions yielded greater variability in pCd (Table 5.1), although re-

digestion of an HCl digested filter with HNO_3 and re-digestion of HCl and HNO_3 digested filters with $HCl+H_2O_2$ (4 hours only) did not recover additional pCd from the filters. Replicate analysis of one sample with the HNO_3 digest gave reproducible pCd and $p\varepsilon^{112/110}Cd$ (P4 75 m, Table 5.1). For workflow reasons and for consistent pCd, the HNO_3 digest was used to process the remainder of the samples. We present only the HNO_3 digest data in tables, figures and for further discussion.

Station	**Lat**	**Long**	**Size Fraction**	**Depth**	**$p\varepsilon^{112/110}Cd$**	**2σ**	$p\delta^{114/110}$**Cd**	**2σ**	**pCd**	**pCd error**
	°N	**°W**		**M**					**pM**	**pM**
P26	50	145	0.8-51 μm	50	2.71	0.14	0.543	0.028	37.59	3.76
P26	50	145	0.8-51 μm	100	-0.84	0.29	-0.169	0.058	6.96	0.70
P26	50	145	0.8-51 μm	150	-2.52	0.37	-0.504	0.074	3.56	0.36
P26	50	145	0.8-51 μm	200	-2.25	0.60	-0.450	0.121	1.61	0.16
P26	50	145	0.8-51 μm	300	-2.52	0.45	-0.504	0.089	1.65	0.16
P26	50	145	0.8-51 μm	400	-2.64	0.27	-0.529	0.054	0.91	0.09
P26	50	145	0.8-51 μm	500[1]	-2.54	0.23	-0.508	0.045	0.98	0.10
P26	50	145	0.8-51 μm	500[2]	-2.07	0.20	-0.415	0.040	1.08	0.11
P26	50	145	0.8-51 μm	600	-2.25	0.29	-0.450	0.058	0.60	0.06
P26	50	145	0.8-51 μm	800	-2.15	0.27	-0.430	0.054	0.28	0.03
P26	50	145	0.8-51 μm	1000	-1.06	0.64	-0.212	0.128	0.28	0.03
P26	50	145	0.8-51 μm	1250	-1.09	0.74	-0.218	0.149	0.18	0.02
P26	50	145	0.8-51 μm	1500	0.27	0.85	0.054	0.171	0.07	0.01
P4	48.65	126.7	0.8-51 μm	25	1.68	0.30	0.335	0.059	35.75	3.57
P4	48.65	126.7	0.8-51 μm	75‡	-0.19	0.84	-0.037	0.167	7.29	0.73
P4	48.65	126.7	0.8-51 μm	75‡	0.22	0.77	0.043	0.154	7.06	0.71
P4	48.65	126.7	0.8-51 μm	150	-1.63	0.24	-0.325	0.048	4.36	0.44
P4	48.65	126.7	0.8-51 μm	300	-2.44	0.20	-0.487	0.040	2.62	0.26
P4	48.65	126.7	0.8-51 μm	400	-2.41	0.39	-0.482	0.079	0.72	0.07
P4	48.65	126.7	0.8-51 μm	500	-2.35	0.21	-0.471	0.042	1.21	0.12
P4	48.65	126.7	0.8-51 μm	600	-2.25	0.17	-0.450	0.034	0.85	0.09
P4	48.65	126.7	≥ 0.8 μm	800*	-0.86	0.20	-0.171	0.039	0.70	0.07
P4	48.65	126.7	0.8-51 μm	1000†	-1.18	0.27	-0.237	0.054	0.88	0.09
P4	48.65	126.7	0.8-51 μm	1250	-1.66	0.40	-0.332	0.079	0.16	0.02

Table 5.2 Line P 2014 particulate $\varepsilon^{112/110}Cd$ and pCd data

[1] = P26 pump cast 1. [2] = P26 pump cast 2. ‡= Duplicates are duplicate subsamples of one sample. *This sampling head was missing the 51 um prefilter on this deployment, therefore the sample is both the 0.8-51 μm and the > 51 μm size fractions. †This sampling head was deployed with only a single filter rather than a doubled filter on this deployment.

5.4.2 pCd and $p\varepsilon^{112/110}Cd$ in the surface ocean

Particulate samples collected from the upper 50 m are isotopically lighter than dissolved samples collected from the same depths (Figure 5.2; Table 5.2; Chapter 4 / Janssen et al., in revision), supporting laboratory (Lacan et al., 2006; John and Conway, 2014) and field (Yang et al., 2012; Chapter 2 / Janssen et al., 2014; Conway and John, 2015a; S.C. Yang et al., 2015) studies showing preferential uptake of isotopically light Cd by marine phytoplankton. While our surface particulates are lighter than surface dCd, they are heavier than both subsurface $p\varepsilon^{112/110}Cd$ from the same 2014 profiles and $d\varepsilon^{112/110}Cd$ samples from the same stations collected in 2012 along Line P (Chapter 4 / Janssen et al., in revision). The generation of heavy surface $p\varepsilon^{112/110}Cd$ may be due to pCd formation from dCd following a closed-system Rayleigh model in a low [dCd], isotopically heavy $d\varepsilon^{112/110}Cd$ pool. Indeed our P4 25 m $d\varepsilon^{112/110}Cd$ and $p\varepsilon^{112/110}Cd$ data appear to fit a Rayleigh model with a fractionation factor (α) of 1.0001 (Figure E.1). However, this may be coincidental as other samples from surface waters at P4 in 2014 do not follow this same fractionation factor. Furthermore it is clear that overall the Rayleigh model does not represent the 2014 $d\varepsilon^{112/110}Cd$ composition of subarctic northeast Pacific surface waters (Figure 4.4 / Janssen et al., in Revision Figure 4) and a Rayleigh model is unable to explain surface $p\varepsilon^{112/110}Cd$ at station P26 under previously reported fractionation factors (Abouchami et al., 2011; Xue et al., 2013) (Figure E.1). Therefore, while uptake under a closed-system Rayleigh model may appear to explain $p\varepsilon^{112/110}Cd$ at P4 25 m, this is unlikely to be the result of a representative causal relationship along Line P with biological uptake incorporating dCd at $\alpha = 1.0001$. Additional mechanisms which may result in a surface $p\varepsilon^{112/110}Cd$ that is heavy with respect to deepwater include biological uptake of unfractionated or minimally fractionated Cd from the heavy surface $d\varepsilon^{112/110}Cd$ pool, adsorption of unfractionated or minimally fractionated heavy surface $d\varepsilon^{112/110}Cd$ onto surface particles, or an external pCd source to the surface ocean.

Based on to the available $p\varepsilon^{112/110}Cd$ data from terrestrial samples, which are enriched in light isotopes relative to ocean water (Schmitt et al., 2009a), the heavy surface $p\varepsilon^{112/110}Cd$ we observe is unlikely to be due to a heavy pCd source to the surface ocean. Organically complexed Zn and adsorbed Zn are heavy with respect to the dissolved pool (John et al., 2008; John and Conway, 2014); however, John et al. (2014) found that Cd adsorbed to degrading cells

was either slightly lighter than or equal to the isotopic composition of the dissolved pool. Cadmium is not a strongly scavenged element (Balistrieri et al., 1981; Bruland, 1980; Boyle et al., 1981; John and Conway, 2014) and therefore it is unlikely that adsorbed Cd is a dominant component of pCd. Our surface $p\varepsilon^{112/110}Cd$ observations are thus likely a signal of Cd uptake or a combination of scavenged and internalized Cd which results in a net dissolved to particulate Cd transfer with only a small isotopic fractionation. Note however that Cd may be susceptible to specific adsorption onto cells with a high abundance of surface binding and transport proteins. See section 5.4.4.2 for further discussion.

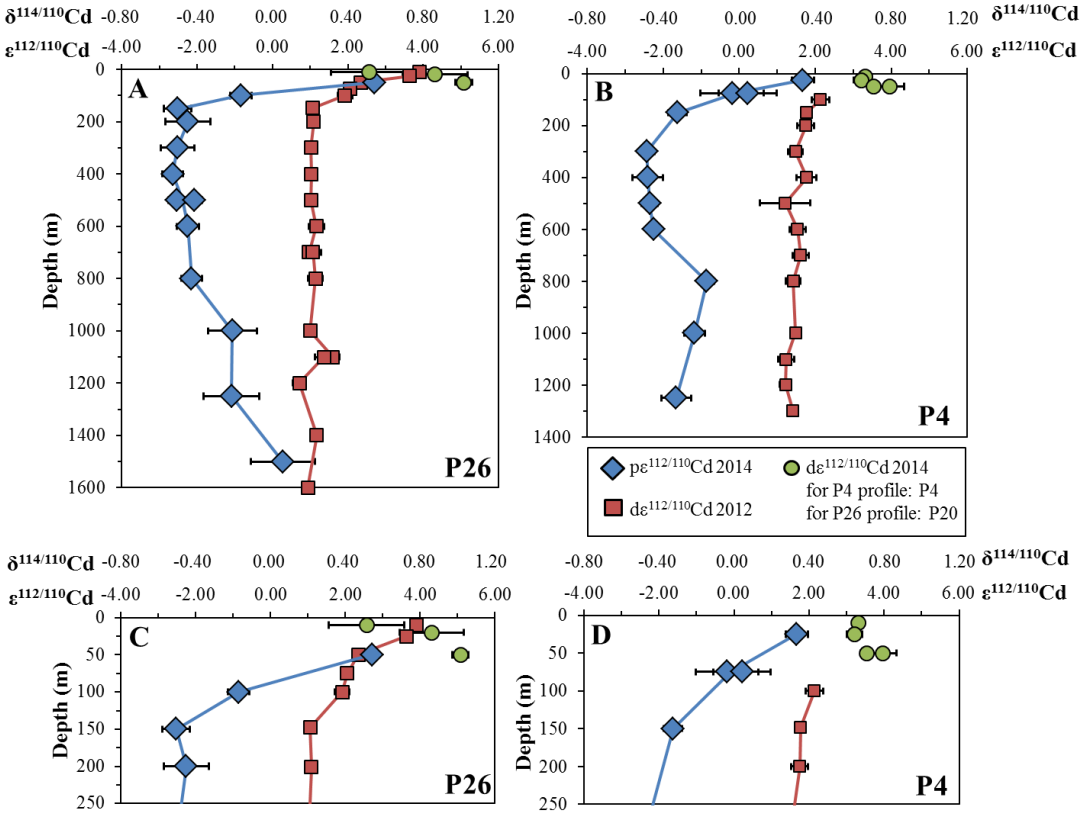

Figure 5.2 Depth profiles of $p\varepsilon^{112/110}Cd$ and $d\varepsilon^{112/110}Cd$ from the subarctic northeast Pacific
Panels A (full profile) and C (surface to 250 m) show profiles from station P26 and panels B (full profile) and D (surface to 250) show profiles from station P4. Particulate $\varepsilon^{112/110}Cd$ are shown as blue diamonds with a solid blue line, which in the case of duplicate analyses from one depth, follows the average while both measurements are shown in symbols. Dissolved $\varepsilon^{112/110}Cd$ from August 2012 are shown as red squares and $d\varepsilon^{112/110}Cd$ from August 2014 are shown as green dots. August 2014 $d\varepsilon^{112/110}Cd$ data are unavailable from station P26. The nearest available 2014 surface $d\varepsilon^{112/110}Cd$ data (station P20) are shown in for panels A and C in green dots. Note that dCd is significantly different between P26 and P20 in 2014 (Table D2).

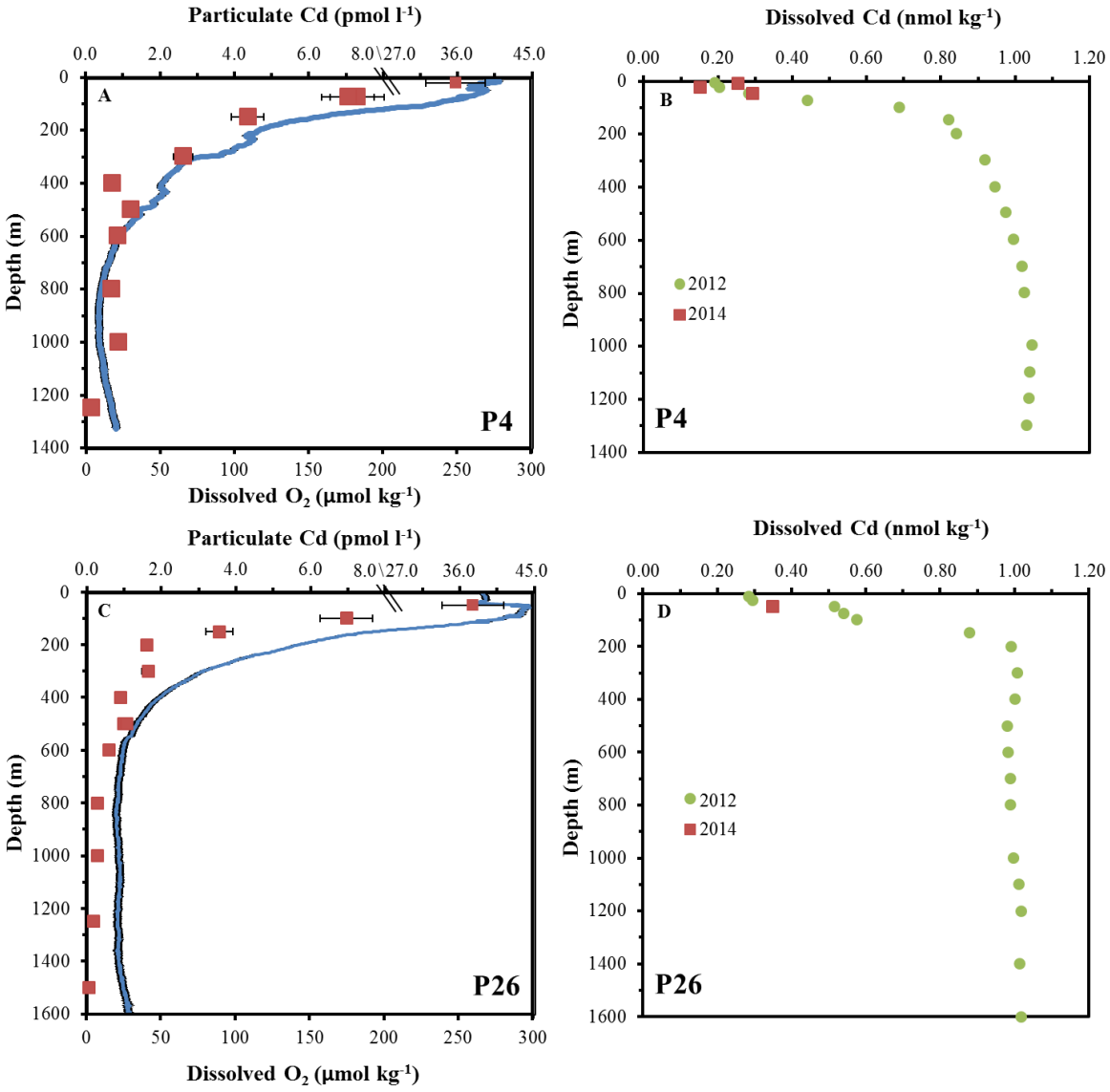

Figure 5.3 Particulate Cd, dissolved O_2 and dissolved Cd depth profiles from Line P
Panels A and C show particulate Cd from 2014 (red squares) and dissolved O_2 from 2014 (blue line). Panels B and D show dissolved Cd from 2012 (green circles) and 2014 (red squares). Particulate Cd profiles are presented with a broken horizontal axis to allow the full profiles to be shown on one plot. The location of the break represents 8 pmol L^{-1} for all data to the left of the break and 27 pmol L^{-1} for the data point to the right of the break. Dissolved O_2, from CTD data calibrated by Winkler titrations, is courtesy of the Line P program, Fisheries and Oceans Canada.

Surface pCd concentrations are high (>30 pmol L^{-1}), which is in agreement with previous reports from the region (Martin et al., 1989). Particulate Cd is rapidly remineralized in the upper water column, with only about 10% of the pCd found in our surface-most samples (50 m at P26 and 25 m at P4) making it to below the permanent halocline and winter mixing depth of 100-150 m (Freeland et al., 1998; Crawford et al., 2007) (Figure 5.3, Table 5.2). This is a more rapid loss of pCd than observed for particulate organic carbon (POC) based on previous work at station P26 (Charette et al., 1999) (see also Martin F curve fits, sections 5.4.3 and 5.4.5; Martin et al., 1987). While surface $p\varepsilon^{112/110}Cd$ is heavy with respect to deep water, $p\varepsilon^{112/110}Cd$ becomes rapidly lighter with depth and $p\varepsilon^{112/110}Cd$ at 150 m is very light. This is in contrast to $p\varepsilon^{112/110}Cd$ reported in sinking particles in the South China Sea, which became heavier with depth in the upper 160 m (S.C. Yang et al., 2015). Therefore in the 0.8-51 um size class, light Cd is preferentially retained in particles with depth, even if surface particles are not light relative to deep water (Tables 5.2 and 5.3). Consequently, in our sample set, it is not the uptake of especially light Cd in the euphotic zone ($p\varepsilon^{112/110}Cd$ = 2.71 ± 0.14 at 50 m at P26 and 1.68 ± 0.30 at 25 m at P4) but the rapid remineralization of heavy Cd and the subsequent export of light $p\varepsilon^{112/110}Cd$ below the winter mixed layer that results in a net removal of light Cd from surface waters and maintains a $d\varepsilon^{112/110}Cd$ which is higher than deepwater (see the simplified schematic in Figure E.2 for a visual representation of this).

5.4.3 pCd and $p\varepsilon^{112/110}Cd$ in subsurface waters

Depth profiles from both stations demonstrate clear $p\varepsilon^{112/110}Cd$ trends (Figure 5.2). In the nutricline while dCd and pCd track inversely to each other, both $p\varepsilon^{112/110}Cd$ and $d\varepsilon^{112/110}Cd$ decrease (Figures 5.2 and 5.3, Table 5.2). Decreasing $d\varepsilon^{112/110}Cd$ with increasing dCd requires that the Cd added to the dissolved phase at these depths be isotopically light relative to the low dCd overlying waters. Therefore the concurrent decrease in $d\varepsilon^{112/110}Cd$ and $p\varepsilon^{112/110}Cd$ is surprising as decreases $p\varepsilon^{112/110}Cd$ requires a loss of heavy Cd from particles. Inferred remineralized $\varepsilon^{112/110}Cd$ in the upper 150 m is comparable to or heavier than $d\varepsilon^{112/110}Cd$ from the same depths in 2012 (Table 5.3). Dissolved $\varepsilon^{112/110}Cd$ data from below 50 m in 2014 are not available for direct comparison to our 2014 particles, and therefore inferred remineralized Cd may be isotopically lighter than $d\varepsilon^{112/110}Cd$ in 2014. However, if $d\varepsilon^{112/110}Cd$ below 50 m is

comparable in 2014 to what was observed in 2012 then remineralization of the 0.8-51 μm particles is unable to explain the dCd and $d\varepsilon^{112/110}Cd$ trends in the upper 150 m.

Station	Depth	$p\varepsilon^{112/110}Cd$	Error	p[Cd]	Inferred Remineralized			
			2σ	pmol L^{-1}	[Cd] (pmol L^{-1})	$\varepsilon^{112/110}Cd$	Max $\varepsilon^{112/110}Cd$	Min $\varepsilon^{112/110}Cd$
P26	50	2.71	0.14	37.59	NA	NA	NA	NA
P26	100	-0.84	0.29	6.96	30.62	3.52	3.76	3.29
P26	150	-2.52	0.37	3.56	3.40	0.91	1.89	-0.07
P26	200	-2.25	0.60	1.61	1.95	-2.74	-1.57	-3.91
P26	300**	-2.52	0.45	1.65	-0.04	-13.84	30.51	-58.18
P26	400	-2.64	0.27	0.91	0.74	-2.37	-1.04	-3.69
P26	500[1]**	-2.38	0.15	1.03	-0.13	-0.55	2.64	-3.73
P26	600	-2.25	0.29	0.60	0.43	-2.58	-1.82	-3.35
P26	800	-2.15	0.27	0.28	0.32	-2.34	-1.55	-3.12
P26	1000	-1.06	0.64	0.28	0.00	NA	NA	NA
P26	1250	-1.09	0.74	0.18	0.11	-1.02	1.90	-3.93
P26	1500	0.27	0.85	0.07	0.11	-1.94	-0.20	-3.69
P4	25	1.68	0.30	35.75	NA	NA	NA	NA
P4	75*	-0.08	0.57	7.18	28.57	2.12	2.63	1.61
P4	150	-1.63	0.24	4.36	1.74	2.30	4.11	0.49
P4	300	-2.44	0.20	2.62	1.74	-0.41	0.49	-1.30
P4	400	-2.41	0.39	0.72	1.90	-2.45	-2.02	-2.87
P4	500**	-2.35	0.21	1.21	-0.49	-2.27	-1.17	-3.37
P4	600	-2.25	0.17	0.85	0.36	-2.60	-1.48	-3.73
P4	800	-0.86	0.20	0.70	0.16	-8.40	-6.61	-10.19
P4	1000**	-1.18	0.27	0.88	-0.18	-2.45	-0.36	-4.54
P4	1250	-1.66	0.40	0.16	0.71	-1.07	-0.65	-1.50

Table 5.3 Calculation of inferred remineralized $p\varepsilon^{112/110}Cd$

Inferred remineralized $\varepsilon^{112/110}Cd$ is calculated by mass balance from the pCd and $p\varepsilon^{112/110}Cd$ differences between adjacent depths by the following equations:

$$p\varepsilon^{112/110}Cd_{depth1} * pCd_{depth1} = p\varepsilon^{112/110}Cd_{depth2} * pCd_{depth2} + p\varepsilon^{112/110}Cd_{remineralized} * pCd_{remineralized}$$

$$pCd\ remineralized = pCd_{depth1} - pCd_{depth2}$$

Maximum and minimum remineralized values are calculated for the maximum range allowable within 2σ error by either adding $2\sigma_{depth1}$ to $p\varepsilon^{112/110}Cd_{depth\ 1}$ and subtracting $2\sigma_{depth2}$ from $p\varepsilon^{112/110}Cd_{depth2}$ or subtracting $2\sigma_{depth1}$ from $p\varepsilon^{112/110}Cd_{depth1}$ and adding $2\sigma_{depth2}$ to $p\varepsilon^{112/110}Cd_{depth2}$ respectively. A version of this table in units of $\delta^{114/110}Cd$ can be found in Appendix E (Table E.2). * = mean of measurements from different subsamples of one filter. [1] = mean of measurements from 2 different samples from this depth. NA = not applicable. ** = a negative inferred remineralization, or an accumulation of Cd, is calculated for these samples.

Particulate $\varepsilon^{112/110}$Cd reaches a minimum of around $p\varepsilon^{112/110}$Cd = -2.5 in the nutricline and remains low ($p\varepsilon^{112/110}$Cd ≤ -2.0) in the upper half of the OMZ where a deficit of dCd is observed (see Chapter 4 / Janssen et al., 2014; in revision). These values are among the lowest observed in natural telluric samples (*cf.* Rehkämper et al., 2012; Schmidt et al., 2009a). A similar mid-depth $p\varepsilon^{112/110}$Cd minimum is observed in the North Atlantic (Chapter 2 / Janssen et al., 2014; Conway and John, 2015a). Whether this mid-depth $p\varepsilon^{112/110}$Cd minimum is a characteristic global feature of $p\varepsilon^{112/110}$Cd profiles or if it is controlled by local or regional conditions remains unclear given the dearth of $p\varepsilon^{112/110}$Cd data. A mid-depth minimum in $p\varepsilon^{112/110}$Cd is difficult to reconcile with simple interpretations of the relatively invariant $d\varepsilon^{112/110}$Cd depth profile. The presence of this surprising feature in the only depth profiles of $p\varepsilon^{112/110}$Cd to date (Chapter 2 / Janssen et al., 2014; Conway and John, 2015a; this study) is in contrast to sinking particulate data collected in sediment traps at 30, 100 and 160 m showing heavier $p\varepsilon^{112/110}$Cd as particles in surface and near-surface waters sink from the euphotic zone (S.C. Yang et al., 2015, South China Sea). It should be noted that these studies of pCd consider different particle size classes: 0.8-51 μm suspended and sinking particles (Chapter 2 / Janssen et al., 2014; Conway and John, 2015a; this study) compared to sinking particles with no size screening (S.C. Yang et al., 2015).

At the oceanic station P26, $p\varepsilon^{112/110}$Cd begins increasing at around 800 m depth until our deepest sample (1500 m) where $p\varepsilon^{112/110}$Cd is indistinguishable from the North Pacific deepwater $d\varepsilon^{112/110}$Cd weighted mean of 1.130 ± 0.023 within 2σ error (Chapter 4 / Janssen et al., in revision; see also Conway and John 2015b). At station P4 this trend is reversed for the deepest two samples (1000 m and 1250 m) with $p\varepsilon^{112/110}$Cd decreasing with depth in these samples, but not to the minimum levels found from 300-600 m. This may be due to a continental slope influence, especially given the proximity of our deepest sample (1250 m) to the sediment-water interface (~1320 m). Although transmissometer data suggests no significant sediment resuspension affecting these samples (transmissometer data available at: https://www.waterproperties.ca/linep/2014-19/index.php), previous work along Line P demonstrated the continental margin can play an important role in suppling particulate Fe to the transect (Lam et al., 2006). Multi-element analysis of our particulate samples should help determine if suspended sediments are influencing our data. This apparent trend may also be

influenced by the P4 800 sample, which is heavier than nearby samples both above and below it, as this sample was inadvertently missing its 51 μm prefilter and therefore represents a > 0.8 μm size class rather than a 0.8-51 μm size class (note that larger particles were found to have increasing $p\varepsilon^{112/110}Cd$ with increasing depth in near-surface waters, S.C. Yang et al., 2015).

Particulate Cd data were fit with Martin F curves following Martin et al. (1987) (Figure E.3). The data show a rapid attenuation of pCd with depth, with a b value of -1.60 at station P26 and -1.14 at station P4. This b value relates the rate at which Cd is lost from the particulate phase, with more negative values signifying more rapid loss. At station P26, the pCd b value is larger than those reported for POC at station P26 (-1.05 and -1.16, Buesseler and Boyd, 2009), suggesting that Cd is remineralized form the particulate phase more rapidly than organic carbon. As macronutrient remineralization is expected to be coupled to organic carbon respiration, the more rapid loss of pCd than POC agrees with dissolved data (Chapter 4 / Janssen et al., in revision), which show a more rapid increase of dCd in than dissolved macronutrients the nutricline. While the pCd profile at P4 generally fit a Martin F curve-type shape, the fit is not as strong as for P26 (log-log $r^2 = 0.96$ at P26, 0.84 at P4). Therefore P4 may show less control form one-dimensional processes, possibly due to the proximity to the continental margin.

The pCd profile at station P26 shows monotonic or nearly monotonic decreases with depth and therefore there appears to be no clear net transfer of Cd from the dissolved to the particulate phase as was observed in low-O_2 waters of the North Atlantic (Chapter 2 / Janssen et al., 2014; Conway and John, 2015a) and the eastern tropical South Pacific (Ohnemus et al., 2016). The lack of a coherent local maximum in subsurface waters does not preclude the mechanisms proposed in the above studies, namely the formation of water column sulphides (Chapter 2 / Janssen et al., 2014; Conway and John, 2015a) and Cd uptake by particle-associated prokaryotes (Ohnemus et al., 2016), from acting in the subarctic northeast Pacific. Rather it shows that if these processes are acting, their impact on Cd partitioning is less pronounced than Cd remineralization and therefore that their observed effect is a partial retention of Cd within particles rather than a net transfer of Cd from the water column to particles (see for example, Figure 3.5 step 6 / Janssen and Cullen 2015, Fig 5 step 6; Waeles et al., 2016). This is discussed further in section 5.4.5.

5.4.4 Control of pε$^{112/110}$Cd Depth Profiles

The mechanism responsible for a transition from heavy surface pε$^{112/110}$Cd to mid-depth light pε$^{112/110}$Cd, in contrast to the trend toward heavier pε$^{112/110}$Cd with depth seen in the upper 160 m in a previous study (S.C. Yang et al., 2015), is unclear at present. Note that because dCd is increasing with increasing depth throughout near-surface nutricline waters, there must be a net transfer of Cd from particles to the dissolved phase in the absence of an external source. Additionally, as dε$^{112/110}$Cd decreases with increasing depth in near surface waters, this transferred Cd must be isotopically light. Therefore any interaction between the dissolved phase and the larger particle class through trophic transfer and/or adsorption as well as changes in particle size class changes (e.g. aggregation) must result in a net transfer of Cd from the composite particle class to the dissolved pool which is isotopically light relative to ambient dε$^{112/110}$Cd.

We consider the following possible explanations: heterogeneity of pε$^{112/110}$Cd export with respect to time and space, multiple pCd pools with variable lability and pε$^{112/110}$Cd, and repackaging of Cd during remineralization resulting in retention of a portion of pCd along with an associated fractionation. For clarity, we will treat these mechanisms as if they operate independently in the following discussion.

5.4.4.1 Mechanism 1: Spatial or temporal variability in surface pε$^{112/110}$Cd

Variability in subsurface pε$^{112/110}$Cd may result from either temporal or spatial differences in exported pε$^{112/110}$Cd. In fact, such variability in surface pε$^{112/110}$Cd would be expected by both Rayleigh and open system fractionation models (see Appendix E, Figure E.1; Abouchami et al., 2014 Figures S1.1 and S1.2; Xie et al., in revision). Based on the available pCd (Martin et al., 1989; this study), dCd (Martin et al., 1989; this study) and dε$^{112/110}$Cd (Chapter 4 / Janssen et al., in revision) from the region, it is clear that surface dCd, dε$^{112/110}$Cd and pCd show temporal variability at our site and spatial variability within the subarctic northeast Pacific. It is therefore quite likely that pε$^{112/110}$Cd is variable as well, and that the signal at depth that we see could be influenced by surface particles formed with lower pε$^{112/110}$Cd and sinking to depth with a preservation of their low pε$^{112/110}$Cd signature.

Station	Lat	Long	Size Fraction	Depth	$p\varepsilon^{112/110}Cd$	Error	$p\delta^{114/110}Cd$	Error	Source
	N	W		m		2σ		2σ	
P26	50.0°	145.0°	0.8-51 μm	50	2.71	0.14	0.543	0.028	this study
P4	48.7°	126.7°	0.8-51 μm	25	1.68	0.30	0.335	0.059	this study
P4	48.7°	126.7°	0.8-51 μm	75*[2]	-0.08	0.57	-0.016	0.114	this study
USGT 10-09	17.35°	18.25°	0.8-51 μm	52	1.74	0.34	0.348	0.068	Janssen et al., 2014; Conway and John, 2015a
USGT 10-09	17.35°	18.25°	0.8-51 μm	85	0.26	0.47	0.051	0.094	Janssen et al., 2014; Conway and John, 2015a
SEATS	18°	116°	10-60 μm	55	1.80	0.90	0.36	0.18	S.C. Yang et al., 2015[1]
SEATS	18°	116°	10-60 μm	65	3.50	0.95	0.70	0.19	S.C. Yang et al., 2015[1]
SEATS	18°	116°	10-60 μm	58	-1.25	0.70	-0.25	0.14	S.C. Yang et al., 2015[1]
SEATS	18°	116°	10-60 μm	58	2.45	0.95	0.49	0.19	S.C. Yang et al., 2015[1]
SEATS	18°	116°	60-150 μm	55	1.85	1.65	0.37	0.33	S.C. Yang et al., 2015[1]
SEATS	18°	116°	60-150 μm	55	3.35	1.25	0.67	0.25	S.C. Yang et al., 2015[1]
SEATS	18°	116°	60-150 μm	65	-4.65	0.40	-0.93	0.08	S.C. Yang et al., 2015[1]
SEATS	18°	116°	60-150 μm	58	-3.20	0.25	-0.64	0.05	S.C. Yang et al., 2015[1]
SEATS	18°	116°	60-150 μm	58	-1.00	0.70	-0.20	0.14	S.C. Yang et al., 2015[1]
SEATS	18°	116°	>150 μm	55	1.15	0.75	0.23	0.15	S.C. Yang et al., 2015[1]
SEATS	18°	116°	>150 μm	55	-0.60	0.70	-0.12	0.14	S.C. Yang et al., 2015[1]
SEATS	18°	116°	>150 μm	65	-0.10	0.70	-0.02	0.14	S.C. Yang et al., 2015[1]
SEATS	18°	116°	>150 μm	58	0.45	0.20	0.09	0.04	S.C. Yang et al., 2015[1]
SEATS	18°	116°	>150 μm	58	2.25	0.30	0.45	0.06	S.C. Yang et al., 2015[1]
SEATS	18°	116°	>100 μm	5*[6]	0.95	0.55	0.19	0.11	S.C. Yang et al., 2015
SEATS	18°	116°	Sed Trap	30	4.35	0.45	0.87	0.09	Yang et al., 2012[1]
SEATS	18°	116°	Sed Trap	30	4.20	0.45	0.84	0.09	S.C. Yang et al., 2015[1]
SEATS	18°	116°	Sed Trap	30	6.40	0.60	1.28	0.12	S.C. Yang et al., 2015[1]
SEATS	18°	116°	Sed Trap	30	4.05	0.60	0.81	0.12	S.C. Yang et al., 2015[1]
Weighted Mean			<60 only	≤85	1.69	2.98	0.338	0.595	

Table 5.4 Compilation of global surface (<100 m) $p\varepsilon^{112/110}Cd$ data
$\varepsilon^{112/110}Cd$ and $\delta^{114/110}Cd$ values were interconverted using the factor of $\delta^{114/110}Cd = 0.2000425*\varepsilon^{112/110}Cd$ (Abouchami et al., 2012, see also table 1.4). Sed Trap = sediment trap samples without any size fraction screening. [1]Denotes samples for which the error is the internal precision of standard and sample measurements rather than the error of that specific measurement. *= a mean from multiple subsample measurements of one sample. The number following the * denotes the number of measurements.
NA = not applicable.

S.C. Yang et al. (2015) found surface particles with $\varepsilon^{112/110}Cd$ similar to particles we sampled in the subsurface. It is difficult to directly invoke the particles of distinct size classes

sampled by S.C. Yang et al. (2015) however, because: (a) only one of four size classes sampled in their study had particles which were sufficiently light to explain our observations, (b) the one light size fraction was different than our sample set (60-150 μm for S.C. Yang et al., 2015 compared to our 0.8-51 μm data), (c) particles matching our size class were much heavier, and (d) sinking particles at 100-160 m were found to be heavier than surface particles (S.C. Yang et al., 2015). Additionally, given our initial conditions of dCd ~1 nmol kg^{-1} and $d\varepsilon^{112/110}Cd$ = 1.1 (Chapter 4 / Janssen et al., in revision), theoretical calculations following closed-system Rayleigh and open-system fractionation models with reported ranges of fractionation factors (from Xue et al., 2013; Abouchami et al., 2014; Chapter 4 / Janssen et al., in review) are unable to produce sufficiently light particles (Figure E.1). Therefore, while spatial or temporal variability in exported $p\varepsilon^{112/110}Cd$ may influence observations, given all available data on particulate samples from the surface ocean (weighted mean $p\varepsilon^{112/110}Cd$ = 1.69 ± 2.98 (2σ), n= 10 particulate samples in the ≤60 μm size class above 100 m depth, range of $p\varepsilon^{112/110}Cd$ = -1.25 to +3.5, Table 5.4, sources: Yang et al., 2012; Chapter 2 / Janssen et al., 2014; Conway and John, 2015a; S.C. Yang et al., 2015; this study) and models of isotope fractionation, it is unlikely that our strongly negative subsurface signal is derived from unmodified surface particles.

5.4.4.2 Mechanism 2: Multiple pCd phases with variable $p\varepsilon^{112/110}Cd$

The presence of pCd pools with different isotopic compositions and relative labilities with respect to remineralization could allow the observed changes from heavy surface $p\varepsilon^{112/110}Cd$, to light mid-depth (200-800 m) $p\varepsilon^{112/110}Cd$, to intermediate $p\varepsilon^{112/110}Cd$ in deepwater (> 800 m) samples in particles sinking from the surface ocean. The largest pCd pool would need to be very labile with respect to remineralization such that it is lost first from the particulate pool as pCd rapidly decreases with depth. Additionally, this pool must be heavy with respect to deepwater $d\varepsilon^{112/110}Cd$ and approximately equal to surface $d\varepsilon^{112/110}Cd$. This pool could be composed of extracellularly adsorbed Cd and/or Cd within slow sinking or more easily degraded cells. If subsurface particles are surface-derived, then this first labile and heavy pCd pool would need to dominate the surface signal, giving surface particles a net heavy $p\varepsilon^{112/110}Cd$ signal.

Recent data of Cd adsorbed onto degrading cells in a pure culture laboratory setting suggested it had the same or very nearly the same isotopic composition as the bulk solution in which the cells were degrading (John and Conway, 2014) which suggests that adsorbed Cd may reflect the ambient $d\varepsilon^{112/110}Cd$ composition. If this is true in field samples as well, then it would contribute the heavy surface $d\varepsilon^{112/110}Cd$ to particles and could contribute to the surface $p\varepsilon^{112/110}Cd$ that we observe, which is heavy with respect to deepwater. Such a condition would require that the most labile and isotopically heavy pool must also be the largest pool. At present, there is not strong support for Cd being a highly scavenged or surface adsorbed element or for an adsorbed fraction dominating the particulate Cd phase. It is possible however, that cells sinking from micronutrient-limiting conditions, such as those found in the HNLC subarctic northeast Pacific, with upregulated expression of divalent metal transporters (e.g. Sunda and Huntsman 1992; 1995; 2000; Cullen et al., 2006; John et al., 2007; Lane et al., 2008) may show a greater tendency to adsorb Cd. This more specific putative metal adsorption, which is dependent on the expression level of extracellular metal binding proteins, may not be properly captured by growth in the elevated metal concentrations found in the controlled media scavenging study (John and Conway, 2014).

The second pCd pool would be less labile in order for pCd in this pool to largely resist degradation until after most of the first pool is remineralized. Additionally, the second pool would be isotopically very light and would dominate the $p\varepsilon^{112/110}Cd$ signal from 200-800 m depth, resulting in the very light $p\varepsilon^{112/110}Cd$ observed in this range. Less labile Cd could be intracellular Cd associated with faster sinking or more refractory cells like coccolithophorids or diatoms. However, as discussed in section 5.4.4.1, this pCd pool must be more negative than previously observed in <60 μm surface particles and than predicted by theoretical calculations based on fractionation models. Finally, a third pool which is more refractory, in order to persist to greater depth, would be necessary to explain the reversal in $p\varepsilon^{112/110}Cd$ trends with an increase below 800 m. Refractory pCd has been reported previously for the upper 200 m at station P26 and in the subarctic northeast Pacific. The deepest samples suggest a refractory Cd pool of around 0.1-0.2 pmol kg^{-1} (Martin et al., 1989), in general agreement with our deep (>800 m) pCd concentrations. Refractory Cd would need an isotopic composition around or slight greater than bulk continental crust ($\varepsilon^{112/110}Cd$ of roughly 0, Schmitt et al., 2009a;

Rehkämper et al., 2012) in order to match our deepwater observations from P26. The deepwater signal could also be influenced by advection of particles and therefore reflect a different source of pCd than overlying waters.

Clearly more experimental work is necessary to determine the $p\varepsilon^{112/110}Cd$ values and labilities of different pCd phases and size classes. Additionally, more research is needed to determine if and how $\varepsilon^{112/110}Cd$ uptake varies among phytoplankton taxa and nutrient conditions in order to understand the depth variability observed in $p\varepsilon^{112/110}Cd$ profiles and the regional and size class variability in surface $p\varepsilon^{112/110}Cd$. Considering the variability of expression of cell surface metal binding and transport proteins across varying micronutrient regimes and among taxa (e.g. Sunda and Huntsman, 1992; Sunda and Huntsman, 1995; Sunda and Huntsman, 2000; Maldonado et al., 2006; John et al., 2007; Lane et al., 2008), there is potential for phytoplankton taxa and growing conditions to alter the potential for metal adsorption in sinking biogenic particles. The fraction of Cd adsorbed to phytoplankton cells either grown in lab settings or from natural assemblages can be separated from intracellular Cd using, for example, diethylenetriamine penta-acetic acid (Lee et al., 1995) or ascorbate (Anderson and Morel, 1982) rinse solutions. This allows the determination of pCd concentration and isotopic compositions of adsorbed (and therefore potentially more labile) and intracellular phases. A similar comparison of adsorbed and intracellular metal isotope composition for Zn showed heavy Zn adsorbed to cells and light Zn internalized (John et al., 2007). Such a composite dissolved-to-particulate transfer of Cd would raise the apparent $p\varepsilon^{112/110}Cd$ in surface biological particles. Sequential leaching of particles, as has been done for refractory and labile pCd (e.g. Martin et al., 1989), can be employed to test if $p\varepsilon^{112/110}Cd$ differs among Cd pools of varying lability.

Data from P4 complicate any multiple pools-type interpretation as $p\varepsilon^{112/110}Cd$ begins to decrease again below 800 m and pCd at 1250 m appears discontinuous with the rest of the profile. It is possible that these data are influenced by interactions with resuspended margin sediments as our sample at 1250 m is within about 70 m of the sediment-water interface (though note that the very low pCd in this sample suggests that any suspended sediments do not have the net effect of adding Cd to the particulate pool compared to overlying waters). These particles would need to be of a size and character that are not detected by the CTD transmissometer (CTD data from this cruise are available at:

https://www.waterproperties.ca/linep/2014-19/index.php). Multi-element analysis of these deep coastal samples would help determine if suspended sediments are influencing the $p\varepsilon^{112/110}Cd$ composition at P4.

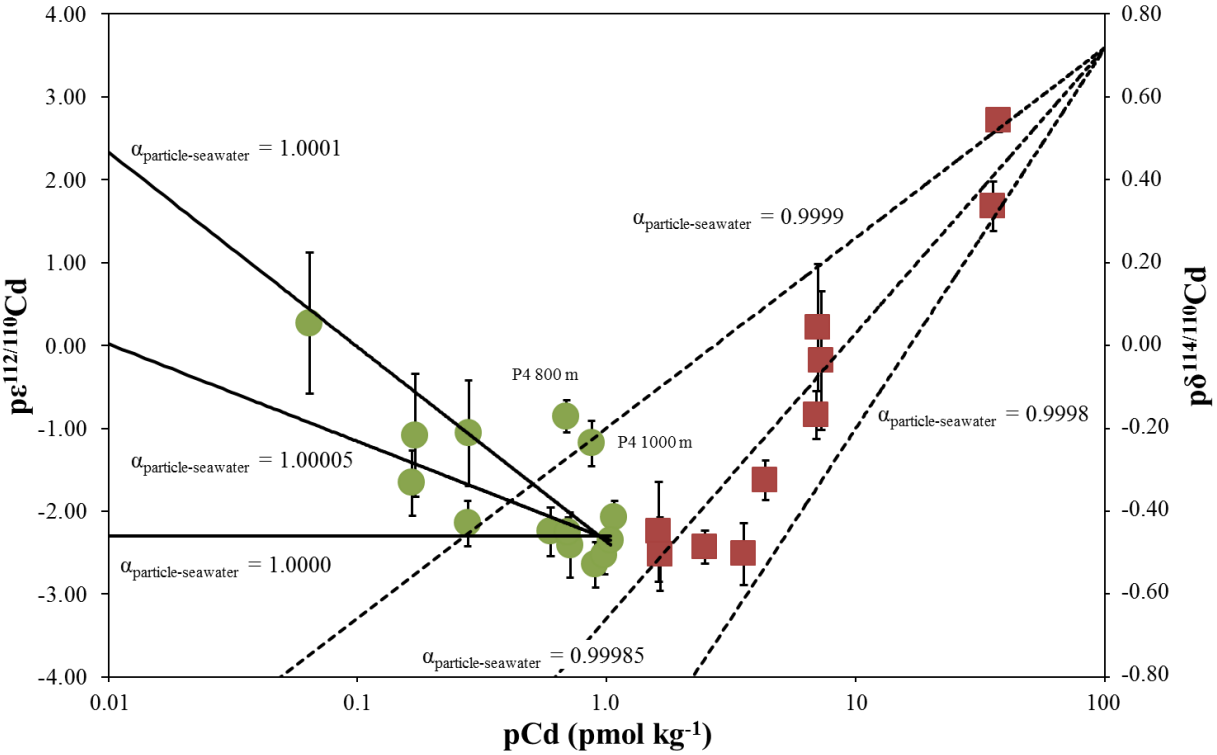

Figure 5.4 Closed-system Rayleigh fractionation model for particulate samples
Samples from above 300 m are shown as red squares and samples from below 300 m are shown as green dots. Dashed lines represent fractionation factors for ≤ 300 m samples with labeled fractionation factors ($\alpha_{particle\text{-}seawater}$). Solid lines represent fractionation factors for > 300 m samples with labeled fractionation factors. P4 800 m and P4 1000 m samples are labeled as they sit apart from the trend of the rest of the data.

5.4.4.3 Mechanism 3: Fractionation due to remineralization and interaction with the dCd pool

In a mechanism involving fractionation from remineralization and interaction with the dissolved pool, we treat the particulate Cd pool in any given sample as homogenous with respect to isotopic composition. We assume that there are not multiple phases which are remineralized at different rates or have different $p\varepsilon^{112/110}Cd$ and therefore that any release of Cd which is isotopically distinct from the composite $p\varepsilon^{112/110}Cd$ is due to a fractionation of Cd during remineralization. Particulate data in the upper 300 m fit a closed system Rayleigh fractionation model with a fractionation factor $\alpha_{particle\text{-}seawater}$ close to 0.99985 (Figure 5.4). This

supports remineralization as the process that may control the distribution of $p\varepsilon^{112/110}Cd$ in the upper 300 m, where most of the pCd remineralization occurs (less than 10% of surface pCd reaches 300 m depth).

The formation of Cd sulphides is associated with an isotopic fractionation, sequestering light Cd isotopes in the solid phase (Schmitt et al., 2009a; J. Yang et al., 2015). The subsurface local $p\varepsilon^{112/110}Cd$ minimum observed in the eastern North Atlantic, which was coincident with a pCd maximum and a dCd depletion, was proposed to originate through the formation of metal sulphides in the water column (Chapter 2 / Janssen et al., 2014; Conway and John, 2015a). In the subarctic northeast Pacific, $p\varepsilon^{112/110}Cd$ reaches its minimum value above depths where dCd deviates from Pacific Cd:PO_4^{3-} correlations (Figure 5.5; see also Janssen et al., in revision / Chapter 4) and above depths where small enrichments in pCd are observed (Figure 5.6). Therefore it is unlikely that the formation of sulphides is the primary mechanism behind decreasing $p\varepsilon^{112/110}Cd$ values in the nutricline (this is discussed further in section 5.4.5). For the same reasons, though biological uptake of Cd is known to accumulate light isotopes in the particulate phase (Lacan et al., 2006; John and Conway, 2014; S.C. Yang et al., 2015; this study) and this has been used to explain pCd enrichments in O_2-depleted waters (Ohnemus et al., 2016), microbial Cd uptake in O_2-depleted water is unlikely to explain the formation of the $p\varepsilon^{112/110}Cd$ minimum we observe. Sulphide formation or biological uptake may help extend the range of the observed light $p\varepsilon^{112/110}Cd$ before the final section of the profiles – an increasing $p\varepsilon^{112/110}Cd$ below 600-800 m (Figures 5.2, 5.4). A mechanism for this increasing $p\varepsilon^{112/110}Cd$ in deepwater is unclear. As deepwater $p\varepsilon^{112/110}Cd$ approaches $d\varepsilon^{112/110}Cd$ at P26, the increasing $p\varepsilon^{112/110}Cd$ may reflect an equilibration with deepwater $d\varepsilon^{112/110}Cd$. Fractionation during remineralization and respiration is also discussed in section 5.4.6.1

5.4.5 Particulate Cd and dissolved Cd depletions in low-O_2 water

Previous studies of pCd cycling in O_2 depleted waters have found subsurface peaks in pCd and/or particulate Cd:P which have been attributed to either the formation of insoluble sulphides in O_2-depleted waters (Chapter 2 / Janssen et al., 2014; Conway and John 2015a; Waeles et al., 2016) or Cd uptake by prokaryotes (Ohnemus et al., 2016). There are two main challenges for using our data set to investigate these potential processes driving depletion of

dCd and enrichments of pCd in O_2-depleted waters. First, we do not have particulate P data to compare particulate Cd:P trends. Second, our samples are of only the 0.8-51 μm size class, and therefore we may be missing signals from larger sized particles, which might be more likely to harbor anoxic microenvironments and more prone to gravitational settling, as well as some small microbes (~0.2-0.8 μm). Previously published work on the 0.8-51 μm particulate size class found pCd maxima associated with this size class in O_2-depleted water; however, these O_2-depleted waters were much closer to the surface (100-200 m depth) (Chapter 2 / Janssen et al., 2014; Conway and John, 2015a; Ohnemus, 2016). Therefore, it is possible, that a greater percentage of surface-derived particles would reach low-O_2 waters without significant decomposition and provide greater potential for particulate microenvironments amenable to sulphide formation.

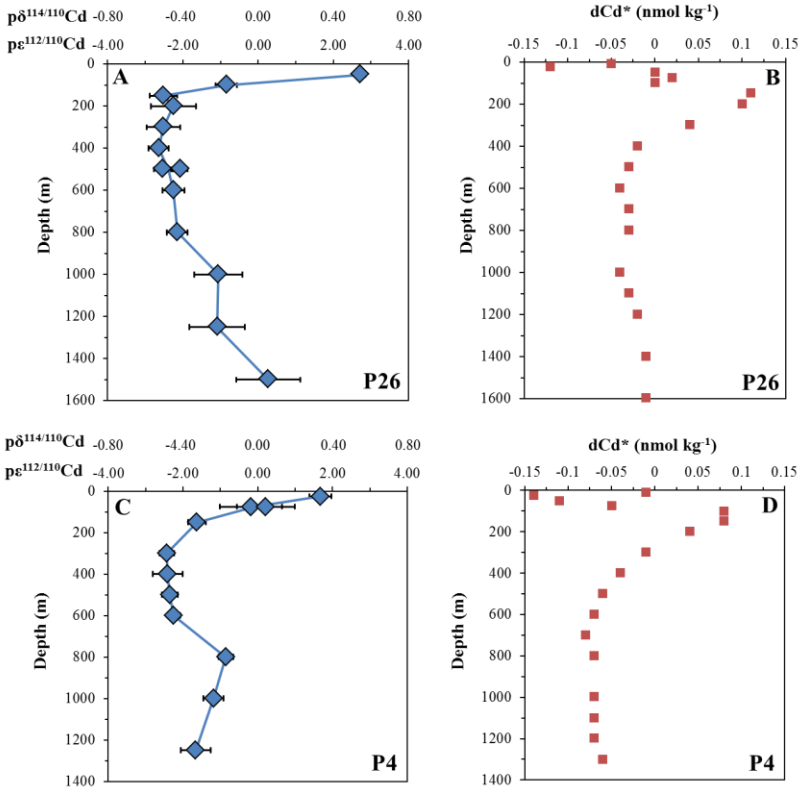

Figure 5.5 Particulate $\varepsilon^{112/110}$Cd and dCd* from Line P
Panels A and B show station P26 and C and D show station P4. Particulate $\varepsilon^{112/110}$Cd are shown in the left panels in blue diamonds. The right panels show Cd* (see equation 2, Chapter 4) in red squares calculated from August 2012 dissolved data.

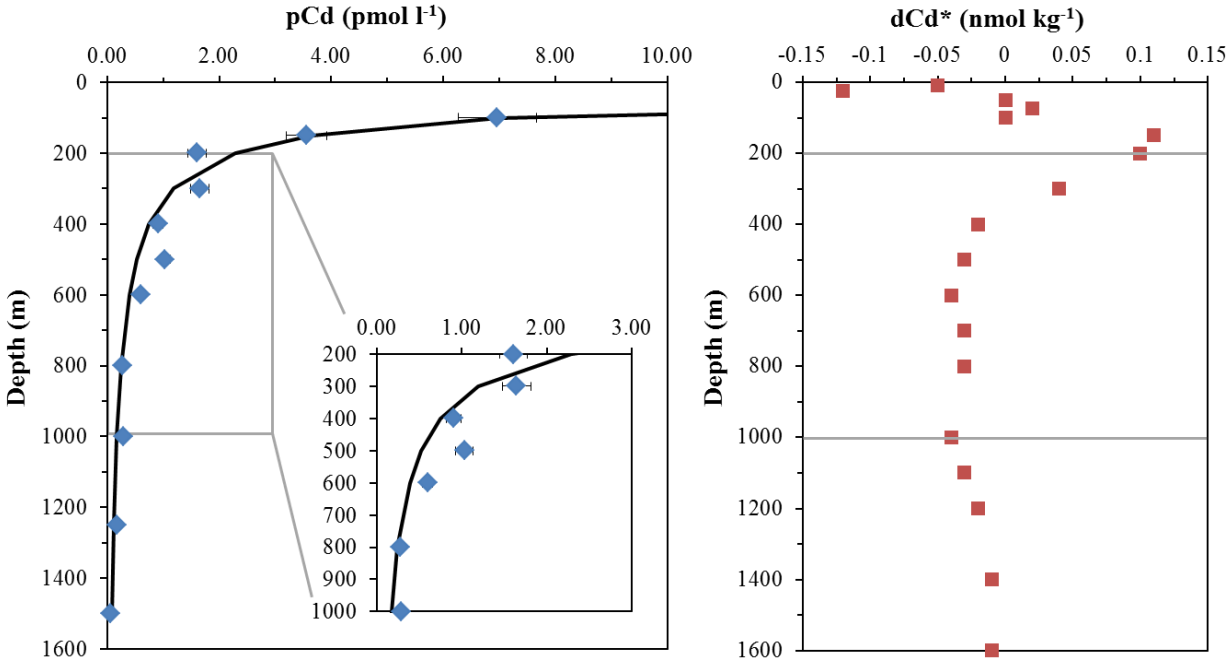

Figure 5.6 Station P26 pCd and dCd*
Particulate Cd are shown in the left panel in blue diamonds with a Martin F curve (solid black line, Martin et al., 1987) fit to the data. The inset of the left panel shows the depth range of 200-1000 m in finer detail. The right panel shows dCd* from August 2012 with horizontal grey lines denoting the depth ranges of the inset in the left panel.

Our sample set shows no clear net transfer of Cd from the dissolved phase to the particulate phase (i.e. no clear local subsurface pCd maximum); however, station P4 shows elevated pCd at 500-1000 m which is slightly larger than or roughly equal to pCd at 400 m. Additionally, subsurface pCd concentrations at P4 are larger than pCd over this depth range at station P26 even though surface pCd is comparable between the two stations. This greater retention of Cd in particles at P4 highlights a different particle cycle between the two stations, either due to the particles themselves (e.g. resuspension and advection of margin sediments (Lam et al., 2006); differences in the composition of particles exported from the surface ocean at these two stations) or water column conditions (e.g. varying aerobic respiration rates or different degrees of sulphide formation due to differences in O_2). A sulphide formation mechanism or decreased aerobic respiration mechanism would likely be more active in water with lower O_2, in agreement with the elevated pCd observed at P4 compared to P26 (see Figure 5.2).

Subsurface pCd data at station P26 generally fit a Martin F curve well (Martin et al., 1987); however, samples between 300 and 1000 m are slightly enriched in pCd relative to the expected profile (Figure 5.6), suggesting that these samples may have retained some of their Cd during remineralization. This depth range of Cd-rich particles corresponds with the depth range of O_2-depleted waters where dCd decouples from phosphate, as shown by the derived tracer Cd* (which tracks enrichments of Cd relative to regional Cd:PO_4^{3-} and measured PO_4^{3-}, Chapter 2 / Janssen et al., 2014; Janssen et al., in revision / Chapter 4) (Figure 5.6). This is consistent with the retention of Cd in particles through the formation of metal sulfides. In low-O_2 waters at station P26 where dCd is depleted and pCd shows a slight enrichment relative to a Martin curve, $p\varepsilon^{112/110}Cd$ is light with respect to $d\varepsilon^{112/110}Cd$, fitting expectations from Cd fractionation during sulphide formation. However, light $p\varepsilon^{112/110}C$ also occurs at shallower depths where dCd is not depleted (Figures 5.5 and 5.6), and $p\varepsilon^{112/110}Cd$ is lighter than theoretical constraints on removed Cd of $\varepsilon^{112/110}Cd \geq -0.37$ (Section 4.5.2.1). Therefore it seems that the light $p\varepsilon^{112/110}Cd$ we observe is formed by a process other than removal of dCd by sulfide formation, either a fractionation during remineralization (mechanism 3 above) or through a light and less labile pCd pool which is retained to depths below the bulk of the Cd respiration. It is unlikely that this light $p\varepsilon^{112/110}Cd$ is derived from surface particles without an alteration of the surface $p\varepsilon^{112/110}Cd$ signal (mechanism 1) due to the very light $p\varepsilon^{112/110}Cd$ minimum values observed, as discussed in section 5.4.4.1. It is possible that this light signal is maintained throughout low-O_2 waters by a mechanism such as sulphide formation, allowing the signal to persist deeper in the water column in the Pacific than observed in the Atlantic (Chapter 2 / Janssen et al., 2014; Conway and John, 2015a). Further $p\varepsilon^{112/110}Cd$ data will help to assess whether: 1) a subsurface minimum $p\varepsilon^{112/110}Cd$ is observed in other oceans in the absence of significant O_2-depletion and 2) whether a light $p\varepsilon^{112/110}Cd$ signal, if present, is maintained through a significant portion of the water column in the presence of higher [O_2].

5.4.6 Deep Pacific and global ocean $\varepsilon^{112/110}Cd$ mass balance

5.4.6.1 $\varepsilon^{112/110}Cd$ mass balance in the deep Pacific

The calculated Cd contributed to the dissolved phase from degrading particles below 150 m is significantly lighter than $d\varepsilon^{112/110}Cd$ in these depths (*cf.* Table 5.3 and Figure 5.2 as

well as Janssen et al., in revision Table A.2 / Chapter 4 Table D.2); however, $d\varepsilon^{112/110}Cd$ shows no variability within a 2σ error over this depth range (Chapter 4 / Janssen et al., in revision). The calculated accumulated deepwater $d\varepsilon^{112/110}Cd$ in subarctic North Pacific deepwater from Southern Component Water (Table D.6, accumulated $\varepsilon^{112/110}Cd$ = +0.65 to +1.05; see Chapter 4 section 4.5.5) is heavier than the integrated inferred remineralized Cd below 300 m ($\varepsilon^{112/110}Cd$ = -2.64 ± 0.5 at station P26 from 300-1500 m, -3.07 ± -0.43 at P4 from 300-1000 m, calculated as described in Table 5.3), suggesting that either the accumulated Cd is spatially variable or the size class of large particles not represented in our data balances the light $\varepsilon^{112/110}Cd$ contributed from small particles. It is possible that there are sink terms for dissolved Cd that remove a smaller amount of isotopically lighter Cd, resulting in a net accumulation of dCd which is not as light as inferred from our particles. However, this is unlikely given the light $p\varepsilon^{112/110}Cd$ of our particle size class and that a sink term would have to be substantially lighter to result in removal of a fraction of the added dCd while increasing the $\varepsilon^{112/110}Cd$ of remaining remineralized Cd into the range of the net accumulated Cd.

Our observations in $p\varepsilon^{112/110}Cd$ and $d\varepsilon^{112/110}Cd$ may be explained by the missing fraction of the Cd pool in our data: the > 51 μm fraction. Transfer of isotopically heavy Cd from smaller particles to larger particles may result in a shift to lighter $p\varepsilon^{112/110}Cd$ in smaller particles without transfer of the full missing heavy Cd inventory to the water column. S.C. Yang et al. (2015) observed sinking particles in sediment trap $p\varepsilon^{112/110}Cd$ becoming heavier from 30 m to 160 m depth. Note that sediment traps may be biased toward larger and denser particles (Baker et al., 1988), which may result in different particle classes in sediment traps compared to our samples. Other stable isotope systems suggest that respiration and trophic transfer of organic matter is accompanied by a retention of heavy isotopes in the particulate phase (e.g. nitrogen: $\delta^{15}N$ (Altabet and Small, 1990; Altabet and Francois, 1994; Sigman and Casciotti, 2001 as presented in Emerson and Hedges, 2008, Figure 5.9)) or proceeds without fractionation (e.g. carbon: $\delta^{13}C$ (Dansgaard, 1965; Knox et al., 1992; Zhang et al., 1995; O'Leary, 1981; Romanek et al., 1992; Lansdown et al., 1992; as presented in Emerson and Hedges, 2008, Figure 5.6 and Table 5.3) and strontium: $\delta^{87/86}Sr$ (Flockhart et al., 2015)). While particulate stable isotope data are available for Fe (Revels et al., 2015) and, in controlled media, for Zn (John and Conway, 2014),

the different particle reactivities of these elements in comparison to Cd complicates a direct comparison.

5.4.6.2 Oceanic $\varepsilon^{112/110}$Cd mass balance

Since the first published oceanic distributions of $d\varepsilon^{112/110}$Cd, a surface to deepwater $d\varepsilon^{112/110}$Cd gradient with heavy surface $d\varepsilon^{112/110}$Cd and light deepwater $d\varepsilon^{112/110}$Cd has been apparent (e.g. Lacan et al., 2006; Ripperger et al., 2007). Isotope fractionation studies in laboratory isolates support the potential of phytoplankton Cd uptake to drive this vertical $d\varepsilon^{112/110}$Cd gradient, with light isotopes sequestered in the biological particulates and the remaining $d\varepsilon^{112/110}$Cd pool enriched in heavy isotopes (Lacan et al., 2006; John and Conway, 2014). However, field particulate data are limited and offer more mixed information regarding large scale transport of light isotopes from surface waters to depth (e.g. S.C. Yang et al., 2015). While $p\varepsilon^{112/110}$Cd in surface waters is light with respect to surface water $d\varepsilon^{112/110}$Cd, available field data indicate that surface particles are generally heavier than or comparable to deepwater $d\varepsilon^{112/110}$Cd (Table 5.4) and, contrary to the trends we observe, that sinking particles may become heavier with depth (S.C. Yang et al., 2015). This presents an isotopic balance disagreement, where source material to surface waters of upwelled deepwater ($d\varepsilon^{112/110}$Cd ~ +1.1 in the Pacific and Southern Ocean, Abouchami et al., 2014; Conway and John, 2015b; Janssen et al., in revision / Chapter 4), crustal material ($\varepsilon^{112/110}$Cd ~ 0, Schmitt et al., 2009a) and river flux ($d\varepsilon^{112/110}$Cd ~ +1, Lambelet et al., 2013)) is light with respect to both surface waters and surface particles. Although particles above 50 m depth are heavier than or comparable to the known Cd sources, $p\varepsilon^{112/110}$Cd rapidly decreases with depth resulting in light $p\varepsilon^{112/110}$Cd below the euphotic zone but above the winter mixed layer. Therefore, heavy surface $d\varepsilon^{112/110}$Cd in our sample set is maintained not by the formation of especially light biological particles but by the isotopic shift in these particles during degradation and the export of light particles below the winter mixing depth.

The bulk oceanic inventory of deepwater $d\varepsilon^{112/110}$Cd (roughly +1.1 in the deep North Pacific and Southern Ocean, +2.4 the North Atlantic, see Figure 4.7) is light with respect to crustal material (Schmitt et al., 2009a; Rehkämper et al., 2012). Known riverine $d\varepsilon^{112/110}$Cd flux, which is constrained only to the Siberian rivers entering the Arctic ocean, suggests that Cd

is either minimally fractionated or unfractionated during weathering, resulting in a riverine flux of $d\varepsilon^{112/110}Cd$ = +0.5 to +1.5 (Lambelet et al., 2013). This is lighter than or comparable to $d\varepsilon^{112/110}Cd$ in the deep Pacific and Southern Component water and is lighter than North Atlantic deepwater, implying that oceanic Cd sink terms must be a net removal of isotopically light Cd. Known authigenic sinks such as incorporation into ferromanganese crusts result in no fractionation from deepwater (Schmitt et al., 2009a; Horner et al., 2010). Sulphide formation removes light isotopes from the dissolved phase (Schmitt et al., 2009a) and this has been proposed as a sink for isotopically light Cd in low-O_2 regions (Janssen et al., 2014; Conway and John, 2015a). Surface particles are insufficiently light to act as an isotopically light Cd sink term (Table 5.4) if these particles are buried in sediments without modification and sinking particles from the upper 160 m (S.C. Yang et al., 2015) are much heavier than the ocean inventory. However, the isotopically light $p\varepsilon^{112/110}Cd$ we observe at intermediate depths can serve as a light $\varepsilon^{112/110}Cd$ sink. While this particulate signal is modified with increasing depth in the open ocean, resulting in higher $p\varepsilon^{112/110}Cd$ in deepwater particles, particles exported to continental shelf sediments would be removed from the water column within the depth range of the isotopically light particles we observe and may therefore act as a globally important sink for isotopically light Cd. It is unclear if the depth range of light $p\varepsilon^{112/110}Cd$ is influenced by sulphide-associated fractionation (or other low-O_2 mediated processes) or not. Data from more oxic regions of the world ocean could help to determine if intermediate-depth light $p\varepsilon^{112/110}Cd$ is a global feature which persists for several hundred meters depth or if this feature is constrained to specific environments like the O_2-depleted regions where it has been observed to date.

5.5 Conclusion

The pCd and $p\varepsilon^{112/110}Cd$ data we present demonstrate an active water column cycling of Cd and Cd isotopes that is neither reflected in nor imprinted upon the dissolved phase. Our results indicate that while the vertical distribution of particulate and dissolved Cd may be driven by biological cycling, the isotopic composition of sinking particles does not support a simple one-dimensional control on Cd stable isotope distributions. Instead, the proximate control on subsurface $d\varepsilon^{112/110}Cd$, which is remarkably uniform (Conway and John, 2015b; Chapter 4 /

Janssen et al., in revision), appears to be an advection of the Southern Component Water $d\varepsilon^{112/110}Cd$ signal. This highlights the potential of $d\varepsilon^{112/110}Cd$ as a tracer of global deepwater circulation (Abouchami et al., 2014). The large particle size class, which is not represented in our particulate data, may balance the inferred remineralized $\varepsilon^{112/110}Cd$ contributed to the dissolved pool from the small particle size class.

Surface particles (<50 m) are isotopically heavy with respect to Cd sources to the mixed layer (upwelled deepwater and river flux); however, particles exported below the winter mixing depth are light with respect to these sources, resulting in the retention of heavy $d\varepsilon^{112/110}Cd$ in the surface ocean. The mechanisms driving the transition from heavy surface $p\varepsilon^{112/110}Cd$ to light $p\varepsilon^{112/110}Cd$ in the nutricline are unclear at present. While subsurface pCd cycling within the water column may not alter $d\varepsilon^{112/110}Cd$ composition, our data demonstrate a dynamic and previously unknown $p\varepsilon^{112/110}Cd$ cycle. This new evidence highlights serious gaps in the global particulate data set, which is currently constrained to 5 depths from the North Atlantic (Chapter 2 / Janssen et al., 2014; Conway and John, 2015a) and 2 depth profiles in the North Pacific (this study), and surface to near-surface (≤160 m depth) samples from the South China Sea (Yang et al., 2012; S.C. Yang et al., 2015). More attention should be given to $p\varepsilon^{112/110}Cd$ samples to better understand the mechanisms driving Cd distributions and cycling, and to constrain Cd source and sink terms in magnitude, isotopic composition, and mechanism, on the global ocean.

Chapter 6

Conclusions

6.1 Dissertation summary

In this dissertation I have presented and discussed Zn and Cd distributions in the subarctic northeast Pacific with the goal to better understand their biogeochemical cycling in this and other ocean basins. A significant portion of the work was focused on O_2-depleted regions and the departures of metal distributions from established global and basin scale metal-macronutrient correlations observed in these regions. Chapter 2 presented such anomalies for Cd in low-O_2 waters of the subarctic northeast Pacific and the eastern North Atlantic. In both regimes Cd:PO_4^{3-} decoupling was observed in O_2-depleted water masses consistent with an O_2-sensitive removal mechanism. Based on available sedimentary data and the water column inventories of Cd, the depletions are unlikely to be explained by a removal process acting at the interface of sediments and low-O_2 waters. Instead, we proposed that Cd is removed by a transfer of Cd from the dissolved to the particulate phase by a process occurring in the water column. A likely vector of Cd transfer from the dissolved to the particulate was is the formation of insoluble sulphides around and within sinking particles in O_2-depleted water. Support for this hypothesis is provided by particulate Cd distributions and isotopic composition in the eastern North Atlantic, where a pronounced mid-depth pCd and particulate Cd:P peak are observed. Particulate $\varepsilon^{112/110}$Cd at this O_2-depleted subsurface pCd peak is light with respect to both overlying particles and the dissolved phase, consistent with previous work by others investigating and modeling metal isotope composition in authigenic CdS (Schmitt et al., 2009a; J. Yang et al., 2015). A water column removal process is also supported by sedimentary silver work done in the subarctic northeast Pacific (McKay and Pedersen, 2008). A first order approximation suggests that water column Cd removal through this process may be a quantitatively important sink term in the marine Cd budget.

Metals with similar sulphide chemistry to Cd like Cu and Zn may be similarly affected in low-O_2 environments. I investigated this possibility by looking at dissolved data for Cu and Zn from the northeast Pacific already present in the literature (Martin et al., 1989) and using my own data collected with a modified fluorescence based detection method in Chapter 3. Together with literature data from the region (Martin et al., 1989; Lohan et al., 2002) these data demonstrate a fundamentally distinct Zn distribution in the subarctic northeast Pacific relative to Si in the global dataset. This distribution can be characterized by depth as follows: 1) low Zn:Si in surface waters with < 25 μmol kg^{-1} Si, 2) high Zn:Si slopes in nutricline waters with 25 μmol kg^{-1} < Si < 90 μmol kg^{-1}, and 3) low Zn:Si slopes in O_2-depleted waters.

The surface water trend is similar to surface Cd:PO_4^{3-} trends observed in Fe-limited regions and could be explained by changes in the uptake of divalent trace metals by phytoplankton uptake under Fe limitation. High Zn:Si in the nutricline may reflect remineralization of Zn-rich biogenic particles formed in surface waters as well as advected high Zn intermediate waters from the western North Pacific. Depth profiles of Zn in the upper 400 m, especially at more oceanic stations, show a remarkably shallow Zn remineralization horizon. Other ocean basins have deeper remineralization horizons for Zn more analogous to "hard part" associated elements like Si, bringing about the strong global correlation with Si. However, the rapid remineralization at station P26 is more comparable to "soft part" macronutrients like PO_4^{3-} and NO_3^-. It is unclear to what degree this shallow Zn remineralization horizon is caused by advected intermediate water with elevated Zn or by regionally distinct specific particulate Zn export and remineralization dynamics in the subarctic northeast Pacific. A future detailed study of particulate trace elements and macronutrients along Line P would help to differentiate between these potential mechanisms.

As is observed for Cd, a deficit of Zn is apparent in O_2-depleted waters along the transect. This is shown in Zn depth profiles, especially at stations P4-P12 where Zn concentrations remain stable or decrease in the depth range of O_2-depleted water. The Zn deficit is also evident in Zn:Si space as a transition to low Zn:Si slopes when O_2 drops below 50 μmol kg^{-1}. Interpretation and quantification of the Zn depletion is more complicated than for Cd as it requires a Zn:Si baseline to determine expected Zn distributions; however, the Zn:Si relationship above the O_2-depleted waters in the subarctic northeast Pacific is fundamentally

different than the relationship seen in the North and South Atlantic, the Southern Ocean and the Indian Ocean. Furthermore, Zn:Si trends from the subarctic northeast Pacific are also distinct from observations in the North Pacific at lower latitudes. Without an oxic Zn:Si baseline which matches our upper water trends, it is not possible to quantify the Zn deficit in O_2-depleted waters.

Chapter 4 expanded the dCd data set available for the subarctic northeast Pacific and introduced the first $d\varepsilon^{112/110}Cd$ data for the region in the form of high-resolution vertical profiles at the major stations along Line P. Dissolved Cd and $Cd:PO_4^{3-}$ from the upper 400 m reflect control of phytoplankton uptake under Fe-limitation. Surface $Cd:PO_4^{3-}$ is low (Cd* is negative) and $Cd:PO_4^{3-}$ in the nutricline is high (Cd* is positive), reflecting the generation of particles rich in Cd relative to PO_4^{3-} and remineralization of these particles in the nutricline. Derived Cd:P remineralization ratios agree well with a recently published compilation of HNLC regions and are roughly double those of non-HNLC regions (Quay et al., 2015). In O_2-depleted waters, dCd data provide a finer scale understanding of the scope of the dCd deficit. The deficit is stronger toward the margin where $[O_2]$ is lower and where particulate export is higher and extends smoothly out to P26.

Cadmium stable isotope data show a uniform deepwater $d\varepsilon^{112/110}Cd$ composition which is indistinguishable from Southern Component Water (Abouchami et al., 2014; Conway and John, 2015b; Jansen et al., in revision / Chapter 4). While dCd is roughly 33% higher in Pacific deepwater compared to the Southern Ocean (Figure 4.7), the uniform $d\varepsilon^{112/110}Cd$ constrains the isotopic composition of Cd contributed to the dissolved phase as water is transported to the North Pacific. This also provides support to previous reports that $d\varepsilon^{112/110}Cd$ of deepwater reflects the source water signal (Abouchami et al., 2014). No $d\varepsilon^{112/110}Cd$ signal is observed within a 2σ error at depths corresponding with the dCd* minimum, which given a constraint of the magnitude of the deficit, places upper limits on the isotopic difference between the bulk dissolved phase and the removed $\varepsilon^{112/110}Cd$. Surface $d\varepsilon^{112/110}Cd$ trends at low dCd do not fit a Rayleigh model and are much lighter than previous reports in the North Pacific at comparable dCd. This may be a systematic artefact of analytical methods or it may be a real regional and/or temporal difference in surface Cd fractionation. In the near future I suggest that an intercalibration of surface $d\varepsilon^{112/110}Cd$ at very low dCd is of crucial importance to the

oceanographic Cd stable isotope community to determine if analytical artefacts affect surface $d\varepsilon^{112/110}Cd$ measurements. Due to the variability in reported surface $d\varepsilon^{112/110}Cd$, it is necessary that this intercalibration take place in a region where especially high $d\varepsilon^{112/110}Cd$ values have been reported previously.

Chapter 5 reports pCd and $p\varepsilon^{112/110}Cd$ data from particles between 0.8 and 51 μm sampled at a subset of stations along Line P. These data on a previously unsampled pool aid our understanding of Cd cycling in the subarctic northeast Pacific and the particulate concentration and isotope data compliment the dCd and $d\varepsilon^{112/110}Cd$ data presented in Chapter 4. Given sampling and analytical constraints, my sampling of particulate Cd was limited in time and space and the > 51 μm size class was not analyzed. Particulate $\varepsilon^{112/110}Cd$ profiles show distinct isotopic cycling which is not explained by simple models linking particles to $d\varepsilon^{112/110}Cd$ profiles. Surface $p\varepsilon^{112/110}Cd$ is lighter than surface $d\varepsilon^{112/110}Cd$, supporting evidence that biological uptake of Cd results in a concentration of lighter isotopes in the particulate pool leaving an enrichment of heavy isotopes in the dissolved pool (Lacan et al., 2006; John and Conway, 2014; C.S. Yang et al., 2015). However, surface $p\varepsilon^{112/110}Cd$ are the heaviest samples observed in the northeast Pacific water column. Particulate $\varepsilon^{112/110}Cd$ becomes lighter with depth, reaching minimum values below the winter mixed layer but above O_2-depleted waters. This suggests that it is not the formation of especially light $p\varepsilon^{112/110}Cd$ in surface waters which results in an enrichment in heavy isotopes but the export of especially light $p\varepsilon^{112/110}Cd$ below the winter mixed layer which acts to remove light isotopes from surface waters.

The mid-depth $p\varepsilon^{112/110}Cd$ minimum extends from roughly 200 m down to 600-800 m and contains some of the lightest telluric $\varepsilon^{112/110}Cd$ values ever measured. This may be an important sink of light Cd in the global ocean if particles of comparable isotopic composition are formed in more coastal regions and are removed at the continental shelf and upper continental slope. Light $p\varepsilon^{112/110}Cd$ is found before Cd* shows a marked deficit of dCd and therefore the development of the light isotopic signature of these particles may be independent of sulphide formation. No distinct particulate signal is observed where dCd depletions are observed, though $p\varepsilon^{112/110}Cd$ remains indistinguishable from the minimum value through most of the depth range of dCd depletion and therefore sulphide formation may extend the range of light $p\varepsilon^{112/110}Cd$. Particulate Cd does not show a clear mid-depth maximum as observed in the

eastern North Atlantic (Janssen et al., 2014 / Chapter 2; Conway and John 2015a), but a small enrichment in particulate Cd is seen at station P26 relative to a Martin F curve (Martin et al., 1987) which describes the exponential nature of particle degradation with water column depth. Particulate P data are not available to compare Cd:P trends with depth. At the open ocean station P26, $p\varepsilon^{112/110}Cd$ increases beginning around 800 m, reaching a value indistinguishable from deepwater $\varepsilon^{112/110}Cd$ at 1500 m. With the exception of this deepest sample, $p\varepsilon^{112/110}Cd$ is always lighter than $d\varepsilon^{112/110}Cd$ at the same depth and station.

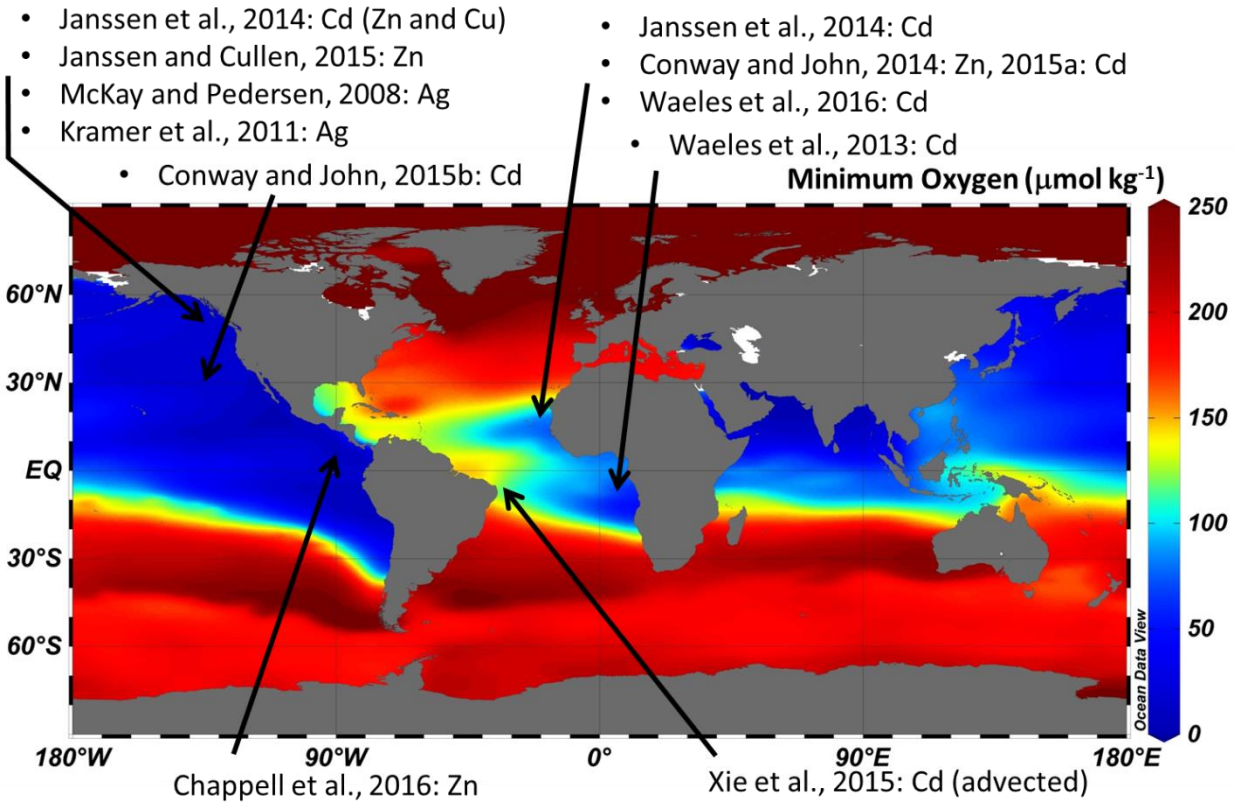

Figure 6.1 Dissolved Cd deficits and metal sulphide formation in the global ocean
This map shows minimum dissolved O2 across the world ocean with the locations of publications which both report dissolved metal deficits and/or particulate metal enrichments in O_2-depleted waters and which propose that metal sulphide formation may explain the observed metal anomalies.

6.2 Water column metal sulphide formation on a global scale

A growing body of data have shown that metals like Zn and Cd have measurable deviations from global and regional metal-macronutrient dissolved phase relationships in O_2-

depleted waters and that particles in O_2-depleted waters are enriched in these metals. We propose this is driven by the formation of metal sulphides in the water column. If metal sulphides are forming in the water column in O_2-depleted regions, we would expect this to be a process which affects multiple sulphide-insoluble metals throughout the world ocean. The presence of a metal depletion signature in oceanographically distinct low-O_2 regions and for multiple metals with similar sulphide coordination chemistry supports that the observed metal depletions are due to conditions related to low O_2 rather than other regional or metal-specific influences. To date, water column sulphide formation has been suggested to explain metal depletions in the North Pacific (Cd, Cu, Zn and Ag), the equatorial Pacific (Zn), the North Atlantic (Cd, Zn) and the South Atlantic (Cd) (Figure 6.1 and sources therein). In addition, data consistent with the sulphide formation hypothesis but not invoking it are found in the Indian Ocean (e.g. Vu and Sohrin, 2013) and the South Pacific (Ohnemus et al., 2016), giving coverage to a metal depletion anomaly in all the open-ocean regions of significant O_2 depletion.

An O_2-sensitive removal of dissolved metals like Zn and Cd has impacts on both the biogeochemistry of the modern ocean and interpretations of records of the paleocean. In the modern ocean, Zn has been shown to influence community composition (Coale et al., 1991; Crawford et al., 2003; Leblanc et al., 2005; Jakuba et al., 2012; Goes et al., 2016) and in some cases Zn may limit primary production (Franck et al., 2003; Jakuba et al., 2012; Chappell et al., 2016). Likewise, through variable toxicity resistance Cd may also influence community composition among primary producers. An O_2-sensitive removal mechanism for Zn and Cd (as well as other metals such as Cu) could shift phytoplankton community composition away from taxa with higher nutrient demands and toxicity resistances for these metals (such as eukaryotic phytoplankton) toward plankton with lower nutrient demands and higher toxicity sensitivity to these metals (such as prokaryotic plankton). Classical assumptions regarding small phytoplankton are that they yield less export production (due to smaller export particle size, e.g. Guidi et al., 2009; and slower settling rates of small particles, e.g. Eppley et al., 1967) and are recycled through more lower trophic levels in the microbial loop, resulting in less efficient transfer of carbon to higher levels of the food chain (e.g. Fenchel, 2008 and references therein). Therefore it would follow that a community composition shift toward smaller cells would lower the efficiency of the biological pump and limit the capacity of a system to support larger

heterotrophic organisms. Note however that the potential role of picoplankton in export production and more direct trophic transfer may have been overlooked due to the potential of picophytoplankton aggregation (Richardson and Jackson, 2007; Lomas and Moran, 2010).

Paleoceanographic reconstructions based on metal records rely on metal distributions to be driven by the same set of processes through geological time and to have generally comparable distributions to the modern ocean. An O_2-dependent depletion of metals may have impacts in paleoceanographic reconstructions as it alters metal:macronutrient dynamics and may also alter the export of metals on sinking particles. For example, reconstructions of ocean nutrient conditions based on Cd preserved in carbonates and a global Cd:PO_4^{3-} relationship requires coupling of Cd:PO_4^{3-}, something which begins to break down in O_2-depleted waters. Ocean oxygen conditions are known to vary over geologic time (e.g. Rosenthal et al., 1995b; Nameroff et al., 2004; Jaccard et al., 2014), with the extent of reducing sediments potentially doubling on glacial-interglacial scales (Rosenthal et al., 1995b). Such variability may therefore alter Cd:$PO4^{3-}$ relationships and complicate interpretations of paleoceanographic records. Comparably for Zn, a reconstruction of particulate organic carbon export via Zn preserved in sponges (e.g. Ellwood et al., 2004) relies on Zn to be exported primarily in the organic carbon phase and for the ratio of Zn:POC to be generally constant. Accumulation of Zn in sinking particles outside of organic phases, for example as a metal sulphide, would lead to greater Zn export per unit carbon and would therefore introduce error in POC export estimates.

The alteration of metal cycles under varying ocean O_2 states is not a new concept, and while this complicates certain paleoceanographic interpretations, it may provide paleoceanographic utility to help answer other questions. For example, accumulation of Cd in sediments may trace the spatial extent of O_2-depleted waters and sediments (e.g. van Geen et al., 1995; Rosenthal et al., 1995a) and other metals such as Ag may have similar utility (McKay and Pedersen, 2008).

6.3 Future directions

This dissertation has presented novel features and identified processes previously not considered in the marine biogeochemical cycles of Zn and Cd. I outline four main areas of focus that I see as important to building off of the work of this thesis: 1) better understanding

and constraining of metal deficits in O_2-depleted waters, 2) filling holes in the global ocean $\varepsilon^{112/110}$Cd inventory and mass balance, 3) a marine Cd stable isotope intercalibration exercise, and 4) investigating the extent of and mechanisms behind anomalous Zn distributions in the upper 400 m of the subarctic northeast Pacific.

6.3.1 Metal deficits in O_2-depleted waters

Although the presented metal removal hypothesis is supported by dissolved and particulate data across the range of O_2-depleted waters, conclusive proof of the mechanism is lacking. While it is not necessary to understand the mechanism(s) driving metal depletions to notice that they are occurring, determining the identity and magnitude of these process(es) is important in terms of understanding global element budgets and metal:macronutrient cycling in the global ocean. The form and therefore lability of metals can regulate the fate of that metal. Incorporation of Zn and Cd into relatively labile organic material compared to inert metal sulphides would result in different potential for long-term removal of Zn and Cd from the system due to burial in sediments. For example, the delivery of Ag sulphides from the water column to sediments has been proposed in the subarctic northeast Pacific as an important mechanism for Ag enrichments in sediments at and below O_2-depleted waters (McKay and Pederson, 2008). Consequently conclusive evidence for or against the proposed metal sulphide removal mechanism is necessary.

It is possible, that while dissolved metals are depleted in low-O_2 waters, the mechanism or one of multiple mechanisms driving this depletion is something other than the formation of water column sulphides. However, because the metal depletions are identified by metal-macronutrient decoupling, any alternate mechanism would need to either remove metal from the dissolved phase without accompanying macronutrients or remove metal to a much greater degree than macronutrients to result in a decoupling from global and regional metal:macronutrient averages. An alternate mechanism to explain the transfer of Cd from the dissolved phase to the particulate phase in the Eastern Tropical South Pacific has recently been proposed – the uptake of metals by particle-associated prokaryotes (Ohnemus et al., 2016).

As discussed above, in order for this mechanism to result in a metal-macronutrient decoupling in the dissolved phase prokaryotes would need to take up metal well in excess of

macronutrients relative to dissolved ratios. No data are available for metal quotas in ODZ prokaryotes to determine whether it is likely that they incorporate a substantial excess of metal; however, available data from prokaryotic metal binding proteins and toxicity resistances would suggest that prokaryotes on the whole are not expected to have disproportionally high inventories of Zn and Cd. Compared to eukaryotes, prokaryotes show a lower biological demand for Zn per protein inventory (Dupont et al., 2006; Dupont et al., 2010) and prokaryotic phytoplankton show an elevated susceptibility to Cd toxicity compared to eukaryotic phytoplankton (Brand et al., 1986; Tortell and Price, 1996; Sunda and Huntsman, 1996; Saito et al., 2003).

Targeted sampling should be undertaken to address the validity of this mechanism, as well as our own of sulphide formation. A first order approach may be to assess the cellular quotas of microbes found in O_2-depleted waters, as nothing is known for these organisms. While prokaryote communities in O_2-depleted waters are likely too small for the sort of cell-specific metal quotas that have been performed on marine phytoplankton (e.g. Twining and Baines, 2013) it may still be possible to assess co-locations of metal and other species such as P and reduced sulphur in particulate material. This may need to be done quantitatively to determine which regions of particles are responsible for accumulation of metal in excess of macronutrient relationships and if those regions are likely within cellular material or as a mineral phase.

Increased interdisciplinary collaboration with sampling may help to address whether or not metal sulphides may be forming. Combining the sorts of measurements which have informed the metal sulphide hypothesis – measurements of dissolved and particulate metals and metal stable isotopes, microbial community composition, respiration rates within sulphate reducing and sulphide oxidizing communities, acid volatile sulphide measurements, etc. – could offer further insight into the likelihood of this mechanism. Ultimately on the analytical side, definitive confirmation or refutation of a metal sulphide formation mechanism will require proof regarding the presence or the absence of metal sulphides. Attempts to do so were carried out during this dissertation by X-Ray Absorption Near Edge Structure (XANES) but were unsuccessful to date due to insufficient metal concentrations.

While mechanistic proof is still needed, the current information available – that metals are depleted in the dissolved phase and enriched in particles in O_2-depleted waters – can be used in modeling studies. This can act to better represent metal distributions and test the sensitivities of these distributions to different environmental conditions such as expansion and intensification of O_2-depleted water. Some of this modeling work, including collaborations born out of results from this dissertation, is already in progress. The results of this work may help to determine the potential for anoxic microenvironments to form within particulate material and the degree to which this may influence metal depletions.

6.3.2 Cadmium isotope mass balance

Considering the attention that the dissolved Cd:PO_4^{3-} relationship has received and the potential utility of Cd in paleoceanographic settings, a thorough understanding of the marine Cd cycle is limited by the poor quantification of known source and sink terms. Data on the isotopic composition of Cd entering the ocean and the magnitude of these sources is sorely lacking, with available riverine $\varepsilon^{112/110}$Cd data restricted to Siberian rivers. The oceanic $d\varepsilon^{112/110}$Cd inventory of roughly +1.1 to +2.4 (this dissertation, Ripperger et al., 2007; Boyle et al., 2012; Xue et al., 2013; Abouchami et al., 2014; Conway and John 2015a; Conway and John 2015b) is heavier than bulk continental crust (~0, Schmitt et al., 2009a) and heavier than or comparable to riverine flux (+0.5 to +1.5, Lambelet et al., 2013), suggesting a light Cd sink from the ocean (Figure 6.2, Table 6.1).

More data for the isotopic composition of Cd sources and sinks are necessary to better constrain the global Cd isotope mass balance and the global marine Cd cycle as a whole. Three important areas where data are lacking are: a more comprehensive and globally representative survey of riverine Cd and $\varepsilon^{112/110}$Cd flux, the Cd stable isotope composition of suspended and sinking particles and the isotopic composition of Cd accumulating on margin sediments. Here we have presented a $p\varepsilon^{112/110}$Cd profile of 5 depths (the eastern North Atlantic, Chapter 2; see also Conway and John, 2015a) and two profiles from the Pacific (10 and 12 depths, Chapter 5). These profiles are the only $p\varepsilon^{112/110}$Cd profiles in the global ocean composed of more than 3 depths and they represent the entire body of marine $p\varepsilon^{112/110}$Cd data below 160 m. Given the distinct isotopic cycling of our data, including the dramatic trend toward light $p\varepsilon^{112/110}$Cd with

depth which is opposite to the trend observed in near-surface sinking particles from sediment traps in the South China Sea (C.S. Yang et al., 2015), more global coverage of $p\varepsilon^{112/110}Cd$ is crucially important.

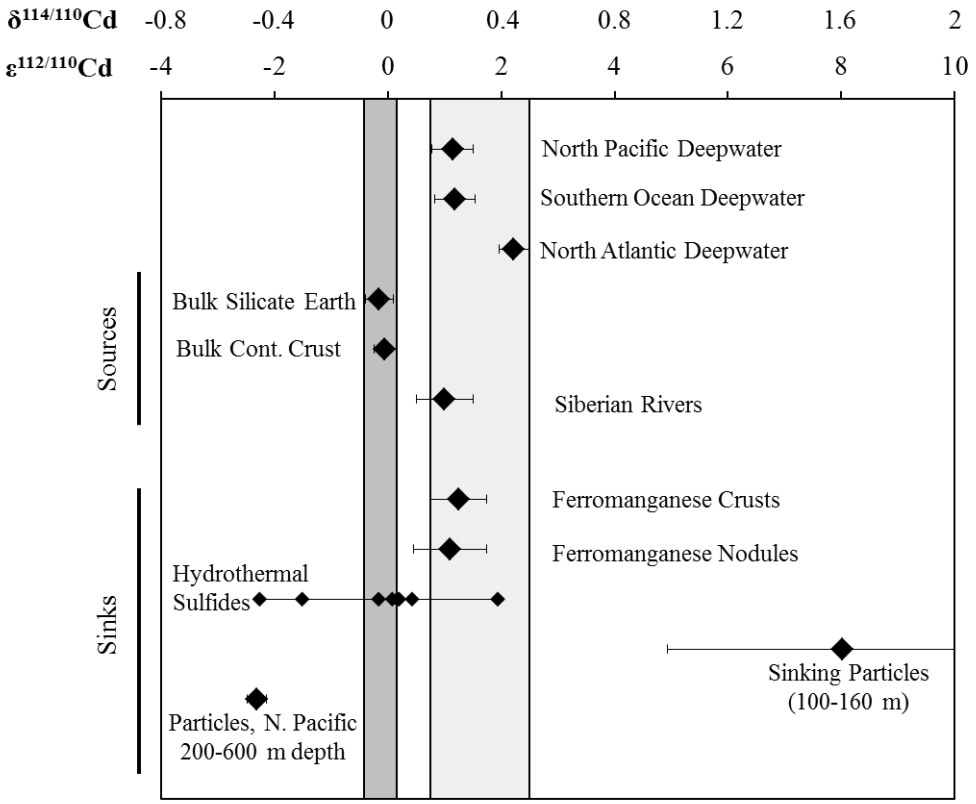

Figure 6.2 Relevant components of the global ocean $\varepsilon^{112/110}Cd$ inventory
The light grey box denotes the range of oceanic deepwater. The dark grey box denotes the range of bulk continental crust and bulk silicate earth. Hydrothermal sulphides are presented as a range with individual points showing different hydrothermal sulphide measurements. Values are presented with references in Table 6.1.

This work should focus on comparing oxic waters with O_2-depleted regions to see if a mid-depth $p\varepsilon^{112/110}Cd$ minimum as observed in both the North Atlantic and the North Pacific is a global feature. Additionally, it appears that either regional conditions or particle size class contributes greatly to $p\varepsilon^{112/110}Cd$ trends with depth. Therefore future studies should consider sampling multiple size classes of particles. Recent work has identified the removal of dissolved Zn to margin sediments as an important process for reconciling the isotopic composition of Zn sources and sinks with the ocean inventory (Little et al., 2016). Given the extremely light values found in particles from 200-600 m depth, the transport of these particles to margin sediments

presents a possible globally relevant sink of light Cd from the ocean; a sink which was previously lacking in the Cd isotope mass balance.

Inventory	**$\varepsilon^{112/110}$Cd**	**2SD**	**$\delta^{114/110}$Cd**	**2SD**	**Reference**
Pacific Deepwater	1.14	0.37	0.23	0.07	This Dissertation
Antarctic Deepwater	1.18	0.36	0.24	0.07	Abouchami et al., 2014
North Atlantic Deepwater	2.22	0.26	0.44	0.05	This Dissertation
Bulk Silicate Earth	-0.15	0.25	-0.03	0.05	Schmitt et al., 2009a; as presented in Rehkämper et al., 2012
Bulk Continental Crust	-0.05	0.2	-0.01	0.04	Schmitt et al., 2009a; as presented in Rehkämper et al., 2012
Sink					
Ferromanganese Crusts	1.25	0.5	0.25	0.10	Horner et al., 2010
Ferromanganese Nodules	1.1	0.65	0.22	0.13	Schmitt et al., 2009a; as presented in Rehkämper et al., 2012
Hydrothermal Sulphides	-2.24 to +1.94		-0.45 to +0.39		Schmitt et al., 2009a
Sinking Particles, S. China Sea, 100-160 m depth, Sediment Trap	8.02	3.08	1.60	0.62	C.S. Yang et al., 2015
Particles, 200-600 m depth, N. Pacific	-2.31	0.17	-0.46	0.03	This Dissertation
Source					
Siberian Rivers	1	0.5	0.20	0.10	Lambelet et al., 2013

Table 6.1 Global $\varepsilon^{112/110}$Cd inventories, sources and sinks
Hydrothermal sulphides are presented as a range of reported values. All others are presented as an average of multiple samples with 2SD error. Pacific particles are 0.8-0.51 μm size fraction. Sediment trap samples have no size fraction screening.

While significant recent advancements have been made to constrain the sources and sinks for isotope systems such as Zn, Cu and nickel (Little et al., 2014; Little et al., 2016; Vance et al., 2016), a comparable understanding of marine Cd cycling through Cd stable isotopes is, at present, lacking. Recent work on Zn has suggested that the Zn residence time may be an order of magnitude shorter than previously estimated (Roshan et al., 2016),

highlighting the considerable gaps remaining to be filled in global trace metal biogeochemical cycling. International programs such as GEOTRACES, which focus on increasing the understanding of trace elements and isotopes in the global ocean through basin-scale transects, international collaboration, and regional cruises and process studies, should help to close these gaps.

6.3.3 A Cd stable isotope intercomparison in surface waters

Among research groups making stable Cd isotope measurements, significant differences are observed at very low dCd in surface in both the North Pacific (*cf*. Ripperger et al., 2007; Conway and John, 2015b; this dissertation, Chapter 4) and the Atlantic (*cf*. Ripperger et al., 2007; Xue et al., 2012; Conway and John, 2015a; Xie et al., in revision). One important difference between these groups is the analytical methodology. Groups measuring $\varepsilon^{112/110}$Cd by ICP-MS have reported $d\varepsilon^{112/110}$Cd 3-10 times the values observed by TIMS at comparable dCd in similar ocean basins. While ICP-MS data are not universally high at low dCd (e.g. Gault-Ringold et al., 2012; as well as some values reported by groups also reporting very high $d\varepsilon^{112/110}$Cd), data collected by TIMS have never produced surface $d\varepsilon^{112/110}$Cd in the range of the high ICP-MS values despite measuring samples with comparable [Cd]. This suggests that the offset may be an analytical artefact. The oceanographic stable Cd isotope community should prioritize an intercalibration at a site where elevated $d\varepsilon^{112/110}$Cd values have been reported previously to determine if this difference is an offset or is a real regionally-variable signal.

6.3.4 Fundamentally distinct Zn:Si distributions in the upper 400 m of the subarctic northeast Pacific

The Line P data presented in Chapter 3 as well as literature data from the subarctic northeast Pacific (Martin et al., 1989; Lohan et al., 2002) highlight a Zn:Si relationship which is unique among data currently available in the global ocean. This suggests a control of Zn:Si distributions which is unique to the region or basin. Surface waters show low Zn:Si and the upper nutricline shows elevated Zn:Si slopes, suggesting remineralization of metal-rich particles in the subarctic northeast Pacific. This is consistent with understanding of phytoplankton physiology and metal uptake under Fe-limitation (e.g. Sunda and Huntsman,

2000; Cullen et al., 2003), but a basin-scale imprint of this has not been reported to date as it has for Cd:PO_4^{3-} (Cullen, 2006; Lane et al., 2009; Quay et al., 2015). Sampling for Zn:Si in sinking particles and for cellular Zn and Si quotas within natural phytoplankton assemblages in the region will help to determine to what degree the observed Zn:Si relationship is driven by biogenic particles formed in the surface water. Sampling the extent of the basin through east-west and north-south transects will help determine the spatial scale of the anomalous distribution and will help to identify any potential advected sources influencing the signal. Recently completed trans-basin GEOTRACES research cruises and GEOTRACES cruises in planning in the subarctic north Pacific (such as the east-west GP-02 and GP-02-bis and a north-south cruise in planning) have great potential to address Zn:Si cycling in the upper 400 m of the subarctic northeast Pacific and the mechanisms responsible.

Appendix A

Pacific data and Cd deficit presented in Chapter 2 and in Janssen et al., 2014

A.1 Pacific dissolved Cd data and the Cd deficit

The two sources of subarctic northeast Pacific dCd data presented in Chapter 2 are Martin et al. (1989) (referred to in this discussion as Martin data) and data from the masters research of former UVic student Dennis Kramer (supporting information about sampling in Kramer, 2006) (referred to in this discussion as UVic data). The Kramer data include filtered samples collected from a trace metal rosette above roughly 600 m and unfiltered samples from a regular CTD rosette below this depth. No evidence for contamination from the use of a regular CTD rosette was found. Martin data were collected from GO-FLO bottles on a Kevlar line and were all filtered. The Martin data were generated by graphite furnace atomic absorption spectroscopy (GF-AAS) following pre-concentration with organic extraction (Bruland et al. 1979). The UVic data were generated by isotope dilution inductively coupled plasma mass spectrometry (ID-ICP-MS) following organic extraction pre-concentration. While these data agree in profile shape, there is an offset between the two (Figure A.1). This offset is roughly 0.15-0.2 nmol kg^{-1}. It should be noted that Cd reference standards were not analyzed along with the UVic data. It was unclear at the time of writing the manuscript presented in Chapter 2 (Janssen et al., 2014) if the difference between the two data sets represented a real oceanographic signal (e.g. a combination of any of the following: annual or interannual variability in dCd in the Pacific, anthropogenic influences on the Cd cycle and oceanic inventory; particulate Cd) or an analytical artefact. A contamination explaining the offset is unlikely given the uniform nature of the offset rather than an erratic distribution of high concentration data points.

Through the subsequent work of this dissertation presented in Chapter 4 (Cd concentrations from samples pre-concentrated by anion exchange chromatography and analyzed by isotope dilution-thermal ionization mass spectrometry (ID-TIMS) (Schmitt et al., 2009b), discussed here as my data or Janssen data) it became clear that the offset of the UVic

data compared Martin data is also present for the UVic data in comparison with my data (Figure A.1, Table B.1). A small offset is also observed between my dCd data and the Martin dCd. A similar offset for Cd was observed by Baars et al. (2014) between their ID-TIMS data and organic extraction GF-AAS data from the Southern Ocean. Some of this offset was within a 5-10% error on the GF-AAS measurements, and therefore the offset could be explained by differences in precision; however, the authors also suggested that incomplete recovery of Cd during organic extraction may account for under-reporting values determined by organic extraction GF-AAS. The UVic data were also processed through organic extraction, but because concentrations were determined by isotope dilution an incomplete Cd recovery would not affect the determined Cd concentration. Considering these factors, it seems that the offset present in the UVic data is an analytical artefact or a combination of multiple artefacts. As this offset is consistent throughout a depth profile, it may have arisen through an analytical error such as incorrect isotope spike calibration and thus provided a regular shift. The same conditions noted by Baars et al. (2014) apply to our data and, therefore, it is possible that the Martin data slightly under-report Cd due to organic extraction, also contributing to an offset between the data sets. This offset impacts the selection of a uniform North Pacific deepwater Cd:PO_4^{3-} ratio. A value of 0.345 is selected to fall between deepwater (>2500 m) ratios observed in Martin et al. (1989) and data from this dissertation (Chapter 4).

Therefore, while the UVic data presented in Chapter 2 do not alter the identification of a Cd deficit in low-O_2 water, they do influence the quantitative treatment of that Cd deficit. In light of the new dCd data collected here, I feel that updating the calculations in Chapter 2 will more accurately reflect a quantitative treatment of the Cd deficit. A conservative calculation of the deficit magnitude relative to known sedimentary sinks for Cd is presented below.

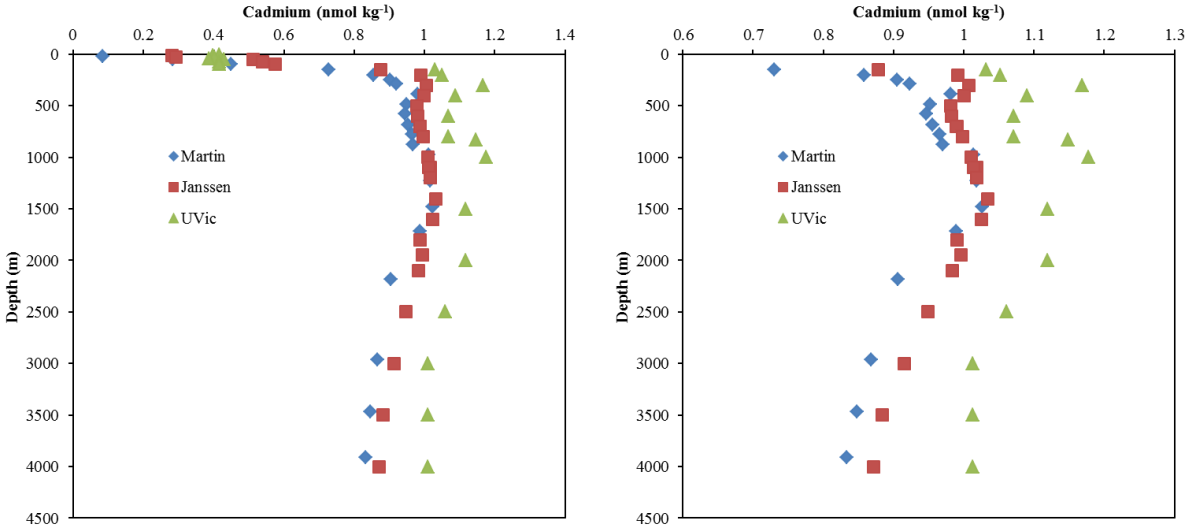

Figure A.1 Comparison of Martin, UVic and my dissolved Cd data from P26
Martin data are shown in blue diamonds, Janssen data are shown in red squares and UVic data are shown in green triangles. The left panel shows the full concentration range and the right panel shows a more narrow range to highlight the deepwater offset.

A.2 Margin sediments as repository of water column Cd deficit

It is possible that, rather than being a water column signal, the observed depletion of Cd in low-O_2 water is due to removal of Cd as waters circulate through or otherwise come into contact with oxygen-depleted sediments. This was addressed in Chapter 2, with a calculated time of 10^4 years necessary to remove sufficient Cd at the sediment-water interface to explain the observed depletion. The calculation is repeated here with the updated information which has become available due to subsequent work as a part of this dissertation. Four different estimates are given (Table A.1, at the end of this appendix) based on different estimations of the Cd deficit. These are:

1) A deficit of 0.044 nm kg^{-1} Cd which exists in a 500 m deep layer of water which extends 1400 km into subarctic northeast Pacific. This deficit estimate is based on the average deficit observed along Line P relative to a deepwater Cd:PO_4^{3-} of 0.345 nmol μmol^{-1} and is calculated from the following:

$$Cd^* = Cd_{measured} - {PO_4^{3-}}_{measured} \times \frac{Cd}{PO_4^{3-}}_{deep}$$

2) A deficit of 0.079 nm kg^{-1} Cd which exists in a 400 m deep layer of water which extends 2200 km into the subarctic northeast Pacific. This is based on the average deficit observed along the VERTEX T transect relative to a deepwater Cd:PO_4^{3-} of 0.345 nmol μmol^{-1}.
3) A deficit 0.13 nm kg^{-1} Cd which exists in a 500 m deep layer of water which extends 1400 km into subarctic north Pacific. This is based on the average deficit observed along Line P relative to a nutricline Cd:PO_4^{3-} relationship of Cd = 0.42*PO_4^{3-} - 0.15. This equation is calculated based on data from Line P in August 2012 as shown in Figure A.3.
4) A deficit of 0.16 nm kg^{-1} Cd which exists in a 400 m deep layer of water which extends 2200 km into the subarctic northeast Pacific. This is based on the average deficit observed along the VERTEX T transect relative to a nutricline Cd:PO_4^{3-} slope of Cd = 0.42*PO_4^{3-} - 0.15.

For the purposes of this calculation, deficits in units of nmol kg^{-1} are approximated as nmol L^{-1}. The deficit volume is calculated as a box with length and width equal to the transect length of the observed deficit and depth equal to the observed depth range of the core of the deficit. Spatial presentations of the deficits are shown in Figure A.4. For this deficit in the subarctic northeast Pacific, the continental slope contacts this box on two sides (the north and the east sides) while the remaining two sides connect to the open ocean. The area of continental slope contact with the Cd deficit box is estimated as two rectangles with sides equal to the box width and height determined from box height taking into account a continental slope angle of 4° (Figure A.2). A high Cd accumulation rate in sediments of 10 ng Cd cm^{-2} y^{-1} (Van Geen et al., 1995) is used to minimize the time necessary to remove sufficient dissolved Cd. This is likely an over-estimate of realistic removal rates as it is the highest Cd accumulation rate measured by Van Geen et al. (1995) in a semi-enclosed marginal basin. An example of the removal time calculation is shown below. The same calculation was repeated for each of the four deficit conditions by swapping in the relevant parameters.

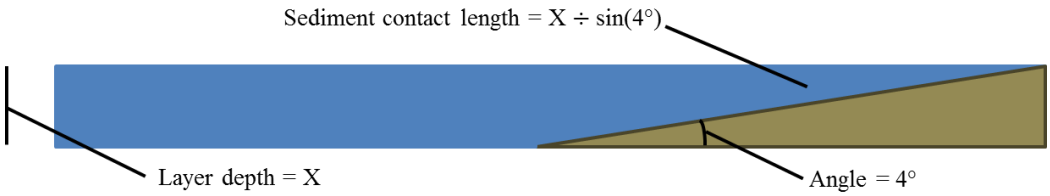

Figure A.2 Illustration of sediment contact length with a layer of water
Given a layer of water with depth X in contact with continental slope with an angle of 4°, the sediment contact length for each 2 dimensional vertical slice through the sediment-water interface = X ÷ sin(4°). In a model where sediments are in contact with two sides of a box of water, this contact length gives the 'depth' of the sediment contact faces. Lengths of these faces are equal to the lengths of the sides of the box of water. Not illustrated to scale.

$$dCd\ deficit = 1{,}400{,}000\ m \times 1{,}400{,}000\ m \times 500\ m \times \frac{1000\ l}{1\ m^3} \times 0.044\ nmol\ l^{-1} = 4.3 \times 10^{16}\ nmol\ Cd$$

$$Sediment\ interface\ area = 500\ m \div \sin(4°) \times 1{,}400{,}000\ m \times 2 \times \frac{100^2 cm^2}{1\ m^2} = 2.0 \times 10^{14}\ cm^2$$

$$Time = (4.3 \times 10^{16}\ nmol\ Cd \times 112.41\ g\ mol^{-1}) \div (2.0 \times 10^{14}\ cm^2 \times 10\ ng\ Cd\ cm^{-2}\ y^{-1}) = 2415\ years$$

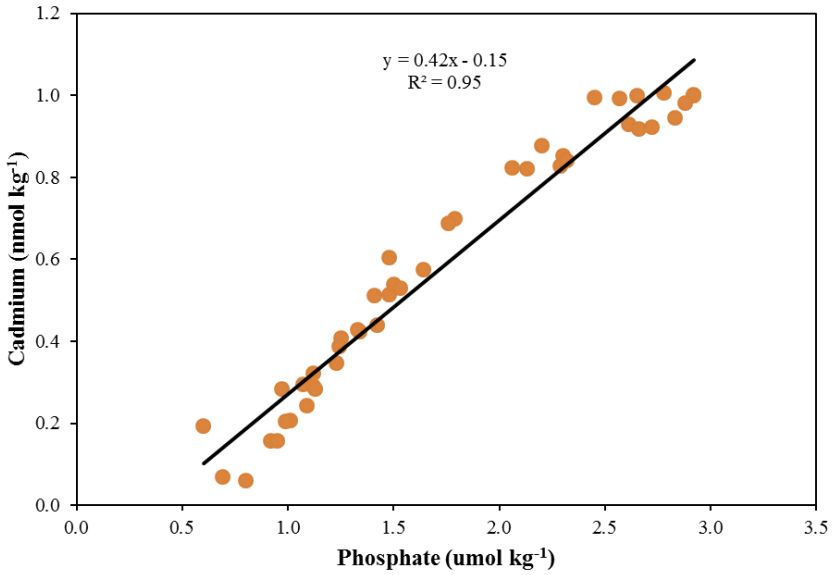

Figure A.3 Cd:PO_4^{3-} relationship in the nutricline on Line P
Data from Janssen et al., in revision (Chapter 4).

A.3 Expected sedimentary Cd concentrations if Cd is lost to slope sediments

The potential of continental slope sediment Cd inventory to account for the observed water column deficit can also be assessed by calculating the necessary sedimentary Cd

concentrations with measured continental slope Cd concentrations. This is shown in Table A.2 (at the end of this appendix). The dissolved Cd deficit (nmol L^{-1}) and the deficit volume were estimated in the same was as described in section A.2. This deficit was split into one cm tall sheets in contact with margin sediments. The sediment contact area of each sheet was calculated as described in section A.2. A sedimentation rate of 3 g cm^{-2} kyr^{-1} was estimated from McKay et al. (2007), which examined Cd accumulation in sediments off of Vancouver Island. This estimate was based on the highest sedimentation rate observed below 400 m depth in their study area (6 cm kyr^{-1}), the porosity of a nearby core (0.8) and the dry grain weight of sediments (2.5 g cm^{-3}), all from McKay et al. (2007).

The necessary shelf enrichment was calculated by transferring the dissolved Cd deficit in each one cm thick sheet into the sediment surface area on a 1000 year time scale in which this surface would accumulate 3 g cm^{-2}. This is certainly an over-estimate of the time available for this process to occur as the residence time of water in the subarctic northeast Pacific is ~10^2 years rather than 10^3 years. Overestimating the time available to accumulate Cd in sediments in this way will underestimate the necessary enrichment by up to one order of magnitude. Sedimentary Cd concentrations were compared to literature data from the region (McKay et al., 2007). Three examples from McKay et al. (2007) were selected for comparison:

1) The maximum sedimentary Cd concentration observed at any depth within any of their cores to place an upper limit on Cd accumulation in sediments.
2) The average Cd concentration in the upper 6 cm of sediments from cores in at least 400 m water depth. This would reflect 1000 years or more of accumulation and therefore would represent the exact process we are trying to approximate.
3) The average Cd concentration from all samples within their cores below 400 m water depth. This was roughly double the upper 6 cm Cd concentration.

An example calculation for necessary shelf sediment enrichment is presented below.

$$Cd\ deficit\ in\ a\ 1\ cm\ sheet$$
$$= 0.044\ nM\ Cd * \frac{1\ \mu mol}{1000\ nmol} \times \frac{1\ l}{1000\ cm^3} \times 1{,}400\ km \times 1{,}400\ km \times \frac{100{,}000^2\ cm^2}{1\ km^2} \times 1\ cm$$
$$= 8.62 \times 10^8\ \mu mol\ Cd$$

$$Sediment\ area\ in\ contact\ with\ each\ 1\ cm\ sheet = 1{,}400\ km \times 2 \times \frac{100{,}000\ \ cm}{1\ km} \times (1\ cm \div \sin(4°))$$
$$= 4.0 \times 10^{9}\ cm^{2}$$

$$Sediment\ Cd\ enrichment$$
$$= 8.62 \times 10^{8}\ \mu mols\ Cd \div 4.0 \times 10^{9}\ cm^{2} \times 3\ g\ cm^{-2} kyr^{-1} \times 1\ kyr \times 112.41\ g\ Cd\ mol^{-1}$$
$$= 8\ \mu g\ Cd\ g^{-1}$$

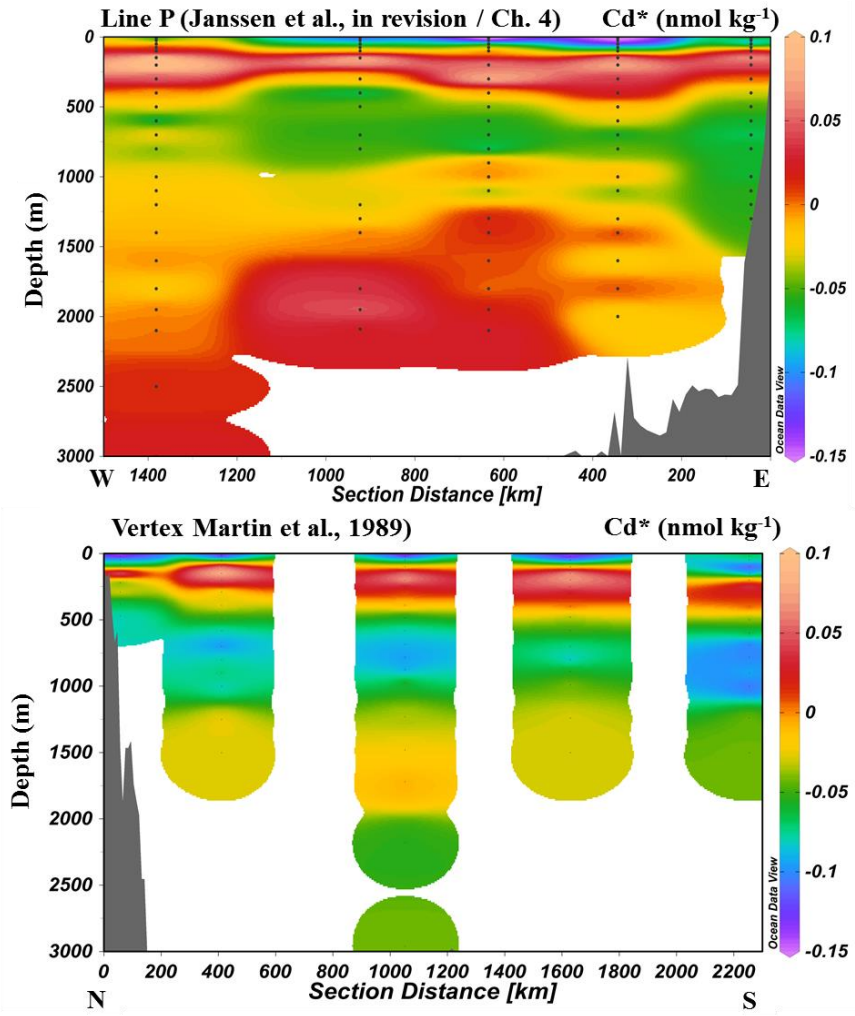

Figure A.4 The dissolved Cd deficit along the Line P and Vertex transects
Cd* was calculated from measured Cd and PO_4^{3-} and a deepwater Cd:PO_4^{3-} of 0.345.

A.4 Interpretation with the refined calculations

The dissolved Cd deficit which is observed in low-O_2 water could be explained by a process acting in the water column or by a process acting at the sediment water interface. In all likelihood both processes are occurring; however, the relative importance of the two is unknown. In order to try to determine the degree to which a water column sink may be important, we estimated the potential of continental slope sediments to hold the missing Cd using two independent approaches. A result indicating that margin sediments are capable of holding the missing Cd does not speak to how the Cd accumulated in these sediments (i.e. delivery of metal-rich particles to sediments or authigenic formation in sediments). A result indicating that margin sediments are unlikely to explain the observed deficit points to a process that does not occur at the sediment-water interface or proximate to the ocean margin.

We tested a range of Cd deficits based on Martin et al. (1989) data and new data presented in Chapter 4 of this dissertation relative to global deepwater and relative to regional nutricline Cd:PO_4^{3-} relationships. These approaches yield substantially different Cd deficits. As the dissolved Cd deficit is found where macronutrient concentrations are still increasing and dissolved O_2 is being consumed, it is likely that expected Cd:PO_4^{3-} relationships in this region are influenced by the Cd:P in remineralizing sinking particulate matter, as inferred from nutricline relationships. Phytoplankton grown in Fe-limiting regions such as Line P have higher cellular Cd:P than when grown under Fe-replete conditions (see the introduction to Chapters 4 and 5 and references therein) and dissolved Cd:PO_4^{3-} slopes in the nutricline in Fe-limited regions are higher than deepwater Cd:PO_4^{3-} (Cullen, 2006; Lane et al., 2009; Quay et al., 2015). Therefore it is likely that the actual dissolved Cd deficit falls between the two end members based on deepwater and nutricline Cd:PO_4^{3-} relationships. Consequently these deficit estimates can serve as end members for the removal time and sedimentary Cd concentration estimates.

The lowest Cd deficit used in the removal time estimate resulted in a removal time of roughly 2400 years. This estimate is larger than the ocean mixing time (~1500 years), and is an order of magnitude longer than the residence time of deepwater in the subarctic northeast Pacific (one hundred to hundreds of years based on ^{14}C age, as presented in Emerson and Hedges, 2008 from Key et al., 2004). Consequently, mixing would likely reset dissolved Cd:PO_4^{3-} and O_2, before sediments in contact with that water could remove sufficient dCd to

explain our observations. Under the conditions which are most likely to result in sediments capable of containing the missing Cd, the removal of Cd to sediments is still insufficient to account for a majority of the deficit and another process is necessary. Similarly, estimates of necessary continental slope Cd enrichments resulted in slope sediments being unlikely to explain the dissolved deficit. Taking the highest sedimentary Cd concentration observed in McKay et al., (2007) from one point in time and space along the continental slope and applying it to all sediments for a duration of 1000 years resulted in a sedimentary sink of roughly 13% of the observed deficit when the smallest deficit estimate was used.

The results of these calculations in combination with literature data identifying water column processes are an important source of sulphide-insoluble metals to continental slope sediments (McKay and Pedersen, 2008) and metal-rich particles in O_2-depleted water columns (Figure 2.3; Waeles et al., 2016; Ohnemus et al., 2016) demonstrate that water column processes are likely to be important in the removal of Cd from the dissolved pool in O_2-depleted waters. While sedimentary processes may also play a role, all of the estimates from our rough calculations resulted in a sedimentary sink term which was at least one order of magnitude smaller than necessary to account for the observed water column deficit.

A.5 Dissolved Cd deficits and the global Cd budget.

In Chapter 2 and Janssen et al. (2014), a global sink of Cd from O_2-depleted waters was calculated based on the observed Pacific Cd depletion and the volume of water in the global ocean with [Cd] < 50 μmol kg^{-1}. These calculations, as they appear in the manuscript, were performed using a Cd deficit of 0.1 nmol kg^{-1} rather than the updated deficits. These calculations are repeated here with the 0.040 nmol kg^{-1} deficit and using the same estimate of waters with less than 50 μmol kg^{-1} O_2 of 1.3-6.0 × 10^{19} L (Bianchi et al., 2009).

$$0.044 \times 10^{-9}\ mol\ Cd\ l^{-1} \times 1.3 \times 10^{19}\ l = 5.7 \times 10^{8}\ mols\ Cd$$
$$0.044 \times 10^{-9}\ mol\ Cd\ l^{-1} \times 6.0 \times 10^{19}\ l = 2.6 \times 10^{9}\ mols\ Cd$$

This deficit yields a yearly loss of 0.057–2.6 × 10^7 mols Cd assuming that this process operates on a time scale from the residence time of water in a low-O_2 basin (~10^2 years) to

ocean mixing (~10^3 years). This range is still of comparable magnitude to the atmospheric and riverine Cd flux (0.6–2.5 × 10^7 mol y^{-1}) and suboxic sedimentary removal rates (0.6–2.3 × 10^7 mol y^{-1}) presented in Rosenthal et al. (1995a). Therefore, the updated Cd deficit does not substantially change the potential relative significance of water column Cd loss on a global scale based on current knowledge of sources and sinks.

Source	Deficit (-Cd*)	Estimation method	Length	Depth	Volume	Volume	Deficit	Sediment Contact length[1]	Sediment Contact area[2]	Removal Rate[3]	Removal time
	nM		km	m	m^3	l	nmol	m	cm^2	ng Cd cm^2 y^{-1}	Years
Janssen, Ch. 4	0.044	Deepwater $Cd:PO_4^{3-}$ = 0.345	1400	500	9.8E+14	9.8E+17	4.3E+16	7168	2.0E+14	10	2415
Martin et al., 1989	0.079	Deepwater $Cd:PO_4^{3-}$ = 0.345	2200	400	1.9E+15	1.9E+18	1.5E+17	5734	2.5E+14	10	6814
Janssen, Ch. 4	0.13	Nutricline $Cd = 0.42*PO_4^{3-}$-0.15	1400	500	9.8E+14	9.8E+17	1.3E+17	7168	2.0E+14	10	7135
Martin et al., 1989	0.16	Nutricline $Cd = 0.42* PO_4^{3-}$-0.15	2200	400	1.9E+15	1.9E+18	3.1E+17	5734	2.5E+14	10	13800

Table A.1 Estimates of time necessary to remove sufficient Cd to explain the water column sink by removal of Cd to margin sediments

[1]Assuming a 4° continental slope angle.

[2]Assuming sediment contact on 2 sides of the missing Cd box

[3]The highest Cd sedimentation rate observed by van Geen et al., 1995.

Calculated Sedimentary Enrichment								
Source	**Deficit**	**Deficit**	**Deficit Length**	**Deficit in a 1 cm tall sheet**	**Sediment surface area in contact with 1 cm sheet[1]**	**Sedimentation Rate[2]**	**Necessary sediment enrichment**	**Necessary sediment enrichment**
	nM	**µmols cm^{-3}**	**km**	**µmols**	**cm^2**	**g cm^{-2} kyr^{-1}**	**µmols g^{-1}**	**µg g^{-1}**
Janssen Line P	0.044	4.0E-08	1400	8.62E+08	4.0E+09	3	0.072	8
Martin et al., 1989	0.079	7.9E-08	2200	3.82E+09	6.3E+09	3	0.20	23
Janssen Line P	0.13	1.2E-07	1400	2.55E+09	4.0E+09	3	0.21	24
Martin et al., 1989	0.16	1.6E-07	2200	7.74E+09	6.3E+09	3	0.41	46

Literature Data		
Source	**Notes**	**Observed concentration**
		µg g^{-1}
McKay et al., 2007	Maximum	1
McKay et al., 2007	Water depth >400 m, upper 6 cm average	0.19
McKay et al., 2007	Water depth >400 m, whole core average	0.32

Table A.2 Comparison of estimated necessary sedimentary Cd enrichment and observed concentrations

[1]Assuming a 4° continental slope angle and sediment contact on two sides.

[2]Estimated from the maximum observed sedimentation rate (6 cm kyr^{-1}) and the dry accumulation rate of 2.5 g cm^{-2} yr^{-1} from a nearby core with an observed sedimentation rate of ~5 cm kyr^{-1}, all from McKay et al., 2007. This study was chosen for comparison and sedimentation parameters because it investigated sediments off of Vancouver Island.

Appendix B

Comparison of P26 Cd and Zn data.

Cruise	Depth	Cd	Cd*	PO_4^{3-}		Cruise	Depth	Cd	Cd*	PO_4^{3-}		Cruise	Depth	Cd	Cd*	PO_4^{3-}
	m	nmol kg^{-1}	nmol kg^{-1}	µmol kg^{-1}			m	nmol kg^{-1}	nmol kg^{-1}	µmol kg^{-1}			m	nmol kg^{-1}	nmol kg^{-1}	µmol kg^{-1}
2012-13	10	0.284	-0.051	0.97		VERTEX	20	0.086	-0.162	0.72		2005-01	4.7	0.43	-0.045	1.34
2012-13	25	0.295	-0.074	1.07		VERTEX	50	0.286	-0.059	1.00		2005-01	11.6	0.41	-0.066	1.35
2012-13	50	0.515	0.004	1.48		VERTEX	100	0.452	-0.024	1.38		2005-01	25.7	0.42	-0.058	1.34
2012-13	75	0.540	0.023	1.50		VERTEX	150	0.73	0.071	1.91		2005-01	40	0.4	-0.073	1.34
2012-13	100	0.576	0.007	1.65		VERTEX	200	0.858	0.089	2.23		2005-01	50.6	0.44	-0.035	1.35
2012-13	148	0.878	0.119	2.20		VERTEX	250	0.905	0.025	2.55		2005-01	74.7	0.43	-0.046	1.35
2012-13	201	0.992	0.105	2.57		VERTEX	290	0.923	0.005	2.66		2005-01	98.5	0.43	-0.049	1.35
2012-13	300	1.007	0.048	2.78		VERTEX	390	0.982	-0.008	2.87		2005-01	149	1.06	0.270	2.23
2012-13	400	1.001	-0.007	2.92		VERTEX	485	0.952	-0.059	2.93		2005-01	203	1.08	0.182	2.54
2012-13	500	0.981	-0.023	2.91		VERTEX	580	0.947	-0.081	2.98		2005-01	301	1.2	0.172	2.90
2012-13	600	0.983	-0.073	3.06		VERTEX	685	0.956	-0.089	3.03		2005-01	403	1.12	0.036	3.06
2012-13	700	0.990	-0.024	2.94		VERTEX	780	0.966	-0.097	3.08		2005-01	599	1.1	-0.018	3.15
2012-13	800	0.998	-0.044	3.02		VERTEX	875	0.97	-0.096	3.09		2005-01	800	1.1	-0.028	3.18
2012-13	1000	1.011	-0.027	3.01		VERTEX	975	1.014	-0.052	3.09		2005-01	828	1.18	0.046	3.20
2012-13	1100	1.017	-0.022	3.01		VERTEX	1230	1.018	-0.034	3.05		2005-01	1000	1.21	0.074	3.21
2012-13	1200	1.019	-0.013	2.99		VERTEX	1480	1.026	-0.023	3.04		2005-01	1501	1.15	0.037	3.14
2012-13	1400	1.034	-0.012	3.03		VERTEX	1720	0.989	-0.008	2.89		2005-01	2002	1.15	0.081	3.02
2012-13	1600	1.025	-0.003	2.98		VERTEX	2180	0.906	-0.053	2.78		2005-01	2500	1.09	0.064	2.89
2012-13	1800	0.990	-0.021	2.93		VERTEX	2960	0.868	-0.043	2.64		2005-01	2999	1.04	0.067	2.75
2012-13	1950	0.996	-0.001	2.89		VERTEX	3470	0.848	-0.039	2.57		2005-01	3501	1.04	0.086	2.69
2012-13	2100	0.984	0.001	2.85		VERTEX	3910	0.834	-0.032	2.51		2005-01	4000	1.04	0.109	2.63
2012-13	2500	0.949	0.014	2.71												
2012-13	3000	0.915	0.022	2.59												
2012-13	3500	0.883	0.017	2.51												
2012-13	4000	0.872	0.010	2.50												

Table B.1 Comparison of Cd data from station P26

Data are from this dissertation (cruise: 2012-13; Chapter 4), Martin et al., 1989 (cruise: VERTEX), and unpublished UVic data (cruise: 2005-01).

Cruise	Depth	Zinc	Zinc Stdev		Cruise	Depth	Zinc
	m	nmol kg^{-1}	nmol kg^{-1}			m	nmol kg^{-1}
2012-13	75	1.45	0.09		VERTEX	20	0.07
2012-13	100	2.13	0.07		VERTEX	50	1.02
2012-13	148	6.02	0.18		VERTEX	100	0.99
2012-13	201	7.77	0.11		VERTEX	150	4.02
2012-13	300	8.58	0.05		VERTEX	200	5.58
2012-13	400	8.96	0.31		VERTEX	250	6.88
2012-13	500	9.00	0.23		VERTEX	290	7.46
2012-13	600	9.01	0.08		VERTEX	390	8.63
2012-13	700	9.06	0.08		VERTEX	485	8.36
2012-13	800	9.10	0.14		VERTEX	580	9.07
2012-13	1000	9.22	0.13		VERTEX	685	9.12
2012-13	1100	9.67	0.11		VERTEX	780	9.52
2012-13	1200	9.60	0.03		VERTEX	875	9.16
2012-13	1399	10.63	0.24		VERTEX	975	9.58
2012-13	1600	10.20	0.05		VERTEX	1230	9.76
2012-13	1800	10.28	0.01		VERTEX	1480	10.15
2012-13	1950	10.87	0.20		VERTEX	1720	10.28
2012-13	2100	10.41	0.05		VERTEX	2180	10.07
2012-13	2500	10.14	0.18		VERTEX	2960	9.59
2012-13	3000	10.19	0.12		VERTEX	3470	9.62
2012-13	3500	9.94	0.14		VERTEX	3910	9.78
2012-13	4000	9.84	0.12				

Table B.2 Comparison of Zn data from station P26
Data are from Chapter 3 / Janssen and Cullen (2015, cruise 2012-13) and Martin et al. (1989, cruise: VERTEX).

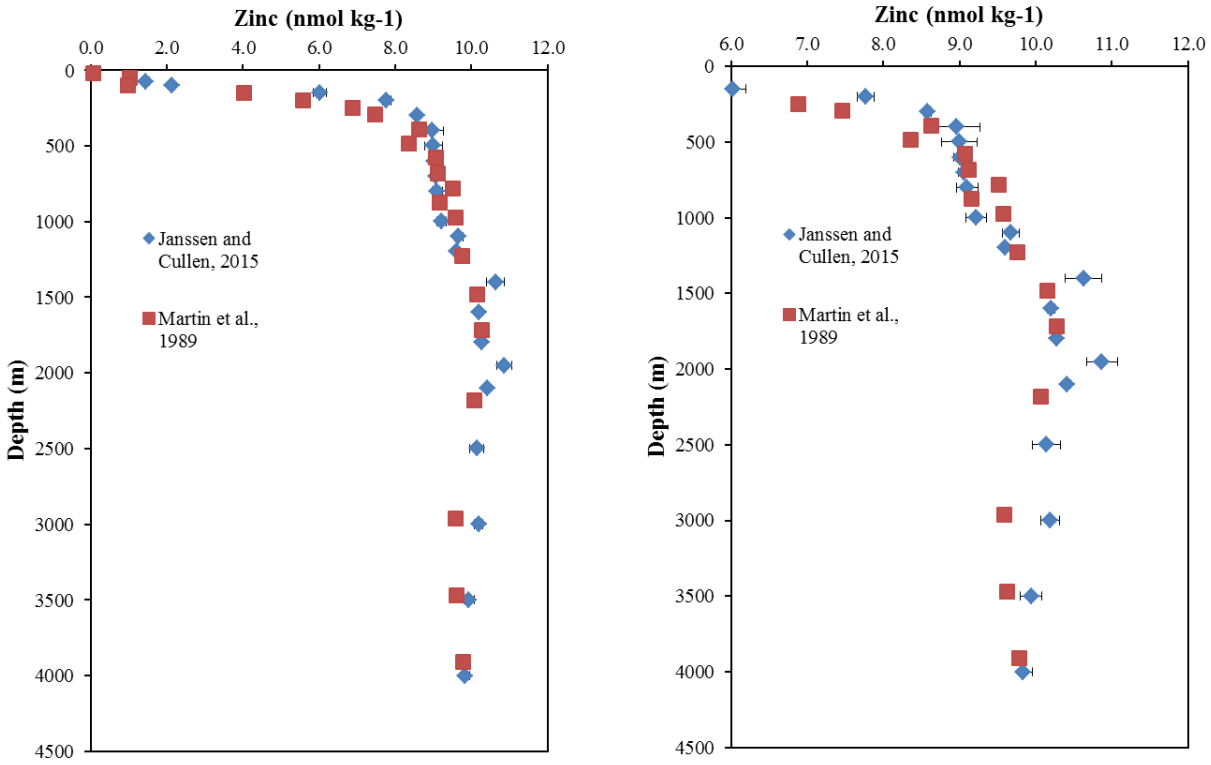

Figure B.1 Comparison of Zn data from station P26
Data from Chapter 2 / Janssen and Cullen (2015, blue diamonds) and Martin et al. (1989, red squares) are shown. Panel A shows the full Zn concentration range and panel B shows a limited range to highlight deepwater samples.

Dissolved Zn data form this dissertation and from Martin et al., (1989) compare well. Unlike as was observed for Cd, no regular offset is seen between my Zn data and literature data.

Appendix C

Supplemental material for Chapter 3 – Zinc in the subarctic northeast Pacific Ocean

C.1 Dissolved Zn data from Line P 2012.

Station	Bottle (Cast)	Lat	Long	Depth	Zn	Zn Stdev	NO_3^-	PO_4^{3-}	Si	O_2
		Deg N	Deg W	m	nmol kg^{-1}	nmol kg^{-1}	µmol kg^{-1}	µmol kg^{-1}	µmol kg^{-1}	µmol kg^{-1}
P26	$11_1(1)$	50	145	75	1.45	0.09	18.1	1.50	31.5	310.48
P26	$9_3(2)$	50	145	100	2.13	0.07	21.6	1.71	36.1	304.98
P26	$10_2(1)$	50	145	148	6.02	0.18	31.8	2.20	55.1	167.66
P26	**$8_{3,9}(2)$**	**50**	**145**	**200**	**8.27**	**0.18**	37.8	2.58	74.3	113.30
P26	**$8_{3,9}(3)$**	**50**	**145**	**201**	**7.77**	**0.11**	37.8	2.57	74.1	113.30
P26	$9_3(1)$	50	145	300	8.58	0.05	41.4	2.78	88.5	64.93
P26	$7_5(2)$	50	145	400	8.96	0.31	42.6	2.90	101.0	41.77
P26	**$8_{3,9}(1)$**	**50**	**145**	**500**	**9.54**	**0.09**	NA	NA	NA	34.30
P26	$7_5(1)$	50	145	500	9.00	0.23	43.0	2.91	110.4	34.30
P26	6 (2)	50	145	600	9.01	0.08	44.0	3.03	120.6	25.23
P26	6(1)	50	145	700	9.06	0.08	44.1	2.94	126.5	23.52
P26	$5_7(2)$	50	145	800	9.10	0.14	44.2	2.92	133.9	23.12
P26	**$4_{12}(3)$**	**50**	**145**	**900**	**2.10**	**0.01**	**20.2**	**1.65**	**34.1**	22.9
P26	$4_{12}(2)$	50	145	1000	9.22	0.13	44.8	3.04	144.4	22.09
P26	$5_7(1)$	50	145	1100	9.67	0.11	44.7	3.01	149.6	22.08
P26	$3_{8,4}(2)$	50	145	1200	9.60	0.03	44.8	2.99	153.1	22.08
P26	**$4_{12}(1)$**	**50**	**145**	**1300**	**1.20**	**0.14**	**16.8**	**1.43**	**30.1**	21.7
P26	$2_{10}(2)$	50	145	1399	10.63	0.24	45.4	2.94	160.4	21.05
P26	$3_{8,4}(1)$	50	145	1600	10.20	0.05	44.3	2.98	165.3	29.89
P26	$1_{11}(2)$	50	145	1800	10.28	0.01	44.0	2.93	168.3	42.52
P26	$2_{10}(1)$	50	145	1950	10.87	0.20	43.2	2.89	169.6	51.35
P26	$1_{11}(1)$	50	145	2100	10.41	0.05	42.8	2.85	170.0	60.90
P26	(L)	50	145	2500	10.14	0.18	40.6	2.71	169.0	81.76
P26	(L)	50	145	3000	10.19	0.12	39.0	2.59	167.1	107.21
P26	(L)	50	145	3500	9.94	0.14	38.2	2.51	165.7	123.86
P26	(L)	50	145	4000	9.84	0.12	37.5	2.50	165.8	133.39
P20	$10_2(1)$	49.57	138.67	150	5.17	0.06	30.5	2.06	51.4	167.93
P20	**$8_A(2)$**	**49.57**	**138.67**	**200**	**>17.5**	**NA**	35.3	2.45	65.8	122.8
P20	$9_3(1)$	49.57	138.67	300	7.41	0.08	39.5	2.72	79.9	75.63

P20	7_5(2)	49.57	138.67	400	8.33	0.03	41.2	2.61	92.7	54.79
P20	8_4(1)	49.57	138.67	498	8.77	0.03	42.6	2.94	102.4	38.51
P20	7_5(1)	49.57	138.67	700	9.18	0.09	43.9	3.05	122.0	23.31
P20	5_7(2)	49.57	138.67	800	9.42	0.06	44.4	3.08	129.9	18.26
P20	$3_{8,4}$(2)	49.57	138.67	1200	10.25	0.11	45.2	3.07	152.7	14.48
P20	5_7(1)	49.57	138.67	1300	10.25	0.06	45.1	3.07	154.3	16.23
P20	2_{10}(2)	49.57	138.67	1400A	9.85	0.16	45.4	3.03	159.7	19.10
P20	2_{10}(2)	49.57	138.67	1400B	10.12	0.10	NA	NA	NA	19.10
P20	**4_8(1)**	**49.57**	**138.67**	**1600**	**11.48**	**0.10**	**15.4**	**1.32**	**24.4**	30.0
P20	**3_9(1)**	**49.57**	**138.67**	**1600**	**12.94**	**0.10**	NA	NA	NA	30.0
P20	1_{11}(2)	49.57	138.67	1800	10.02	0.17	43.6	2.82	167.2	43.85
P20	2_{10}(1)	49.57	138.67	1950	10.61	0.10	42.7	2.74	167.9	54.43
P20	1_{11}(1)	49.57	138.67	2090	10.70	0.19	42.3	2.79	168.9	63.37
P16	9_3(1)	49.28	134.67	149	4.16	0.20	28.9	2.00	43.9	154.18
P16	8_4(2)	49.28	134.67	200	5.68	0.07	33.0	2.30	56.9	130.27
P16	8_4(1)	49.28	134.67	300A	7.36	0.15	38.8	2.65	74.0	85.97
P16	8_4(1)	49.28	134.67	300B	7.25	0.03	NA	NA	NA	85.97
P16	7_5(2)	49.28	134.67	400	8.28	0.17	40.9	2.88	89.1	60.99
P16	7_5(1)	49.28	134.67	500	8.80	0.11	42.8	2.96	100.4	37.90
P16	6(2)	49.28	134.67	600	8.86	0.14	43.8	2.73	112.1	24.13
P16	6(1)	49.28	134.67	699	9.24	0.08	44.5	3.08	122.2	21.16
P16	5_7(2)	49.28	134.67	800	9.36	0.03	44.5	3.15	127.0	15.69
P16	6(3)	49.28	134.67	900	9.06	0.13	44.4	2.96	134.7	13.76
P16	**4_8(2)**	**49.28**	**134.67**	**1000**	**1.69**	**0.14**	**7.1**	**0.80**	**3.7**	11.04
P16	5_7(3)	49.28	134.67	1000	9.11	0.09	44.9	2.98	141.2	11.04
P16	5_7(1)	49.28	134.67	1100	9.21	0.08	45.3	3.11	146.0	11.71
P16	**3_9(2)**	**49.28**	**134.67**	**1200**	**10.09**	**0.06**	44.9	2.72	140.1	12.5
P16	**4_8(1)**	**49.28**	**134.67**	**1300**	**7.41**	**0.13**	**39.0**	**2.65**	**72.7**	15.30
P16	2_{10}(3)	49.28	134.67	1300	9.84	0.13	45.3	2.94	154.7	15.30
P16	2_{10}(2)	49.28	134.67	1400	10.25	0.12	45.1	2.94	156.9	18.79
P16	**3_9(1)**	**49.28**	**134.67**	**1600**	**13.14**	**NA**	44.2	2.98	163.1	29.68
P16	1_{11}(3)	49.28	134.67	1600	9.91	0.14	44.5	2.93	164.6	29.68
P16	1_{11}(1)	49.28	134.67	1800	10.13	0.12	43.8	2.90	166.1	44.37
P16	2_{10}(1)	49.28	134.67	1949	10.73	0.09	43.1	2.89	169.8	55.77
P16	1_{11}(1)	49.28	134.67	2100	10.66	0.12	42.2	2.81	171.2	64.08
P12	10(1)	48.97	130.67	150	1.83	0.04	NA	NA	NA	206.05
P12	**9(1)**	**48.97**	**130.67**	**150**	**18.57**	**NA**	20.6	1.48	27.7	206.05
P12	8(2)	48.97	130.67	200	4.22	0.13	26.1	1.79	39.8	172.73
P12	8(1)	48.97	130.67	300	5.92	0.05	33.0	2.29	59.2	126.30

P12	7(2)	48.97	130.67	400	7.05	0.10	38.0	2.61	75.3	78.95
P12	7(1)	48.97	130.67	500A	7.73	0.05	41.8	2.91	91.0	43.75
P12	7(1)	48.97	130.67	500B	7.79	0.04	NA	NA	NA	43.75
P12	6(2)	48.97	130.67	600	8.32	0.03	43.3	2.95	100.7	24.70
P12	6(1)	48.97	130.67	700	8.73	0.05	44.2	3.05	114.4	20.13
P12	5(2)	48.97	130.67	800	8.57	0.15	44.9	3.08	120.3	12.95
P12	4(2)	48.97	130.67	1000	8.73	0.11	44.5	3.02	133.1	9.82
P12	**5(1)**	**48.97**	**130.67**	**1100**	**5.08**	**0.17**	45.1	3.10	142.4	11.4
P12	3(2)	48.97	130.67	1201	9.29	0.06	41.5	2.78	145.6	14.48
P12	4(1)	48.97	130.67	1301	9.77	0.14	44.9	3.09	151.8	18.08
P12	2(2)	48.97	130.67	1401	9.80	0.18	43.5	2.96	156.1	25.78
P12	3(1)	48.97	130.67	1600	9.96	0.32	NA	NA	NA	35.5
P12	2(1)	48.97	130.67	1600	9.94	0.04	44.1	3.00	162.8	35.5
P12	1(2)	48.97	130.67	1800	10.30	0.10	43.4	2.96	166.4	45.6
P12	1(1)	48.97	130.67	1999	10.19	0.06	42.7	2.92	170.8	60.18
P4	6(1)	48.65	126.67	148	2.86	0.01	30.5	2.13	40.6	118.38
P4	7(2)	48.65	126.67	200	3.73	0.07	32.6	2.32	47.1	97.77
P4	5(1)	48.65	126.67	300	5.21	0.11	38.1	2.66	62.9	59.07
P4	6(2)	48.65	126.67	400	6.03	0.07	39.2	2.83	70.4	39.94
P4	4(1)	48.65	126.67	498	7.30	0.14	41.9	2.97	82.7	29.17
P4	5(2)	48.65	126.67	600	7.14	0.03	42.4	3.07	90.1	16.67
P4	3(1)	48.65	126.67	700	7.55	0.03	43.9	3.15	103.3	12.12
P4	4(2)	48.65	126.67	799A	7.19	0.10	43.2	3.14	107.4	8.86
P4	4(2)	48.65	126.67	799B	7.33	0.08	NA	NA	NA	8.86
P4	3(2)	48.65	126.67	998	8.00	0.07	44.2	3.21	123.0	9.93
P4	2(1)	48.65	126.67	1101	8.28	0.07	44.9	3.17	134.6	13.56
P4	2(2)	48.65	126.67	1198	8.42	0.05	44.5	3.17	140.5	16.64
P4	1(1)	48.65	126.67	1300	9.14	0.07	44.6	3.14	145.8	20.33

Table C.1 Data from the 2012-13 Line P research cruise

Red trace metal data show signs of contamination. Blue data suggest a leaking/improperly sealing bottle (note that Zn from P12 1100 m suggests a leak but macronutrient data do not). One sample (P26 200 m cast 3) shown in orange was collected in a GO-FLO which consistently gave high Zn measurements but which seemed to be approaching accurate values the more it was used. This was the final use of this GO-FLO on the cruise and reliable data are not available to address whether this sample is high or accurate. Replicate subsamples collected from the same GO-FLO bottle are noted with an "A" or "B" following the depth. The subscript number between bottle and cast numbers denotes previous positions this bottle occupied during the cruise. For example, the P26 1200 m sample labeled as $3_{8,4}$(2) was collected from the GO-FLO in position 3 on cast 2 at P26. The GO-FLO in position 3 on this cast was previously in position 8 (P16 casts 1 and 2, P20 cast 1), and in position 4 (P4 and P12 casts) before being in position 8. Cast L at Station P26 was a 4 bottle cast of GO-FLO bottles on a Kevlar line tripped by Teflon messenger rather than a TMR cast. Bottle and CTD data for additional parameters from this cruise is available at https://www.waterproperties.ca/linep/2012-13/index.php. Nutrient data (bottle) and oxygen data (CTD) are courtesy of Line P program chief scientist Marie Robert and the Institute of Ocean Sciences, DFO

(Sidney, BC). Phosphate data was erratic and at times these data are interpolated due to erratic values or no data available at the stations and depth. Interpolated data are as follows: P26: 1800 m, P20: 1200 m, 1400 m, 1800 m. Values form samples taken from the conventional rosette are as follows: P16: 400 m, 800 m, 1400 m. The P12 1800 m sample was lost due to a cracked nutrient tube and therefore nitrate and phosphate data are interpolated.

Bottles positions were changed multiple times throughout the cruise. The first swap was at Station 16 before any casts were made. This switch affected all bottles except position 6. The second switch occurred at Station P20 between the two casts. This cast affected 4 bottles (positions 3, 4, 8 and 12). During this switch, the bottle from position 3 (consistently high Zn) was removed from the lineup. Positions were changed for bottles formerly in positions 4, 8 and 12 and an alternate bottle, which had not previously been used on the cruise, was placed in position 8. A third swap was made at station P26. The bottle which had been removed from position 3 at Station 20 (which had been consistently giving high values) was brought in to replace the bottle in position 8. Table C.2 shows positions occupied by each bottle throughout the cruise.

Bottle Number	**Stations P4-P12**	**Stations P16-P20 Cast 1**	**Station P20 Cast 2**	**Station P26, P16 Cast 3**
	Position	**Position**	**Position**	**Position**
1	1	11	11	11
2	2	10	10	10
3	3	9	9	9
4	4	8	3	3
5	5	7	7	7
6	6	6	6	6
7	7	5	5	5
8	8	4	12	12
9	9	3	NA	8
10	10	2	2	2
11	11	1	1	1
12	12	12	4	4
Alternate	NA	NA	8	NA

Table C.2 GO-FLO bottle positions throughout the cruise

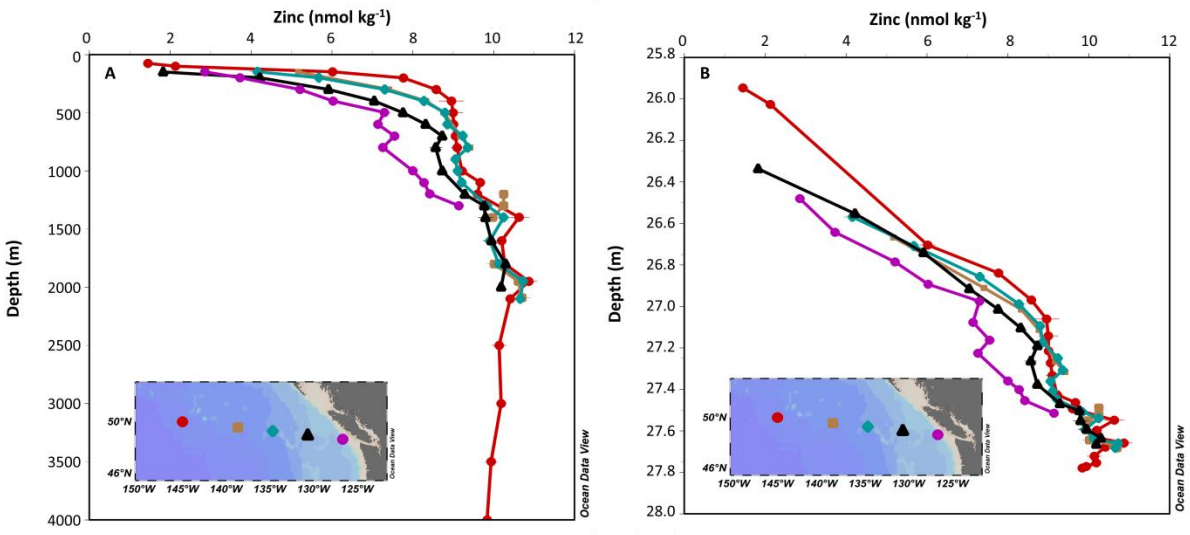

Figure C.1 Dissolved Zn depth profiles along the Line P transect
Zinc data is from all major stations along the transect (stations shown in inlay map). Moving from the coastal to oceanic stations, P4 is shown in purple, P12 in black, P16 in light blue, P20 in tan and P26/OSP in red. Panel A shows the concentrations plotted in depth space and panel B shows the trend in density space.

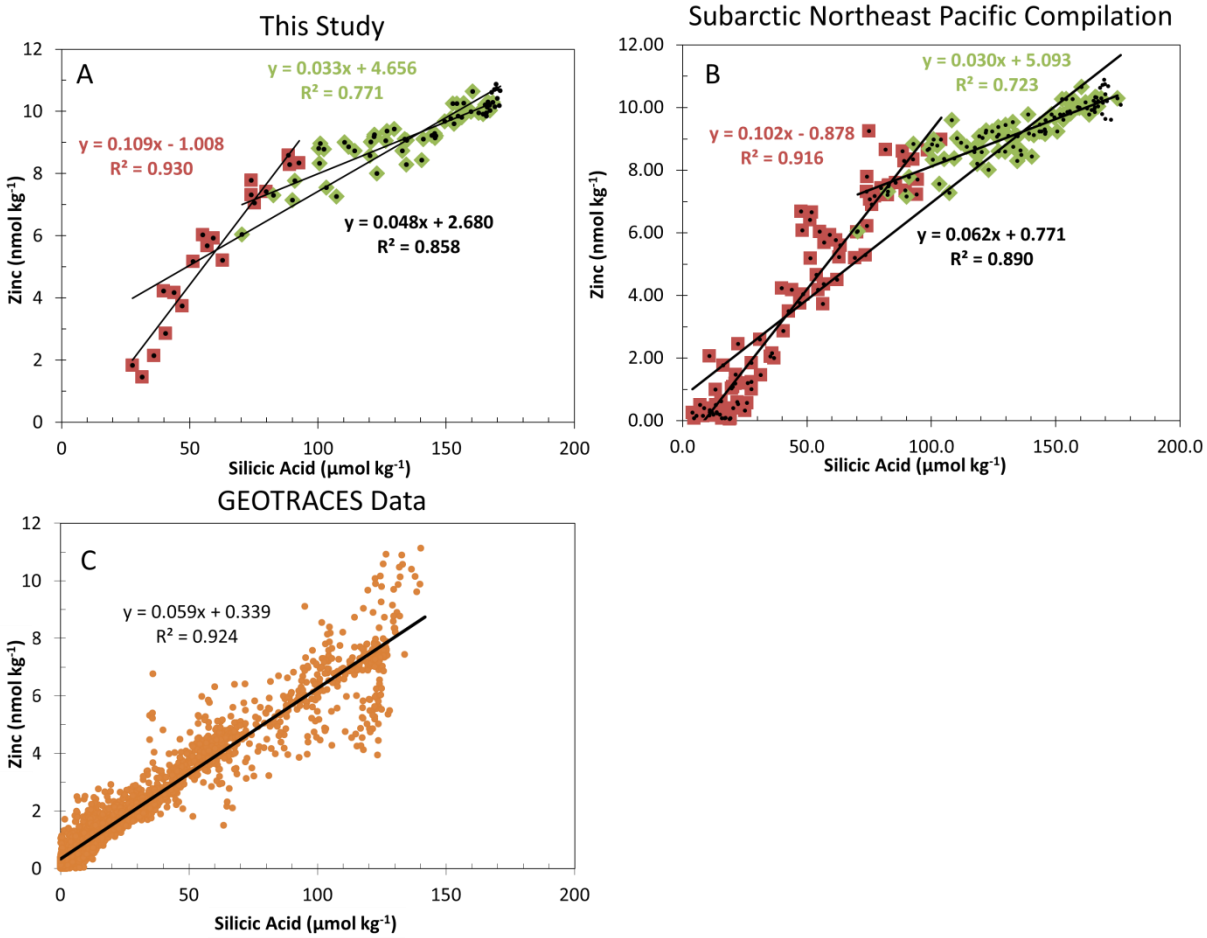

Figure C.2 The Zn:Si relationship in the northeast Pacific and the world ocean
Data from this study along Line P is shown in panel A and a compilation of subarctic northeast Pacific data (this study; Lohan et al., 2002 (station P4 is omitted); Martin et al., 1989) is shown in panel B. Red squares denote samples with both $[O_2] > 50$ µmol kg^{-1} and depths above 510 m. Green diamonds denote samples with $[O_2] < 50$ µmol kg^{-1} (samples within the subarctic northeast Pacific ODZ). Black dots denote all samples, including the previous two categories as well as samples from below the ODZ. Trendline slopes and intercepts are color coordinated to these red, green, and black data groupings. Panel C shows the global average comprised only of GEOTRACES data from the intermediate data product (2014) and excluding the subarctic northeast Pacific.

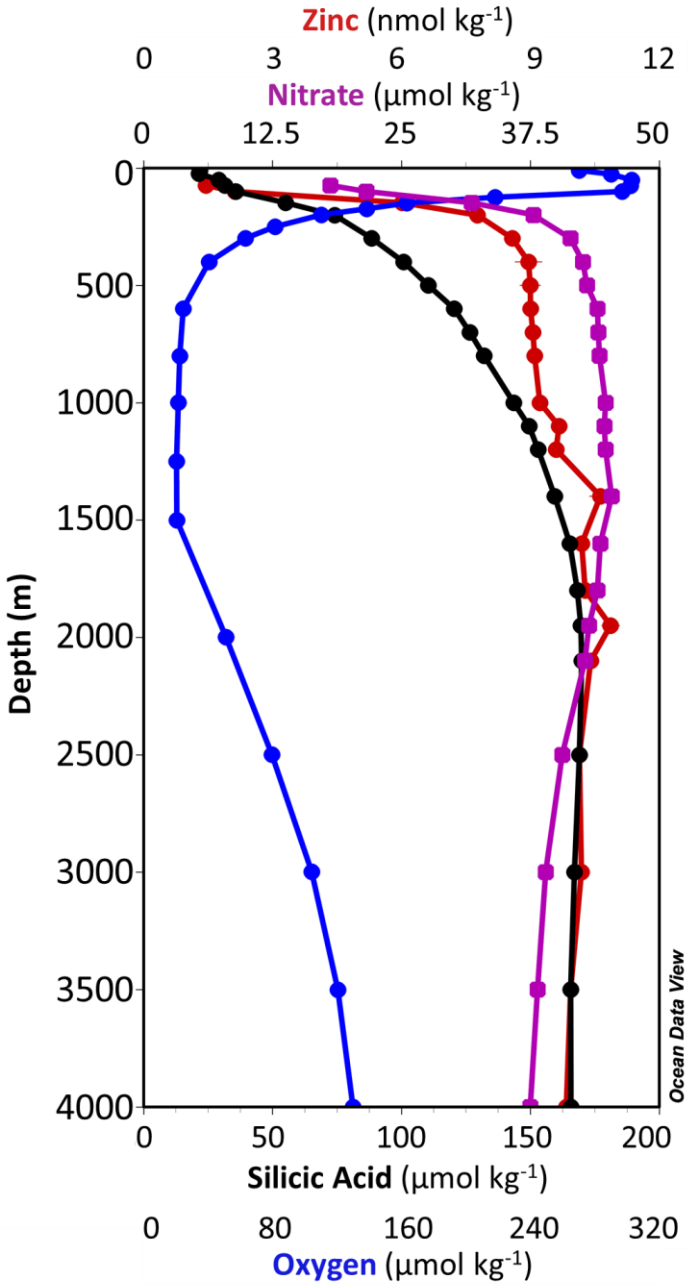

Figure C.3 Depth profiles for dissolved zinc, nitrate, silicic acid, and oxygen at P26
Zinc is shown in red, NO_3^- in purple, Si in black and O_2 in blue. The rapid remineralization of Zn in the upper 400 m tracks well with NO_3^- but not with Si. In the ODZ below 400 m both Zn and NO_3^- show relatively stable values while Si continues increasing. Dissolved Zn and Si concentrations increase below 1000 m to a maximum value at around 2000 m while O_2 and NO_3^- reach their respective minimum and maximum and O_2 and NO_3^- concentrations begin increasing and decreasing respectively over this range. Below 2000 m both Zn and Si maintain relatively stable high deep-water values while O_2 and NO_3^- concentrations continue to increase and decrease respectively.

C.2 Global Zn:Si with O_2

The GEOTRACES global Zn:Si data set is shown in Figure C.4. Indian Ocean data (GI04, Vu and Sohrin, 2013) show a mixed trend, with 4 of the 6 profiles with $[O_2]$ < 50 µmol kg^{-1} falling below the bulk of the global composite. Of the remaining two stations, the one converges with the low Zn:Si cluster at intermediate [Zn] (station ER-2, the station with lower $[O_2]$ of the two remaining stations) while the other more oxic station (ER-3, $[O_2]_{min}$ = 45.6 µmol kg^{-1}) remains above the global trend. The $[O_2]_{min}$ of the stations falling below the global average ranges from 2-35 µmol kg^{-1} (data from Vu and Sohrin, 2013). Low O2 samples from elevated Zn (7-11 nmol kg-1) and Si (90-170 µmol kg-1) are from the subarctic northeast Pacific. The tracking of the Pacific data is shown in Figure 3.4, Table 3.1, and Figure C.1, and profiles have not been included in Figure C.4 for clarity of the other data.

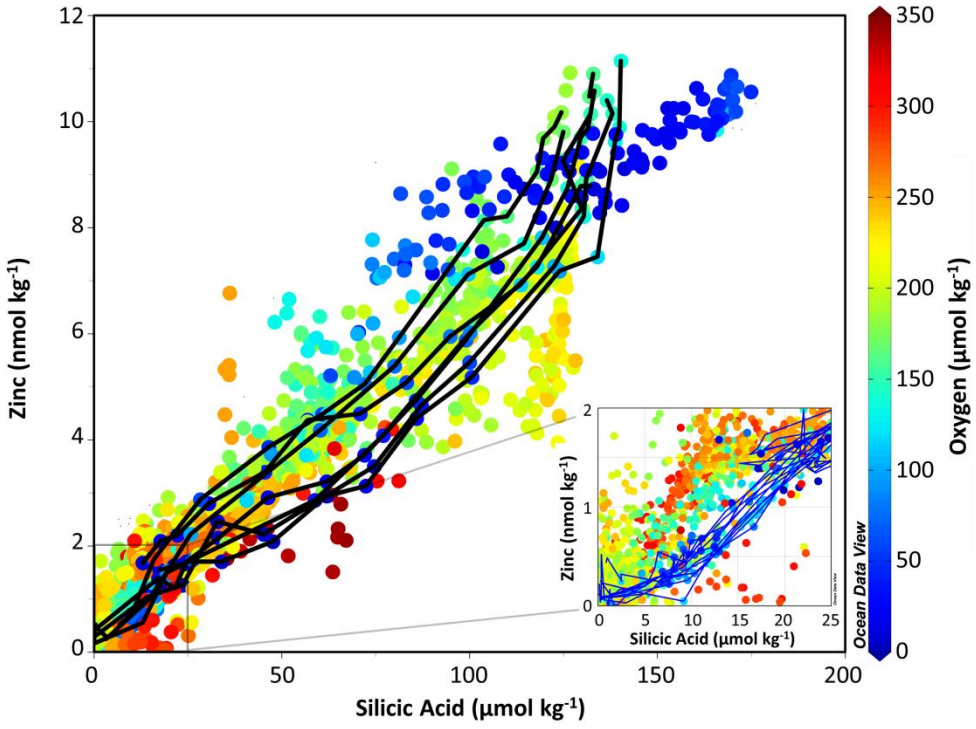

Figure C.4 Dissolved Zn:Si and O_2 in the global ocean
The global Zn:Si trend from the GEOTRACES data set (GEOTRACES, 2014) and subarctic northeast Pacific data (Martin et al., 1989; Lohan et al., 2002; this study) is shown with dissolved O_2 (analogous to figure 4 panel C with the data shown in panels A and B). Indian Ocean profiles with low [O2] samples (<50 µmol kg^{-1}) are shown with black lines (GEOTRACES cruise GI04, Vu and Sohrin, 2013). Atlantic profiles with low $[O_2]$ samples (<100 µmol kg^{-1}) are shown with blue lines in the insert (0-2 nmol kg^{-1} Zn, 0-25 µmol kg^{-1} Si; GEOTRACES cruises GA03, Conway and John 2014; GA02 de Baar, unpublished data; GA10, Wyatt et al., 2014). Low $[O_2]$ samples in the insert without profile lines are from the Indian Ocean and are left unmarked in the insert to allow for clarity in the Atlantic profiles.

Atlantic data with low [O_2] (<100 µmol kg^{-1}) are shown as blue lines in the insert (GA02 de Baar unpublished data; GA03 Conway and John, 2014; GA10 Wyatt et al., 2014). Though these data cover the eastern North Atlantic, the western equatorial Atlantic and the eastern South Atlantic, their trending is consistent. The low [O_2] Atlantic data consistently sit below the bulk of the Zn:Si compilation, including more oxic samples from the Atlantic, over the concentration range of 0-2 nmol kg^{-1} Zn, 0-25 µmol kg^{-1} Si. The samples sitting below this O_2-depleted Atlantic cluster are primarily either surface HNLC Pacific Ocean samples (high [O_2]) or O_2-depleted Indian Ocean samples.

The similar anomalous tracking relative to a global composite of Zn:Si is consistent across ODZs from different ocean basins and covering different depth ranges. This depth- and basin-independent depletion of Zn relative to Si in oceanic ODZs does not support basin-specific (*e.g.* anomalous pre-formed Zn:Si, localized advected Zn or Si sources) or depth specific (*e.g.* particle density driven, stratification and mixing) forcings and instead supports the decoupling being driven by a common underlying mechanism related to O_2 depletion such as the formation of solid sulphides in the water column. Similar decoupling of other sulphide-insoluble metal-macronutrient pairs in these environments (Janssen et al., 2014 / Chapter 2; Conway and John, 2015a) provides further support to such an oxygen specific mechanism.

C.3 Zn*

Following the definition of Wyatt et al. (2014) Zn*, denoting enrichments or deficiencies in Zn relative to Si and a chosen Zn:Si relationship, is calculated for the Line P transect by the following:

$$Zn^* = [Zn]_{meas} - [Si]_{meas} * 0.065 + 0.21$$

Given the difficulties in establishing an accurate baseline Zn:Si relationship (including the possibility of variable basin-scale relationships as observed for Cd:PO_4^{3-} (de Baar et al., 1994)), the tracking of Zn* throughout the water column should be treated with more confidence than the Zn* value at a given depth. The tracking of Zn* shows how Zn:Si is changing throughout a depth profile or transect regardless of the linear Zn:Si trend chosen and therefore allows comparisons within a data set of enrichment and depletion of Zn relative to Si without requiring full confidence in the Zn:Si relationship chosen. Zn* based on the composite subarctic northeast Pacific linear relationship can also be visualized for a given data point by tracking to that data point from the subarctic northeast Pacific Zn:Si relationship trendline (Figure 3.4 panel A, Figure C.1). Samples lying above the Zn:Si trend are enriched

with Zn by the degree to which they lie above the trendline and samples below the trendline are depleted with Zn by the same amount relative to Si and the average whole water column subarctic northeast Pacific trend.

Zn* is shown for the Line P transect along with dissolved O_2 contours (Figure C.5, including Lohan et al. (2002) stations P12-P26 and Martin et al. (1989) station T7/P26). For the Line P transect maximum of Zn* is observed at 300-500 m depth, corresponding with the kink in Zn:Si at [Si] = 90-100 µmol kg^{-1} and [O2] > 50 µmol kg^{-1}. From this point Zn* values decrease throughout the ODZ, reaching minimum values between 1600 m and 1700 m ([O_2] < 50 µmol kg^{-1}) before increasing (P12 shows a second minimum at 2000 m and P26 shows a second minimum below 2000 m). Station P4 (bottom depth = 1324 m) shows a minimum at 1200 m. Zn* profiles against O_2 for the composite of subarctic northeast Pacific data are shown in Figure C.6 (Martin et al., 1989; Lohan et al., 2002 stations P12-P26; this study). The same general trend is visible, with Zn* increases with decreasing [O_2] until [O_2] is roughly 50 µmol kg^{-1}. At this point Zn* begins tracking toward the negative direction, signaling a Zn:Si trendline slope below the global average. Zn* reaches a minimum for most stations below the core of the ODZ as [O_2] begins to increase (20 µmol kg^{-1} < [O_2] < 50 µmol kg^{-1}, corresponding to 1500-2000 m depth) though some stations show similarly low Zn* at elevated [O_2] below the ODZ.

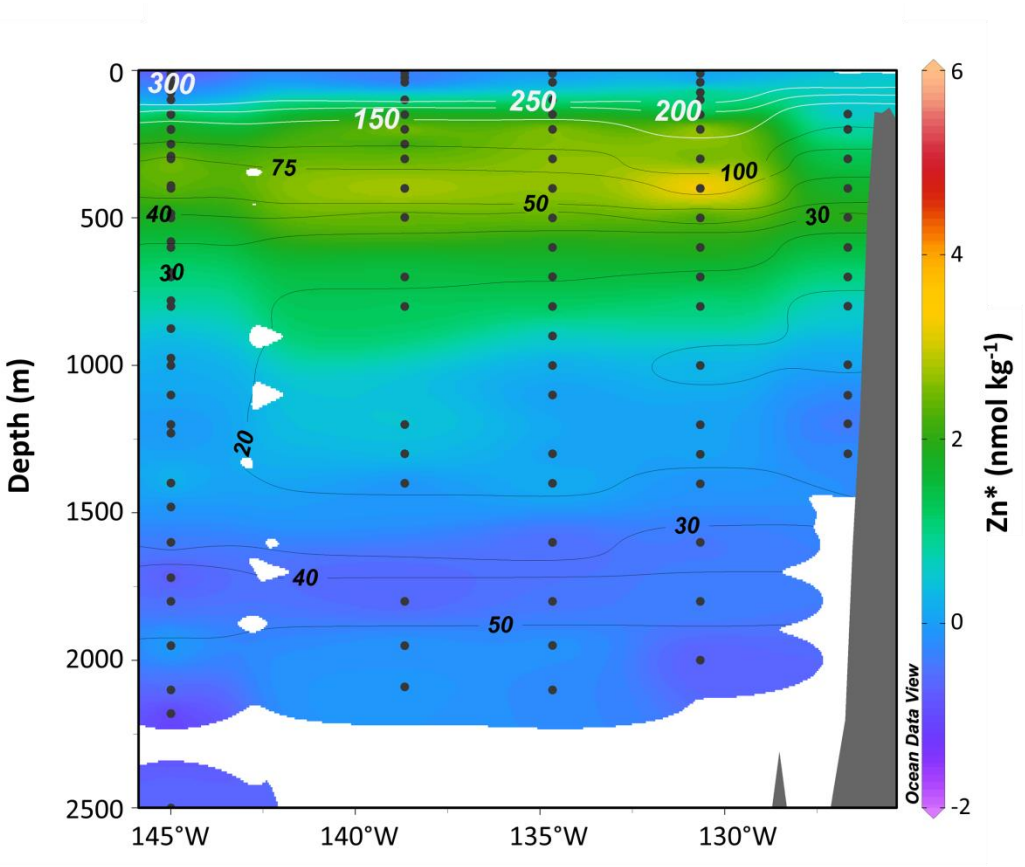

Figure C.5 Zn* along the Line P transect
Zn* values are shown as calculated following the definition of Wyatt et al. (2014). Dissolved [O_2] (μmol kg^{-1}) is shown with contours. Zinc and Si data are from Martin et al. (1989, station T7), Lohan et al. (2002, excepting station P4) and this study. Dissolved [O_2] is from August 2012 (the same cruise as the Zn and Si data in this study) and is courtesy of the Line P program (Institute of Ocean Sciences, Sidney, BC).

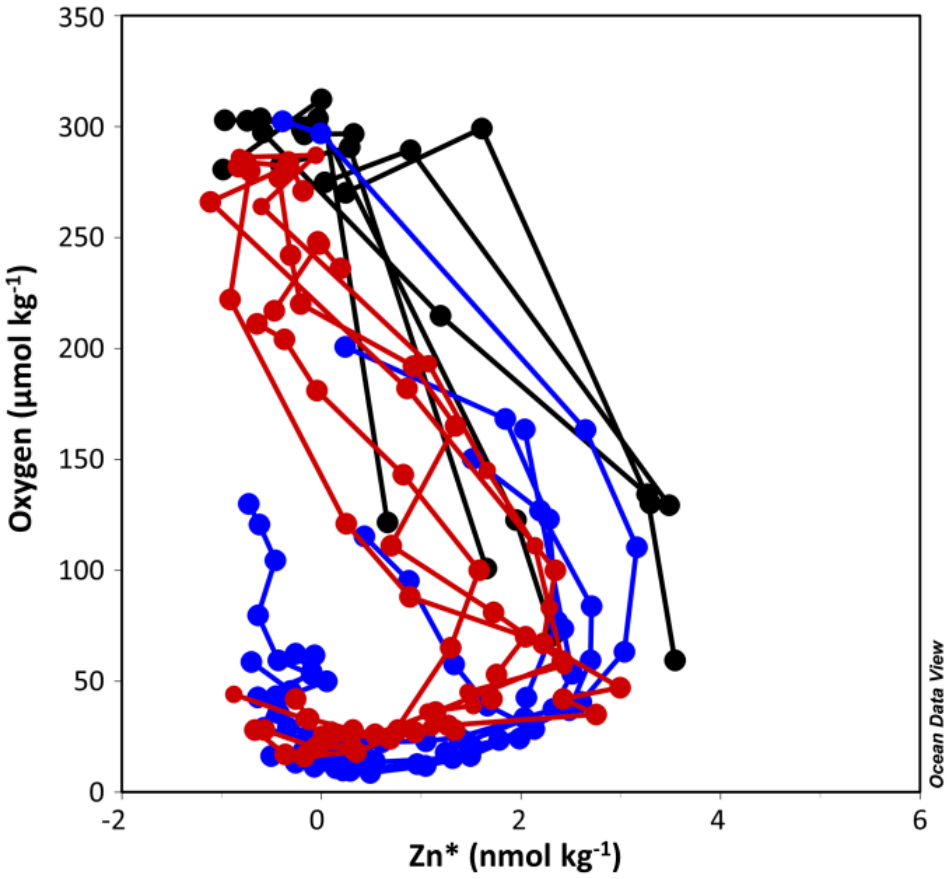

Figure C.6 Zn* and O_2 in the subarctic northeast Pacific
Zn* values are calculated following the definition of Wyatt et al. (2014). Data from Martin et al. (1989) is shown in red. Data from Lohan et al. (2002) is shown in black. This study is shown in blue.

Appendix D

Supplemental material for Chapter 4 – Dissolved Cd and $\varepsilon^{112/110}$Cd in the subarctic northeast Pacific

D.1 NIST SRM-3108 reference standards

ng Cd Loaded	^{110}Cd/^{112}Cd	standard error	$\varepsilon^{112/110}$Cd	2σ	$\delta^{114/110}$Cd	2σ	N
≥50	0.520121	3.6E-07	0.00	0.01	0.000	0.002	53
10	0.520127	2.0E-06	-0.11	0.08	-0.022	0.016	9
5	0.520132	2.5E-06	-0.21	0.10	-0.042	0.020	12
1	0.520143	8.3E-06	-0.41	0.32	-0.082	0.064	10
0.5	0.520139	2.0E-05	-0.35	0.77	-0.07	0.15	4

Table D.1 $\varepsilon^{112/110}$Cd of NIST SRM-3108 reference standards
Weighted mean $\varepsilon^{112/110}$Cd values from NIST SRM-3108 reference standards, double-spiked and run between October 2013 and March 2016. Standard runs are grouped by the mass of NIST Cd loaded for each analysis. 2σ ^{110}Cd/^{112}Cd errors for the weighted mean ^{110}Cd/^{112}Cd ratio were determined by:

$$\text{Weighted Mean } {}^{110}\text{Cd}/{}^{112}\text{Cd } 2\sigma = 2 \times \left(\frac{1}{\Sigma \left(\frac{1}{Individual\ Measurement\ 1\sigma^2} \right)} \right)^{-0.5}$$

$\varepsilon^{112/110}$Cd values are referenced to ^{110}Cd/^{112}Cd = 0.520121 (Abouchami et al., 2011; this study).

A trend of decreasing $\varepsilon^{112/110}$Cd is observed as the amount of Cd analyzed decreases in replicate analyses of the NIST-SRM 3108 reference standard (Table D.1). The trend to slightly more negative $\varepsilon^{112/110}$Cd as the amount of loaded Cd decreases is real, though is only marginally outside the error of measurement. This can be shown to be due to the presence of small hydrocarbon isobars during TIMS analyses using silica gel activator. In spectrum scans on the ion counter these peaks are seen on the high-mass side of the major inorganic Cd masses, amounting to a few hundred counts. Such count rates are potentially capable of biasing the Cd isotope data by up to around an ε-unit when measured ^{112}Cd beams are 0.1 pA or less. Ion statistics and these hydrocarbon interferences appear to constitute the ultimate limit on precision of Cd isotope measurements by TIMS for small samples.

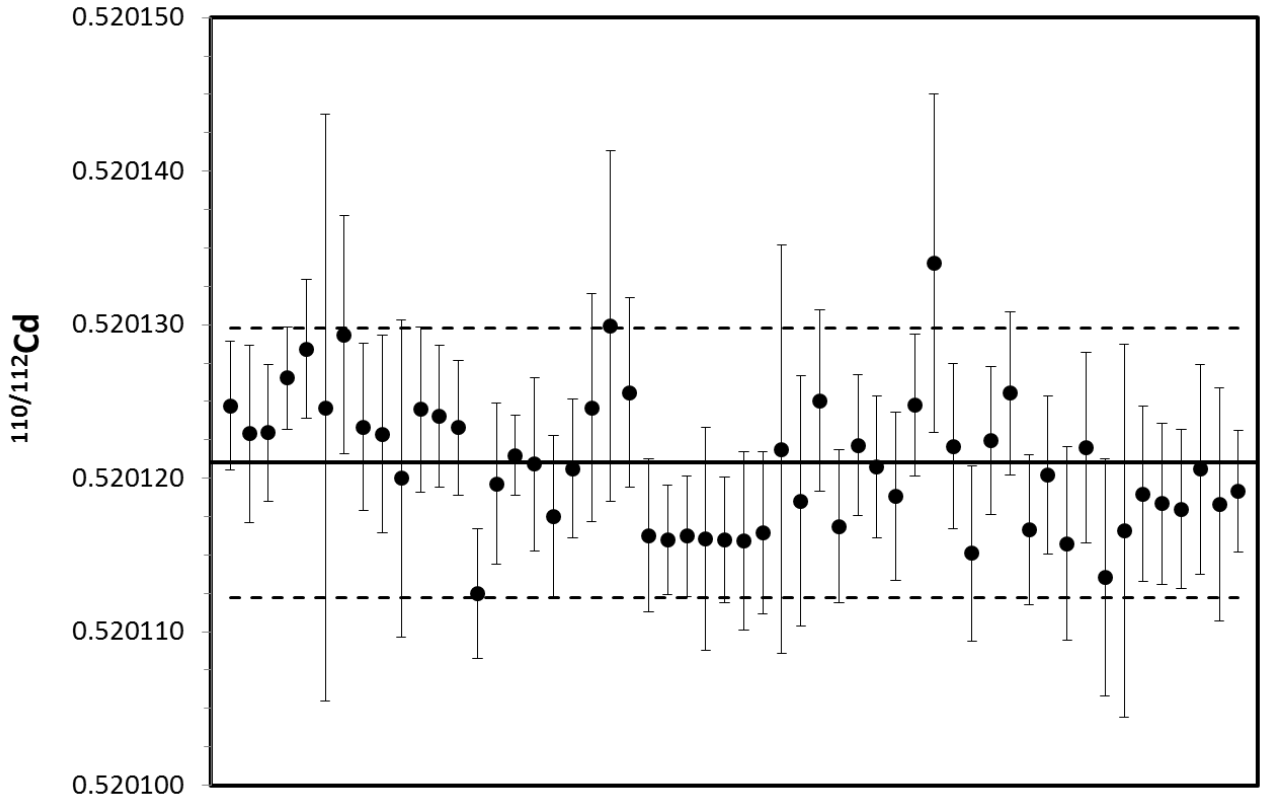

Figure D.1 Long term reproducibility of $^{110/112}$Cd ratios of the NIST SRM-3108 standard for ≥50 ng Cd loads

Standards were analyzed with each set of samples and were measured between October 2013 and April 2016. Error bars correspond to 2σ. The mean value agrees well with that reported by Abouchami et al. (2011, 2013). The solid black line shows the arithmetic mean $^{110/112}$Cd of 0.520121 and the dashed lines show the 2SD error around this mean (0.520121± 0.0000088).

D.2 Data tables and alternate plots in $\delta^{114/110}$Cd notation

Lat	Long	Station	Cruise	TM Sample	Depth	$\varepsilon^{112/110}$Cd	$\delta^{114/110}$Cd	[Cd]	Cd	Cd*	NO_3^-	Si	PO_4^{3-}	CTD Temp	Salinity	CTD σ_0	CTD O_2
°N	°E			ID #	m			nmol kg^{-1}	% max	nmol kg^{-1}	µmol kg^{-1}	µmol kg^{-1}	µmol kg^{-1}	°C	psu		µmol kg^{-1}
50	-145	P26	2012-13	659	10	3.91 ± 0.12	0.78 ± 0.02	0.284	27.5	-0.049	10.3	21.8	0.97	12.6	32.564	24.60	275.1
50	-145	P26	2012-13	638[P]	25	3.64 ± 0.12	0.73 ± 0.02	0.295	28.5	-0.075	11.3	21.5	1.07	11.0	32.587	24.92	287.6
50	-145	P26	2012-13	506	50	2.35 ± 0.13	0.47 ± 0.03	0.515	49.8	0.004	15.5	29.1	1.48	5.5	32.710	25.83	307.4
50	-145	P26	2012-13	505	75	2.05 ± 0.10	0.41 ± 0.02	0.540	52.2	0.022	18.1	31.5	1.50	4.6	32.736	25.95	308.8
50	-145	P26	2012-13	656	100	1.92 ± 0.12	0.38 ± 0.04	0.576	55.7	0.008	21.4	35.8	1.65	4.1	32.771	26.03	302.8
50	-145	P26	2012-13	504	148	1.06 ± 0.09	0.21 ± 0.02	0.878	84.9	0.119	31.8	55.1	2.20	4.2	33.636	26.70	165.3
50	-145	P26	2012-13	655	201	1.09 ± 0.12	0.22 ± 0.02	0.992	96.0	0.105	37.8	74.1	2.57	3.9	33.763	26.84	111.3
50	-145	P26	2012-13	503	300	1.02 ± 0.09	0.20 ± 0.02	1.007	97.4	0.050	41.4	88.5	2.78	3.8	33.918	26.97	61.6
50	-145	P26	2012-13	654	400	1.03 ± 0.10	0.21 ± 0.02	1.001	96.8	-0.007	43.3	100.8	2.92	3.8	34.030	27.06	41.1
50	-145	P26	2012-13	501	500	1.02 ± 0.11	0.21 ± 0.02	0.981	94.9	-0.023	43.0	110.4	2.91	3.7	34.124	27.14	33.4
50	-145	P26	2012-13	653	600	1.17 ± 0.20	0.23 ± 0.04	0.983	95.1	-0.073	43.7	120.5	3.06[3]	3.6	34.202	27.22	27.0
50	-145	P26	2012-13	500	700	0.97 ± 0.17 1.07 ± 0.22	0.19 ± 0.03 0.21 ± 0.04	0.990	95.8	-0.024	44.1	126.5	2.94	3.4	34.252	27.27	22.9
50	-145	P26	2012-13	652	800	1.14 ± 0.19	0.23 ± 0.04	0.998	96.5	-0.044	44.4	132.1	3.02[3]	3.2	34.305	27.33	23.9
50	-145	P26	2012-13	650	1000	1.00 ± 0.14	0.20 ± 0.03	1.011	97.8	-0.027	44.3	143.6	3.01	2.9	34.381	27.43	22.2
50	-145	P26	2012-13	499	1100	1.60 ± 0.19 1.36 ± 0.22	0.32 ± 0.04 0.27 ± 0.04	1.017	98.6	-0.019	44.7	149.6	3.01	2.7	34.411	27.46	21.5
50	-145	P26	2012-13	534	1200	0.72 ± 0.17	0.14 ± 0.03	1.019	98.6	-0.012	44.8	153.1	2.99	2.6	34.436	27.49	21.5
50	-145	P26	2012-13	648	1400	1.17 ± 0.15	0.23 ± 0.03	1.034	100.0	-0.010	45.4	159.5	3.03	2.4	34.492[2]	27.55	20.5
50	-145	P26	2012-13	497	1600	0.94 ± 0.10	0.19 ± 0.02	1.025	99.2	-0.002	44.3	165.3	2.98	2.2	34.523	27.60	29.1
50	-145	P26	2012-13	532	1800	1.33 ± 0.19	0.27 ± 0.04	0.990	95.8	-0.021	44.0	168.3	2.93[1]	2.1	34.566[2]	27.64	41.4
50	-145	P26	2012-13	496	1950	1.21 ± 0.17	0.24 ± 0.03	0.996	96.4	-0.001	43.2	169.6	2.89	2.0	34.583[2]	27.66	50.0
50	-145	P26	2012-13	495	2100	1.27 ± 0.28	0.25 ± 0.06	0.984	95.2	0.000	42.8	170.0	2.85	1.9	34.597[2]	27.68	59.3
50	-145	P26	2012-13	600[L]	2500	0.89 ± 0.14 0.91 ± 0.19	0.18 ± 0.03 0.18 ± 0.04	0.949	91.8	0.012	40.6	169.0	2.71	1.7	34.629	27.72	84.2
50	-145	P26	2012-13	599[L]	3000	1.29 ± 0.15	0.26 ± 0.03	0.915	88.6	0.022	39.0	167.1	2.59	1.6	34.655[2]	27.75	109.8
50	-145	P26	2012-13	598[L]	3500	1.24 ± 0.18 1.29 ± 0.25	0.25 ± 0.04 0.26 ± 0.05	0.883	85.5	0.017	38.2	165.7	2.51	1.5	34.672[2]	27.77	126.7
50	-145	P26	2012-13	597[L]	4000	1.11 ± 0.14	0.22 ± 0.03	0.872	84.4	0.009	37.5	165.8	2.50	1.5	34.682[2]	27.78	137.0

496	-138.7	P20	2012-13	429	10.6	ND	ND	0.244	23.5	-0.133	11.5	18.6	1.09	13.8	32.513	24.34	271.6
49.6	-138.7	P20	2012-13	428	25.3	ND	ND	0.292	28.1	-0.095	11.9	19.3	1.12	9.1	32.601	25.25	306.8
49.6	-138.7	P20	2012-13	427	50	ND	ND	0.346	33.3	-0.078	13.6	23.3	1.23	6.6	32.675	25.67	314.1
49.6	-138.7	P20	2012-13	368	75	ND	ND	0.425	40.9	-0.036	15.4	25.2	1.34	5.4	32.718	25.84	305.7
49.6	-138.7	P20	2012-13	426	100	2.11 ± 0.23	0.42 ± 0.05	0.530	51.0	0.002	19.3	29.3	1.53	4.7	32.769	25.97	300.2
49.6	-138.7	P20	2012-13	367	150	1.71 ± 0.36	0.34 ± 0.07	0.823	79.2	0.110	30.5	51.4	2.06	5.1	33.714	26.67	161.5
49.6	-138.7	P20	2012-13	425	200	1.24 ± 0.17	0.25 ± 0.03	0.995[†]	95.8	0.149	35.3	65.8	2.45	4.5	33.792	26.80	122.8
49.6	-138.7	P20	2012-13	366	300	1.52 ± 0.32	0.30 ± 0.06	0.922	88.8	-0.015	39.5	79.9	2.72	4.3	33.905	26.91	80.7
49.6	-138.7	P20	2012-13	424	400	1.19 ± 0.24	0.24 ± 0.05	0.953	91.8	-0.071	41.2	92.7	2.97[3]	4.2	34.014	27.00	60.0
49.6	-138.7	P20	2012-13	365	498	1.15 ± 0.20	0.23 ± 0.04	0.969	93.3	-0.046	42.6	102.4	2.94	4.0	34.101	27.10	37.5
49.6	-138.7	P20	2012-13	364	700	1.26 ± 0.23	0.25 ± 0.05	0.997	96.0	-0.055	43.9	122.0	3.05	3.5	34.239	27.26	22.7
49.6	-138.7	P20	2012-13	422	800	1.33 ± 0.27	0.27 ± 0.05	1.012	97.4	-0.050	44.4	129.9	3.08	3.3	34.295	27.32	18.8
49.6	-138.7	P20	2012-13	420	1200	1.11 ± 0.17	0.22 ± 0.03	1.028	99.0	-0.030	45.2	152.7	3.07[1]	2.7	34.434	27.49	14.1
49.6	-138.7	P20	2012-13	362	1300	1.06 ± 0.14	0.21 ± 0.03	1.030	99.2	-0.028	45.1	154.3	3.07	2.5	34.460	27.52	15.8
49.6	-138.7	P20	2012-13	419 B	1400	1.20 ± 0.16	0.24 ± 0.03	1.039	100.0	0.003	45.4	159.7	3.00[1]	2.4	34.492[2]	27.55	18.6
49.6	-138.7	P20	2012-13	418	1800	0.80 ± 0.18	0.16 ± 0.04	1.009	97.2	0.036	43.6	167.2	2.82[1]	2.1	34.567[2]	27.64	42.7
49.6	-138.7	P20	2012-13	359	1950	1.04 ± 0.14	0.21 ± 0.03	1.000	96.3	0.050	42.7	167.9	2.75	2.0	34.581[2]	27.66	53.0
49.6	-138.7	P20	2012-13	358	2090	0.92 ± 0.16	0.18 ± 0.03	0.995	95.7	0.024	42.3	168.9	2.81	1.9	34.599[2]	27.69	61.7
49.3	-134.7	P16	2012-13	351	10.5	ND	ND	0.061	5.9	-0.216	6.6	3.5	0.80	14.7	32.518	24.14	264.7
49.3	-134.7	P16	2012-13	350	24.5	ND	ND	0.157	15.2	-0.159	7.8	5.3	0.92	11.1	32.550	24.88	296.5
49.3	-134.7	P16	2012-13	349	50	ND	ND	0.407	39.4	-0.023	12.9	20.8	1.25	7.6	32.663	25.53	304.7
49.3	-134.7	P16	2012-13	280	74	ND	ND	0.428	41.5	-0.029	15.3	23.0	1.33	6.3	32.695	25.72	297.8
49.3	-134.7	P16	2012-13	348	100	2.15 ± 0.23	0.43 ± 0.05	0.513	49.6	0.025	18.5	26.1	1.41	5.7	32.937	25.98	267.9
49.3	-134.7	P16	2012-13	347	200	1.70 ± 0.25	0.34 ± 0.05	0.853	82.5	0.060	33.0	56.9	2.30	5.6	33.855	26.72	130.5
49.3	-134.7	P16	2012-13	277	300	1.31 ± 0.14	0.26 ± 0.03	1.001	96.9	0.087	38.8	74.0	2.65	4.6	33.911	26.88	78.3
49.3	-134.7	P16	2012-13	346	400	1.00 ± 0.26	0.30 ± 0.06	0.982	95.1	-0.012	40.9	89.1	2.88[3]	4.3	33.992	26.98	57.7
49.3	-134.7	P16	2012-13	276	500	1.34 ± 0.19	0.20 ± 0.05	0.978	94.7	-0.043	42.8	100.4	2.96	4.1	34.084	27.08	36.9
49.3	-134.7	P16	2012-13	345	600	1.54 ± 0.18	0.27 ± 0.04	0.980	94.9	-0.058	43.8	112.1	3.01[3]	3.8	34.160	27.16	26.1
49.3	-134.7	P16	2012-13	275	699	0.79 ± 0.61	0.31 ± 0.04	1.003	97.1	-0.058	44.5	122.2	3.08	3.6	34.222	27.23	20.6
49.3	-134.7	P16	2012-13	344	800	1.73 ± 0.26	0.16 ± 0.12	1.009	97.7	-0.079	44.5	127.0	3.15[3]	3.4	34.275	27.30	16.8
49.3	-134.7	P16	2012-13	664	900	1.17 ± 0.25	0.35 ± 0.05	1.025	99.2	0.004	44.4	134.7	2.96	3.2	34.333	27.36	13.4

49.3	-134.7	P16	2012-13	663	1000	1.11 ± 0.15	0.23 ± 0.05	1.030	99.7	0.003	44.9	141.2	2.98	3.0	34.372	27.41	11.4
49.3	-134.7	P16	2012-13	274	1100	1.29 ± 0.20	0.22 ± 0.03	1.032	99.9	-0.043	45.3	146.0	3.11	2.9	34.409	27.45	11.4
49.3	-134.7	P16	2012-13	342*	1200	1.32 ± 0.31*	0.26 ± 0.04	1.020*	98.8*	0.084*	44.9*	140.1*	2.72*	2.7	34.439	27.49	12.5
49.3	-134.7	P16	2012-13	661	1298	1.12 ± 0.13	0.26 ± 0.06	1.033	100.0	0.019	45.3	154.7	2.94	2.6	34.461	27.52	14.8
49.3	-134.7	P16	2012-13	341	1400	1.10 ± 0.16	0.22 ± 0.03	1.029	99.6	0.014	45.1	156.9	2.94[1]	2.5	34.486[2]	27.55	18.3
49.3	-134.7	P16	2012-13	660	1600	0.87 ± 0.21	0.22 ± 0.03	1.017	98.5	0.007	44.5	164.6	2.93	2.3	34.526	27.60	28.9
49.3	-134.7	P16	2012-13	340	1800	1.01 ± 0.14	0.18 ± 0.04	1.002	97.0	0.002	43.8	166.1	2.90	2.1	34.562[2]	27.64	43.2
49.3	-134.7	P16	2012-13	271	1949	0.83 ± 0.26	0.20 ± 0.03	1.016	98.3	0.019	43.1	169.8	2.89	2.0	34.584[2]	27.67	54.2
49.3	-134.7	P16	2012-13	270	2100	0.96 ± 0.17	0.17 ± 0.05	0.997	96.5	0.027	42.2	171.2	2.81	1.9	34.606[2]	27.69	62.4
49	-130.7	P12	2012-13	245	11	ND	ND	0.070	6.7	-0.170	5.3	2.8	0.69	15.0	32.519	24.08	261.7
49	-130.7	P12	2012-13	244	25	ND	ND	0.157	15.0	-0.170	8.5	8.8	0.95	13.1	32.585	24.53	278.2
49	-130.7	P12	2012-13	243	50	ND	ND	0.208	19.9	-0.142	9.6	11.8	1.01	8.6	32.647	25.36	306.0
49	-130.7	P12	2012-13	196	75	ND	ND	0.322	30.9	-0.065	11.5	15.4	1.12	7.3	32.702	25.60	291.3
49	-130.7	P12	2012-13	242	100	3.15 ± 0.29	0.63 ± 0.06	0.387	37.1	-0.040	14.3	18.6	1.24	7.0	32.808	25.72	280.5
49	-130.7	P12	2012-13	195	149	1.37 ± 0.31	0.27 ± 0.06	0.604	57.9	0.093	20.6	27.7	1.48	7.1	33.687	26.39	207.9
49	-130.7	P12	2012-13	241	200	1.37 ± 0.28	0.27 ± 0.06	0.700	67.1	0.082	26.1	39.8	1.79	6.8	33.891	26.60	172.3
49	-130.7	P12	2012-13	193	300	1.59 ± 0.24	0.32 ± 0.05	0.829	79.4	0.039	33.0	59.2	2.29	5.4	33.876	26.76	127.2
49	-130.7	P12	2012-13	240	400	1.47 ± 0.18	0.29 ± 0.04	0.929	89.0	0.029	38.0	75.3	2.61	4.6	33.937	26.90	79.7
49	-130.7	P12	2012-13	192A	500	1.38 ± 0.16	0.28 ± 0.03	0.988	94.6	-0.017	41.8	91.0	2.91	4.4	34.044	27.01	42.6
49	-130.7	P12	2012-13	239	600	1.34 ± 0.16	0.27 ± 0.03	0.993	95.1	-0.025	43.3	100.7	2.95	4.1	34.130	27.11	24.8
49	-130.7	P12	2012-13	191	700	1.52 ± 0.19	0.30 ± 0.04	0.987	94.5	-0.064	44.2	114.4	3.05	3.8	34.196	27.19	19.6
49	-130.7	P12	2012-13	238	800	1.71 ± 0.31	0.34 ± 0.06	1.016	97.4	-0.045	44.9	120.3	3.08	3.6	34.252	27.25	13.9
49	-130.7	P12	2012-13	237	1000	1.13 ± 0.16	0.23 ± 0.03	1.032	98.8	-0.009	44.5	133.1	3.02	3.3	34.351	27.37	10.7
49	-130.7	P12	2012-13	190	1100	1.22 ± 0.11	0.24 ± 0.02	1.025	98.2	-0.046	45.1	142.4	3.10	3.1	34.391	27.42	11.4
49	-130.7	P12	2012-13	236	1201*	0.99 ± 0.14	0.20 ± 0.03	1.032*	98.9	0.072*	41.5*	145.6*	2.78*	2.9	34.430	27.46	14.1
49	-130.7	P12	2012-13	189	1301	1.16 ± 0.19	0.23 ± 0.04	1.044	100.0	-0.021	44.9	151.8	3.09	2.8	34.458	27.50	17.6
49	-130.7	P12	2012-13	235	1401	1.46 ± 0.17	0.29 ± 0.03	1.034	99.1	0.013	43.5	156.1	2.96	2.5	34.495[2]	27.55	25.2
49	-130.7	P12	2012-13	188A	1600	1.28 ± 0.15	0.26 ± 0.03	1.010	96.8	-0.024	44.1	162.8	3.00	2.3	34.530	27.60	35.5
49	-130.7	P12	2012-13	234	1800	1.07 ± 0.21	0.21 ± 0.04	1.028	98.5	0.007	43.4[1]	166.4	2.96[1]	2.1	34.558[2]	27.63	45.6
49	-130.7	P12	2012-13	186	1999	1.03 ± 0.12	0.21 ± 0.02	0.985	94.3	-0.023	42.7	180.4	2.92	2.0	34.587[2]	27.67	58.4

48.7	-126.7	P4	2012-13	112	9.6	ND	ND	0.192	18.4	-0.013	1.7	3.9	0.60	13.6	31.214	23.37	338.8
48.7	-126.7	P4	2012-13	111	25	ND	ND	0.204	19.5	-0.136	8.2	12.0	0.99	8.8	32.595	25.29	283.4
48.7	-126.7	P4	2012-13	110	50	ND	ND	0.284	27.1	-0.107	14.1	15.7	1.13	7.7	32.710	25.55	267.1
48.7	-126.7	P4	2012-13	109	74	ND	ND	0.440	42.1	-0.051	17.4	21.2	1.42	7.4	33.039	25.84	216.3
48.7	-126.7	P4	2012-13	108	100	2.14 ± 0.23	0.43 ± 0.05	0.689	65.9	0.080	24.1	29.7	1.76	7.4	33.555	26.24	177.0
48.7	-126.7	P4	2012-13	65	148	1.77 ± 0.12	0.35 ± 0.04	0.821	78.6	0.085	30.5	40.6	2.13	7.4	33.848	26.48	118.2
48.7	-126.7	P4	2012-13	107	200	1.75 ± 0.23	0.35 ± 0.05	0.842	80.6	0.042	32.6	47.1	2.32	6.8	33.935	26.63	91.9
48.7	-126.7	P4	2012-13	64	300	1.48 ± 0.19	0.30 ± 0.04	0.919	88.0	0.002	38.1	62.9	2.66	6.1	34.008	26.79	59.3
48.7	-126.7	P4	2012-13	106	400	1.77 ± 0.26	0.35 ± 0.05	0.945	90.4	-0.033	39.2	70.4	2.83	5.6	34.066	26.89	40.0
48.7	-126.7	P4	2012-13	63	498	1.21 ± 0.66	0.24 ± 0.13	0.975	93.3	-0.050	41.9	82.7	2.97	5.2	34.114	26.97	28.4
48.7	-126.7	P4	2012-13	105	600	1.53 ± 0.21	0.31 ± 0.04	0.996	95.4	-0.062	42.4	90.1	3.07	4.9	34.177	27.06	17.6
48.7	-126.7	P4	2012-13	62	700	1.61 ± 0.21	0.32 ± 0.04	1.018	97.4	-0.070	43.9	103.3	3.15	4.6	34.237	27.15	11.8
48.7	-126.7	P4	2012-13	104 A	799	1.42 ± 0.19	0.28 ± 0.04	1.023	97.9	-0.061	43.2	107.4	3.14	4.2	34.293	27.2	9.8
48.7	-126.7	P4	2012-13	103	998	1.48 ± 0.12	0.30 ± 0.02	1.045	100.0	-0.063	44.2	123.0	3.21	3.7	34.392[2]	27.35	10.6
48.7	-126.7	P4	2012-13	61	1101	1.23 ± 0.21	0.25 ± 0.04	1.040	99.5	-0.055	44.9	134.6	3.17	3.4	34.440[2]	27.41	13.2
48.7	-126.7	P4	2012-13	102	1198	1.22 ± 0.15	0.24 ± 0.03	1.038	99.3	-0.057	44.5	140.5	3.17	3.2	34.464[2]	27.45	16.2
48.7	-126.7	P4	2012-13	60	1300	1.41 ± 0.13	0.28 ± 0.03	1.031	98.6	-0.054	44.6	145.8	3.14	3.0	34.483[2]	27.49	19.8
50	-145.0	P26	2013-18	510	200	0.87 ± 0.12 1.11 ± 0.19	0.17 ± 0.02 0.22 ± 0.04	1.035	ND	0.074	38.6[3]	73.5[3]	2.79[3]	3.6	33.699[2]	26.80	128.4
50	-145.0	P26	2013-18	509	250	1.05 ± 0.14	0.21 ± 0.03	1.015	ND	-0.006	41.6[3]	83.4[3]	2.96[3]	3.6	33.803[2]	26.88	86.9
50	-145.0	P26	2013-18	575	350	0.96 ± 0.15	0.19 ± 0.03	1.029	ND	-0.011	43.5[1]	94.8[1]	3.01[1]	3.7	33.989[2]	26.99	53.5
50	-145.0	P26	2013-18	573	500	1.07 ± 0.12	0.21 ± 0.02	0.986	ND	-0.072	44.0[1]	107.5[1]	3.07[1]	3.7	34.195[2]	27.14	27.4
50	-145.0	P26	2013-18	572	650	1.08 ± 0.14 1.34 ± 0.13	0.22 ± 0.03 0.27 ± 0.03	0.986	ND	-0.084	43.9[1]	111.3[1]	3.10[1]	3.5	34.298[2]	27.25	25.3
50	-145.0	P26	2013-18	570	1000	1.06 ± 0.12 1.24 ± 0.16	0.21 ± 0.02 0.25 ± 0.03	1.008	ND	-0.067	44.8[3]	140.4[3]	3.11[3]	2.9	34.451[2]	27.43	21.6
49.3	-134.7	P16	2013-18	278	250	1.31 ± 0.15	0.26 ± 0.03	0.868	ND	0.049	34.3[3]	58.3[3]	2.38[3]	5.5	33.852[2]	26.74	118.6
49.3	-134.7	P16	2013-18	277	300	1.35 ± 0.17	0.27 ± 0.03	0.920	ND	0.033	37.4[3]	67.0[3]	2.57[3]	5.0	33.904[2]	26.82	92.6
49.3	-134.7	P16	2013-18	276	400	1.25 ± 0.11	0.25 ± 0.02	0.967	ND	-0.007	41.0[3]	81.5[3]	2.82[3]	4.6	33.995[2]	26.95	54.9
49.3	-134.7	P16	2013-18	275	550	1.31 ± 0.12	0.26 ± 0.02	0.989	ND	-0.048	43.3[1]	99.5[1]	3.01[1]	4.1	34.129[2]	27.11	24.2
49.3	-134.7	P16	2013-18	274	700	1.45 ± 0.16	0.29 ± 0.03	0.999	ND	-0.064	44.3[1]	114.8[1]	3.08[1]	3.7	34.222[2]	27.23	16.0

49.3	-134.7	P16	2013-18	272	1000	1.35 ± 0.13	0.27 ± 0.03	1.032	ND	-0.053	45.3[3]	136.4[3]	3.14[3]	3.1	34.360[2]	27.39	11.3
49	-130.7	P12	2013-18	199	300	1.20 ± 0.13	0.24 ± 0.03	0.874	ND	0.004	35.9[3]	65.5[3]	2.52[3]	5.1	33.906[2]	26.80	103.6
49	-130.7	P12	2013-18	198	400	1.22 ± 0.13	0.24 ± 0.03	0.952	ND	-0.022	40.3[3]	80.0[3]	2.82[3]	4.6	33.973[2]	26.94	62.2
49	-130.7	P12	2013-18	197	450	1.17 ± 0.14	0.23 ± 0.03	0.971	ND	-0.024	41.1[1]	85.7[1]	2.88[1]	4.5	34.023[2]	26.97	51.2
49	-130.7	P12	2013-18	196	600	1.30 ± 0.13	0.26 ± 0.03	0.988	ND	-0.070	43.6[3]	102.8[3]	3.07[3]	4.1	34.148[2]	27.12	26.5
49	-130.7	P12	2013-18	195	800	1.25 ± 0.24	0.25 ± 0.05	1.018	ND	-0.080	44.8[3]	121.0[3]	3.18[3]	3.6	34.371[2]	27.27	12.3
49	-130.7	P12	2013-18	194	1100	1.12 ± 0.12	0.22 ± 0.02	1.046	ND	-0.069	45.5[1]	141.5[1]	3.23[1]	3.0	34.430[2]	27.37	11.7
48.7	-126.7	P4	2013-18	131	350	1.67 ± 0.16	0.33 ± 0.03	0.947	ND	-0.016	39.4[1]	66.8[1]	2.79[1]	5.9	34.015[2]	26.81	53.9
48.7	-126.7	P4	2013-18	130	425	1.52 ± 0.21	0.30 ± 0.04	0.962	ND	-0.049	41.2[1]	75.1[1]	2.93[1]	5.4	34.063[2]	26.90	38.7
48.7	-126.7	P4	2013-18	128	700	1.32 ± 0.12	0.26 ± 0.02	1.000	ND	-0.100	44.4[1]	103.7[1]	3.19[1]	4.3	34.215[2]	27.17	11.3
48.7	-126.7	P4	2013-18	127	800	1.27 ± 0.11	0.25 ± 0.02	1.019	ND	-0.096	45.0[3]	113.1[3]	3.23[3]	4.1	34.315[2]	27.25	8.9
48.7	-126.7	P4	2013-18	663	1000	1.29 ± 0.15	0.26 ± 0.03	1.040	ND	-0.062	45.4[3]	127.7[3]	3.19[3]	3.6	34.378[2]	27.37	9.2
49.6	-138.7	P20	2014-19	505	10	2.57 ± 1.01	0.51 ± 0.20	0.005	ND	-0.122	ND	1.7[3]	0.37[3]	16.8	32.236	23.46	250.8
49.6	-138.7	P20	2014-19	504	25	4.31 ± 0.86	0.86 ± 0.17	0.006	ND	-0.124	ND	1.5[3]	0.38[3]	16.4	32.240	23.56	253.0
49.6	-138.7	P20	2014-19	503	50	5.08 ± 0.22	1.02 ± 0.04	0.105	ND	-0.214	7.6[3]	9.6[3]	0.92[3]	9.0	32.419	25.12	282.2
49.3	-134.7	P16	2014-19	384	10	ND	ND	0.001	ND	-0.130	ND	1.6[3]	0.38[3]	17.6	32.299	23.34	248.8
49.3	-134.7	P16	2014-19	383	25	4.87 ± 1.44	0.97 ± 0.29	0.004	ND	-0.126	ND	1.6[3]	0.38[3]	15.6	32.305	23.79	271.8
49.3	-134.7	P16	2014-19	382	50	5.19 ± 0.23	1.04 ± 0.05	0.034	ND	-0.252	6.0[3]	7.1[3]	0.83[3]	9.8	32.482	25.04	281.5
49	-130.7	P12	2014-19	319	10	1.82 ± 0.41	0.36 ± 0.08	0.011	ND	-0.125	ND	3.9[3]	0.40[3]	18.6	32.215	23.01	242.2
49	-130.7	P12	2014-19	318	25	1.17 ± 0.41	0.23 ± 0.08	0.012	ND	-0.138	ND	4.8[3]	0.43[3]	18.6	32.217	23.02	244.0
49	-130.7	P12	2014-19	317	50	4.49 ± 0.19	0.90 ± 0.04	0.053	ND	-0.244	6.6[3]	9.4[3]	0.86[3]	11.3	32.268	24.62	279.0
48.7	-126.7	P4	2014-19	92	10	3.31 ± 0.11	0.66 ± 0.02	0.253	ND	0.108	ND	6.7[3]	0.42[3]	14.6	32.031	23.79	278.9
48.7	-126.7	P4	2014-19	91	25	3.21 ± 0.20	0.64 ± 0.04	0.153	ND	-0.162	7.0[3]	10.3[3]	0.91[3]	12.2	32.117	24.34	259.3
48.7	-126.7	P4	2014-19	90	50	3.96 ± 0.38 3.53 ± 0.16	0.79 ± 0.08 0.71 ± 0.0	0.293	ND	-0.118	12.5[3]	14.3[3]	1.19[3]	8.7	32.422	25.17	267.6

Table D.2 Cadmium, macronutrient, and other oceanographic data

Data from cruise 2012-13 (August 2012), 2013-18 (August 2013) and 2014-19 (August 2014) are shown. Macronutrient, temperature, salinity, density and O_2 data are courtesy of the Line P program run by the Institute of Ocean Sciences (DFO, Canada).[P] Denotes a trace metal sample from the Teflon bellows pump. [L] Denotes a trace metal sample collected from GO-FLO bottles on a Kevlar line. All others were collected on a trace metal rosette. [1] = interpolated nutrient concentration, all others are bottle data.[2] = bottle salinity data, all others are CTD data. [3] = Nutrient sample

from a conventional rosette. * = suspected bottle leak † = Suspected bottle contamination (suspected contamination seen for Zn in same sample, Janssen and Cullen, 2015 / Chapter 3), data not included in plots. ND = Not Determined.

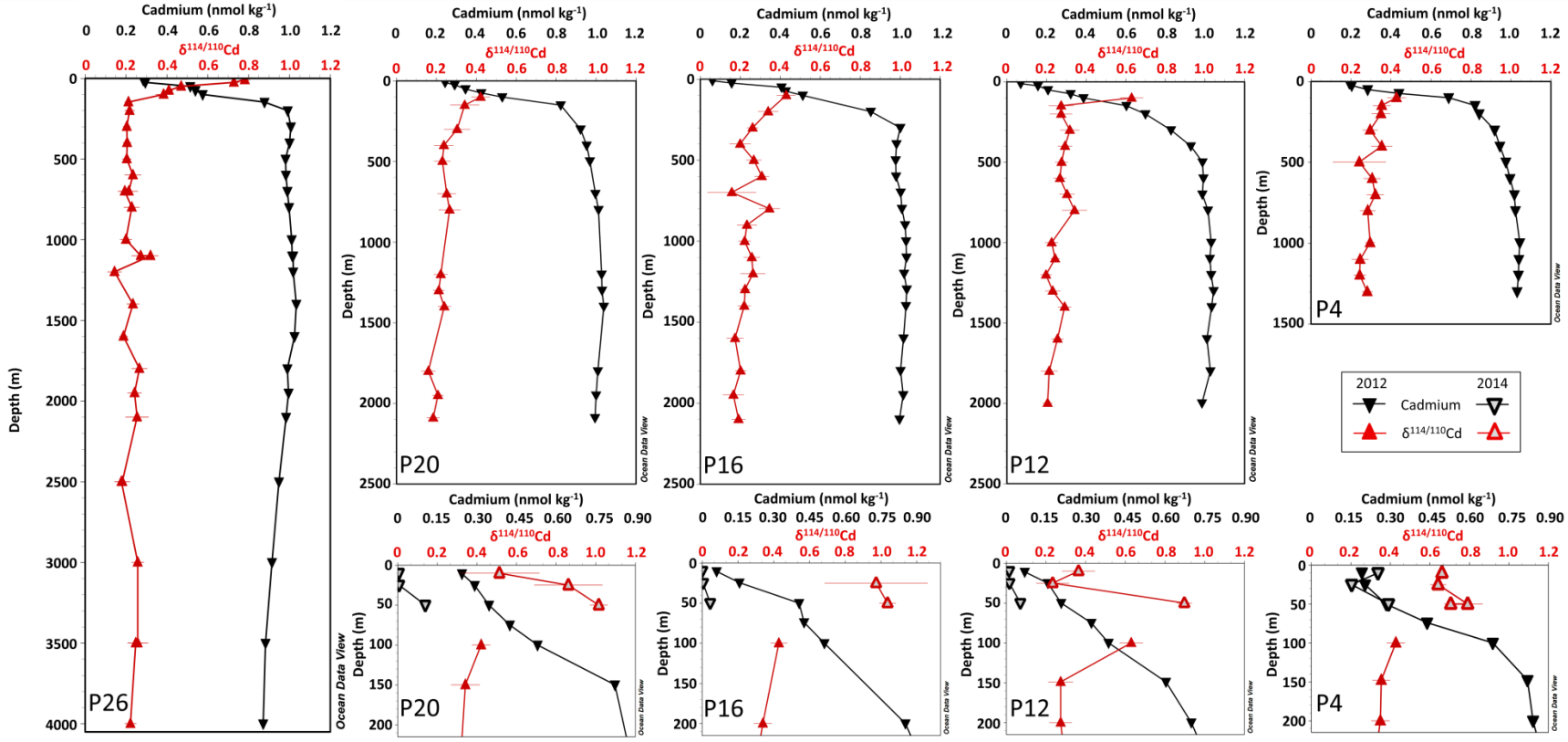

Figure D.2 Dissolved [Cd] and $\delta^{114/110}$Cd from August 2012 and August 2014
Cadmium concentrations are presented as black inverted triangles and $\delta^{114/110}$Cd as red triangles. Duplicate analyses (station P26 700 m, 1100 m, 2500 m and 3500 m) are shown for $\delta^{114/110}$Cd. The upper plots show only 2012 data. $\delta^{114/110}$Cd and [Cd] data from the upper 200 m are shown again in the lower plots for stations P4-P20, with 2012 data as solid symbols and 2014 data as open symbols. Note that the [Cd] scaling is different for the surface plots and full water column plots and that the surface plot for station P16 has different [Cd] and $\delta^{114/110}$Cd scaling than the other surface plots. 2013 are not shown here but are included in Table A.2. Figure 4.3 presents a version of this figure in $\varepsilon^{112/110}$Cd notation. An alternate version of this figure with Cd stable isotopes in units of $\varepsilon^{112/110}$Cd is shown as Figures 4.3 and D.3.

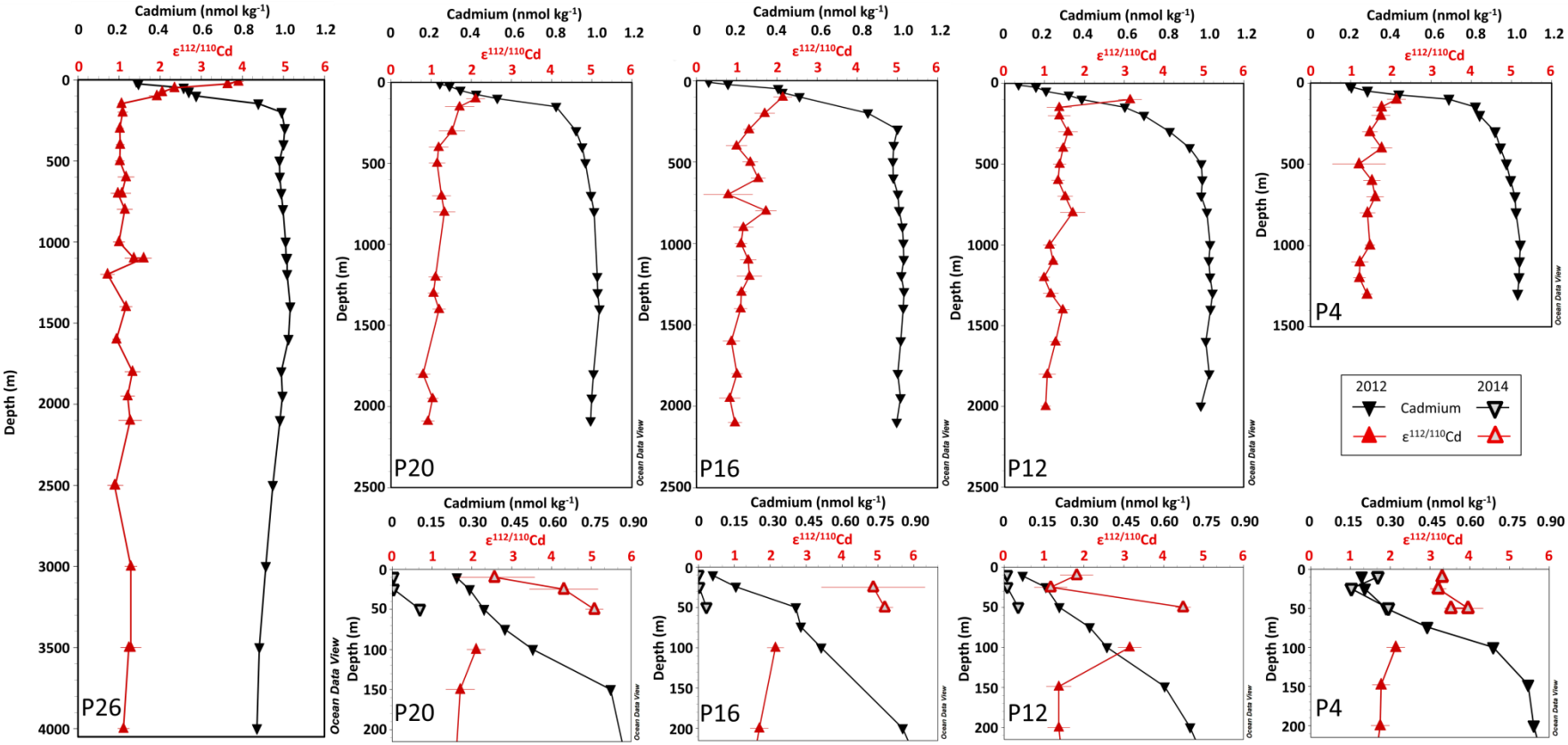

Figure D.3 Enlarged version of Figure 4.3

This is the same as Figure 4.3 but enlarged. Cadmium concentrations are presented as black inverted triangles and $\varepsilon^{112/110}$Cd as red triangles. Duplicate analyses (station P26 700 m, 1100 m, 2500 m and 3500 m) are shown for $\varepsilon^{112/110}$Cd. The upper plots show only 2012 data. $\varepsilon^{112/110}$Cd and [Cd] data from the upper 200 m are shown again in the lower plots for stations P4-P20,with 2012 data as solid symbols and 2014 data as open symbols. Note that the [Cd] scaling is different for the surface plots and full water column plots and that the surface plot for station P16 has different [Cd] and $\varepsilon^{112/110}$Cd scaling than the other surface plots. 2013 are not shown here but are included in Table D.2. Figure D.2 presents a version of this figure in $\delta^{114/110}$Cd notation.

D.3 Isotopic range possible for the observed Cd deficit as determined by Cd*

If the formation of Cd sulphides is driving the observed deficit of Cd in the subarctic northeast Pacific based on Cd*, then the lack of an apparent $\varepsilon^{112/110}Cd$ signal in O_2-depleted waters constrains the potential range of the Cd removed from the dissolved phase. This range can be calculated given measured dissolved $\varepsilon^{112/110}Cd$ and [Cd] as well as an expected $\varepsilon^{112/110}Cd$ and [Cd] in the absence of sulphide formation from the following:

$$[Cd]_{obs} + [Cd]_{mis} = [Cd]_{expect}$$
$$[Cd]_{obs} \times \varepsilon^{112/110}Cd_{obs} + [Cd]_{mis} \times \varepsilon^{112/110}Cd_{mis} = [Cd]_{expect} \times \varepsilon^{112/110}Cd_{expect}$$

where the subscript "obs" represents the measured Cd, "mis" is the missing Cd as determined by Cd*, and "expect" is the expected Cd in the absence of a Cd deficit. Since the exact deficit and observed Cd varies with depth and station, the following approximations are made for the sake of this calculation:

$[Cd]_{obs}$ = 1 nmol kg^{-1}, $\varepsilon^{112/110}Cd_{obs}$ = 1.28 to 0.98 ($\varepsilon^{112/110}Cd_{obs} \pm 0.15$ 2σ)
$[Cd]_{mis}$ = 0.05 to 0.1 nmol kg^{-1}
$[Cd]_{expect}$ = 1.1 nmol kg^{-1}, $\varepsilon^{112/110}Cd_{expect}$ = 1.13

The range of $[Cd]_{mis}$ is chosen to encompass maximum observed Cd* (0.1 nmol kg^{-1}) and a value more representative of the average observed deficit (0.05 nmol kg^{-1}), therefore reflecting the most narrow range of tolerable $\varepsilon^{112/110}Cd_{mis}$ (Cd* = 0.1 nmol kg^{-1}) as well as a value more generally representative of the entire Cd deficit in low-O_2 water. The range of $\varepsilon^{112/110}Cd_{obs}$ spans the largest possible range of observed values which would still result in a measurement indistinguishable from deep subarctic northeast Pacific $\varepsilon^{112/110}Cd$ within a 2σ error for a given measurement of roughly 0.15. The potential ranges of missing Cd are shown in Table A.4. Under the more restrictive scenario, the missing Cd must have an $\varepsilon^{112/110}Cd$ between -0.37 and +2.63. As Cd sulphide formation is expected to disproportionally sequester light Cd isotopes in the solid phase (Schmitt et al., 2009a; Yang et al., 2015), we can focus on

the lower end of this range. This constrains the missing Cd to have $\varepsilon^{112/110}Cd \geq -0.37$, a value within the reported range measured in hydrothermal sulphides (Schmitt et al., 2009a).

A minimum fractionation factor between seawater Cd (sw) and the removed Cd (removed), $\alpha_{sw\text{-}removed}$ can be calculated similarly from the following equation (from Mariotti et al., 1981 as presented in Ripperger et al., 2007 equation A.2).

$$\varepsilon^{112/110}Cd_{obs} = \varepsilon^{112/110}Cd_{expect} + 10{,}000 \times \left(\frac{1}{\propto} - 1\right) \times ln\left(\frac{[Cd]_{obs}}{[Cd]_{expect}}\right)$$

Using the above conditions for the minimum $\varepsilon^{112/110}Cd$ of removed Cd, the calculated fractionation factor ($\alpha_{sw\text{-}removed}$) must be ≤ 1.00016.

	Cd*	Deep Pacific	2σ	Missing Cd Min	Missing Cd Max
$\varepsilon^{112/110}Cd$	0.05	1.13	0.15	-0.74	5.26
	0.1	1.13	0.15	-0.37	2.63
$\delta^{114/110}Cd$	0.05	0.226	0.030	-0.34	0.80
	0.1	0.226	0.030	-0.17	0.40

Table D.3 Potential isotopic ranges of the Cd deficit observed in the subarctic northeast Pacific

D.4 $\varepsilon^{112/110}Cd$ at low [Cd]

Region	Lat	Long	Station	Cruise	Cd	$\varepsilon^{112/110}Cd$	2σ	$\delta^{114/110}Cd$	2σ
	°N	°W			pmol kg^{-1}				
North Pacific[1]	24.3	-170.3	7	IOC 2002	3.1	18.54	3.00	3.71	0.60
North Pacific[1]	24.3	-170.3	7	IOC 2002	15.3	7.54	1.15	1.51	0.23
North Pacific[1]	24.3	-170.3	7	IOC 2002	2.1	-3.45	3.00	-0.69	0.60
North Pacific[1]	22.8	158	9 (ALOHA)	IOC 2002	4.8	2.64	1.35	0.53	0.27
North Pacific[1]	22.8	158	9 (ALOHA)	IOC 2002	7.6	2.14	1.25	0.43	0.25
North Pacific[2]	30 N	140	SAFe	IC2	16.7	16.87	1.60	3.37	0.32
North Pacific[2]	30 N	140	SAFe	IC2	2.7	14.82	2.00	2.96	0.40
Marginal N. Pacific Basin[2]	33.80	118.40	SPOTS	Sep-08	39.9	0.8	4.23	0.42	0.85
Subarctic North	49.6	138.7	P20	2014-19	5.0	2.57	1.01	0.51	0.2

Pacific[3]									
Subarctic North Pacific[3]	49.6	138.7	P20	2014-19	6.0	4.31	0.86	0.86	0.17
Subarctic North Pacific[3]	49.3	134.7	P16	2014-19	4.0	4.87	1.44	0.97	0.29
Subarctic North Pacific[3]	49.3	134.7	P16	2014-19	34.0	5.19	0.23	1.04	0.05
Subarctic North Pacific[3]	49	130.7	P12	2014-19	11.0	1.82	0.41	0.36	0.08
Subarctic North Pacific[3]	49	130.7	P12	2014-19	12.0	1.17	0.41	0.23	0.08
Subarctic North Pacific[3]	49	130.7	P12	2014-19	53.0	4.49	0.19	0.9	0.04
South China Sea[4]	18.27	-115.7	SEATS	Oct-06	48	4.65	1.35	0.93	0.27
South China Sea[4]	18.27	-115.7	SEATS	Oct-06	37	4.5	0.4	0.90	0.08
South China Sea[4]	18.27	-115.7	SEATS	Oct-06	41	4.2	0.4	0.84	0.08
West Philippine Sea[5]	22.00	125.00	16	10/06/1902	50	0.1	4.2	0.3	0.84
Subantarctic S. Pacific[6]	-45.78	170.91	1	28/11/2008	43.5	3.95	0.70	0.79	0.14
Subantarctic S. Pacific[6]	-45.79	170.95	2	28/11/2008	31.8	4.40	0.85	0.88	0.17
Subantarctic S. Pacific[6]	-45.80	171.07	3	28/11/2008	41.9	4.85	0.90	0.97	0.18
Subantarctic S. Pacific[6]	-45.80	171.16	4	28/11/2008	18.9	7.10	2.00	1.42	0.40
Subantarctic S. Pacific[6]	-45.81	171.25	5	28/11/2008	22.8	4.00	1.15	0.80	0.23
Subantarctic S. Pacific[6]	-45.82	171.34	6	28/11/2008	21.4	7.45	1.35	1.49	0.27
Subantarctic S. Pacific[6]	-45.83	171.44	7	28/11/2008	36.5	5.50	0.90	1.10	0.18
Subantarctic S. Pacific[6]	-45.83	171.54	8	28/11/2008	33.5	4.95	0.95	0.99	0.19

Subantarctic S. Pacific[6]	-45.78	170.91	1	25/03/2009	31.6	5.55	1.15	1.11	0.23
Subantarctic S. Pacific[6]	-45.79	170.93	1-2	25/03/2009	16.4	3.40	1.35	0.68	0.27
Subantarctic S. Pacific[6]	-45.79	170.95	2	25/03/2009	17.0	1.70	1.25	0.34	0.25
Subantarctic S. Pacific[6]	-45.83	171.44	7	25/03/2009	28.9	5.50	1.25	1.10	0.25
Subantarctic S. Pacific[6]	-45.83	171.49	7-8	25/03/2009	23.2	4.00	1.00	0.80	0.20
Subantarctic S. Pacific[6]	-45.83	171.54	8	25/03/2009	23.2	4.85	1.45	0.97	0.29
Subantarctic S. Pacific[6]	-45.78	170.91	1	08/12/2009	22.7	3.35	1.20	0.67	0.24
Subantarctic S. Pacific[6]	-45.82	171.34	6	08/12/2009	26.4	4.35	0.85	0.87	0.17
Subantarctic S. Pacific[6]	-45.83	171.44	7	08/12/2009	37.3	3.40	0.65	0.68	0.13
Subantarctic S. Pacific[6]	-45.83	171.54	8	08/12/2009	30.0	3.45	0.90	0.69	0.18
Subantarctic S. Pacific[6]	-45.78	170.91	1	15/01/2010	36.5	4.00	0.55	0.80	0.11
Subantarctic S. Pacific[6]	-45.80	171.07	3	15/01/2010	15.3	2.15	1.15	0.43	0.23
Subantarctic S. Pacific[6]	-45.80	171.16	4	15/01/2010	19.0	4.50	0.90	0.90	0.18
Subantarctic S. Pacific[6]	-45.81	171.25	5	15/01/2010	4.8	-1.70	1.90	-0.34	0.38
Subantarctic S. Pacific[6]	-45.82	171.34	6	15/01/2010	3.2	2.55	1.55	0.51	0.31
Subantarctic S. Pacific[6]	-45.83	171.54	8	15/01/2010	3.2	2.80	1.65	0.56	0.33
North Atlantic[1]	45.8	5.5	69/6-4	ANTXXIII/1	31.4	3.74	0.60	0.75	0.12
North Atlantic[1]	45.8	5.5	69/6-4	ANTXXIII/1	28.4	5.19	0.50	1.04	0.10
North Atlantic[7]	31.8	64.1	BATS (GS1)	GEOTRACES IC1	1.2	11.14	2.65	2.23	0.53
North Atlantic[7]	31.8	64.1	BATS (GPr1)	GEOTRACES IC1	2.2	6.84	2.65	1.37	0.53
North Atlantic[7]	31.8	64.1	BATS (GPr1)	GEOTRACES IC1	1.7	5.99	2.65	1.20	0.53
North Atlantic[8]	31.8	64.1	BATS (GS1)	GEOTRACES IC1	1.3	11.40	4.35	2.28	0.87
North	31.8	64.1	BATS	GEOTRACES	1.3	6.55	3.60	1.31	0.72

Atlantic[8]			(GS1)	IC1					
North Atlantic[8]	31.8	64.1	BATS (GPr1)	GEOTRACES IC1	1.9	3.60	3.20	0.72	0.64
North Atlantic[8]	31.8	64.1	BATS (GPr1)	GEOTRACES IC1	2.7	8.20	3.70	1.64	0.74
North Atlantic[8]	31.8	64.1	BATS (GPr1)	GEOTRACES IC1	32.8	2.70	0.40	0.54	0.08
North Atlantic[9]	38.32	9.66	1	KN199-4	23.3	3.31	0.97	0.66	0.19
North Atlantic[9]	38.32	9.66	1	KN199-4	11.8	2.80	0.85	0.56	0.17
North Atlantic[9]	38.32	9.66	1	KN199-4	15.3	3.14	0.74	0.63	0.15
North Atlantic[9]	38.32	9.66	1	KN199-4	16.7	1.99	0.81	0.40	0.16
North Atlantic[9]	38.32	9.66	1	KN199-4	8.5	1.52	1.08	0.30	0.22
North Atlantic[9]	38.32	9.66	1	KN199-4	50.1	2.54	0.44	0.51	0.09
North Atlantic[9]	35.2	16	3	KN199-4	0.9	10.83	3.90	2.17	0.78
North Atlantic[9]	35.2	16	3	KN199-4	1.2	5.88	2.97	1.18	0.59
North Atlantic[9]	35.2	16	3	KN199-4	21.1	3.51	0.61	0.70	0.12
North Atlantic[9]	35.2	16	3	KN199-4	36.3	3.26	0.46	0.65	0.09
North Atlantic[9]	35.2	16	3	KN199-4	53.8	2.75	0.42	0.55	0.08
North Atlantic[9]	31	22	5	KN199-4	0.7	6.53	5.16	1.31	1.03
North Atlantic[9]	31	22	5	KN199-4	0.8	15.69	5.90	3.14	1.18
North Atlantic[9]	31	22	5	KN199-4	1.0	7.05	3.12	1.41	0.62
North Atlantic[9]	31	22	5	KN199-4	0.7	8.09	5.77	1.62	1.15
North Atlantic[9]	31	22	5	KN199-4	13.8	2.86	1.08	0.57	0.22
North Atlantic[9]	31	22	5	KN199-4	22.5	3.23	1.17	0.65	0.23
North Atlantic[9]	31	22	5	KN199-4	42.5	2.65	0.68	0.53	0.14
North Atlantic[9]	17.35	18.25	9	KN199-4	1.4	25.23	1.91	5.05	0.38
North Atlantic[9]	17.35	18.25	9	KN199-4	3.5	17.61	1.55	3.52	0.31
North	17.35	20.82	10	KN199-4	1.6	23.54	2.47	4.71	0.49

Atlantic[9]									
North Atlantic[9]	17.35	20.82	10	KN199-4	4.4	13.25	1.53	2.65	0.31
North Atlantic[9]	17.35	22.78	11	KN199-4	39.9	5.49	0.36	1.10	0.07
North Atlantic[9]	17.4	22.45	12	KN199-4	13.5	10.03	1.00	2.01	0.20
North Atlantic[9]	39.7	69.8	1	KN204-01b	50.4	3.82	0.73	0.76	0.15
North Atlantic[9]	39.7	69.8	1	KN204-01b	34.5	4.00	0.70	0.80	0.14
North Atlantic[9]	39.7	69.8	1	KN204-01b	34.1	2.88	0.57	0.58	0.11
North Atlantic[9]	39.7	69.8	1	KN204-01b	41.3	2.53	0.47	0.51	0.09
North Atlantic[9]	39.35	69.54	2	KN204-01b	25.2	ND	ND	ND	ND
North Atlantic[9]	39.35	69.54	2	KN204-01b	28.3	3.23	1.09	0.65	0.22
North Atlantic[9]	39.35	69.54	2	KN204-01b	49.6	2.60	0.56	0.52	0.11
North Atlantic[9]	38.69	69.09	3	KN204-01b	1.1	ND	ND	ND	ND
North Atlantic[9]	38.69	69.09	3	KN204-01b	1.0	6.18	3.20	1.24	0.64
North Atlantic[9]	38.69	69.09	3	KN204-01b	27.9	2.17	0.55	0.43	0.11
North Atlantic[9]	38.69	69.09	3	KN204-01b	32.6	2.23	0.53	0.45	0.11
North Atlantic[9]	38.69	69.09	3	KN204-01b	19.7	2.07	0.60	0.41	0.12
North Atlantic[9]	37.57	68.45	6	KN204-01b	7.3	3.71	1.68	0.74	0.34
North Atlantic[9]	37.57	68.45	6	KN204-01b	6.5	5.97	2.38	1.19	0.48
North Atlantic[9]	37.57	68.45	6	KN204-01b	0.6	5.46	0.94	1.09	0.19
North Atlantic[9]	37.57	68.45	6	KN204-01b	23.3	2.83	0.48	0.57	0.10
North Atlantic[9]	35.42	66.53	8	KN204-01b	1.3	9.50	3.12	1.90	0.62
North Atlantic[9]	35.42	66.53	8	KN204-01b	12.1	3.37	0.90	0.67	0.18
North Atlantic[9]	35.42	66.53	8	KN204-01b	11.7	2.93	0.83	0.59	0.17
North Atlantic[9]	35.42	66.53	8	KN204-01b	26.2	2.22	0.72	0.44	0.14
North	35.42	66.53	8	KN204-01b	19.7	3.09	0.82	0.62	0.16

Atlantic[9]									
North Atlantic[9]	35.42	66.53	8	KN204-01b	21.1	2.76	0.87	0.55	0.17
North Atlantic[9]	35.42	66.53	8	KN204-01b	27.4	2.24	0.82	0.45	0.16
North Atlantic[9]	31.75	64.17	10	KN204-01b	8.8	3.43	0.93	0.69	0.19
North Atlantic[9]	31.75	64.17	10	KN204-01b	8.0	4.04	0.85	0.81	0.17
North Atlantic[9]	31.75	64.17	10	KN204-01b	17.5	2.82	0.59	0.56	0.12
North Atlantic[9]	31.75	64.17	10	KN204-01b	21.6	3.30	0.56	0.66	0.11
North Atlantic[9]	31.75	64.17	10	KN204-01b	21.5	3.10	0.51	0.62	0.10
North Atlantic[9]	31.75	64.17	10	KN204-01b	52.2	3.06	0.28	0.61	0.06
North Atlantic[9]	29.7	56.82	12	KN204-01b	4.7	4.87	1.95	0.97	0.39
North Atlantic[9]	29.7	56.82	12	KN204-01b	17.7	4.39	0.93	0.88	0.19
North Atlantic[9]	29.7	56.82	12	KN204-01b	19.3	5.80	0.88	1.16	0.18
North Atlantic[9]	29.7	56.82	12	KN204-01b	23.4	3.13	0.49	0.63	0.10
North Atlantic[9]	29.7	56.82	12	KN204-01b	34.0	3.06	0.38	0.61	0.08
North Atlantic[9]	29.7	56.82	12	KN204-01b	46.9	1.22	0.32	0.24	0.06
North Atlantic[9]	27.58	49.63	14	KN204-01b	1.6	13.54	7.35	2.71	1.47
North Atlantic[9]	27.58	49.63	14	KN204-01b	1.2	9.34	2.95	1.87	0.59
North Atlantic[9]	27.58	49.63	14	KN204-01b	9.4	5.09	0.81	1.02	0.16
North Atlantic[9]	27.58	49.63	14	KN204-01b	22.4	4.08	0.46	0.82	0.09
North Atlantic[9]	27.58	49.63	14	KN204-01b	29.1	4.82	0.72	0.96	0.14
North Atlantic[9]	27.58	49.63	14	KN204-01b	43.0	2.66	0.38	0.53	0.08
North Atlantic[9]	26.14	44.83	16	KN204-01b	0.3	11.40	6.10	2.28	1.22
North Atlantic[9]	26.14	44.83	16	KN204-01b	0.5	7.31	6.68	1.46	1.34
North Atlantic[9]	26.14	44.83	16	KN204-01b	13.2	3.25	0.76	0.65	0.15
North	26.14	44.83	16	KN204-01b	26.9	2.60	0.77	0.52	0.15

Atlantic[9]									
North Atlantic[9]	26.14	44.83	16	KN204-01b	34.4	2.74	0.49	0.55	0.10
North Atlantic[9]	26.14	44.83	16	KN204-01b	48.9	2.61	0.47	0.52	0.09
North Atlantic[9]	24.15	40.22	18	KN204-01b	0.4	7.86	7.29	1.57	1.46
North Atlantic[9]	24.15	40.22	18	KN204-01b	0.4	12.59	5.78	2.52	1.16
North Atlantic[9]	24.15	40.22	18	KN204-01b	1.1	20.00	3.08	4.00	0.62
North Atlantic[9]	24.15	40.22	18	KN204-01b	21.6	3.72	0.52	0.74	0.10
North Atlantic[9]	24.15	40.22	18	KN204-01b	37.5	2.65	0.31	0.53	0.06
North Atlantic[9]	22.33	35.87	20	KN204-01b	0.4	23.89	7.46	4.78	1.49
North Atlantic[9]	22.33	35.87	20	KN204-01b	1.6	5.72	1.47	1.14	0.29
North Atlantic[9]	22.33	35.87	20	KN204-01b	17.5	5.31	0.79	1.06	0.16
North Atlantic[9]	22.33	35.87	20	KN204-01b	17.6	3.71	0.86	0.74	0.17
North Atlantic[9]	22.33	35.87	20	KN204-01b	47.7	4.00	0.38	0.80	0.08
North Atlantic[9]	22.33	35.87	20	KN204-01b	46.8	3.38	0.42	0.68	0.08
North Atlantic[9]	19.43	29.38	22	KN204-01b	11.3	9.33	1.08	1.87	0.22
North Atlantic[9]	17.4	24.5	24	KN204-01b	2.2	15.28	1.95	3.06	0.39
North Atlantic[9]	17.4	24.5	24	KN204-01b	11.1	6.07	1.62	1.21	0.32
Subantarctic S. Atlantic[10]	-42.34	-8.99	PS71-101-2	ANTXXIV/III	36.0	3.32	1.12	0.66	0.22
South Atlantic[11]	-28.11	-9.49		GA02 Leg 3	0.49	3.14	2.88	0.7162	0.03
South Atlantic[11]	-28.45	-5.79		GA02 Leg 3	0.99	3.91	1.32	0.7502	0.02
South Atlantic[11]	-28.88	-2.80		GA02 Leg 3	1.74	2.86	1.36	0.5781	0.03
South Atlantic[11]	-29.26	-13.01		GA02 Leg 3	1.11	3.68	1.34	0.9122	0.55
South Atlantic[11]	-30.57	-16.89		GA02 Leg 3	0.28	6.71	2.91	0.6641	0.11
South Atlantic[11]	-41.22	-37.99		GA02 Leg 3	1.87	2.38	1.36	0.6276	0.17

South Atlantic[11]	-42.54	-40.05		GA02 Leg 3	3.1336	3.14	0.85	0.4761	0.27
South Atlantic[11]	-45.43	-44.59		GA02 Leg 3	3.94	3.32	0.56	1.3423	0.58
South Atlantic[11]	-45.55	-44.70		GA02 Leg 3	5.96	4.56	2.74	0.7362	0.27
South Atlantic[11]	-47.33	-47.07		GA02 Leg 3	19.65	2.89	0.16	0.6281	0.58
South Atlantic[11]	-48.20	-48.18		GA02 Leg 3	80.86	3.75	0.11	0.7822	0.26
South Atlantic[11]	-52.26	-49.49		GA02 Leg 3	31.47	3.58	0.17	0.5721	0.27

Table D.4 Cadmium stable isotope data at less than 50 pmol kg^{-1} dissolved Cd
[1]Ripperger et al., 2007.
[2]Conway and John, 2015b.
[3]This dissertation / Janssen et al., in revision.
[4]Yang et al., 2012.
[5]Yang et al., 2014.
[6]Gault-Ringold et al., 2012.
[7]Xue et al., 2012.
[9]Conway et al., 2013.
[9]Conway and John, 2015a.
[10]Abouchami et al., 2011.
[11]Xie et al., in revision.

D.5 Assessing the effect of dust addition on low-Cd surface waters $\varepsilon^{112/110}$Cd

Due to the Cd isotopic fractionation associated with biological uptake (Lacan et al., 2006; John and Conway, 2014), it would follow that significant biological uptake in surface waters, resulting in very low [Cd], would result in highly fractionated surface $\varepsilon^{112/110}$Cd (up to ~+20) as is observed in many regions of the world ocean (e.g. Ripperger et al., 2007; Xue et al., 2012; Conway and John, 2015a; Conway and John, 2015b). At very low [Cd], the input of Cd from dust deposition may alter surface $\varepsilon^{112/110}$Cd due to the near-zero $\varepsilon^{112/110}$Cd of continental crust material (-0.05 ± 0.2; Schmitt et al., 2009; Rehkämper et al., 2012) in comparison to the elevated $\varepsilon^{112/110}$Cd predicted by biological Cd uptake. This potential dust influence may explain our low surface $\varepsilon^{112/110}$Cd (up to 5.19 ± 0.23) observed at very low [Cd] in comparison with the high values (up to +18.5 ± 3.0, Ripperger et al., 2007) reported from the subtropical North Pacific. To assess the potential for dust deposition to depress ambient surface $\varepsilon^{112/110}$Cd and result in our low $\varepsilon^{112/110}$Cd observations, we determined the necessary

dust flux to explain our observations at 10 m depth at station P16 (4 pmol kg^{-1} Cd, $\varepsilon^{112/110}Cd$ = 4.87 ± 1.44).

We assume that a putative dust deposition, with $\varepsilon^{112/110}Cd_{dust} = 0$ due to the near-zero value of continental crust (Schmitt et al., 2009; Rehkämper et al., 2012), would contribute half of the observed Cd to our surface sample. This results in the following conditions:

$$[Cd_{dust}] = 2 \text{ pmol } kg^{-1},\ \varepsilon^{112/110}Cd_{dust} = 0$$
$$[Cd_{sw}] = 2 \text{ pmol } kg^{-1},\ \varepsilon^{112/110}Cd_{sw} = 10$$
$$[Cd_{obs}] = 4 \text{ pmol } kg^{-1},\ \varepsilon^{112/110}Cd_{obs} = 5$$

based off of the mass balance where:

$$[Cd_{dust}] \times \varepsilon^{112/110}Cd_{dust} + [Cd_{sw}] \times \varepsilon^{112/110}Cd_{sw} = [Cd_{obs}] \times \varepsilon^{112/110}Cd_{obs}$$

The subscript "dust" reflects the Cd contributed by dust, "sw" is the Cd contributed by seawater before the addition of dust, and "obs" is the observed Cd after the putative dust deposition. This assumption, which is the foundation for determining the theoretical dust flux, was based on 1) balancing the need for a small amount of dust in order to keep the calculated deposition as close to reasonable as possible and 2) the fact that a larger amount of dust allows for the pre-dust surface $\varepsilon^{112/110}Cd$ to be larger, which is necessary if dust will reconcile our low observed $\varepsilon^{112/110}Cd$ and elevated $\varepsilon^{112/110}Cd$ in the literature.

Based off of an average crustal [Cd] of ~0.1 ppm, or 0.1 μg g^{-1} (Schmitt et al., 2009a), the necessary dust deposition to explain our observations given the above conditions is calculated as follows, assuming that all of the Cd present in dust reaching the ocean dissolves in the upper 10 m. If some Cd remained insoluble or dissolved below 10 m, then a larger dust input will be necessary to result in a 2 pmol kg^{-1} addition in the upper 10 m. Therefore this calculation represents the minimum dust deposition necessary to result in a 2 pmol kg^{-1} addition to the surface at P16.

Volume = 10 m^3 (a 10 m deep box with a surface exposed to the atmosphere of 1 m^2)

Added Cd in this box = 10 m^3 × 1000 kg m^{-3} × 2 pmol kg^{-1} added = 20,000 pmol Cd

pmol Cd in dust = (0.1 μg g^{-1} ÷ 112 μg $μmol^{-1}$ Cd) × 1000^2 pmol $μmol^{-1}$ = 893 pmol Cd in 1 g of dust

Dust deposited to 1 m^2 of surface = 20,000 pmol Cd added ÷ 893 pmol Cd g^{-1} dust = 22 g dust

This calculated addition of dust, which would be necessary to explain our results given the assumed equal contributions of Cd_{dust} and Cd_{sw}, would need to be deposited in a sufficiently short timeframe such that it is not mixed out of the upper 10 m (i.e. much less than 1 year). However, the calculated deposition is an order of magnitude or more greater than the yearly dust deposition in the subarctic northeast Pacific of ~1 g m^{-2} (Han et al., 2008; Serno et al., 2014) and therefore cannot explain our observations. The necessary dust deposition can be decreased if the Cd_{dust}:Cd_{sw} is lowered; however, such a modification to the calculation results in the $\varepsilon^{112/110}Cd_{sw}$ signal dominating $\varepsilon^{112/110}Cd_{obs}$ such that $\varepsilon^{112/110}Cd_{sw}$ would already be significantly lower than the previous range of reported values from the North Pacific of up to 18.5± 3.0 (Ripperger et al., 2007) and 16.9 ± 1.6 (Conway and John, 2015b), rendering the theoretical exercise unnecessary. For example, halving the dust contribution to our observations would still result in an unrealistically high dust deposition of 11 g m^{-2} while lowering $\varepsilon^{112/110}Cd_{sw}$ to +6.67.

D.6 Subsurface $\varepsilon^{112/110}$Cd trends along Line P

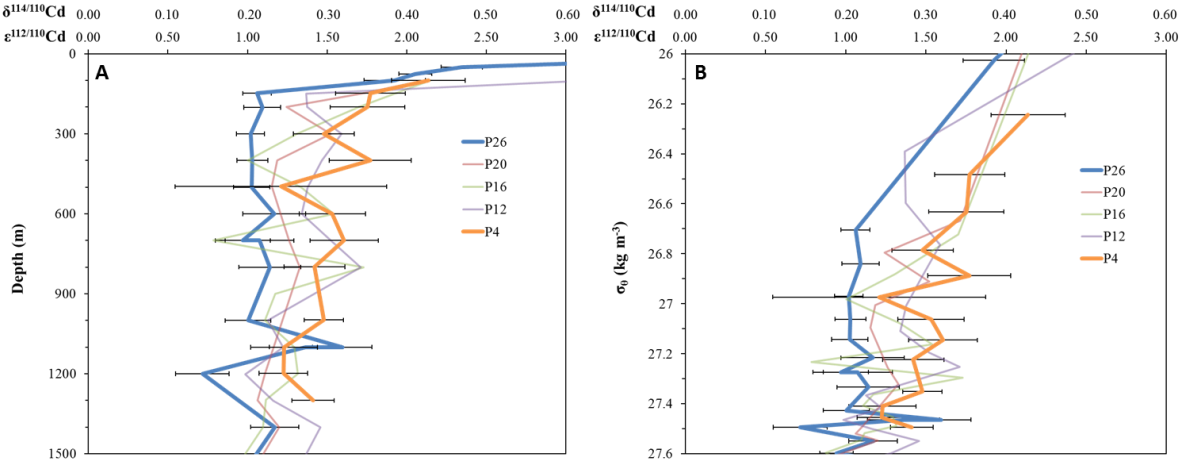

Figure D.4 $\varepsilon^{112/110}$Cd depth profiles along Line P in O_2-depleted water
$\varepsilon^{112/110}$Cd is plotted against depth (panel A) and σ_θ (panel B). Stations P26 (blue) and P4 (orange) are highlighted to show potential variability in deepwater $\varepsilon^{112/110}$Cd along the Line P transect. Error bars are 2σ. Intermediate stations P20, P16 and P12 are shown in red, green and purple respectively and are plotted without error bars for clarity.

D.7 Accumulated deepwater [Cd]

A homogeneous North Pacific deepwater $\varepsilon^{112/110}$Cd and a Southern Component Water source $\varepsilon^{112/110}$Cd (Xue et al., 2013; Abouchami et al., 2014) as well as constraints of [Cd] in these two end members allows a calculation for the isotopic composition of Cd which accumulates in Pacific deepwater from the following fundamental mass balance as Equations:

$$Cd_{SCW} + Cd_{acm} = Cd_{Pac}$$

$$Cd_{SCW} * \varepsilon^{112/110}Cd_{SCW} + Cd_{acm} * \varepsilon^{112/110}Cd_{acm} = Cd_{Pac} * \varepsilon^{112/110}Cd_{Pac}$$

where the suffix "SCW" is deep Southern Component Water, "acm" is accumulated, and "Pac" is deep subarctic northeast Pacific. This calculation is carried out for both $\varepsilon^{112/110}$Cd and $\delta^{114/110}$Cd in two ways:

1) Using the arithmetic mean deepwater isotopic composition from each water mass and the 2SD error on this mean.
2) Using a weighted mean and 2σ of each water mass based on the errors associated with individual measurements, where the weighting is equal to ($^{110/112}$Cd standard error)$^{-2}$.

Deep SCW [Cd]	**Deep Pacific [Cd]**		**Arithmetic Mean**					
nmol kg^{-1}	nmol kg^{-1}		Deep SCW	2SD	Deep Pacific	2SD	Maximum Accumulated	Minimum Accumulated
0.76	1	$\boldsymbol{\varepsilon^{112/110}Cd}$	1.21	0.36	1.14	0.37	3.61	-1.75
		$\boldsymbol{\delta^{114/110}Cd}$	0.241	0.072	0.228	0.074	0.72	-0.35
Deep SCW [Cd]	**Deep Pacific [Cd]**		**Weighted mean**					
nmol kg^{-1}	nmol kg^{-1}		Deep SCW	2σ	Deep Pacific	2σ	Maximum Accumulated	Minimum Accumulated
0.76	1	$\boldsymbol{\varepsilon^{112/110}Cd}$	1.219	0.033	1.130	0.023	1.05	0.65
		$\boldsymbol{\delta^{114/110}Cd}$	0.244	0.007	0.226	0.005	0.21	0.13

Table D.5 Derived isotopic composition of Cd accumulated in North Pacific deepwater from a Southern Component source

Appendix E

Supplementary material for Chapter 5 - Particulate cadmium concentrations and stable isotopes in the subarctic northeast Pacific

Station	Lat	Long	Size Fraction	Depth	$p\varepsilon^{112/110}Cd$	2σ	$p\delta^{114/110}Cd$	2σ	pCd	pCd error
	N	W		m					pM	pM
P26	50°	145°	0.8-51 µm	50	2.71	0.14	0.543	0.028	37.59	3.76
P26	50°	145°	0.8-51 µm	100	-0.84	0.29	-0.169	0.058	6.96	0.70
P26	50°	145°	0.8-51 µm	150	-2.52	0.37	-0.504	0.074	3.56	0.36
P26	50°	145°	0.8-51 µm	200‡	-2.25	0.60	-0.450	0.121	1.61	0.16
P26	50°	145°	0.8-51 µm	200†‡	-3.16	0.34	-0.633	0.068	1.93	0.19
P26	50°	145°	0.8-51 µm	300	-2.52	0.45	-0.504	0.089	1.65	0.16
P26	50°	145°	0.8-51 µm	400	-2.64	0.27	-0.529	0.054	0.91	0.09
P26	50°	145°	0.8-51 µm	500	-2.54	0.23	-0.508	0.045	0.98	0.10
P26	50°	145°	0.8-51 µm	500‡	-2.07	0.20	-0.415	0.040	1.08	0.11
P26	50°	145°	0.8-51 µm	500†‡	-2.42	0.34	-0.484	0.069	0.53	0.05
P26	50°	145°	0.8-51µm	600	-2.25	0.29	-0.450	0.058	0.60	0.06
P26	50°	145°	0.8-51 µm	800	-2.15	0.27	-0.430	0.054	0.28	0.03
P26	50°	145°	0.8-51 µm	1000	-1.06	0.64	-0.212	0.128	0.28	0.03
P26	50°	145°	0.8-51 µm	1250	-1.09	0.74	-0.218	0.149	0.18	0.02
P26	50°	145°	0.8-51 µm	1500	0.27	0.85	0.054	0.171	0.07	0.01
P4	48.65°	126.7°	0.8-51 µm	25	1.68	0.30	0.335	0.059	35.75	3.57
P4	48.65°	126.7°	0.8-51 µm	75‡	-0.19	0.84	-0.037	0.167	7.29	0.73
P4	48.65°	126.7°	0.8-51 µm	75‡	0.22	0.77	0.043	0.154	7.06	0.71
P4	48.65°	126.7°	0.8-51 µm	150	-1.63	0.24	-0.325	0.048	4.36	0.44
P4	48.65°	126.7°	0.8-51 µm	300	-2.44	0.20	-0.487	0.040	2.62	0.26
P4	48.65°	126.7°	0.8-51 µm	400	-2.41	0.39	-0.482	0.079	0.72	0.07
P4	48.65°	126.7°	0.8-51 µm	500	-2.35	0.21	-0.471	0.042	1.21	0.12
P4	48.65°	126.7°	0.8-51 µm	600	-2.25	0.17	-0.450	0.034	0.85	0.09
P4	48.65°	126.7°	≥ 0.8 µm	800	-0.86	0.20	-0.171	0.039	0.70	0.07
P4	48.65°	126.7°	0.8-51 µm	1000	-1.18	0.27	-0.237	0.054	0.88	0.09
P4	48.65°	126.7°	0.8-51 µm	1250	-1.66	0.40	-0.332	0.079	0.16	0.02
USGT 10-09	17. 35°	18.25°	0.8-51 µm	52	1.74	0.34	0.348	0.068	2.37	0.24
USGT 10-09	17.35°	18.25°	0.8-51 µm	85	0.26	0.47	0.051	0.094	2.35	0.24
USGT 10-09	17.35°	18.25°	0.8-51 µm	185	-0.04	0.45	-0.007	0.091	3.00	0.30

USGT 10-09	17.35°	18.25°	0.8-51 µm	235	-0.10	0.44	-0.020	0.089	2.83	0.29
USGT 10-09	17.35°	18.25°	0.8-51 µm	390	0.85	0.47	0.170	0.095	1.82	0.19
SEATS	18°	116°	10-60 µm	55	1.80	0.90	0.36	0.18	0.64	
SEATS	18°	116°	10-60 µm	65	3.50	0.95	0.7	0.19	0.4	
SEATS	18°	116°	10-60 µm	58	-1.25	0.70	-0.25	0.14	0.97	
SEATS	18°	116°	10-60 µm	58	2.45	0.95	0.49	0.19	0.89	
SEATS	18°	116°	10-60 µm	**mean**	1.65	2.05	0.33	0.41	0.82	0.28
SEATS	18°	116°	60-150 µm	55‡	1.85	1.65	0.37	0.33	0.14	
SEATS	18°	116°	60-150 µm	55‡	3.35	1.25	0.67	0.25	0.14	
SEATS	18°	116°	60-150 µm	65	-4.65	0.40	-0.93	0.08	0.18	
SEATS	18°	116°	60-150 µm	58	-3.20	0.25	-0.64	0.05	0.37	
SEATS	18°	116°	60-150 µm	58	-1.00	0.70	-0.2	0.14	0.18	
SEATS	18°	116°	60-150 µm	**mean**	-0.75	3.00	-0.15	0.60	0.2	0.09
SEATS	18°	116°	>150 µm	55‡	1.15	0.75	0.23	0.15	0.19	
SEATS	18°	116°	>150 µm	55‡	-0.60	0.70	-0.12	0.14	0.14	
SEATS	18°	116°	>150 µm	65	-0.10	0.70	-0.02	0.14	0.11	
SEATS	18°	116°	>150 µm	58	0.45	0.20	0.09	0.04	0.26	
SEATS	18°	116°	>150 µm	58	2.25	0.30	0.45	0.06	0.18	
SEATS	18°	116°	>150 µm	**mean**	0.65	1.00	0.13	0.20	0.18	0.05
SEATS	18°	116°	>100 µm	5‡	1.25	0.75	0.25	0.15	0.09	
SEATS	18°	116°	>100 µm	5‡	1.35	0.85	0.27	0.17	0.09	
SEATS	18°	116°	>100 µm	5‡	-0.10	0.55	-0.02	0.11	0.07	
SEATS	18°	116°	>100 µm	5‡	0.35	0.90	0.07	0.18	0.17	
SEATS	18°	116°	>100 µm	5‡	1.20	0.90	0.24	0.18	0.19	
SEATS	18°	116°	>100 µm	5‡	1.60	0.85	0.32	0.17	0.22	
SEATS	18°	116°	>100 µm	**mean**	0.95	0.55	0.19	0.11	0.15	0.06
									µmol m^{-2}d^{-1}	
SEATS	18°	116°	Sed Trap	30	4.35	0.45	0.87	0.09	0.3	
SEATS	18°	116°	Sed Trap	100	5.75	0.50	1.15	0.10	0.21	
SEATS	18°	116°	Sed Trap	30	4.20	0.45	0.84	0.09	1.09	
SEATS	18°	116°	Sed Trap	100	6.65	0.60	1.33	0.12	0.21	
SEATS	18v	116°	Sed Trap	160	9.00	0.70	1.8	0.14	0.04	
SEATS	18°	116°	Sed Trap	30	6.40	0.60	1.28	0.12	0.07	
SEATS	18°	116°	Sed Trap	100	7.65	0.55	1.53	0.11	0.08	
SEATS	18°	116°	Sed Trap	160	8.00	0.70	1.6	0.14	0.03	
SEATS	18°	116°	Sed Trap	30	4.05	0.60	0.81	0.12	0.6	
SEATS	18°	116°	Sed Trap	100	10.40	0.55	2.08	0.11	0.1	
SEATS	18°	116°	Sed Trap	160	8.70	0.55	1.74	0.11	0.08	

Table E.1 Compilation of all global marine suspended and sinking pε$^{112/110}$Cd data

There are no size fraction constraints on the sediment trap samples and Cd is measured as a flux (μmol $m^{-2}d^{-1}$) rather than concentration. Sources: Line P data: this dissertation. USGT data: Janssen et al., 2014 / Chapter 2; Conway and John 2015a. SEATS data: S.C. Yang et al., 2015 except the first 30 m sediment trap sample, which is from Yang et al., 2012. ‡ = analysis of replicate subsamples from the same sample. † = an error was made in spiking this sample whereby samples were underspiked by roughly a factor of 10, resulting in a far from optimal $^{106}Cd/^{112}Cd$ ratio and greater imprecision in analysis. For this reason, these data are omitted from presentation or discussion for both pCd and $p\varepsilon^{112/110}Cd$ in the rest of the dissertation.

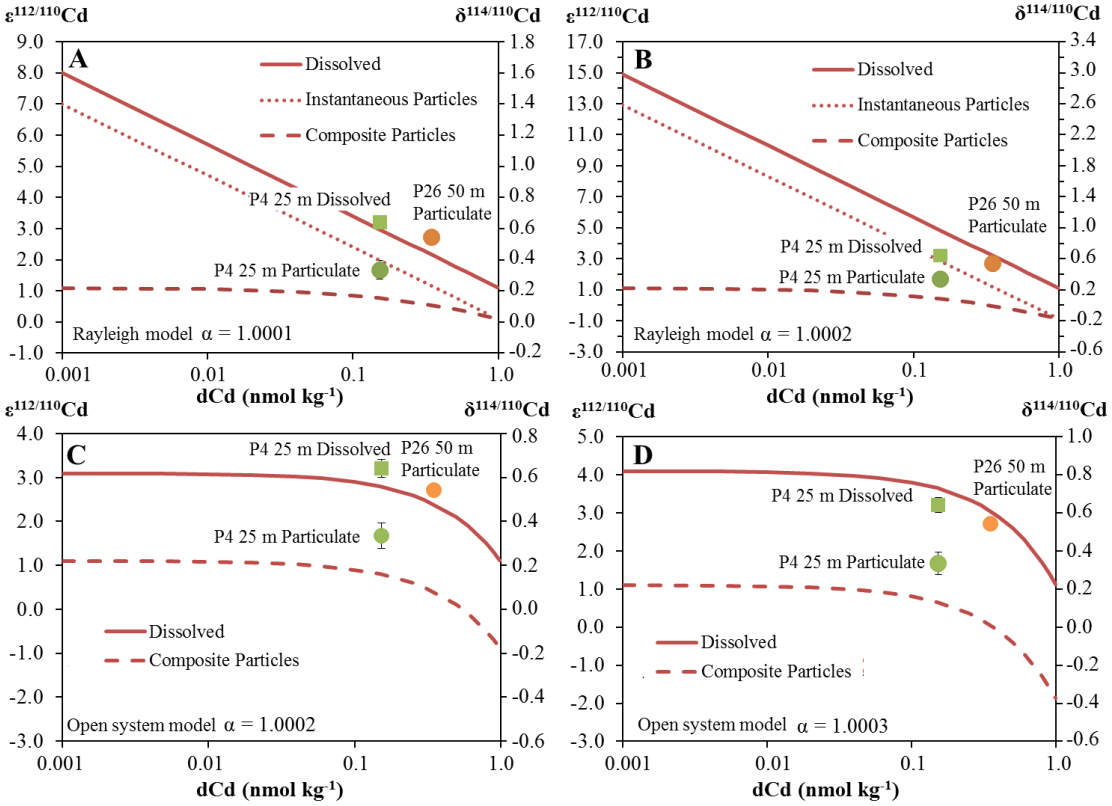

Figure E.1 Cadmium isotope fractionation models

Panels A and B show Rayleigh model fractionation and panels C and D show open system model fractionation. Seawater-particle fractionation factors (α) are presented for each panel. Composite particles represent the integrated isotopic composition of all particles formed until a given point during transfer of Cd from the dissolved to the particulate phase. Fractionation models are calculated for conditions of the subarctic northeast Pacific deepwater: dCd = ~1 nM kg^{-1} and $d\varepsilon^{112/110}Cd$ ~ +1.1. P4 25 m, the only sample for which we have dissolved and particulate concentrations and $\varepsilon^{112/110}Cd$, is included as a green dot ($p\varepsilon^{112/110}Cd$) and a green square ($d\varepsilon^{112/110}Cd$). Particulate $\varepsilon^{112/110}Cd$ for P26 50 m is presented as an orange circle. Dissolved Cd at P26 50 m (0.349 nmol kg^{-1}) was measured by ICP-MS. Dissolved $\varepsilon^{112/110}Cd$ is not available for P26 at 50 m in 2014. Note the varying $\varepsilon^{112/110}Cd$ scale among the different panels. Note also that these models are tuned to deepwater Cd following Abouchami et al., 2014, but that the exact fits are sensitive to the source Cd. An initial term with elevated $\varepsilon^{112/110}Cd$ (such as upwelling of intermediate depth water) would result in the model lines shifting up. The subarctic northeast Pacific is insulated from this potential source of error in the models due to the shallow depths at which near-deepwater d[Cd] and $d\varepsilon^{112/110}Cd$ are reached (~200 m at P26 in 2012, see Table D.2, Figure 4.3).

Station	Depth	$p\delta^{114/110}Cd$	Error	pCd	Inferred Remineralized			
			2σ	pmol L^{-1}	[Cd] (pmol L^{-1})	$\delta^{114/110}Cd$	Max $\delta^{114/110}Cd$	Min $\delta^{114/110}Cd$
P26	50	0.54	0.03	37.59	NA	NA	NA	NA
P26	100	-0.17	0.06	6.96	30.62	0.70	0.75	0.66
P26	150	-0.50	0.07	3.56	3.40	0.18	0.38	-0.01
P26	200	-0.45	0.12	1.61	1.95	-0.55	-0.31	-0.78
P26	300	-0.50	0.09	1.65	-0.04	-2.77	-11.64	6.10
P26	400	-0.53	0.05	0.91	0.74	-0.47	-0.21	-0.74
P26	500[1]**	-0.48	0.03	1.03	-0.13	-0.11	-0.75	0.53
P26	600	-0.45	0.06	0.60	0.43	-0.52	-0.36	-0.67
P26	800	-0.43	0.05	0.28	0.32	-0.47	-0.31	-0.63
P26	1000	-0.21	0.13	0.28	0.00	NA	NA	NA
P26	1250	-0.22	0.15	0.18	0.11	-0.20	0.38	-0.79
P26	1500	0.05	0.17	0.07	0.11	-0.39	-0.04	-0.74
P4	25	0.34	0.06	35.75	NA	NA	NA	NA
P4	75*	-0.02	0.11	7.18	28.57	0.42	0.53	0.32
P4	150	-0.33	0.05	4.36	2.82	0.46	0.82	0.10
P4	300	-0.49	0.04	2.62	1.74	-0.08	0.10	-0.26
P4	400	-0.48	0.08	0.72	1.90	-0.49	-0.40	-0.57
P4	500**	-0.47	0.04	1.21	-0.49	-0.45	-0.67	-0.23
P4	600	-0.45	0.03	0.85	0.36	-0.52	-0.30	-0.75
P4	800	-0.17	0.04	0.70	0.16	-1.68	-1.32	-2.04
P4	1000**	-0.24	0.05	0.88	-0.18	-0.49	-0.91	-0.07
P4	1250	-0.33	0.08	0.16	0.71	-0.21	-0.13	-0.30

Table E.2 Calculation of inferred remineralized $p\delta^{114/110}Cd$

Inferred remineralized $\delta^{114/110}Cd$ is calculated by mass balance from the pCd and $p\delta^{114/110}Cd$ differences between adjacent depths by the following equations:

$$p\delta^{114/110}Cd_{depth1} * pCd_{depth1} = p\delta^{114/110}Cd_{depth2} * pCd_{depth2} + p\delta^{114/110}Cd_{remineralized} * pCd_{remineralized}$$

$$pCd\ remineralized = pCd_{depth1} - pCd_{depth2}$$

Maximum and minimum remineralized values are calculated for the maximum range allowable within 2σ error by either adding $2\sigma_{depth1}$ to $p\delta^{114/110}Cd_{depth\ 1}$ and subtracting $2\sigma_{depth2}$ from $p\delta^{114/110}Cd_{depth2}$ or subtracting $2\sigma_{depth1}$ from $p\delta^{114/110}Cd_{depth1}$ and adding $2\sigma_{depth2}$ to $p\delta^{114/110}Cd_{depth2}$ respectively.

A version of this table in units of $\varepsilon^{112/110}Cd$ can be found in Section 5.4.3 (Table 5.3).

* = mean of measurements from different subsamples of one filter.

[1] = mean of measurements from 2 different samples from this depth. NA = not applicable.

** = a negative inferred remineralization, or an accumulation of Cd, is calculated for these samples.

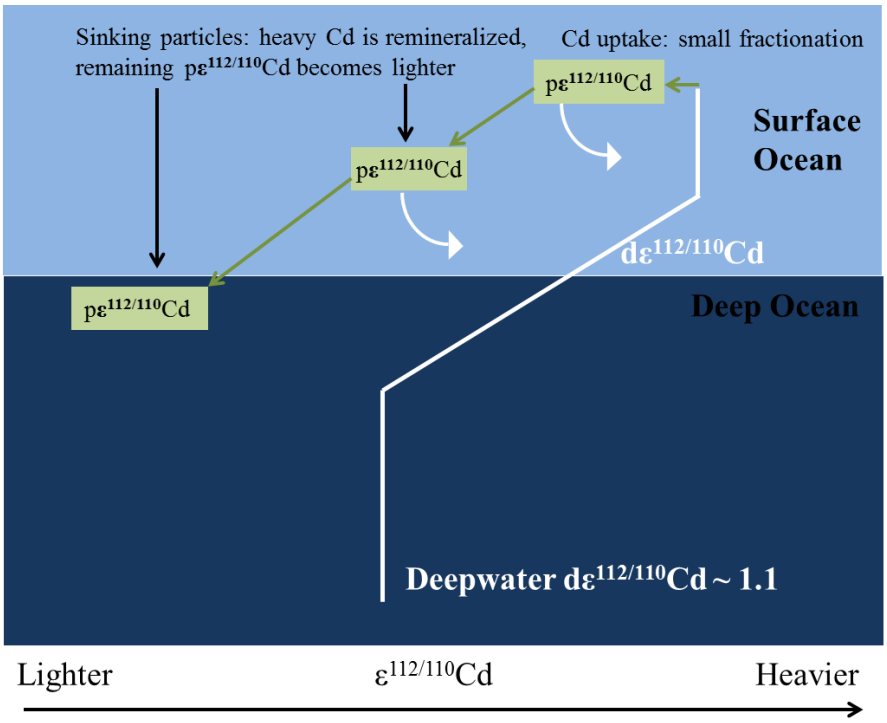

Figure E.2 Simple schematic showing particulate composition with depth and inferred remineralization
The dissolved phase and transfer from dissolved to particulates are shown in while lines. The particulate phase and transfer from dissolved to particulates are shown in green lines.

A heavy surface $d\varepsilon^{112/110}Cd$ is maintained not by the transfer of especially light Cd to the particulate phase, but by the remineralization of heavy Cd with depth resulting in the transfer of very light $p\varepsilon^{112/110}Cd$ to depth. This schematic reflects the 0.8-51 μm size class sampled in this dissertation, which gives an incomplete picture of the pCd pool. S.C. Yang et al. (2015) sampled sinking particles without size screening (all size classes of sinking particles represented) in sediment traps in the South China Sea and observed the opposite trend with depth – particulates becoming isotopically heavier with depth. If the > 51 μm size class in the subarctic northeast Pacific, which we did not sample, follows a different trend than the 0.8-51 μm size class, the composite of the trends these two classes follow will dictate net cycling in the surface ocean.

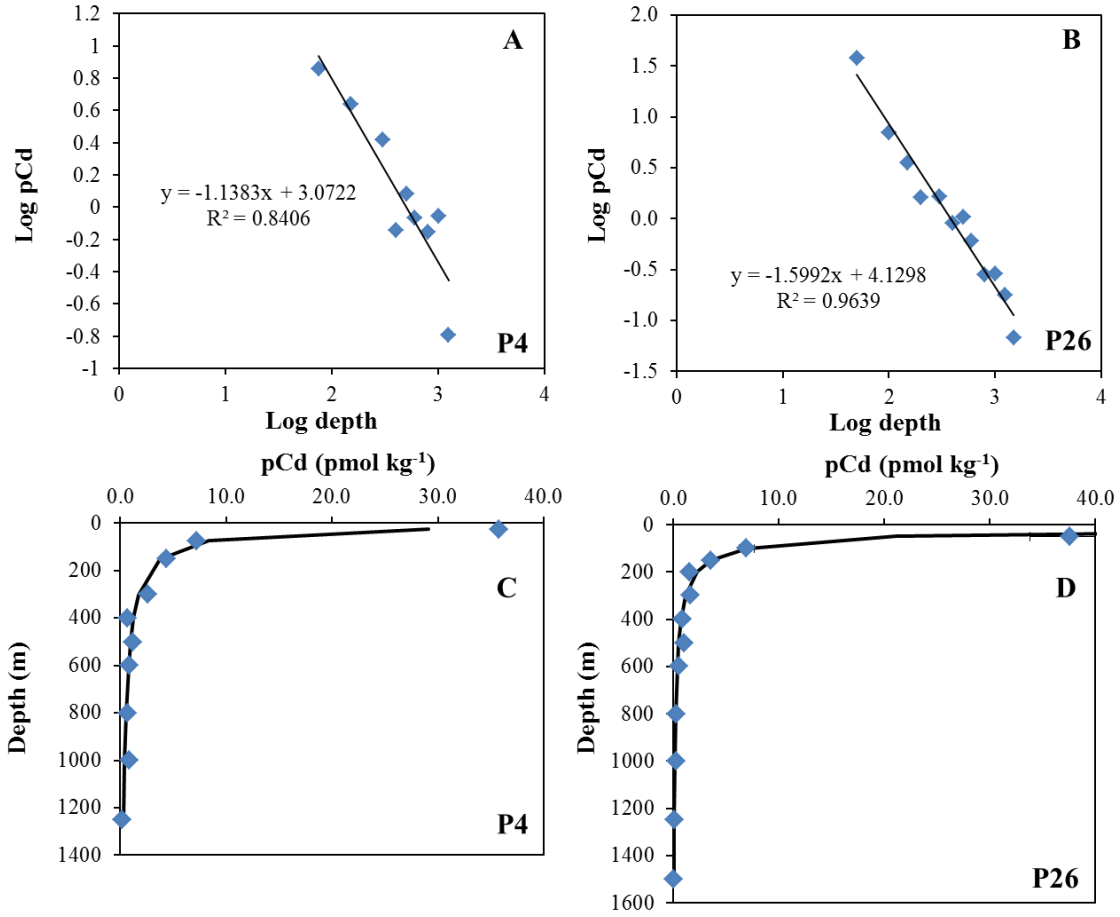

Figure E.3 Martin F curves for pCd
Panels A (P4) and B (P26) show the log-log transformation of pCd data for the derivation of B values. Panels C (P4) and D (P26) show the pCd data with Martin F curve fits (see Martin et al., 1987) calculated from:

$$F_z = F_{100} \times \left(\frac{z}{100}\right)^b$$

where F_z is the flux at depth z and F_{100} is the flux at 100 m. The F curves in C and D are tuned to the data with b values equal to the slope of the log-log plots. For station P26, pCd at 100 m at is used for F100. For station P4, a pCd value of 6 pmol kg^{-1} (between the values at 75 m and 150 m) is used as pCd data are not available for 100 m.

Bibliography

Abe, K. (2002). Preformed Cd and PO_4 and the relationship between the two elements in the northwestern Pacific and the Okhotsk Sea. *Marine Chemistry*. 79:27-36. doi: 10.1016/S0304-4203(02)00038-5.

Abouchami, W., Galer, S.J.G., de Baar, H.J.W., Alderkamp, A.C., Middag, R., Laan, P., Feldmann, H., Andreae, M.O. (2011). Modulation of the Southern Ocean cadmium isotope signature by ocean circulation and primary productivity. *Earth and Planetary Science Letters*. 305:83–91. doi: 10.1016/j.epsl.2011.02.044.

Abouchami, W., Galer, S.J.G., Horner, T.J., Rehkämper, M., Wombacher, F., Xue, Z. ,Lambelet, M., Gault-Ringold, M., Stirling, C.H., Schönbächler, M., Shiel, A.E., Weis, D., Holdship, P.F. (2012). A common reference material for cadmium isotope studies – NIST SRM 3108. *Geostandards and Geoanalytical Research*. 37:5–17. doi: 10.1111/j.1751-908X.2012.00175.x.

Abouchami, W., Galer, S.J.G., de Baar, H.J.W., Middag, R., Vance, D., Zhao, Y., Klunder, M., Mezger, K., Feldmann, H., Andreae, M.O. (2014). Biogeochemical cycling of cadmium isotopes in the Southern Ocean along the Zero Meridian. *Geochimica et Cosmochimica Acta*. 127:348-367. doi: 10.1016/j.gca.2013.10.022

Abouchami, W., Koschinsky A., Haßler, K., Galer, S.J.G. (2015). Cadmium and Lead isotopes in high temperature hydrothermal vents at 5°S on the Mid-AtlanticRidge. *Goldschmidt Abstracts*, 2015, 8.

Ahlgren, N.A., Noble, A., Patton, A.P., Roache-Johnson, K., Jackson, L., Robinson, D., McKay, C., Moore, L.R., Saito, M.A., Rocap, G. (2014). The unique trace metal and mixed layer conditions of the Costa Rica upwelling dome support a distinct and dense community of *Synechococcus*. *Limnology and Oceanography*. 59(6):2166-2184. doi: 10.4319/lo.2014.59.6.2166.

Al-Farawati, R., van den Berg, C.M.G. (1999). Metal-sulfide complexation in seawater. *Marine Chemistry*. 63(3-4):331-352. doi: 10.1016/S0304-4203(98)00056-5.

Altabet, M.A., Small, L.F. (1990). Nitrogen isotopic ratios in fecal pellets produced by marine zooplankton. *Geochimica et Cosmochimica Acta*. 54(1):155-163. doi: 10.1016/0016-7037(90)90203-W.

Altabet, M.A., Francois, R. (1994). Sedimentary nitrogen isotopic ratio as a recorder for surface ocean nitrate utilization. *Global Biogeochemical Cycles*. 8(1):103-116. doi: 10.1029/93GB03396.

Anderson, M.A., Morel, F.M.M., Guillard, R.R.L. (1978). Growth limitation of a coastal diatom by low zinc ion activity. *Nature*. 276:70-71. doi: 10.1038/276070a0.

Anderson, M.A., Morel, F.M.M. (1982). The influence of aqueous iron chemistry on the uptake of iron by the coastal diatom *Thalassiosira weissflogii*. *Limnology and Oceanography*. 27(5), 789-813. doi: 10.4319/lo.1982.27.5.0789.

Baars, O., Abouchami, W., S. J.G. Galer, Boye, M., and Croot, P.L. (2014). Dissolved cadmium in the Southern Ocean: Distribution, speciation, and relation to phosphate. *Limnology and Oceanography*. 59:385–399. doi: 10.4319/lo.2014.59.2.0385.

Baker, E.T., Milburn, H.B., Tennant, D.A. (1988). Field assessment of sediment trap efficiency under varying flow conditions. *Journal of Marine Research*. 46, 573-592. doi: 10.1357/002224088785113522.

Barwell-Clarke, J., Whitney, F. (1996). Institute of Ocean Sciences nutrient methods and analysis. *Canadian Technical Report of Hydrography and Ocean Sciences*. 182:43pp. ISSN Fs-7-18/182E.

Balistrieri, L., Brewer, P.G., Murray, J.W. (1981). Scavenging residence times of trace metals and surface chemistry of sinking particles in the deep ocean. *Deep-Sea Research*. 28A:101-121. doi: 10.1016/0198-0149(81)90085-6.

Berner, R.A. (1981). A new geochemical classification of sedimentary environments. *Journal of Sedimentary Research*. 51(2):359-365. doi: 10.1306/212F7C7F-2B24-11D7-8648000102C1865D.

Bianchi, D., Dunne, J.P., Sarmiento, J.L., Galbraith, E.D. (2012). Data-based estimates of suboxia, denitrification, and N_2O production in the ocean and their sensitivities to dissolved O_2. *Global Biogeochemical Cycles*. 26(2):13pp. doi: 10.1029/2011GB004209.

Bishop, J.K.B. (1988). The barite-opal-organic carbon association in oceanic particulate matter. *Nature*. 332(6162):341-343. doi: 10.1038/332341a0.

Bishop, J.K.B., Lam, P.J., Wood, T.J. (2012). Getting good particles: Accurate sampling of particles by large volume In-situ filtration. *Limnology and Oceanography Methods*. 10:681-710. doi: 10.4319/lom.2012.10.681.

Blain, S., Bonnet, S., Guieu, C., 2008. Dissolved iron distribution in the tropical and sub tropical South Eastern Pacific. Biogeosciences. 5(1):269-280. doi: 10.5194/bg-5-269-2008.

Bond, N.A., Cronin, M.F., Freeland, H., Mantua, N. (2015). Causes and impacts of the 2014 warm anomaly in the NE Pacific. *Geophysical Research Letters*. 42:3414-3420. doi: 10.1002/2015GL063306.

Bopp, L., Resplandy, L., Orr, J.C., Doney, S.C., Dunne, J.P., Gehlen, M., Halloran, P., Heinze, C., Ilyina, T., Séférian, R., Tjiputra, J., Vichi, M. (2013). Multiple stressors of ocean ecosystems in the 21st century: projections with CMIP5 models. *Biogeosciences*. 10:6225-6245. doi: 10.5194/bg-10-6225-2013.

Boyd, P., Harrison, P.J. (1999). Phytoplankton dynamics in the NE subarctic Pacific. *Deep-Sea Research Part II*. 46:2405-2432. doi: 10.1016/S0967-0645(99)00069-7.

Boyle, E.A., Edmund, J.J. (1975). Copper in surface waters of South New Zealand. *Nature*. 253:107-109. doi: 10.1038/253107a0.

Boyle, E.A., Sclater, F., Edmond, J.M. (1976). On the marine geochemistry of cadmium. *Nature*. 263:42-44. doi: 10.1038/263042a0.

Boyle, E.A., Huested, S.S., Jones, S.P. (1981). On the distribution of copper, nickel, and cadmium in the surface waters of the North Atlantic and North Pacific Ocean. *Journal of Geophysical Research*. 86(C9):8048-8066. doi: 10.1029/JC086iC09p08048.

Boyle, E.A., Keigwin, L. (1987). North Atlantic thermohaline circulation during the past 20,000 years linked to high-latitude surface temperature. *Nature*. 330:35-40. doi: 10.1038/330035a0.

Boyle, E.A., 1988. Cadmium: chemical tracer of deepwater paleoceanography. *Paleoceanography*. 3(4):471-489. doi: 10.1029/PA003i004p00471.

Boyle, E.A., John, S., Abouchami, W., Adkins, J.F., Echegoyen-Sanz. Y., Ellwood, M., Flegal, A.R., Fornace, K., Gallon, C., Galer, S., Gault-Ringold, M., Lacan, F., Radic, A., Rehkämper, M., Rouxel, O., Sohrin, Y., Stirling, C., Thompson, C., Vance, D., Xue, Z., Zhao, Y. (2012). GEOTRACES IC1 (BATS) contamination-prone trace element isotopes Cd, Fe, Pb, Zn, Cu, and Mo intercalibration. *Limnology and Oceanography Methods*. 10:653-665. doi: 10.4319/lom.2012.10.653.

Brand, L.E., Sunda, W.G., Guillard, R.R.L. (1983). Limitation of marine phytoplankton reproductive rates by zinc, manganese and iron. *Limnology and Oceanography*. 28(6):1182-1198. doi: 10.4319/lo.1983.28.6.1182.

Brand, L.E., Sunda, W.G., Guillard, R.R.L. (1986). Reduction of marine phytoplankton reproduction rates by copper and cadmium. *Journal of Experimental Marine Biology and Ecology*. 96(3):225-250. doi: 10.1016/0022-0981(86)90205-4.

Bridgestock, L., van de Flierdt, T., Rehkämper, M., Paul, M., Middag, R., Milne, A., Lohan, M.C., Baker, A.R., Chance, R., Khonosker, R., Strekopytov, S., Humphreys-Williams, E., Achterberg, E.P., Rijkenberg, M.J.A., Gerringa, L.J.A., de Baar, H.J.W. (2016).

Return of naturally sourced Pb to Atlantic surface waters. *Nature Communications*. 7:12pp. doi: 10.1038/ncomms12921.

Bruland, K.W., Knauer, G.A., Martin, J.H. (1978). Cadmium in northeast Pacific waters. *Limnology and Oceanography*. 23:618-625. doi: 10.4319/lo.1978.23.4.0618.

Bruland, K.W., Knauer, G.A., Martin, J.H. (1978). Zinc in north-east Pacific water. *Nature*. 271:741-743. doi: 10.1038/271741a0.

Bruland, K.W., Franks, R.P., Knauer, G.A., Martin, J.H. (1979) Sampling and analytical methods for the determination of copper, cadmium, zinc and nickel at the nanogram per liter level in sea water. *Analytica Chimica Acta*. 105:223-245. doi: 10.1016/S0003-2670(01)83754-5.

Bruland, K.W. (1980). Oceanographic distributions of cadmium, zinc, nickel, and copper in the North Pacific. *Earth and Planetary Science Letters*. 47(2):176-198. doi: 10.1016/0012-821X(80)90035-7.

Bruland, K.W., Franks, R.P. (1983). Mn, Ni, Cu, Zn and Cd in the Western North Atlantic. In Trace Metals in Sea Water. *NATO Conference Series Volume 9*. 395-414. doi: 10.1007/978-1-4757-6864-0_23.

Bruland, K.W. (1989). Complexation of zinc by natural organic ligands in the central North Pacific. *Limnology and Oceanography*. 34(2):269-285. doi: 10.4319/lo.1989.34.2.0269.

Bruland, K.W., Lohan, M.C. (2006). 6.02 Controls of trace metals in seawater. Elderfield, H. (Ed.), The Oceans and Marine Geochemistry. Elsevier, Oxford, pp. 23-47. doi: 10.1016/B0-08-043751-6/06105-3.

Buesseler, K.O., Bacon, M.P., Cochran, J.K., Livingston, H.D. (1992). Carbon and nitrogen export during the JGOFS North Atlantic Bloom experiment estimated from ^{234}Th:^{238}U disequilibria. *Deep Sea Research Part* A. 39(7-8):1115-1137. doi:10.1016/0198-0149(92)90060-7.

Byrne, R.H., Kump, L.R., Cantrell, K.J. (1988). The influence of temperature and pH on trace metal speciation in seawater. *Marine Chemistry*. 25(2):163-181. doi:10.1016/0304-4203(88)90062-X.

Byrne, R.H. (2002). Inorganic speciation of dissolved elements in seawater: the influence of pH on concentration ratios. *Geochemical Transactions*. 3:11-16. doi: 10.1186/1467-4866-3-11.

Calvert, S.E., Pedersen, T.F. (1993). Geochemistry of recent oxic and anoxic marine sediments: Implications for the geological record. *Marine Geology*. 113(1-2):67-88. doi: 10.1016/0025-3227(93)90150-T.

Canfield. D.E., Stewart, F.J., Thamdrup, B., De Brabandere, L., Dalsgaard, T., Delong, E.F., Revsbech, N.P., Ulloa, O. (2010). A cryptic sulfur cycle in oxygen-minimum-zone waters off the Chilean coast. *Science*. 330:1375-1378. doi: 10.1126/science.1196889.

Carolan, M.T., Smith, J.M., Beman, J.M. (2015). Transcriptomic evidence for the microbial sulfur cycling in the eastern tropical North Pacific oxygen minimum zone. *Frontiers in Microbiology*. 6(334):8pp. doi: 10.3389/fmicb.2015.00334.

Chandler, P.C., King, S.A., and Perry, R.I. (Eds.). (2015). State of the physical, biological and selected fishery resources of Pacific Canadian marine ecosystems in 2014. *Canadian Technical Report of Fisheries and Aquatic Sciences*. 3131: vi + 211p. http://www.dfo-mpo.gc.ca/Library/358018.pdf.

Chappell, P.D., Vedmati, J., Selph, K.E., Cyr, H.A., Jenkins, B.D., Landry, M.R., Moffett, J.W. (2016). *Journal of Plankton Research*. 38(2):244-255. doi: 10.1093/plankt/fbw018.

Charette, M.A., Moran, S.B., Bishop, J.K. (1999). ^{234}Th as a tracer of particulate organic carbon export in the subarctic northeast Pacific Ocean. *Deep-Sea Research Part II*. 46:2833-2861. doi: 10.1016/S0967-0645(99)00085-5.

Conway, T.M., Rosenberg, A.D., Adkins, J.F., John, S.G. (2013). A new method for precise determination of iron, zinc and cadmium stable isotope ratios in seawater by double-spike mass spectrometry. *Analytica Chimica Acta*. 793:44-52. doi: 10.1016/j.aca.2013.07.025.

Conway, T.M., John, S.G. (2013). Sources of Fe to the North Atlantic: Insights from Fe isotopes. *Mineralogical Magazine*. 77(5):912.

Conway, T.M., John. S.G. (2014). The biogeochemical cycling of zinc and zinc isotopes in the North Atlantic Ocean. *Global Biogeochemical Cycles*. 28(10):1111-1128. doi: 10.1002/2014GB004862.

Conway, T.M., John, S.G. (2015a). Biogeochemical cycling of cadmium isotopes along a high-resolution section through the North Atlantic Ocean. *Geochimica et Cosmochimica Acta*. 148:269-283. doi: 10.1016/j.gca.2014.09.032.

Conway, T.M., John, S.G. (2015b). The cycling of iron, zinc and cadmium in the North East Pacific Ocean – Insights from stable isotopes. *Geochimica et Cosmochimica Acta*. 164:262-283. doi: 10.1016/j.gca.2015.05.023.

Crawford, D.W., Lipsen, M.S., Purdie, D.A., Lohan, M.C., Statham, P.J., Whitney, F.A., Putland, J.N., Johnson, W.K., Sutherland, N., Peterson, T.D., Harrison, P.J., Wong, C.S. (2003). Influence of zinc and iron enrichments on phytoplankton growth in the

northeastern subarctic Pacific. *Limnology and Oceanography*. 48(4):1583-1600. doi: 10.4319/lo.2003.48.4.1583.

Crawford, W., Galbraith, J., Bolingbroke, N. (2007). Line P ocean temperature and salinity, 156-2005. *Progress in Oceanography*. 75:161-178. doi: 10.1016/j.pocean.2007.08.017.

Croot, P.L., Moffett, J.W., Brand, L.E. (2000). Production of extracellular Cu complexing ligands by eukaryotic phytoplankton in response to Cu stress. *Limnology and Oceanography*. 45(3):619-627. doi: 10.4319/lo.2000.45.3.0619.

Croot, P.L., Baars, O., Streu, P. (2011). The distribution of dissolved zinc in the Atlantic sector of the Southern Ocean. *Deep-Sea Research Part II*. 58:2797-2719. doi: 10.1016/j.dsr2.2010.10.041.

Cullen, J.J., Franks, P.J.S., Karl, D.M., Longhurst, A. (2002). Physical influences on marine ecosystem dynamics. In The Sea A.R. Robinson, J.J. McCarthy, B.J. Rothschild (Eds).Wiley & Sons Inc. ISBN 0-471-18901-4.

Cullen, J.T., Sherrell, R.M. (1999). Techniques for determination of trace metals in small samples of size-fractionated particulate matter: phytoplankton metals off central California. *Marine Chemistry*. 67(3-4):233-247. doi: 10.1016/S0304-4203(99)00060-2.

Cullen, J.T., Chase, Z., Coale, K.H., Fitzwater, S.E., Sherrell, R.M. (2003). Effect of iron limitation on the cadmium to phosphorus ratio of natural phytoplankton assemblages from the Southern Ocean. *Limnology and Oceanography*. 48:1079–1087. doi: 10.4319/lo.2003.48.3.1079.

Cullen, J.T., Sherrell, R.M. (2005). Effects of dissolved carbon dioxide, zinc, and manganese on the cadmium to phosphorus ratio in natural phytoplankton assemblages. *Limnology and Oceanography*. 50:1193-1204. doi: 10.4319/lo.2005.50.4.1193.

Cullen, J.T. (2006). On the nonlinear relationship between dissolved cadmium and phosphate in the modern global ocean: Could chronic iron limitation of phytoplankton growth cause the kink? *Limnology and Oceanography*. 51:1369–1380. doi: 10.4319/lo.2006.51.3.1369.

Cummins, P.F., Freeland, H.J. (2007). Variability of the North Pacific Current and its bifurcation. *Progress in Oceanography*. 75:253-265. doi: 10.1016/j.pocean.2007.08.006.

Cutter, G., Andersson, P., Codispoti, L., Croot, P., François, R., Lohan, M.C., Obata, H., Rutgers v. d. Loeff, M. (2010). Sampling and sample-handling protocols for GEOTRACES cruises. Hdl: 10013/epic.42722.

Dansgaard, W. (1965). Stable isotopes in precipitation. Tellus. 16(4):436-468. doi: 10.3402/tellusa.v16i4.8993.

de Baar, H.J.W., Saager, P.M., Nolting, R.F., van der Meer, J. (1994). Cadmium versus phosphate in the world ocean. *Marine Chemistry*. 46:261-281. doi: 10.1016/0304-4203(94)90082-5.

De La Rocha, C.L., Hutchins, D.A., Brzezinski, M.A., Zhang, Y. (2000). Effects of iron and zinc deficiency on elemental composition and silica production in diatoms. *Marine Ecology*. 195:71-79. doi: 10.3354/meps195071.

Diaz, R.J., Rosenberg, R. (2008). Spreading dead zones and consequences for marine ecosystems. *Science*. 321(5891):926-929. doi: 10.1126/science.1156401.

Dugdale, R.C., Goering, J.J., Barber, R.T., Smith, R.L., Packard, T.T. (1977). Denitrification and hydrogen sulfide in the Peru upwelling region during 1976. *Deep Sea Research*. 24(6):601-608. doi: 10.1016/0146-6291(77)90530-6.

Dupont, C.L., Yang, S., Palenik, B., Bourne, P.E. (2006). Modern proteomes contain putative imprints of ancient shifts in trace metal geochemistry. *Proceedings of the National Academy of Sciences of the United States of America*. 103(47):17822-17827. doi: 10.1073/pnas.0605798103.

Dupont, C.L., Butcher, A., Valas, R.E., Bourne, P.E., Caetano-Anollés, G. (2010). History of biological metal utilization inferred through phylogenomic analysis of protein structures. *Proceedings of the National Academy of Sciences of the United States of America*. 107(23):10567-10572. doi: 10.1073/pnas.0912491107.

Dyrssen, D., Kremling, K. (1990). Increasing hydrogen sulfide concentration and trace metal behavior in the anoxic Baltic waters. *Marine Chemistry*. 30:193-204. doi: 10.1016/0304-4203(90)90070-S.

Elderfield, H., Rickaby, R.E.M. (2000). Oceanic Cd/P ratio and nutrient utilization in the glacial Southern Ocean. *Nature*. 405:305-310. doi: 10.1038/35012507.

Ellwood, M.J., Hunter, K.A. (2000). The incorporation of zinc and iron into the frustule of the marine diatom *Thalassiosira pseudonana*. *Limnology and Oceanography*. 45(7):1517-1524. doi: 10.4319/lo.2000.45.7.1517.

Ellwood, M.J., Van den Berg, C.M.G. (2000). Zinc speciation in the Northeastern Atlantic Ocean. *Marine Chemistry*. 68(4):295-306. doi: 10.1016/S0304-4203(99)00085-7.

Ellwood, M.J., Kelly, M., Noddler, S.D., Carter, L. (2004). Zinc/silicon ratios of sponges: A proxy for carbon export to the seafloor. *Geophysical Research Letters*. 31(12):L12308 4pp. doi: 10.1029/2004GL019648.

Emerson, S.R., Hedges, J.I. (2008). Chemical Oceanography and the Marine Carbon Cycle. Cambridge University Press. 453 pp. ISBN: 978-0-521-83313-4.

Eppley, R.W., Holmes, R.W., Strickland, J.D.H. (1967). Sinking rates of marine phytoplankton measured with a fluorometer. *Journal of Experimental Marine Biology and Ecology*. 1(2):191-208. doi: 10.1016/0022-0981(67)90014-7.

Esther, T.A., Hammond, D.E., Hautala, S.L., Johnson, H.P., Schwartz, R.J., Paukert, A.N. (2010). Evaluation of the budget for silicic acid in Cascadia Basin deep water. *Deep-Sea Research Part II*. 57(5):677-686. doi: 10.1016/j.dsr.2010.02.002.

Fenchel, T. (2008). The microbial loop – 25 years later. *Journal of Experimental and Marine Biology and Ecology*. 366(1-2):99-103. doi: 10.1016/j.jembe.2008.07.013.

Flockhart, D.T.T., Kyser, T.K., Chipley, D.C., Miller, N.G., Norris, D.R. (2015). Experimental evidence shows no fractionation of strontium isotopes (87Sr/86Sr) among soil, plants, and herbivores: implications for tracking wildlife and forensic science. *Isotopes in Environmental Health Studies*. 51(3):372-381. doi: 10.1080/10256016.2015.1021345.

Franck, V.M., Bruland, K.W., Hutchins, D.A., Brzezinski, M.A. (2003). Iron and zinc effects on silicic acid and nitrate uptake kinetics in three high-nutrient, low-chlorophyll (HNLC) regions. *Marine Ecology Progress Series*. 252:15-33. doi: doi:10.3354/meps252015.

Freeland, H.J. (2007). A short history of Ocean Station Papa and Line P. *Progress in Oceanography*. 75:120-125. doi: 10.1016/j.pocean.2007.08.005.

Freeland, H., Denman, K., Wong, C.S., Whitney, F., Jacques, R. (1998). Evidence of change in the winter mixed layer in the Northeast Pacific Ocean. *Deep Sea Research Part I*. 44(12):2117-2129. doi: 10.1016/S0967-0637(97)00083-6.

Freeland, H.J. (2006). What proportion of the North Pacific current finds its way into the Gulf of Alaska? *Atmosphere Ocean*. 44(4):321-330. doi: 10.3137/ao.440401.

Frew, R.D. (1995). Antarctic bottom water formation and the global cadmium to phosphorus relationship. *Geophysical Research Letters*. 22(17):2349-2352. doi:10.1016/0304-4203(95)00057-7.

Froelich, P.N., Bender, M.L., Luedtke, N.A., Heath, G.R., DeVries, T. (1982). The marine phosphorus cycle. *American Journal of Science*. 282(4):474-511. doi: 10.2475/ajs.282.4.474.

Garcia, H.E., Locarnini, R.A., Boyer, T.P., Antonov, J.I., Baranova, O.K., Zweng, M.M., Johnson, D.R. (2010). World Ocean Atlas 2009. Volume 3: Dissolved oxygen, apparent oxygen utilization, and oxygen saturation. S. Levitus (Ed.), NOAA Atlas NESDIS 70, US Government Printing Office, Washington DC. 344 pp.

Gault-Ringold, M., Stirling, C.H. (2012). Anomalous isotopic shifts associated with organic resin residues during cadmium isotopic analysis by double spike MC-ICP-MS. *Journal of Analytical Atomic Spectrometry*. 27:449-459. doi: 10.1039/C2JA10360E.

Gault-Ringold, M., Adu, T., Stirling, C.H., Frew, R.D., Hunter, K.A. (2012). Anomalous biogeochemical behavior of cadmium in subantarctic surface waters: Mechanistic constraints from cadmium isotopes. *Earth and Planetary Science. Letters*. 341-344:94-103. doi: 10.1016/j.epsl.2012.06.005.

Georgiev, S.V., Horner, T.J., Stein, H.J., Hannah, J.L., Bingen, B., Rehkämper, M. (2015). Cadmium-isotopic evidence for increasing primary productivity during Late Permian anoxic event. *Earth and Planetary Science Letters*. 410:84-96. doi: 10.7185/geochemlet.1704.

Gilly, W.F., Berman, J.M., Litvin, S.Y., Robinson, B.H. (2013). Oceanographic and biological effects of shoaling of the oxygen minimum zone. *Annual Reviews in Marine Science*. 5:393-420. doi: 10.1146/annurev-marine-120710-100849.

Glud, R.N., Grossart, H.P., Larsen, M., Tang, K.W., Arendt K.E., Rysgaard, S., Thamdrup, B., Nielsen, T.G. (2015). Copepod carcasses as microbial hot spots for pelagic denitrification. *Limnology and Oceanography*. 60(6):2026-2036. doi: 10.1002/lno.10149.

Goes, J.I., do Rosario Gomes, H., Selph, K.E., Landry, M.R. (2016). Biological response of Costa Rica Dome phytoplankton to light, silicic acid and trace metals. *Journal of Plankton Research*. 38(2): 290-304. doi: 10.1093/plankt/fbv108.

Guidi, L., Stemmann, L., Jackson, G.A., Ibanez, F., Claustre, H., Legendre, L., Picheral., M., Gorskya, G. (2009). Effects of phytoplankton community on production, size, and export of large aggregates: A world-ocean analysis. *Limnology and Oceanography*. 54(6):1951-1963. doi: 10.4319/lo.2009.54.6.1951.

Han, Q., Moore, J.K., Zender, C., Measures, C., Hydes, D. (2008). Constraining oceanic dust deposition using surface ocean dissolved Al. *Global Biogeochemical Cycles*. 22(GB2003):14 pp. doi: 10.1029/2007GB002975.

Hastings, D., Emerson, S. (1988). Sulfate reduction in the presence of low oxygen levels in the water column of the Cariaco Trench. *Limnology and Oceanography*. 33(3):391-396. doi: 10.4319/lo.1988.33.3.0391.

Ho, T.Y., Quigg, A., Finkel, Z.V., Milligan, A.J., Wyman, K., Falkowski, P.G., Morel, F.M.M. (2003). The elemental composition of some marine phytoplankton. *Journal of Phycology*. 39(6):1145-1159. doi: 10.1111/j.0022-3646.2003.03-090.x.

Hohl, S.V., Galer, S.J.G., Gamper, A., Becker, H. (2017). Cadmium isotope variations in Neoproterozoic carbonates – A tracer of biologic production? *Geochemical Perspectives Letters*. 3:32-44. doi: 10.7185/geochemlet.1704.

Homoky, W.B., Severmann, S., McManus, J., Berelson, W.M., Riedel, T.E., Statham, P.J., Mills, R.A. (2012). Dissolved oxygen and suspended particles regulate the benthic flux of iron from continental margins. *Marine Chemistry*. 134-135:59-70. doi: 10.1016/j.marchem.2012.03.003.

Horner, T.J., Schönbächler, M., Rehkämper, M., Nielsen, S.G., Williams, H., Halliday, A.N., Xue, Z., Hein, J.R. (2010). Ferromanganese crusts as archives of deep water Cd isotope composition. *Geochemistry Geophysics Geosystems*. 11(4):10pp. doi: 10.1029/2009GC002987.

Jaccard, S.L., Galbraith, E.D., Frölicher, T.L., Gruber, N. (2014). Ocean (de)oxygenation across the last deglaciation: Insights for the future. *Oceanography*. 27(1):26-35. doi: 10.5670/oceanog.2014.05.

Hutchins, D.A., Bruland, K.W. (1998). Iron-limited diatom growth and Si:N uptake ratios in a coastal upwelling regime. *Nature*. 393:561-564. doi: 10.1038/31203.

Hutchins, D.A., Witter, A.E., Butler, A., Luther III, G.W. (1999). Competition among marine phytoplankton for different chelated iron species. *Nature*. 400:858-861. doi: 10.1038/23680.

Jacobs, L., Emerson, S. (1982). Trace-metal solubility in an anoxic fjord. *Earth and Planetary Science Letters*. 60(2):237-252. doi:10.1016/0012-821X(82)90006-1.

Jacobs, L., Emerson, S., Skei, J. (1985). Partitioning and transport of metals across the O2/H2S interface in a permanently anoxic basin - Framvaren Fjord, Norway. *Geochimica Cosmochimica Acta*. 49:1433-1444. doi: 10.1016/0016-7037(85)90293-5.

Jakuba, R.W., Saito, M.A., Moffett, J.W., Xu, Y. (2012). Dissolved zinc in the subarctic North Pacific and Bering Sea: Its distribution, speciation, and importance to primary producers. *Global Biogeochemical Cycles*. 26:15pp. doi: 10.1029/2010GB004004.

Janssen, D.J., Conway, T.M., John, S.G., Christian, J.R., Kramer, D.I., Pedersen, T.F., Cullen, J.T. (2014). Undocumented water column sink for cadmium in open ocean oxygen-deficient zones. *Proceedings of the National Academy of Sciences of the United States of America*. 111:6888-6893. doi: 10.1073/pnas.1402388111.

Janssen, D.J., Cullen, J.T. (2015). Decoupling of zinc and silicic acid in the subarctic northeast Pacific interior. *Marine Chemistry*. 177:124-133. doi: 10.1016/j.marchem.2015.03.014.

Janssen, D.J., Abouchami, W., Galer, S.J.G., Cullen, J.T. In Revision at *Earth and Planetary Science Letters*. Dissolved cadmium concentration and isotopes in the subarctic northeast Pacific.

John, S.G., Geis, R.W., Saito, M.A., Boyle, E.A. (2007). Zinc isotope fractionation during high-affinity and low-affinity zinc transport by the marine diatom *Thalassiosira oceanica*. *Limnology and Oceanography*. 52(6):2710-2714. doi: 10.4319/lo.2007.52.6.2710.

John, S.G., Rouxel, O.J., Craddock, P.R., Engwall, A.M., Boyle, E.A. (2008). Zinc stable isotopes in seafloor hydrothermal vent fluids and chimneys. *Earth and Planetary Science Letters*. 269:17-28. doi: 10.1016/j.epsl.2007.12.011.

John, S.G., Conway, T.M. (2014). A role for scavenging in the marine biogeochemical cycling of zinc and zinc isotopes. *Earth and Planetary Science Letters*. 394:159-167. doi: 10.1016/j.epsl.2014.02.053.

Johnson, H.P., Hautala, S.L., Bjorklund, T.A., Zarnetske, M.R. (2006). Quantifying the north Pacific silica plume. *Geochemistry Geophysics Geosystems*. 7(5):14 pp. doi: 10.1029/2005GC001065.

Johnston, D.T., Gill, B.C., Beirne, M.E., Casciotti, K.L., Knapp, A.N., Berelson, W. (2014). Placing an upper limit on cryptic marine sulphur cycling. *Nature*. 513(7519):530-533. doi: 10.1038/nature13698.

Keeling, R.F., Kortzinger, A., Gruber, N. (2010) Ocean deoxygenation in a warming world. *Annual Reviews in Marine Science*. 2:199-229. doi: 10.1146/annurev.marine.010908.163855.

Key, R.M., Kozyr, A., Sabine, C.L., Lee, K., Wanninkhof, R., Bullister, J.L., Feely, R.A., Millero, F.J., Mordy, C., Peng, T.-H. (2004). A global ocean carbon climatology: Results from Global Data Analysis Project (GLODAP). *Global Biogeochemical Cycles*. 18(4):23 pp. doi: 10.1029/2004GB002247.

Kim, T., Obata, H., Kondo, Y., Ogawa, H., Gamo, T. (2015). Distribution and speciation of dissolved zinc in the western North Pacific and its adjacent seas. *Marine Chemistry*. 173:330-341. doi: 10.1016/j.marchem.2014.10.016.

Klinkhammer, G.P., Palmer, M.R. (1991). Uranium in the oceans - where it goes and why. *Geochimica et Cosmochimica Acta*. 55(7):1799-1806. doi: 10.1016/0016-7037(91)90024-Y.

Knox, M., Quay, P.D., Wilbur, D. (1992). Kinetic isotopic fractionation during air-water gas transfer of O_2, N_2, CH_4, and H_2. *Journal of Geophysical Research*. 97(C12):20335-20343. doi: 10.1029/92JC00949.

Kramer, D. (2006). An exploration of the marine silver cycle in coastal and open ocean environments of the North Pacific. M.Sc. Thesis. University of Victoria.

Kramer, D., Cullen, J.T., Christian, J.R., Johnson, W.K., Pedersen, T.F. (2011) Silver in the subarctic northeast Pacific Ocean: Explaining the basin scale distribution of silver. *Marine Chemistry*. 123(1-4):133-142. doi: 10.1016/j.marchem.2010.11.002.

Lacan, F., Francois, R., Yongcheng, Y., Sherrell, R.M. (2006). Cadmium isotopic composition in the ocean. *Geochimica Cosmochimica Acta*. 70:5104–5118. doi: 10.1016/j.gca.2006.07.036.

Lagerström, M.E., Field, M.P., Séguret, M., Fischer, L., Hann, S., Sherrell, R.M. (2013). Automated on-line flow-injection ICP-MS determination of trace metals (Mn, Fe, Co, Ni, Cu, Zn) in open ocean seawater: Application to the GEOTRACES program. *Marine Chemistry*. 155:71-80. doi: 10.1016/j.marchem.2013.06.001

Lam, P.J., Bishop, J.K.B., Henning, C.C., Marcus, M.A., Waychunas, G.A., Fung, I.Y. (2006). Wintertime phytoplankton bloom in the subarctic Pacific supported by continental margin iron. *Global Biogeochemical Cycles*. 20(GB1006):12pp. doi: 10.1029/2005GB002557.

Lam, P.J., Morris, P.J., Patent US 20130298702 A1. In Situ Marine Sample Collection System and Methods.

Lambelet, M., Rehkämper, M., van de Flierdt, T., Xue, Z., Kreissig, K., Coles, B., Porcelli, D., Andersson, P. (2013). Isotopic analysis of Cd in the mixing zone of Siberian rivers with the Arctic Ocean – New constraints on marine Cd cycling and the isotopic composition of riverine Cd. *Earth and Planetary Science Letters*. 361:64-73. doi: 10.1016/j.epsl.2012.11.034.

Lambelet, M., Flierdt, T., Crocket, K., Rehkämper, M., Kreissig, K., Coles, B., Rijkenberg, M.J.A., Gerringa, L.J.A., de Baar, H.J.W., Steinfeldt, R. (2016). Neodymium isotopic composition and concentration in the western North Atlantic Ocean: Results from the GEOTRAES GA02 section. *Geochimica Cosmochimica Acta*. 117:1-29. doi: 10.1016/j.gca.2015.12.019.

Lane, E.S., Jang, K., Cullen, J.T., Maldonado, M.T. (2008). The interaction between inorganic iron and cadmium uptake in the marine diatom Thalassiosira oceanica. *Limnology and Oceanography*. 53(5):1784-1789. doi: 10.4319/lo.2008.53.5.1784.

Lane, E.S., Semeniuk, D.M., Strzepek, R.F., Cullen, J.T., Maldonado, M.T. (2009). Effects of iron limitation on intracellular cadmium of cultured phytoplankton: Implications for surface dissolved cadmium to phosphate ratios. *Marine Chemistry*. 115:155–162. doi: 10.1016/j.marchem.2009.07.008.

Lane, T.W., Morel, F.M.M. (2000). A biological function for cadmium in marine diatoms. *Proceedings of the National Academy of Sciences of the United States of America*. 97:4627-4631. doi: 10.1073/pnas.090091397.

Lane, T.W., Saito, M.A., George, G.N., Pickering, I.J., Prince, R.C., Morel, F.M.M. (2005). Biochemistry: A cadmium enzyme from a marine diatom. *Nature*. 435:42. doi: 10.1038/435042a.

Lansdown, J.M., Quay, P.D., King, S.L. (1992). CH4 production via CO2 reduction in a temperate bog: A source of 13C-depleted CH4. *Geochimica et Cosmochimica Acta*. 56(9):3493-3503. Doi: 10.1016/0016-7037(92)90393-W.

Leal, M.F.C., Vasconcelos, M.T.S.D., van den Berg, C.M.G. (1999) Copper-induced release of complexing ligands similar to thiols by *Emiliania huxleyi* in seawater cultures. *Limnology and Oceanography*. 44(7):1750-1762. doi: 10.4319/lo.1999.44.7.1750.

Leblanc, K., Hare, C.E., Boyd, P.W., Bruland, K.W., Sohst, B., Pickmere, S., Lohan, M.C., Buck, K., Ellwood, M., Hutchins, D.A. (2005). Fe and Zn effects on the Si cycle and diatom community structure in two contrasting high and low-silicate HNLC areas. *Deep-Sea Research Part I*. 52(10):1842-1864. doi: 10.1016/j.dsr.2005.06.005.

Lee, J.G., Roberts, S.B., Morel, F.M.M. (1995). Cadmium: A nutrient for the marine diatom *Thalassiosira weissflogii*. *Limnology and Oceanography*. 40(6):1056-1063. doi: 10.3354/meps127305.

Li, W.K.W., Subba Rao, D.V., Harrison, W.G., Smith, J.C., Cullen, J.J., Irwin, B., Platt, T. (1983). Autotrophic picoplankton in the tropical ocean. *Science*. 219(4582):292-295. doi: 10.1126/science.219.4582.292.

Lide, D.R. (Ed.) (2006). CRC Handbook of Chemistry and Physics, 87th Edition. CRC Press, Taylor & Francis Group. ISBN: 0-8493-0487-3.

Little, S.H., Vance, D., Walker-Brown, C., Landing, W. (2014). The oceanic mass balance of copper and zinc isotopes, investigated by analysis of their inputs, and outputs to ferromanganese oxide sediments. *Geochimica Cosmochimica Acta*. 125:673-693. doi: 10.1016/j.gca.2013.07.046.

Little, S.H., Vance, D., McManus, J., Severmann, S. (2016). Key role of continental margin sediments in the oceanic mass balance of Zn and Zn isotopes. *Geology*. 44(3):207-210. doi: 10.1130/G37493.1.

Lohan, M.C., Statham, P.J., Crawford, D.W. (2002). Total dissolved zinc in the upper water column of the subarctic North East Pacific. *Deep-Sea Research Part II*. 49:5793-5808. doi: 10.1016/S0967-0645(02)00215-1.

Lohan, M.C., Crawford, D.W., Purdie, D.A., Statham, P.J. (2005). Iron and zinc enrichments in the northeastern subarctic Pacific: Ligand production and zinc availability in response to phytoplankton growth. *Limnology and Oceanography*. 50(5):1427-1437. doi: 10.4319/lo.2005.50.5.1427.

Lohan, M.C., Bruland, K.W. (2008). Elevated Fe(II) and Dissolved Fe in Hypoxic Shelf Waters off Oregon and Washington: And Enhanced Source of Iron to coastal upwelling regimes. *Environmental Science and Technolog*y. 42(17):6462-6468. doi: 10.1021/es800144j.

Luther, G.W. III, Rickard, D.T. (2005) Metal sulfide cluster complexes and their biogeochemical importance in the environment. *Journal of Nanoparticle Research*. 7(6):713-733. doi:10.1007/s11051-005-4272-4.

Luther, G.W. III., Tsamakis, E. (1989). Concentration and form of dissolved sulfide in the oxic water column of the ocean. *Marine Chemistry*. 27(3-4):165-177. doi: 10.1016/0304-4203(89)90046-7.

Macdonald, A.M., Mecking, S., Robbins, P.E., Toole, J.M., Johnson, G.C., Talley, L., Cook, M., Wijffels, S.E. (2009). The WOCE-era 3-D Pacific Ocean circulation and heat budget. *Progress in Oceanography*. 82:281-325. doi: 10.1016/j.pocean.2009.08.002.

Maldonado, M.T., Allen, A.E., Chong, J.S., Lin, K., Leus, D., Karpenko, N., Harris, S.L. (2006). *Limnology and Oceanography*. 51(4):1729-1743. doi: 10.4319/lo.2006.51.4.1729.

Mann, E.L., Ahlgren, N., Moffett, J.W., Chisholm, S.W. (2002). Copper toxicity and cyanobacteria ecology in the Sargasso Sea. *Limnology and Oceanography*. 47(4):976-988. doi: 10.4319/lo.2002.47.4.0976.

Marchetti, A., Hutchins, P.J. (2007). Couple changes in the cell morphology and the elemental (C, N, and Si) composition of the pennate diatom Pseudo-nitzschia due to iron deficiency. *Limnology and Oceanography*. 52(5):2270-2284. doi: 10.4319/lo.2007.52.5.2270.

Marchitto, T.M. Jr., Curry, W.B., Oppo, D.W. (2000). Zinc concentrations in benthic foraminifera reflect seawater chemistry. *Paleoceanography*. 15(3):299-306. doi: 10.1029/1999PA000420.

Marchitto, T.M. Jr., Oppo, D.W., Curry, W.B. (2002). Paired benthic foraminiferal Cd/Ca and Zn/Ca evidence for a greatly increased presence of Southern Ocean Water in the glacial North Atlantic. *Paleoceanography*. 17(3):10-1 – 10-18. doi: 10.1029/2000PA000598.

Mariotti, A., Germon, J.C., Hubert, P., Kaiser, P., Letolle, R., Tardieux, A., Tardieux, P. (1981). Experimental determination of nitrogen kinetic isotope fractionation: some principles; illustration for the denitrification and nitrification processes. *Plant and Soil*. 62(3):413-430. doi: 10.1007/BF02374138.

Marschall, C., Frenzel, P., Cypionka, H. (1993). Influence of oxygen on sulfate reduction and growth of sulfate-reducing bacteria. *Archives of Microbiology*. 159(2):168-173. doi: 10.1007/BF00250278.

Martin, J.H., Knauer, G.A. (1984). VERTEX: manganese transport through oxygen minima. *Earth and Planetary Science Letters*. 67(1):35-47. doi: 10.1016/0012-821X(84)90036-0.

Martin, J.H., Knauer, G.A., Broenkow, W.W. (1985). VERTEX: the lateral transport of manganese in the northeast Pacific. *Deep-Sea Research*. 32(11):1414-1427. doi:10.1016/0198-0149(85)90056-1.

Martin, J.H., Knauer, G.A., Karl, D.M., Broenkow, W.W. (1987). VERTEX: carbon cycling in the northeast Pacific. *Deep-Sea Research*. 34(2):267-285. doi: 10.1016/0198-0149(87)90086-0.

Martin, J.H., Gordon, R.M., Fitzwater, S., Broenkow, W.W. (1989). VERTEX: phytoplankton/iron studies in the Gulf of Alaska. *Deep-Sea Research*. 36:649-680. doi: 10.1016/0198-0149(89)90144-1.

Martin, J.H. (1990). Glacial-interglacial CO2 change: The iron hypothesis. *Paleoceanography*. 5(1):1-13. doi: 10.1029/PA005i001p00001.

Martinez-Garcia, A., Rosell-Melé, A., Jaccard, S.L., Geibert, W., Sigman, D.M., Haug, G.H. (2011). Southern Ocean dust-climate coupling over the past four million years. *Nature*. 476:312-315. doi: 10.1038/nature10310.

Mawji et al. (137 others) (2015). GEOTRACES Intermediate Data Product 2014. *Marine Chemistry*. 177:1-8. doi: 10.1016/j.marchem.2015.04.005.

McDonough, W.F., Sun, S.-s. (1995). The composition of the Earth. *Chemical Geology*. 120(3-4):223-253. doi: 10.1016/0009-2541(94)00140-4.

McKay, J.L., Pedersen, T.F., Mucci, A. (2007). Sedimentary redox conditions in continental margin sediments (N.E. Pacific) – Influence on the accumulation of redox-sensitive trace metals. *Chemical Geology*. 238:180-196. doi: 10.1016/j.chemgeo.2006.11.008.

McKay, J.L., Pedersen, T.F. (2008). The accumulation of silver in marine sediments: A link to biogenic Ba and marine productivity. *Global Biogeochemical Cycles*. 22:GB4010, 17pp. doi:10.1029/2007GB003136.

Measures, C.I., Vink, S. (2000). On the use of dissolved aluminum in surface waters to estimate dust deposition on the ocean. *Global Biogeochemical Cycles*. 14(1):317-327. doi: 10.1029/1999GB001188.

Measures, C.I., Landing, W.M., Brown, M.T., Buck, C.S. (2008). A commercially available rosette system for trace metal-clean sampling. *Limnology and Oceanography Methods*. 6:384-394. doi: 10.4319/lom.2008.6.384.

Mecking, S., Warner, M.J., Bullister, J.L. (2006). Temporal changes in pCFC-12 ages and AOU along two hydrographic sections in the eastern subtropical north Pacific. *Deep-Sea Research Part I*. 53(1):169-187. doi: 10.1016/j.dsr.2005.06.018.

Mofett, J.W., Zika, R.G., Brand, L.E. (1990). Distribution and potential sources and sinks of copper chelators in the Sargasso Sea. *Deep Sea Research*. 37(1):27-36. doi: 10.1016/0198-0149(90)90027-S.

Morel, F.M.M., Reinfelder, S.B., Roberts, S.B., Chamberlain, C.P., Lee, J.G., Yee, D. (1994). Zinc and carbon co-limitation of marine phytoplankton. *Nature*. 369:740-742. doi: 10.1038/369740a0.

Morford, J.L., Emerson, S. (1999). The geochemistry of redox sensitive trace metals in sediments. *Geochimica Cosmochimica Acta*. 63(11-12):1735-1750. doi: 10.1016/S0016-7037(99)00126-X.

Mullaugh, K., Luther, G.W. III. (2011). Growth kinetics and long-term stability of CdS nanoparticles in aqueous solution under ambient conditions. *Journal of Nanoparticle Research*. 13(1):393-404. doi: 10.1007/s11051-010-0045-9.

Murphy, K., Rehkämper, M., Kreissig, K., Coles, B., van de Flierdt, T. (2016). Improvements in Cd stable isotope analyses achieved through use of liquid-liquid extraction to remove organic residues from Cd separates obtained by extraction chromatography. *Journal of Analytical Atomic Spectrometry*. 31:319-327. doi: 10.1039/C5JA00115C.

Nameroff, T.J., Balistrieri, Murray, J.W. (2002). Suboxic trace metal geochemistry in the eastern tropical North Pacific. *Geochimica Cosmochimica Acta*. 66(7):1139-1158. doi: 10.1016/S0016-7037(01)00843-2.

Nameroff, T.J., Calvert, S.E., Murray, J.W. (2004). Glacial-interglacial variability in the eastern tropical North Pacific oxygen minimum zone by redox-sensitive trace metals. *Paleoceanography*. 19:PA1010. doi: 10.1029/2003PA000912.

Nowicki, J.L., Johnson, K.S., Coale, K.H., Elrod, V.A., Lieberman, S.H. (1994). Determination of zinc in seawater using flow injection analysis with fluorometric detection. *Analytical Chemistry*. 66:2732-2738. doi: 10.1021/ac00089a021.

O'Leary, M.H. (1981). Carbon isotope fractionation in plants. *Phytochemistry*. 20(4):553-567. doi: 10.1016/0031-9422(81)85134-5.

Ohnemus, D.C., Rauschenberg, S., Cutter, G.A., Fitzsimmons, J.N., Sherrell, R.M., Twining, B.S. (2016). Elevated trace metal content of prokaryotic communities associated with marine oxygen deficient zones. *Limnology and Oceanography*. doi: 10.1002/lno.10363.

Ono, T., Midorikawa, T., Watanabe, Y.W., Tadokoro, K., Saino, T. (2001). Temporal increases of phosphate and apparent oxygen utilization in the subsurface waters of western subarctic Pacific from 1968 to 1998. *Geophysical Research Letters*. 28(17):3285-3288. doi: 10.1029/2001GL012948.

Parker, C.E., Brown, M.T., Bruland, K.W. (2016). Scandium in the open ocean: A comparison with other group 3 trivalent metals. *Geophysical Research Letters*. 43(6):2758-2764. doi: 10.1002/2016GL067827.

Pearson, R.G. (1963). Hard and soft Lewis acids. *Journal of the American Chemical Society*. 85(22):3533-3539. doi: 10.1021/ja00905a001.

Peers, G., Price, N.M. (2006). Copper-containing plastocyanin used for electron transport by an oceanic diatom. *Nature*. 441(7091):341-344. doi: 10.1038/nature04630.

Peña, M.A., Varela, D.E. (2007). Seasonal and interannual variability in phytoplankton and nutrient dynamics along Line P in the NE subarctic Pacific. *Progress in Oceanography*. 75:200-222. doi: 10.1016/j.pocean.2007.08.009.

Peterson, W., Robert, M., Bond, N. (2016). The blob (part three): Going, going, gone? *PICES Press*. (24)1:46-48. ISSN: 11952512.

Ploug, H., Bergkvist, J. (2015). Oxygen diffusion limitation and ammonium production within sinking diatom aggregates under hypoxic and anoxic conditions. *Marine Chemistry*. 176:142-149. doi: 10.1016/j.marchem.2015.08.012.

Price, N.M., Morel, F.M.M. (1990). Cadmium and cobalt substitution for zinc in a marine diatom. *Nature*. 344:658-660. doi: 10.1038/344658a0.

Podlaska, A., Wakeham, S.G., Fanning, K.A., Taylor, G.T. (2012). Microbial community structure and productivity in the oxygen minimum zone of the eastern tropical north Pacific. *Deep-Sea Research Part I*. 66:77-89. doi: 10.1016/j.dsr.2012.04.002.

Quay, P., Cullen, J., Landing, W., Morton, P. (2015). Processes controlling the distributions of Cd and PO_4 in the ocean. *Global Biogeochemical Cycles*. 29:12pp. doi: 10.1002/2014GB004998.

Rehkämper, M., Wombacher, F., Horner, T.J., Xue, Z. (2012). Natural and anthropogenic Cd isotope variations. In Handbook of Environmental Isotope Geochemistry. M. Baskaran (Ed.) Springer Berlin Heidelberg. 125-154. doi: 10.1007/978-3-642-10637-8_8.

Revels, B.N., Ohnemus, D.C., Lam, P.J., Conway, T.M., John, S.G. (2015). The isotopic signature and distribution of particulate iron in the North Atlantic Ocean. *Deep-Sea Research II*. 116:321-331. doi: 10.1016/j.dsr2.2014.12.004.

Richardson, T.L., Jackson, G.A. (2008). Small phytoplankton and carbon export from the surface ocean. *Science*. 315:838-841. doi: 10.1126/science.1133471.

Ripperger, S., Rehkämper, M., Porcelli, D., Halliday, A.N. (2007). Cadmium isotope fractionation in seawater – A signature of biological activity. *Earth and Planetary Science Letters*. 261:670-684. doi: 10.1016/j.epsl.2007.07.034.

Romanek, C.S., Grossman, E.L., Morse, J.W. (1992). Carbon isotope fractionation in synthetic aragonite and calcite: Effects of temperature and precipitation rate. *Geochimica et Cosmochimica Acta*. 56(1):419-430. doi: 10.1016/0016-7037(92)90142-6.

Rosenthal, Y., Lam, P., Boyle, E.A., Thomson, J. (1995a). Authigenic cadmium enrichments in suboxic sediments: Precipitation and postdepositional mobility. *Earth and Planetary Science Letters*. 132:99–111. doi: 10.1016/0012-821X(95)00056-I.

Rosenthal, Y., Boyle, E.A., Labeyrie, L., Oppo, D. (1995b). Glacial enrichments of authigenic Cd and U in subantarctic sediments: A climatic control on the elements' ocean budget? *Paleoceanography*. 10(3):395-413. doi: 10.1029/95PA00310.

Rosenthal, Y., Boyle, E.A., Labeyrie, L. (1997). Last glacial maximum paleochemistry and deepwater circulation in the Southern Ocean: Evidence from foraminiferal cadmium. *Paleoceanography* 12(6):787-796. doi: 10.1029/97PA02508.

Roshan, S., Wu, J., Jenkins, W.J. (2016). Long-range transport of hydrothermal dissolved Zn in the tropical South Pacific. *Marine Chemistry*. 183:25-32. doi: 10.1016/j.marchem.2016.05.005.

Rozan, T.F., Lassman, M.E., Ridge, D.P., Luther, G.W. III. (2000). Evidence for iron, copper and zinc complexation as multinuclear sulphide clusters in oxic rivers. *Nature*. 406:879-882. doi: 10.1038/35022561.

Rue, E.L., Bruland, K.W. (1995). Complexation of iron(III) by natural organic ligands in the Central North Pacific as determined by a new competitive ligand equilibration/adsorptive cathodic stripping voltammetric method. *Marine Chemistry*. 50(1-4):117-138. doi: 10.1016/0304-4203(95)00031-L.

Rue, E.L., Bruland, K.W. (1997). The role of organic complexation on ambient iron chemistry in the equatorial Pacific Ocean and the response of a mesoscale iron addition experiment. *Limnology and Oceanography*. 42(5):901-910. doi: 10.4319/lo.1997.42.5.0901.

Ruttenberg, K.C. (1993). Reassessment of the oceanic residence time of phosphorus. *Chemical Geology*. 107, 405-409. doi: 10.1016/0009-2541(93)90220-D.

Ruttenberg, K.C., Berner, R.A. (1993). Authigenic apatite formation and burial in sediments from no-upwelling continental margin environments. *Geochimica et Cosmochimica Acta*. 57(5):991-1007. doi: 10.1016/0016-7037(93)90035-U.

Saito, M.A., Sigman, D.M., Morel, F.M.M. (2003). The bioinorganic chemistry of the ancient ocean: the co-evolution of the cyanobacterial metal requirements and biogeochemical cycles at the Archean-Proterozoic boundary? *Inorganica Chimica Acta*. 356:308-318. doi: 10.1016/S0020-1693(03)00442-0.

Saito, M.A., Gabrielle, R., Moffett, J.W. (2005). Production of cobalt binding ligands in a Synechococcus feature at the Costa Rica upwelling dome. *Limnology and Oceanography*. 50(1):279-290. doi: 10.4319/lo.2005.50.1.0279.

Saito, M.A., Goepfert, T.J. (2008). Zinc-cobalt colimitation of *Phaeocystis antarctica*. *Limnology and Oceanography*. 53(1):266-275. doi: 10.4319/lo.2008.53.1.0266.

Saito, M.A., Goepfert, T.J., Ritt, J.T. (2008) Some thoughts on the concept of colimitation: Three definition and the importance of bioavailability. *Limnology and Oceanography*. 53(1):276-290. doi: 10.4319/lo.2008.53.1.0276.

Sakamoto-Arnold, C.M., Hanson, A.K., Huizenga, D.L., Kester, D.R. (1987). Spatial and temporal variability of cadmium in Gulf Stream warm-core rings and associated waters. *Journal of Marine Research*. 45(1):201-230. doi: 10.1357/002224087788400909.

Sarmiento, J.L., Gruber, N., Brzezinski, M.A., Dunne, J.P. (2004). High-latitude controls of thermocline nutrients and low latitude biological productivity. *Nature*. 427:56-60. doi: 10.1038/nature02127.

Schlitzer, R. (2014). Ocean Data View (version 4.6.3). Available at http://odv.awi.de.

Schmitt, A.D., Galer, S.J.G., Abouchami, W. (2009a). Mass-dependent cadmium isotopic variations in nature with emphasis on the marine environment. *Earth and Planetary Science Letters*. 277:262-272. doi: 10.1016/j.epsl.2008.10.025.

Schmitt, A.D., Galer, S.J.G., Abouchami, W. (2009b). High-precision cadmium stable isotope measurements by double spike thermal ionization mass spectrometry. *Journal of Analytical Atomic Spectrometry*. 24:1079-1088. doi: 10.1039/B821576F.

Schunck, H., Lavik, G., Desai, D.K., Großkopf, T., Kalvelage, T., Löscher, C.R., Paulmier, A., Contreras, S., Siegel, H., Holtappels, M., Rosentiel, P., Schilhabel, M.B., Graco, M., Schmitz, R.A., Kuypers, M.M.M., LaRoche, J. (2013) Giant hydrogen sulfide plume in the oxygen minimum zone off Peru supports chemolithoautotrophy. *PLOs One*. 8(8):18pp. doi: 10.1371/journal.pone.0068661

Selavka, C.M., Jiao, K.S., Krull, I.S. (1987). Construction and comparison of open tubular reactors for postcolumn reaction detection in liquid chromatography. *Analytical Chemistry*. 59:2221-2224. doi: 10.1021/ac00144a048.

Semeniuk, D.M., Cullen, J.T., Johnson, W.K., Gagnon, K., Ruth, T.J., Maldonado, M.T. (2009). Plankton copper requirements and uptake in the subarctic northeast Pacific Ocean. *Deep-Sea Research Part I*. 56(7):1130-1142. doi: 10.1016/j.dsr.2009.03.003.

Shaffer, G., Olsen, S.M., Pedersen, J.O.P. (2009). Long-term ocean oxygen depletion in response to carbon dioxide emissions from fossil fuels. *Nature Geoscience*. 2:105-109. doi: 10.1038/ngeo420.

Shaked, Y., Xu, Y., Leblanc, K., Morel, F.M.M. (2006). Zinc availability and alkaline phosphatase activity in Emiliania huxleyi: Implications for Zn-P co-limitation in the ocean. *Limnology and Oceanography*. 51(1):299-309. doi: 10.4319/lo.2006.51.1.0299.

Shcherbina, A.Y., Talley, L.D., Rudnick, D.L. (2003). Direct Observations of North Pacific Ventilation: Brine Rejection in the Okhotsk Sea. *Science*. 302:1952-1955. doi: 10.1126/science.1088692.

Shen, G.T., Boyle, E.A. (1987). Lead in corals: reconstruction of historical industrial fluxes to the surface ocean. *Earth and Planetary Science Letters*. 82(3-4):289-304. doi:10.1016/0012-821X(87)90203-2.

Sherrell, R.M., Boyle, E.A. (1992). The trace metal composition of suspended particles in the oceanic water column near Bermuda. *Earth and Planetary Science Letters*. 111:155-174. doi: 10.1016/0012-821X(92)90176-V.

Shiel, A.E., Barling, J., Orians, K.J., Weis, D. (2009). Matrix effects on the multi-collector inductively coupled plasma mass spectrometric analysis of high-precision cadmium and zinc isotope ratios. *Analytica Chimica Acta*. 633:29-37. doi: 10.1016/j.aca.2008.11.026.

Shiller, A.M., Boyle, E. (1985). Dissolved zinc in rivers. *Nature*. 317:49-52. doi: 10.1038/317049a0.

Sigman, D.M., Casciotti, K.L., (2001). Nitrogen isotopes in the ocean. In Encyclopedia of Ocean Sciences, eds J.H. Steele, K.K. Turekian, S.A. Thorpe, pp. 1884-1894. London: Academic Press.

Stewart, F.J., Ulloa, O., DeLong, E.F. (2012). Microbial metatranscriptomics in a permanent marine oxygen minimum zone. *Environmental Microbiology*. 14(1):23-40. doi: 10.1111/j.1462-2920.2010.02400.x.

Slater, J.C. (1964). Atomic Radii in Crystals. *Journal of Chemical Physics*. 41:3199-3204. doi: 10.1063/1.1725697.

Stewart, F.J. (2011). Dissimilatory sulfur cycling in oxygen minimum zones: an emerging metagenomics perspective. *Biochemical Society Transactions*. 39:1859-1863. doi: 10.1042/BST20110708.

Stramma, L., Schmidtko, S., Levil, L.A., Johnson, G.C. (2010). Ocean oxygen minima expansions and their biological impacts. *Deep-Sea Research Part I*. 57:587-595. doi: 10.1016/j.dsr.2010.01.005.

Stukel, M.R., Decima, M., Selph, K.E., Taniguchi, D.A.A., Landry, M.R., 2013. The role of Synechococcus in vertical flux in the Costa Rica upwelling dome. *Progress in Oceanography*. 112:49-59. doi: 10.1016/j.pocean.2013.04.003.

Sunda, W.G. Huntsman, S.A. (1992). Feedback interactions between zinc and phytoplankton in seawater. *Limnology and Oceanography*. 37(1):25-40. doi: 10.4319/lo.1992.37.1.0025.

Sunda, W.G., Huntsman, S.A., (1995). Cobalt and zinc interreplacement in marine phytoplankton: Biological and geochemical implications. *Limnology and Oceanography*. 40(8):1404-1417. doi: 10.4319/lo.1995.40.8.1404.

Sunda, W.G., Huntsman, S.A. (1996). Antagonisms between cadmium and zinc toxicity and manganese limitation in a coastal diatom. *Limnology and Oceanography*. 41(3):373-387. doi: 10.4319/lo.1996.41.3.0373

Sunda, W.G., Huntsman, S.A. (1998). Control of Cd concentrations in a coastal diatom by interactions among free ionic Cd, Zn, and Mn in seawater. *Environmental Science and Technology*. 32(19):2961-2968. doi: 10.1021/es980271y.

Sunda, W.G., Huntsman, S.A. (2000). Effect of Zn, Mn, Fe on Cd accumulation in phytoplankton: Implications for oceanic Cd cycling. *Limnology and Oceanography*. 45:1501-1516. doi: 10.4319/lo.2000.45.7.1501.

Takano, S., Tanimizu, M., Hirata, T., Sohrin, Y. (2014). Isotopic constraints on biogeochemical cycling of copper in the ocean. *Nature Communications*. 5:5663. doi: 0.1038/ncomms6663.

Talley, L.D. (1993). Distribution and formation of North Pacific Intermediate Water. *Journal of Physical Oceanography*. 23:517-537. doi: 10.1175/1520-0485(1993)023<0517:DAFONP>2.0.CO;2.

Taylor, A.G., Landry, M.R., Fruibott, A., Selph, K.E., Gutierrez-Rodriguez, A. (2015). Patterns of microbial community biomass, composition and HPLC diagnostic pigments in the Costa Rica upwelling dome. *Journal of Plankton Research*. 38(2):183-198. doi: 10.1093/plankt/fbv086.

Thamdrup, B., Dalsgaard, T., Revsbech, N.P. (2012). Widespread functional anoxia in the oxygen minimum zone of the Eastern South Pacific. *Deep-Sea Research Part I*. 65:36-45. doi: 10.1016/j.dsr.2012.03.001.

Theberge, S.M., Luther, G.W. III., Farrenkopf, A.M. (1997). On the existence of free and metal complexed sulfide in the Arabian Sea and its oxygen minimum zone. *Deep-Sea Research Part II*. 44(6-7):1381-1390. doi: 10.1016/S0967-0645(97)00012-X.

Thomson, R.E., Krassovski, M.V. (2010). Poleward reach of the California Undercurrent extension. *Journal of Geophysical Research*. 115:9pp. doi: 10.1029/2010JC006280.

Tortell, P.D., Price, N.M. (1996). Cadmium toxicity and zinc limitation in centric diatoms of the genus Thalassiosira. *Marine Ecology Progress Series*. 138:245-254. doi: 10.3354/meps138245.

Twining, B.S., Baines, S.B., Fisher, N.S., Maser, J., Vogt, S., Jacobsen, C., Tovar-Sanchez, A., Sañudo-Wilhelmy, S.A. (2003). Quantifying trace elements in individual aquatic protest cells with a synchrotron X-ray fluorescence microprobe. *Analytical Chemistry*. 75:3806-3816. doi: 10.1021/ac034227z.

Twining, B.S., Baines, S.B. (2004). Element Stoichiometry of individual plankton cells collected during the Southern Ocean Iron Experiment (SOFeX). *Limnology and Oceanography*. 49(6):2115-2128. doi: 10.4319/lo.2004.49.6.2115.

Twining, B.S., Baines, S.B. (2013). The Trace Metal Composition of Marine Phytoplankton. *Annual Reviews in Marine Science*. 5:191-215. doi: 10.1146/annurev-marine-121211-172322.

Twining, B.S., Nodder, S.D., King, A.L., Hutchins, D.A., LeCleir, G.R., DeBruyn, J.M., Maas, E.W., Vogt, S., Willhelm, S.W., Boyd, P.W. (2014). Differential remineralization of major and trace elements in sinking diatoms. *Limnology and Oceanography*. 59(3):689-704. doi: 10.4319/lo.2014.59.3.0689.

Ulloa, O., Pantoja, S. (2009). The oxygen minimum zone of the eastern South Pacific. *Deep-Sea Research Part II*. 56(16):987-991. doi: 10.1016/j.dsr2.2008.12.004.

Ulloa, O., Canfield, D.E., DeLong, E.F., Letelier, R.M., Stewart, F.J. (2012). Microbial oceanography of anoxic oxygen minimum zones. *Proceedings of the National Academy of Sciences of the United States of America*. 109(40):15996-16003. doi: 10.1073/pnas.1205009109.

van Geen A., McCorkle, D.C., Klinkhammer, G.P. (1995). Sensitivity of the phosphate-cadmium-carbon isotope relation in the ocean to cadmium removal by suboxic sediments. *Paleoceanography*. 10:159–169. doi: 10.1029/94PA03352.

Vance, D., Little, S.H., Archer, C., Cameron, V., Andersen, M.B., Rijkenberg, M.J.A., Lyons, T.W. (2016). The oceanic budgets of nickel and zinc isotopes: the importance of sulfidic environments as illustrated by the Black Sea. *Philosophical Transactions of the Royal Society of London A*. 374: 20150294. doi:10.1098/rsta.2015.0294.

Vraspir, J.M., Butler, A. (2009). Chemistry of marine ligands and siderophores. *Annual Reviews in Marine Science*. 1:43-63. doi: 10.1146/annurev.marine.010908.163712.

Vu, H.T.D., Sohrin, Y. (2013). Diverse stoichiometry of dissolved trace metals in the Indian Ocean. *Science Reports*. 3(1745):5 pp. doi:10.1038/srep01745.

Waeles, M., Maguer, J.F., Baurand, F., Riso, R.D. (2013). Off Congo waters (Angola Basin, Atlantic Ocean): A hot spot for cadmium-phosphate fractionation. *Limnology and Oceanography*. 58:1481-1490. doi: 10.4319/lo.2013.58.4.1481.

Waeles, M., Planquette, H., Afandi, I., Delebecque, N., Bouthir, F., Donval, A., Shelley, R.U., Auger, P.A., Riso, R.D., de Morias, L.T. (2016). Cadmium in the waters off South Morocco; nature of particles hosting Cd and insights into the mechanisms fractionating Cd from phosphate. *Journal of Geophysical Research: Oceans*. 121, 3106-3120. doi: 10.1002/2016JC011688.

Wedepohl, K.H. (1995) The composition of the continental crust. *Geochimica et Cosmochimica Acta*. 59(7):1217-1232. doi: 10.1016/0016-7037(95)00038-2.

Whitney, F.A., Freeland, H.J. (1999). Variability in upper-ocean water properties in the NE Pacific Ocean. *Deep-Sea Research Part II*. 46:2351-2370. doi: 10.1016/S0967-0645(99)00067-3.

Whitney, F.A., Freeland, H.J., Robert. M. (2007). Persistently declining oxygen levels in the interior waters of the eastern subarctic Pacific. *Progress in Oceanography*. 75:179-199. doi: 10.1016/j.pocean.2007.08.007.

Wright, J.J., Konwar, K.M., Hallam, S.J. (2012). Microbial ecology of expanding oxygen minimum zones. *Nature Reviews Microbiology*. 10:381-394. doi: 10.1038/nrmicro2778.

Wu, J., Boyle, E.A. (1997). Lead in the western North Atlantic Ocean: Completed response to leaded gasoline phaseout. *Geochimica et Cosmochimica Acta*. 61(15):3279-3283. doi:10.1016/S0016-7037(97)89711-6.

Wyatt, N.J., Milne, A., Woodward, E.M.S., Rees, A.P., Browning, T.J., Bouman, H.A., Worsfold, P.J., Lohan, M.C. (2013). Biogeochemical cycling of dissolved zinc along the GEOTRACES south Atlantic transect GA10 at 40°S. *Global Biogeochemical Cycles*. 28:44-56. doi: 10.1002/2013GB004637.

Wyrtki, K. (1962). The oxygen minima in relation to ocean circulation. *Deep-Sea Research and Oceanographic Abstracts*. 9(1-2):11-23. doi: 10.1016/0011-7471(62)90243-7.

Xie, R.C., Galer, S.J.G., Abouchami, W., Rijkenberg, M.J.A., De Jong, J., de Baar, H.J.W., Andreae, M.O. (2015). The cadmium-phosphate relationship in the western South Atlantic – The importance of mode and intermediate waters on the global systematics. *Marine* Chemistry. 177(1):110-123. doi: 10.1016/j.marchem.2015.06.011.

Xie, R.C., Galer, S.J.G., Abouchami, W., Rijkenberg, M.J.A., de Baar, H.J.W., De Jong, J., Andreae, M.O., in revision at *Earth and Planetary Science Letters*. Non-Rayleigh control of upper ocean Cd isotope fractionation in the western South Atlantic.

Xu, Y., Feng, L., Jeffrey, P.D., Shi, Y.G., Morel, F.M.M. (2008). Structure and metal exchange in the cadmium carbonic anhydrase of marine diatoms. *Natur*e. 452(7183):56-58. doi: 10.1038/nature06636.

Xu, Y., Morel, F.M.M. (2013). Cadmium in Marine Phytoplankton. In Cadmium: From Toxicity to Essentiality, Metal Ions in Life Sciences, eds Sigel, A., Sigel, H., Sigel, R.K.O. (Springer Netherlands), Vol 11, pp 509-528. doi: 10.1007/978-94-007-5179-8_16.

Xue, Z., Rehkämper, M., Schönbächler, M., Statham, P.J., Coles, B.J. (2012). A new methodology for precise cadmium isotope analyses of seawater. *Analytical and Bioanalytical Chemistry*. 402:883-893. doi 10.1007/s00216-011-5487-0.

Xue, A., Rehkämper, M., Horner, T.J., Abouchami, W., Middag, R., van de Flierd, T., de Baar, H.J.W. (2013). Cadmium isotope variations in the Southern Ocean. *Earth and Planetary Science Letters*. 382:161-172. doi: 10.1016/j.epsl.2013.09.014.

Yang, J., Li, Y., Liu, S., Tian, H., Chen, C., Liu, J., Shi, Y. (2015). Theoretical calculations of Cd stable isotope fractionation in hydrothermal fluids. *Chemical Geology*. 391:74-82. doi: 10.1016/j.chemgeo.2014.10.029.

Yang, S.C., Lee, D.C., Ho, T.Y. (2012). The isotopic composition of cadmium in the water column of the South China Sea. *Geochimica et Cosmochimica Acta*. 98:66-77. doi: 10.1016/j.gca.2012.09.022.

Yang, S.C., Lee, D.C., Ho, T.Y., Wen, L.S., Yang, H.H. (2014). The isotopic composition of dissolved cadmium in the water column of the West Philippine Sea. *Frontiers in Marine Science*. 1:13 pp. doi: 10.3389/fmars.2014.00061.

Yang, S.C., Lee, D.C., Ho, T.Y. (2015). Cd isotopic composition in the suspended and sinking particles of the surface water of the South China Sea: The effects of biotic activities. *Earth and Planetary Science Letters*. 428:63-72. doi: 10.1016/j.epsl.2015.07.025.

Zhang, J., Quay, P.D., Wilbur, D.O. (1995). Carbon isotope fractionation during gas-water exchange and dissolution of CO_2. *Geochimica et Cosmochimica Acta*. 59(1):107-114. doi: 10.1016/0016-7037(95)91550-D.

Zhang, J.Z., Millero, F.J. (1994). Investigation of metal sulfide complexes in sea water using cathodic stripping square wave voltammetry. *Analytica Chimica Acta*. 284(3):497-504. doi:10.1016/0003-2670(94)85056-9.

Zhao, Y., Vance, D., Abouchami, W., de Baar, H.J.W. (2014). Biogeochemical cycling of zinc and its isotopes in the Southern Ocean. *Geochimica et Cosmochimica Acta*. 125:653-672. doi: 10.1016/j.gca.2013.07.045.